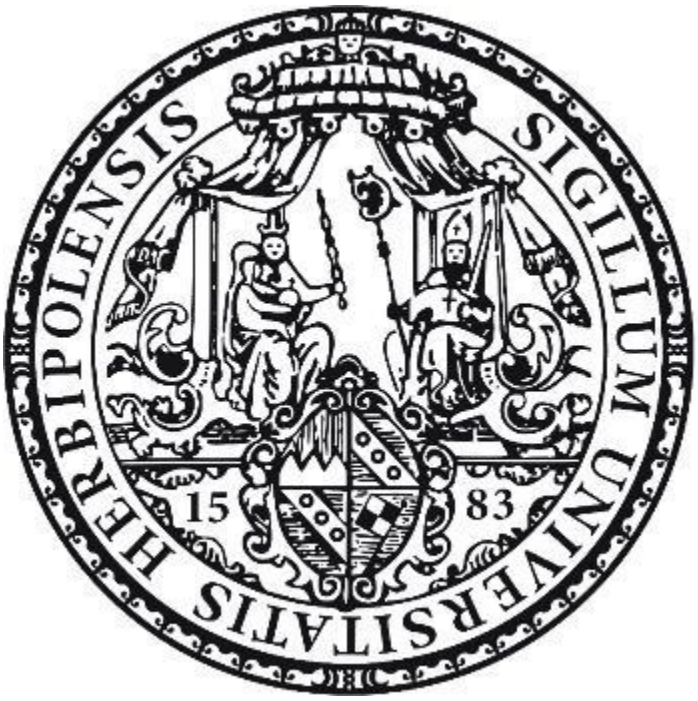

Adrenergic-induced ERK3 pathway drives lipolysis and suppresses energy dissipation

♦♦♦♦♦

Der adrenerge induzierte ERK3-Signalweg verstärkt Lipolyse und unterdrückt Energiedissipation

Doctoral thesis for a doctoral degree
at the Graduate School of Life Sciences,
Julius-Maximilians-Universität Würzburg,
Section Biomedicine

Submitted by

Rabih El Merahbi
from Beirut, Lebanon

Würzburg, 2020

Submitted on: ……..……..

Office stamp

Members of the Thesis Committee

Chairperson: Prof. Dr. Manfred Gessler

Primary Supervisor: Dr. Grzegorz Sumara

Supervisor (Second): Prof. Dr. Antje Gohla

Supervisor (Third): Prof. Dr. Christian Wolfrum

Supervisor (Fourth):

Date of Public Defence: ……

Date of Receipt of Certificates: ……

ABSTRACT

Obesity-induced diabetes affects over 400 million people worldwide. Obesity is a complex metabolic disease and is associated with several co-morbidities, all of which negatively affect the individual's quality of life. It is commonly considered that obesity is a result of a positive energy misbalance, as increased food intake and lower expenditure eventually lead to the development of this disease. Moreover, the pathology of obesity is attributed to several genetic and epigenetic factors that put an individual at high risk compared to another. Adipose tissue is the main site of the organism's energy storage. During the time when the nutrients are available in excess, adipocytes acquire triglycerides, which are released during the time of food deprivation in the process of lipolysis (free fatty acids and glycerol released from adipocytes). Uncontrolled lipolysis is the consequent event that contributes to the development of diabetes and paradoxically obesity. To identify the genetic factors aiming for future therapeutic avenues targeting this pathway, we performed a high-throughput screen and identified the Extracellular-regulated kinase 3 (ERK3) as a hit. We demonstrate that β-adrenergic stimulation stabilizes ERK3 leading to the formation of a complex with the co-factor MAP kinase-activated protein kinase 5 (MK5) thereby driving lipolysis. Mechanistically, we identify a downstream target of the ERK3/MK5 pathway, the transcription factor FOXO1, which promotes the expression of the major lipolytic enzyme ATGL. Finally, we provide evidence that targeted deletion of ERK3 in mouse adipocytes inhibits lipolysis, but elevates energy dissipation, promoting lean phenotype and ameliorating diabetes. Moreover, we shed the light on our pharmacological approach in targeting ERK3/MK5 pathways using MK5 specific inhibitor. Already after 1 week of administering the inhibitor, mice showed signs of improvement of their metabolic fitness as showed here by a reduction in induced lipolysis and the elevation in the expression of thermogenic genes. Taken together, our data suggest that targeting the ERK3/MK5 pathway, a previously unrecognized signaling axis in adipose tissue, could be an attractive target for future therapies aiming to combat obesity-induced diabetes.

Zusammenfassung

Adipositas-induzierter Diabetes betrifft weltweit über 400 Millionen Menschen. Adipositas ist eine komplexe Stoffwechselerkrankung und geht mit mehreren Komorbiditäten einher, die sich alle negativ auf die Lebensqualität der Betroffenen auswirken. Es wird generell angenommen, dass Adipositas aus einem positiven Energieungleichgewicht resultiert, da eine erhöhte Nahrungsaufnahme und ein geringerer Verbrauch zu der Ausbildung dieser Krankheit führen. Darüber hinaus ist die Pathologie von Adipositas auf mehrere genetische und epigenetische Faktoren zurückzuführen, wodurch Individuen einem erhöhtem Risiko ausgesetzt sein können. Das Fettgewebe ist der vorwiegende Energiespeicher des Organismus. In Zeiten eines Nährstoffüberschusses speichern Adipozyten Triglyceride, die im Falle eines Nahrungsmangels durch den Prozess der Lipolyse in Form von freien Fettsäuren und Glycerin freigesetzt werden. Unkontrollierte Lipolyse ist ein Folgeereignis, welches zur Entwicklung von Diabetes und paradoxerweise zu Adipositas beiträgt. Um die genetischen Faktoren zu identifizieren, die in Zukunft therapeutische Angriffspunkte darstellen könnten, haben wir ein Hochdurchsatz-Screening durchgeführt und die extrazellulär regulierte Kinase 3 (ERK3) als Treffer identifiziert. Wir zeigen, dass β-adrenerge Stimulation ERK3 stabilisiert, was zur Bildung eines Komplexes mit dem Cofactor MAP-Kinase-aktivierte Proteinkinase 5 (MK5) führt und dadurch die Lipolyse vorantreibt. Mechanistisch identifizieren wir den Transkriptionsfaktor FOXO1, der dem ERK3/MK5-Signalweg nachgeschaltet ist und die Expression des wichtigsten lipolytischen Enzyms ATGL fördert. Darüber hinaus belegen wir, dass die gezielte Deletion von ERK3 in Maus-Adipozyten die Lipolyse hemmt, aber die Energiedissipation erhöht, den mageren Phänotyp fördert und Diabetes lindert. Außerdem nutzen wir einen pharmakologischen Ansatz durch Verwendung eines MK5 spezifischen Inhibitors, um auf den ERK3/MK5-Signalweg abzuzielen. Bereits eine Woche nach Verabreichung des Inhibitors zeigen Mäuse Anzeichen einer verbesserten metabolischen Fitness, die sich durch einer Verringerung der induzierten Lipolyse und eine verstärkte Expression von thermogenen Genen auszeichnet. Zusammenfassend legen unsere Daten nahe, dass der ERK3/MK5-Signalweg, eine zuvor nicht erkannte Signalachse im Fettgewebe, ein attraktiver Ansatzpunkt für zukünftige Therapien zur Bekämpfung von Adipositas-induziertem Diabetes sein könnte.

TABLE OF CONTENTS

1 OBESITY AND METABOLIC SYNDROME

1.1 Obesity as a worldwide pandemic

Obesity is generally characterized by impaired energy homeostasis and disordered body metabolism. Obesity has been considered as pandemic disease, its prevalence has doubled worldwide since 1980 to an extent that nearly a third of the world population is now classified as overweight or obese (Tabarés Seisdedos 2017).

Obesity constitutes a significant threat to public health; it unfavorably affects nearly all the body's physiological functions. It increases the risk for developing multiple disease conditions, such as diabetes mellitus (Kahn, Hull et al. 2006), cardiovascular disease (Van Gaal, Mertens et al. 2006), several types of cancers (Khandekar, Cohen et al. 2011), an array of musculoskeletal disorders (Wearing, Hennig et al. 2006), and poor mental health (Halfon, Larson et al. 2013) all of which might lead to reduced quality of life, unemployment, lower productivity, and social disadvantages.

Despite this relatively simplistic definition, obesity is a multifactorial disease that is not only be attributed to one single reason, which is the positive alteration of the individual energy balance between increase dietary energy intake exceeds energy expenditure, but rather is a combination of many factors. While genetic predisposition is one of the causes, the rising pandemic is mainly identified as behavioral (Bouchard 1991).

According to the World Health Organization (WHO), obesity is a pandemic disease defined as an abnormal or excessive fat accumulation that presents a risk to health (De Onis, Blössner et al. 2010). For adults, current guidelines define a normal BMI range as18.5 to 24.9, whereas a BMI ≥25 kg/m2 is considered to be overweight, and a BMI ≥30 kg/m2 is classified as obese, with severe obesity defined as a BMI ≥40 kg/m2 (De Onis, Blössner et al. 2010). The rise of industrialization negatively affected society's physical health. The globalization of food systems that produce more processed and affordable food, and promote passive overconsumption from energy-dense, nutrient-poor foods and beverages have been identified as a major driver of the obesity epidemic disease (Popkin, Adair et al. 2012) although a decrease in physical activity owing to the modernization of lifestyles is also likely involved (Marti, Moreno-Aliaga et al. 2004). Obesity can occur at any age. Previous studies assessing trends in obesity found that its prevalence has increased in both adults and children of all ages, indiscriminate of geographical locality, ethnicity or socioeconomic status (Chooi, Ding et al. 2019).

1.2 Genetic and Epigenetic factors

Evolutionarily, our ancestors had to withstand various survival challenges that had a lot of influence on shaping the current human beings. Among that, they would go through cycles where food is in abundance but also, they had to survive periods of undernutrition. Therefore, selection pressure most likely contributed to a genetic profile that would favor the ability to resorb calories to a higher degree and to enlarge energy stores in adipose tissue (AT) more efficiently (Zucoloto 2011). Humans who could handle longer periods of starvation and who could store and efficiently mobilize energy might have higher chances to reproduce more than those without these adaptations might. Consequently, leading to the overrepresentation of certain genetic variants among the population. However, only in the past few years, more people are dying from the consequences of obesity rather than underweight (Organization 2002).

Today, we must consider the epigenetic effects on feeding and metabolic processes. Epigenetics can be defined as a process in which genes can be activated or deactivated in a new environmental situation, enabling the organism to better performance without modification of its genome (Gibney and Nolan 2010). In this regard, a period of caloric restriction leads to persistent changes in mitochondrial biogenesis and fatty acid oxidation, thereby shifting cellular metabolism preferentially toward fatty acid oxidation rather than glucose oxidation in the mitochondria. Similarly, prolonged mild cold exposure is associated with metabolic adaptation in skeletal muscle and adipose tissue by inducing a switch from carbohydrate metabolism to fatty acid oxidation (Chouchani and Kajimura 2019). From an evolutionary viewpoint, such metabolic shifts are considered protective mechanisms to secure enough glucose for the brain, while other fuels, such as fatty acids and amino acids, are allocated to the peripheral metabolic organs (Kajimura, Spiegelman et al. 2015). Importantly increasing evidence indicates that this process can be passed to future generations. That is, the genes are activated or deactivated in a generation and transmitted to the following generation(Eaton, Konner et al. 2009). Results also showed that the number of adipocytes is genetically determined. Moreover accumulating evidence suggests that childhood and adolescence are critical periods for shaping adipose tissue properties and thereby determining the risk of obesity and metabolic disease (McMorrow, Connaughton et al. 2015). As explained, if during the growth phase the individual ingests more food than necessary in such a way that the organism's adipocyte capacity is exhausted, then this number can increase proportionately with the excess ingestion. This study has highlighted that overweight at kindergarten age was shown to increase the risk of later obesity by 4-fold (Cunningham, Kramer et al. 2014). This may explain why the individual who reaches adulthood

while overweight has more difficulty resuming a normal weight than an individual who became overweight during adulthood (Kaufman, Montalvo-Ortiz et al. 2018). Taken together, these findings highlight a role for environment and social stressors that might lead to substantial epigenetic alterations in adipocytes as well as adipocyte progenitor cells, eventually influencing the individual susceptibility to develop obesity.

1.3 Obesity-related complications

As mentioned earlier, overweight and obesity are the consequence of a chronic imbalance between energy intake and energy expenditure. Adipose tissue has remarkable plasticity in turn of expanding in size and number which helps maintaining blood sugar and free fatty acids (FFAs) level in the physiological range (Wang, Tao et al. 2013). However, chronic overfeeding leads to a pathophysiological expansion of AT which causes hypoxia, fibrosis, as well as infiltration of immune cells, promoting chronic low-grade inflammation and eventually leading to adipocyte death (Figure 1) (Sun, Tordjman et al. 2013, Choe, Huh et al. 2016). This impairment in the ability of AT in culminating in the excess of fat results in the pathological expansion of AT around the heart and kidneys and also the ectopic storage of lipids in peripheral organs, such as liver and skeletal muscle (Robbins, Danforth Jr et al. 1979, Robbins, Horton et al. 1982). Moreover, circulating proinflammatory cytokines and FFAs derived from the inflamed adipose tissue impair peripheral insulin sensitivity in the periphery, which is the major cause in the development of type 2 diabetes mellitus (T2D) and a number of other metabolic disorders or comorbidities (Stefan and Häring 2013).

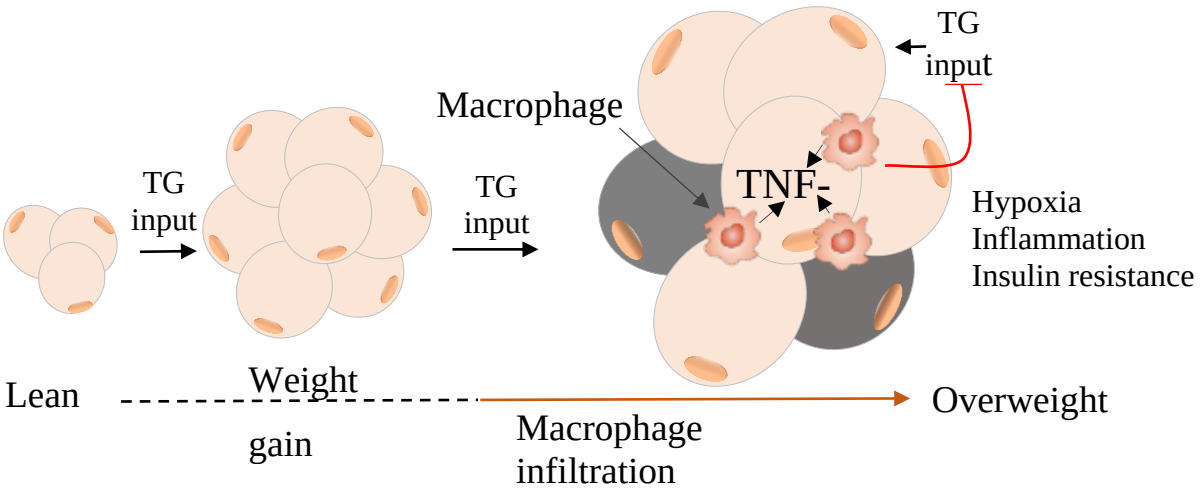

Figure 1. Development of adipose tissue in the course of prolonged over nutrition.

Excessive TG input causes an increase of adipose tissue in size and number of adipocytes. When the expansion limit is reached, hypertrophic adipocytes undergo fibrotic changes and become maladaptive due to hypoxia and inflammation which causes cell death and contributes to the development of insulin resistance (modified from (Rosen and Spiegelman 2014)). Triglycerides (TG), tumor necrosis factor α (TNFα).

Type 2 diabetes mellitus is the most common metabolic disorder associated with obesity and affecting 422 million people worldwide (Okemah, Peng et al. 2018). Systemically ectopic lipid deposition in the pancreases together with the increasing demand for insulin production to maintain normoglycemia causes β cell failure (Prentki, Joly et al. 2002). However, the major pathophysiological event contributing to the development of T2D is the resistance of target tissues to insulin signaling, which is clinically referred to as insulin resistance(Ferrannini and Stern 1995). On the cellular level, insulin signaling is involved in multiple metabolic and mitogenic aspects of cellular function. Briefly, the binding of insulin to its receptor triggers autophosphorylation of the receptor, leading to the binding of insulin receptor substrate proteins (IRS) together with various other scaffold proteins (Lee, Li et al. 1993). The Insulin Receptor Substrate proteins are a family of cytoplasmic adaptor proteins (IRS1-6) containing two extracellular (α) and two intracellular (β) subunits and are mainly expressed on the surface of metabolically active cells (White 2002). Importantly, IRS1 mediates insulin-stimulated glucose uptake in muscle and adipose tissue, whereas IRS2 mainly acts in the liver. Phosphorylation of IRS1 and IRS2 leads to activation of phosphatidylinositol 3-kinase (PI3K)/ AKT pathway which eventually facilitates the translocation of glucose transporter-4 (GLUT4)-containing vesicles to the cell surface (Bryant, Govers et al. 2002). Therefore, insulin resistance defines the ineffective strength of insulin to signal downstream its receptor to its final substrates, thereby affecting insulin-stimulated glucose uptake and storage.

2 THE THREE DIFFERENT SHADES OF FAT

2.1 Adipose tissue biology

Adipose tissue comprises adipocytes and many other cell types that engage in dynamic crosstalk in a highly innervated and vascularized tissue matrix. Although adipose tissue has been studied for decades, it has been only recently that our understanding of adipose biology and its crosstalk with other vital organs was effectively enhanced. This field of study gained global attention by scientists and their interest in excessively studying adipose tissue functions beyond what was previously assumed to be limited to be the place of storage of extra fat. Nowadays, it is commonly known that adipose tissue has a strong influence on the whole-body glucose metabolism and lipid metabolism through its signaling effects on the body's major metabolic organs such as skeletal muscle, liver, heart, and brain (Guilherme, Virbasius et al. 2008, Antonopoulos, Margaritis et al. 2016). In this regard, it was further illustrated that this communication with different organs happens through the adipocyte's secretion of endocrine and paracrine factors also called adipokines. Locally, adipose tissue modulates infiltrated immune cell cytokine secretion (Mancuso 2016) thereby affecting tissue inflammation. Through its direct interaction with the vasculature, adipocytes regulate the endothelium blood flow (Cao 2013) and signal other organs through their adipokines secretion. Moreover, studies showed that innervated sympathetic neurons project polysynaptically from the brain to the adipose tissue, thereby sending and receiving signals to the central nervous system (Stanley, Pinto et al. 2010). Importantly, energy homeostasis is regulated by a complex network of electrical or chemical stimulation that controls lipid storage mobilization(de Kloet and Herman 2018).

The adipose tissue is a large organ that stretches along the whole body, providing support and responding to the organism's energy needs. According to their anatomical location and function, two major cell types have been classified. The white adipose tissue (WAT) is noted for its energy-storing function while the brown adipose tissue (BAT) plays a crucial role in whole-body heat production, through its non-shivering thermogenesis. As nutrient shortage and cold can occur transiently and independently from each other, both WAT and BAT undergo adaptive and dynamic changes in response to starvation or overfeeding, as well as in response to cold or thermoneutrality (Cannon and Nedergaard 2004, Cinti 2012). While short term changes might only involve the altered expression of proteins, continuous stimulations for 2–3 days, induces marked changes in the adipose tissue morphology and

functional properties (Cinti 2012). In this light, came the identification of a third population of adipocytes called beige adipocytes referring to the emergence of brown-like cells within the white adipose tissue(Cousin, Cinti et al. 1992). Altogether, adipocytes drive and modulate the whole-body energy balance.

2.2 White adipose tissue

A major shift in our understanding of white adipose tissue biology occurred only in this last decade. The realization that WAT is not just a passive storage organ for excess calories, has opened the field for more discoveries in the function of this tissue. Currently, white adipose tissue is observed as the main determinant of healthy metabolism and metabolic dysfunction. It is a highly dynamic organ that can rapidly remodel in response to environmental inputs (Figure 2). White adipose tissue accounts for anywhere from 5% to 50% of human body weight. It was long assumed that the number of adipocytes within the white adipose tissue is formed by puberty and persists throughout life, while its variable size is due to its expansion or involution according to the organism's diet. However, tracer studies had disproved this misconception by revealing that adipocytes undergo a classical turnover with a rate of 8–10% per year (Arner, Bernard et al. 2011). The generation of new adipocytes involves the proliferation of a residing preadipocyte which later differentiates into a mature adipocyte, capable of storing and releasing energy. The noninflammatory clearance of dying adipocytes occurs by the recruitment of tissue macrophages which offloads the adipocyte from its lipids content before engulfing it (Cinti, Mitchell et al. 2005). On one hand, the development of obesity is accompanied by a rapid expansion of the tissue by increasing its lipid storage capacity (hypertrophy) and by increasing the number of adipocytes (hyperplasia) (Lee, Wu et al. 2010). On the other hand, involution of tissue size occurs within the first 24 hours of fasting while prolonged fasting causes the shrinkage in the number of mature adipocytes (MacLean, Higgins et al. 2006).

Taking this together, WAT major physiological function is to serve as the body's fuel reservoir where the surplus energy is efficiently deposited in the form of neutral triglycerides (TGs) through the lipogenic pathway ref. However, when food is scarce or energy expenditure requirements are stimulated, stored TGs are hydrolyzed into glycerol and fatty acids through the lipolytic pathway (Bernard 1856). This released glycerol and fatty acids from adipose tissue can then be transported through the bloodstream and subsequently infiltrated and oxidized in the peripheral organs such as the skeletal muscles and liver.

2.3 Brown adipose tissue

Brown adipose tissue was first described in the 16th century however, it was not until the 1960s that its function and physiology were discovered (Betz and Enerbäck 2018). BAT is characterized by a dense vasculature and sympatho-adrenergic innervation that differs markedly from that of WAT (Figure 2). Under physiological conditions, BAT gets activated in response to cold exposure by the innervated sympathetic neurons. Through a process defined as cold-induced thermogenesis or non-shivering thermogenesis, activated BAT converts it chemical energy from TGs stored in numerous lipid droplets into heat(Horowitz and Plant 1978). This process results from an evocable short circuit at the inner membrane capacitor of the tissue's most abundant organelle, the mitochondria(de Meis, Arruda et al. 2006).

Heat production by BAT is an extremely energy-expensive process that burns nutrients stores. Therefore, to avoid hyperthermia, thermogenesis in this tissue must be tightly controlled, so that heat is specifically produced in response to thermogenic stimuli. Humans and other mammals register cooling of the skin with high sensitivity thermoreceptors, especially on their trunk and neck regions (Ouzzahra, Havenith et al. 2012). Modest cooling of the skin activates a transient receptor in sensory neurons, which acts as a sensor for mild, non-noxious cold and mediates this sensation to the thermoregulatory areas in the central nervous system. The perception of cold temperature is integrated in the preoptic area (POA) of the hypothalamus then afferent command signals leading to the defense of body temperature are sent through the POA somatic outflow to stimulate the shivering behavior in skeletal muscles as well as through its sympathetic neurons to stimulate the non-shivering thermogenesis in BAT (Nakamura and Morrison 2008).

Subsequently, BAT is an active metabolic organ that can be clearly detected as hot spots of glucose uptake when imaged using ^{18}F-FDG-PET/CT scans in the cervical, supraclavicular, axillary, and paravertebral regions of adult humans (Hadi, Chen et al. 2007). Studies showed that repeated cold exposure leads to an increase of BAT activity, which is associated with an induced increase in energy expenditure by non-shivering thermogenesis, together with a self-reported decrease in sensitivity to cold (van der Lans, Hoeks et al. 2013).

2.4 Beige adipose tissue

Subcutaneous WAT depots contain a second form of thermogenic adipocytes, often referred to as beige adipocytes (or brite adipocytes). Similar to brown adipocytes, beige adipocytes also contain multilocular lipid droplets and densely packed mitochondria (Figure 2). However, despite their morphological similarity, beige adipocytes are distinct from brown adipocytes in their cellular heterogeneity within adipose tissues (Wu, Boström et al. 2012, Lee, Kim et al. 2017). While the interscapular BAT depot is separated from the surrounding WAT by a layer of connective tissue, beige adipocytes are found to exists within the WAT and without any separation by a distinct later of connective tissue from the surrounding white unilocular cells (Sidossis and Kajimura 2015). Moreover, it was well demonstrated that beige adipocytes are essentially regulated by the sympathetic nervous system. Following a cold exposure or just with the feeling of cold, clusters of beige adipocytes are prone to emerge within the WAT and surrounding the areas in which tyrosine-hydroxylase expressing nerve fibers are densely innervated (Murano, Barbatelli et al. 2009). A number of studies showed that the release of norepinephrine from the sympathetic nerves is the main driver of browning and its experimental inhibition with 6-hydroxydopamina prior to cold exposure, impairs beige adipocyte formation (Barbatelli, Murano et al. 2010, Paulo, Wu et al. 2018).

As mentioned before, stimuli such as fasting or cold exposure induce tissue plasticity. thereby a study investigating the origin of cold-induced beige adipocyte showed that a large part of the newly formed beige adipocytes in subcutaneous WAT are negative for proliferation markers such as BrdU or Ki67, indicating that browning occurred from mature white adipocytes rather than the differentiation of precursor cells (Himms-Hagen, Melnyk et al. 2000, Lee, Petkova et al. 2012, Frontini, Vitali et al. 2013). Furthermore, a recent genetic lineage–tracing study showed that beige adipocytes dedifferentiated back to mature white adipocytes after only some weeks of warm adaptation. These white adipocytes' plasticity allows them to reconvert into beige adipocytes after additional cold stimulation (Rosenwald, Perdikari et al. 2013). In contrast, pulse-chase fate-mapping experiments performed by others on mature adipocytes to find out that the majority of newly evolved beige adipocytes originates from de novo differentiation of progenitors in subcutaneous WAT (Wang, Tao et al. 2013). At the molecular level, various transcriptional regulators are characterized for their activity in response to sympathetic stimulation, driving the beiging process. Specifically, studies showed that PRDM16 acts primarily through co-regulating C/EBP β a member of CCAAT/enhancer-binding protein (C/EBP) family which in turn promotes that activity of PPAR γ , PPAR α , and

PGC-1 α to induce brown adipocyte lineage or enhances white adipocyte browning (Seale, Kajimura et al. 2007, Hondares, Rosell et al. 2011, Giralt and Villarroya 2013). Altogether, the theory of beige trans-differentiation needs to be critically investigated to help us better understand the physiological and genetic mediators of the beiging phenotype.

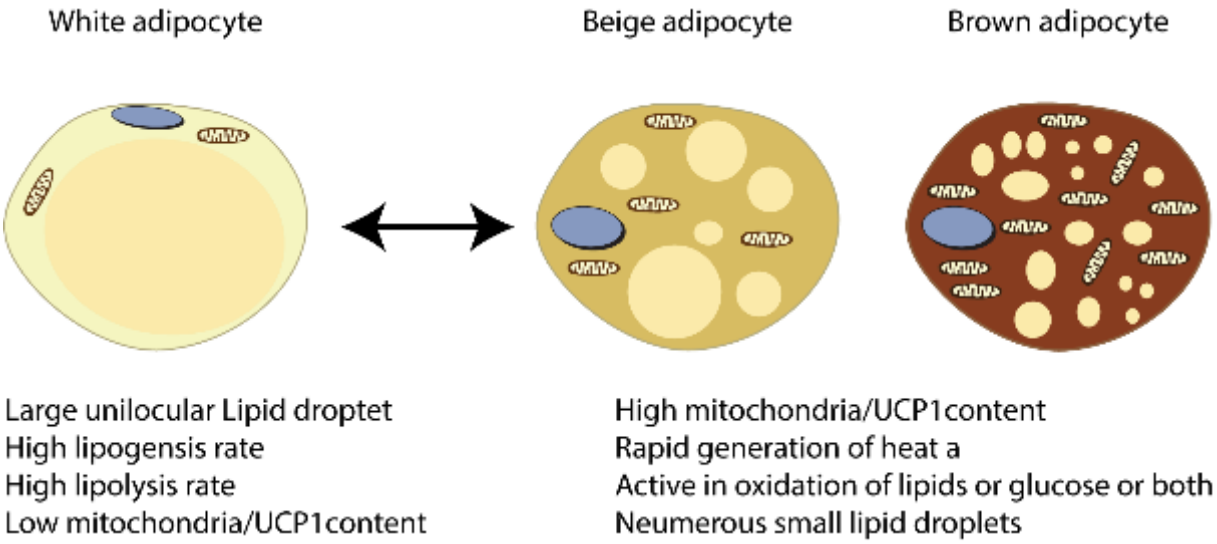

Figure 2. Different characteristics of adipose tissue cells.

White adipose tissue on the left panel is characterized by a single unilocular lipid droplet with high potential for energy storage and its release. On the right panel, brown adipocytes are dense in mitochondria and cauterized by their high potential for energy dissipation and heat production. Beige/Bright adipocytes on the middle panel combine the characteristics of both cells.

3 METABOLIC ADAPTATION IN ADIPOSE TISSUE

3.1 Physiological adaptation to food ingestion

Fatty acids are essential for sustaining the body physiological needs. They construct the integral parts of biological membranes, contains a high energy density source and are also used as precursors for the generation of numerous lipid mediators. Therefore, humans adapted their food behavior for up taking FFAs rich food from plant and animal sources. However, other major dietary components, such as monosaccharides and amino acids, can be converted into FFAs. Despite their important role in cellular and physiological functions, high concentrations of FFAs in the bloodstream are rather toxic to the body because of their amphipathic nature and limited solubility in blood and their hostile acidic nature which impacts cellular homeostasis. Collectively, these destructive effects of accumulation and conversion into cytotoxic lipid species are referred to as lipotoxicity. As a defensive mechanism to avoid lipotoxicity, FFAs are directly esterification to the trivalent alcohol glycerol to form triacylglycerols. Triacylglycerols (also named as Fat) are hydrophobic in nature, thereby providing an optimal packaging of FFAs for efficient transport and storage.

During the feeding stage, insulin governs the accumulation of excess calorie intake as fat stored in the WAT (Figure 3). However, The FFAs sources used for TG synthesis is obtained from two distinct origins, that is, circulating TG and de novo lipogenesis (DNL) (Song, Xiaoli et al. 2018). On one hand, absorbed FFAs are packed as TGs in chylomicrons or very-low-density lipoproteins (VLDL), in the intestine or liver respectively. These lipoproteins travel the bloodstream to ATs. There, insulin stimulates the action of lipoprotein lipase within the AT vascular endothelium to hydrolyze TGs into non-esterified fatty acids (NEFA) (Cryer 1981). This process allows the released NEFAs to be uptaken by the adipocytes through fatty acid transporters such as CD36 and fatty acid transport protein-1 (FATP1) (Goldberg, Eckel et al. 2009) (Figure 3).

On the other hand, insulin also stimulates glucose uptake in cells expressing the GLUT 4, essentially driving the DNL majorly in adipocytes but also in other active metabolic tissues, such as the liver and skeletal muscles(Garvey, Maianu et al. 1992). After being internalized, glucose follows a series of coordinated enzymatic reactions that occur in the adipocytes to allow the flow of carbons from glucose to fatty acids. Importantly, glucose provides its own metabolite acetyl-CoA as the substrate for de novo synthesis of fatty acids. In parallel, it induces the expression of rate-limiting enzymes such as acetyl-CoA carboxylases 1 (ACC1)

(Park, Kaushik et al. 2002) and fatty acid synthase (FASN) which plays key roles to convert glucose to FFAs (Menendez and Lupu 2007) (Figure 3). In the same time, insulin activates glycolytic and lipogenic enzymes, and stimulates the expression of lipogenic gene sterol regulatory element-binding protein 1 (SREBP1) and carbohydrate response element-binding protein (ChREBP), both proteins are shown to control the expression of genes required for cholesterol, fatty acids, TG and phospholipid synthesis (Ferre and Foufelle 2007, Eissing, Scherer et al. 2013). Finally, glycerol 3-phosphate, a glucose derivative, is used as a backbone to synthesize and store TG from both FFAs sources in lipid droplets (Cao, Li et al. 2006). Therefore, adipocyte DNL is an important source of endogenous fatty acids and plays a key role in maintaining systemically metabolic homeostasis.

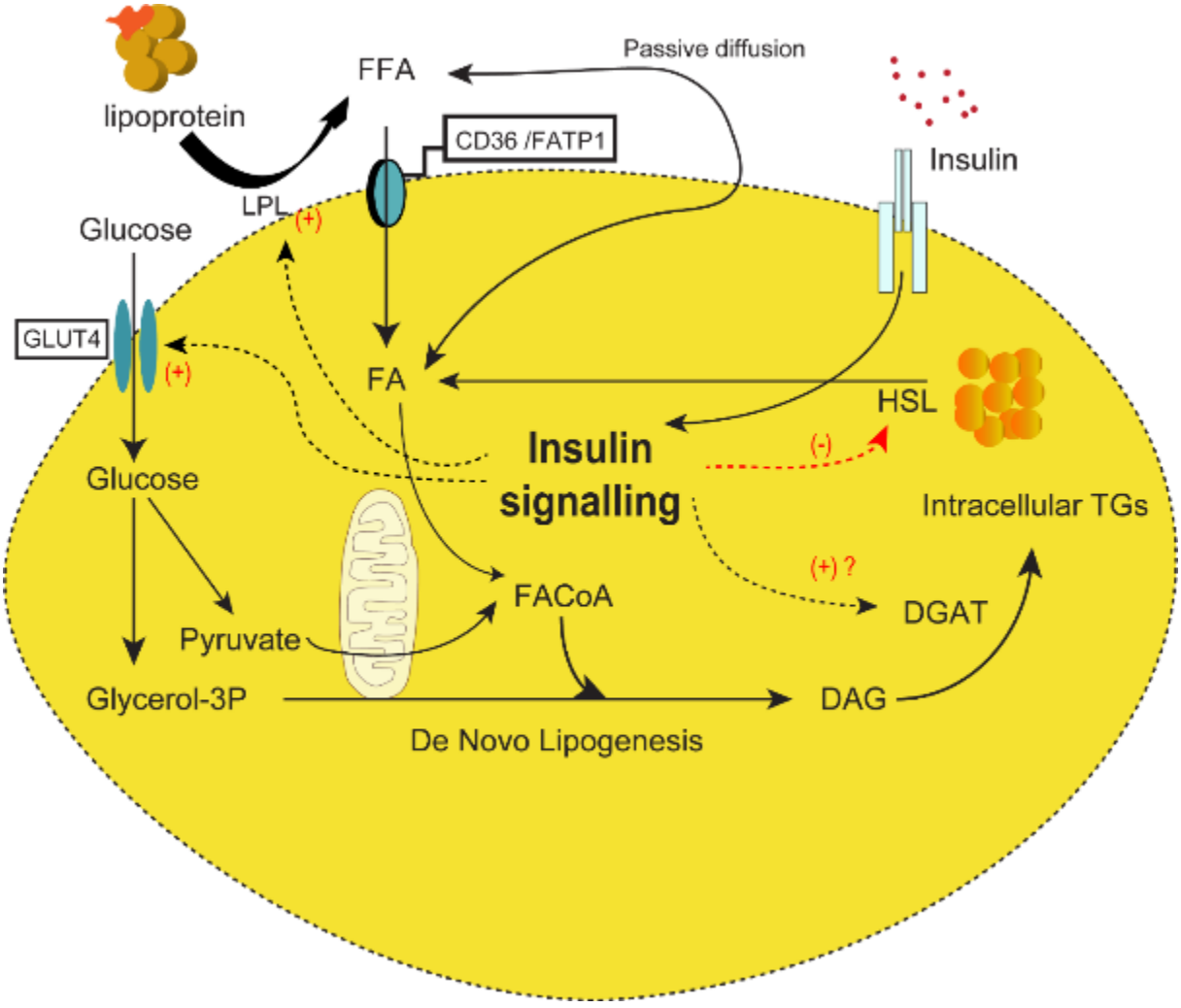

Figure 3. Adipocytes de novo lipogenesis.

Adipocytes internalize circulating FFA and glucose to generate TG for energy storage. Solid lines indicate flux of metabolic substrates, and dashed lines indicate stimulatory or inhibitory

effects of insulin. (+) Indicates a stimulatory effect of insulin, and (-) indicates an inhibitory effect of insulin. Insulin binds to its receptor and it's signaling pathways, promotes FFA uptake into the adipocyte by stimulating the LPL-mediated release of FFA from lipoprotein triglyceride. Fatty acids enter the adipocyte both by diffusion down a concentration gradient as well as by facilitated transport. Insulin regulation of fatty acid transporters such as CD36 and FATP1. Insulin stimulates glucose transport into the adipocyte through GLUT4, thereby increasing the availability of glycerol-3 phosphate (Glycerol-3P) for triglyceride (TG) synthesis. Insulin may have a direct stimulatory effect on lipogenic enzymes such as DGAT. By inhibiting HSL, it reduces the intracellular lipolysis of cytosolic triglycerides, thereby promoting adipocyte triglyceride storage. (adopted and modified from (Chouchani and Kajimura 2019)).

3.2 Physiological Adaptation to energy expenditure

Adipocytes possess a unique morphology, consisting of a lipid droplet (TGs store) occupying the majority of the intracellular region while the nucleus and cytosome are squeezed to the periphery. The mobilization of fatty acids in and out of these TGS stores is termed Lipogenesis and lipolysis, respectively. These processes provide essential help to maintain the whole-body energy balance, in response to altered nutrient needs, which is considered a major evolutionary adaptation to sustain the body's increasing demands of energy supplies during the periods of food deprivation, physical exercise, and cold. Therefore, to avoid the extinction of lipid fuel, the trigger for initiation of lipolysis is dependent upon sympathetic innervation of the adipose tissue which is under direct control from the central nervous system (Hücking, Hamilton-Wessler et al. 2003).

3.2.1 Fasting response

In most mammals, the primary source of energy is glucose, which is mainly stored in the liver in the form of glycogen. During short term food deprivation, glucose level starts to drop in the circulation. This low amount of glucose is directly sensed by the sensory receptors in CNS. Together with dropping levels of insulin, pancreatic alpha cells responses to fasting signals by secreting glucagon to the circulation. Glucagon acts in opposition to insulin and primary targets the liver by triggering the cyclic AMP cascade leading the inhibition of glycogen synthase; thereby, increasing glycogenolysis and gluconeogenesis while inhibiting glycogen synthesis(Cross, Watt et al. 1997). In parallel, glucagon inhibits the synthesis of free fatty acids by diminishing the production of pyruvate while maintaining acetyl CoA carboxylase in its unphosphorylated state(Kudo, Barr et al. 1995). Glucose metabolism is

shown to be critical for brain physiology. Therefore, its tight regulation through this process is essential to protect the brain from the alteration in the blood glucose levels.

However, when fasting signals are prolonged, sympathetic neurons sense the depletion of the hepatic glycogen and signals a metabolic in which non-hepatic glucose, fat-derived ketone bodies are used as energy sources to sustain the nervous system while free fatty acids are utilized for energy in the other tissues(Song and Thomas 2007). Regarding adipose tissue, fasting promotes the utilization of lipids from adipose tissue as an energy substrate at the expense of glucose and protein(Carlson, Snead et al. 1994). On the cellular level, the release of noradrenaline by adipose efferent nerves activates the β-adrenergic receptors (β-AR) which induces the activation and assembly of lipolytic pathways that eventually lead to the hydrolyzation of TGs stocks and the release of FFAs and glycerol to the circulation (Figure 4). In the periphery, Fatty acids enter the mitochondria and serve through its β-oxidation (FAO) a key metabolic pathway for ATP production and energy homeostasis in metabolic organs such as the liver, heart, and skeletal muscle(Houten and Wanders 2010). In parallel, ketone bodies are generated by the liver in a process that is dependent on FAO. Ketone bodies provide an additional source of energy that could be used by all tissues including the brain(McGarry and Foster 1980).

3.2.2 Physical exercise

Activity-induced energy expenditure is considered the most variable component of the body's daily energy balance. During exercise skeletal muscles requires high amounts of ATP to conduct its proposed action. During prolonged exercise, the fuel substrates are switched from carbohydrate, stored as muscle and liver glycogen, to the use of FFA, mainly deposited as triacylglycerol (TG) in subcutaneous and deep visceral adipose tissue. In this sense, exercise-induced sympathetic nervous system stimulation activates β-adrenergic signaling to release of FFAs from adipocytes and deliver them to working muscles. There, FFAs are used as a substrate for ATP production through β-oxidation (van Loon, Koopman et al. 2003).

3.2.3 Cold exposure

As mentioned before, in response to cold exposure, BAT is the specialized organ that can convert its stored chemical energy from TGs found in numerous lipid droplets directly into heat upon their activation by the innervated sympathetic neurons. This process is termed cold-induced thermogenesis or non-shivering thermogenesis. Heat production precisely occurs at the mitochondrial inner membrane; uncouples electron transport from ATP synthesis, and

causes the electron transport chain to run at its maximum rate, thereby by channeling fatty acids into β-oxidation and dissipating the generated energy as heat (Figure 4) (Wallace, Fan et al. 2010). In brief, following a sympathetic signal, thermogenesis gets activated in the BAT as well as in beige cells. As a result, free fatty acids are transferred into mitochondria by carnitine palmitoyltransferase 1 (CPT1) which is located at the outer membrane of mitochondria. At the inner side of the mitochondria, FFAs are the fuel source for β-oxidation, which in turn produces NADHs and FADHs that are later oxidized in the electron transport chain(Dalgaard and Pedersen 2001). This process is primarily facilitated by uncoupling protein 1 (UCP1) which activity is essential to dissociate cellular respiration from the generation of ATP, thereby promoting proton reentry into mitochondrial membrane, and ultimately dissipates energy as heat (Petrovic, Walden et al. 2010).

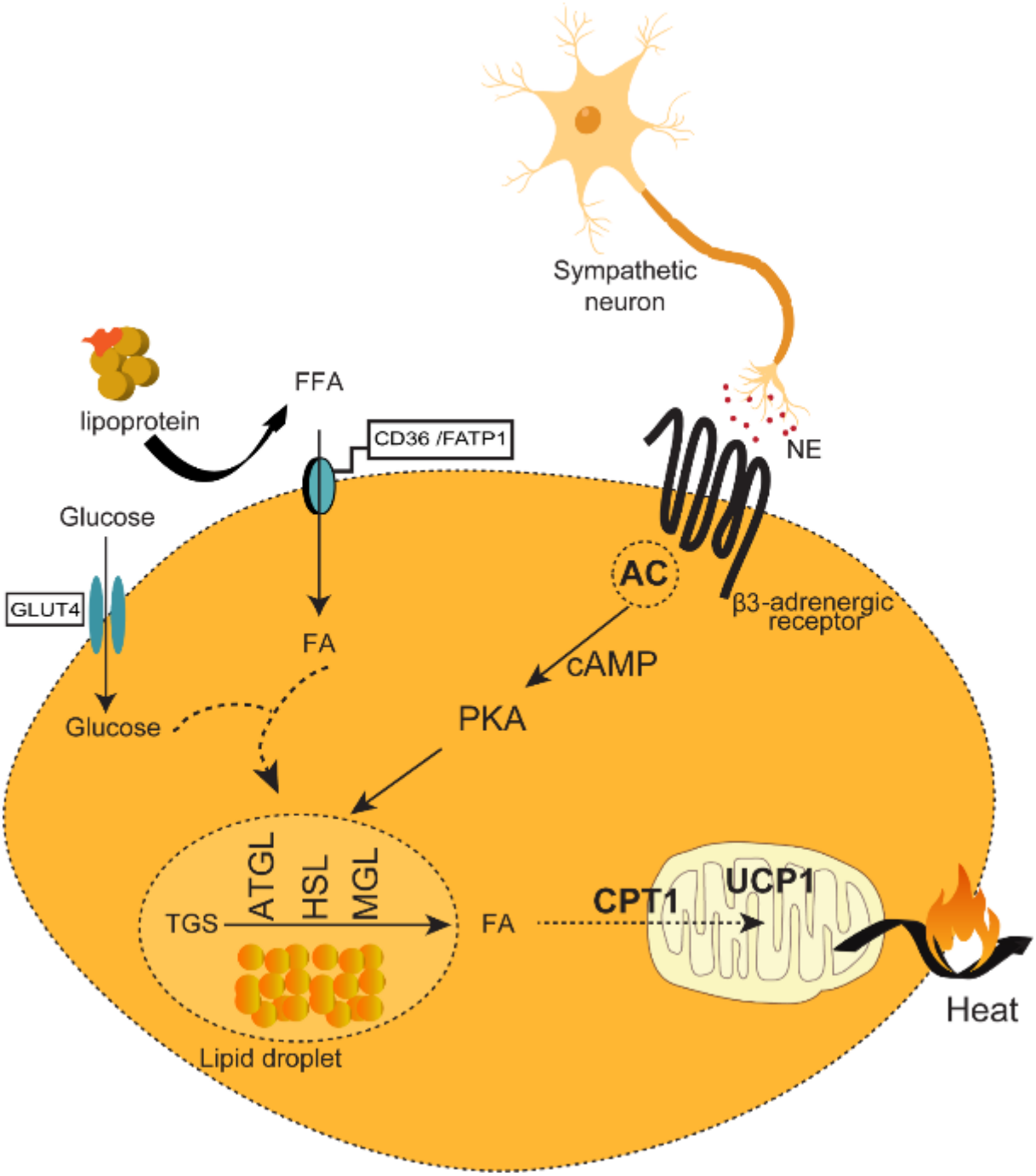

Figure 4. Activation of energy expenditure via the Sympathetic Nervous System.

Upon enhanced sympathetic activity, norepinephrine (NE) is released from nerve endings near brown/beige adipocytes. β3-adrenergic receptor stimulates cyclic AMP (cAMP) production by adenylyl cyclase (AC). cAMP activates protein kinase A (PKA), which drives lipolysis through phosphorylation of hormone-sensitive lipase (HSL) and induces transcription of genes involved in mitochondrial biosynthesis and thermogenesis. Fatty acids (FA) that are released from lipid droplets are directed towards the mitochondria via carnitine palmitoyltransferase I (CPT1) to be combusted or may allosterically activate uncoupling protein 1 (UCP1). Intracellular lipid stores need to be replenished by uptake of glucose and triglyceride (TG) derived FA from the circulation. (adopted and modified from (Kooijman, van den Heuvel et al. 2015)).

4 MOLECULAR EVENTS IN LIPOLYSIS.

4.1 The Fat machinery

Most of the body's storage pool of lipids is located in adipocytes as lipid droplets (LDs). These cytosolic lipid droplets are composed of a TGs core that is surrounded by a monolayer of phospholipids and lipid droplet-associated proteins, including structural proteins and enzyme co-activators. As mentioned before, the release of these fat stores occurs during the induction of lipolysis(Murphy, Martin et al. 2009). Upon its activation, the assembly of lipolytic enzymes takes place at the lipid droplet outer surface, where adipose triglyceride lipase (ATGL), hormone-sensitive lipase (HSL) and monoglyceride lipase (MGL) are the three known lipases responsible for the sequential hydrolysis of TGs into diacylglycerol, monoacylglycerol, and glycerol, liberating one molecule of fatty acids at each step respectively. The major positive regulators of human lipolysis are catecholamines and their activity in adipocytes is acutely regulated intracellularly by protein kinase A (PKA)(Figure 5) (Zechner, Kienesberger et al. 2009).

4.2 Catecholamines

The sympathetic nervous system plays an important role in the regulation of adipocyte metabolism and also affects their differentiation and proliferation(Zhu, He et al. 2003, Bowers, Festuccia et al. 2004). The stress hormones adrenaline and noradrenaline, also known as norepinephrine and epinephrine, are the primary mediators for adrenergic signaling in adipose tissue. Both hormones are able to stimulate and inhibit lipolysis depending on their relative affinity for different adrenergic receptors (Lafontan and Langin 2009). Catecholamines, secreted locally from innervated neurons, promote lipolysis by acting through β-adrenoceptor subtypes 1–3, while antilipolytic signals are transmitted by the a2-AR(Robidoux, Martin et al. 2004). Adrenergic receptors are all members of the G-protein coupled receptors (GPCRs) large family that are integral membrane proteins of the plasma membrane. βARs are expressed in white and brown adipocytes in all three subtypes. However, the relative proportions of these subtypes vary between fat species, fat depots, and metabolic status (Lafontan and Berlan 1993). The activation of the receptors causes the G-proteins to interact with adenylyl cyclase which converts ATP to cAMP, resulting in an increase in intracellular cAMP levels. Elevated cAMP concentrations activate protein kinase

A (PKA) which in turn phosphorylate multiple target proteins at specific serine residues to induce lipolysis(Taskén and Aandahl 2004).

4.3 Adipose triglyceride lipase

The identification of ATGL as a major triglyceride lipase came from three independent laboratories in 2004 (Figure 5) (Zimmermann, Strauss et al. 2004). *Atgl* gene (officially annotated as PNPLA2) encodes a 504-amino acid protein with a molecular weight of 55 kilodaltons (in humans and mice) and belongs to the family patatin domain-containing proteins including nine human and eight murine members. ATGL exhibits a high substrate affinity for TGs, a very weak activity against diacylglycerol, and almost no activity against cholesterol or retinyl ester bonds; thus it is considered the rate-limiting enzyme in the lipolytic cascade(Schweiger, Schreiber et al. 2006). At least two serine residues in ATGL can be phosphorylated (S406 and S430 in the murine enzyme) (Bartz, Zehmer et al. 2007). However, ATGL phosphorylation is PKA-independent(Zimmermann, Strauss et al. 2004), suggesting the role of another kinase may regulate its activity.

4.4 Comparative gene identification 58

Comparative gene identification 58 (CGI-58) is a co-activator of ATGL for its full TG hydrolase activity. The gene is now officially named α/β hydrolase domain-containing protein-5 (ABHD5), due to the existence of an α/β hydrolase domain frequently found in esterases, thioesterases, and lipases. CGI-58 binds to the lipid droplet associated protein 1 also known as (PLIN1). Under basal conditions, ATGL activity remains low. However, the phosphorylation of both PLIN1 and CGI-58 by PKA leads to a dissociation of these two proteins, facilitating ATGL co-activation (Sahu-Osen, Montero-Moran et al. 2015).on the other hand, The G0/G1 switch gene 2 (G0S2) protein binds to the C-terminal lipid-binding domain of ATGL, inhibiting ATGL triglyceride hydrolase activity and preventing localization to the lipid droplet (Figure 5) (Schweiger, Paar et al. 2012).

4.5 Hormone-sensitive lipase

HSL was initially characterized as the critical lipase essential for the hydrolysis of TAGs in adipose tissue. It exhibits both triglyceride and diglyceride hydrolase activities, yet the relative hydrolase activity is 11-fold higher against diglyceride than triglyceride in vitro(Fredrikson, Strålfors et al. 1981). *Hsl* essentially mirrors the *Atgl* expression profile,

showing the highest mRNA and protein expression levels in AT depots(WAT and BAT) while low expression levels are detected in other metabolic active tissues including muscles, steroidogenic tissues and pancreatic islets(Holm, Østerlund et al. 2000). Functional studies have described in HSL an NH2-terminal lipid-binding region, the α/β hydrolase fold domain with a catalytic triad, and the regulatory module holding all known phosphorylation sites critical for regulation of enzyme activity(Holm 2003) Moreover, adrenergic stimulation regulates HSL through PKA-catalyzed phosphorylation (Strålfors and Belfrage 1983). HSL has five identified potential phosphorylation sites, of which S660 and S663 seem to be predominantly important for hydrolytic activity (Figure 5) (Anthonsen, Rönnstrand et al. 1998).

4.6 The lipid storage lipid droplet protein, the perilipin 1

In pre-adipocytes or differentiating fibroblasts, small lipid droplets are found coated with ADRP (adipocyte differentiation-related protein). Once these cells undergo differentiation into mature adipocytes, these lipid droplets start to grow and accumulate more fat to a point that may comprise around 95% of the total adipocyte cell volume(Listenberger, Ostermeyer-Fay et al. 2007). However, during differentiation perilipin 1 gene (PLIN1) expression ensues and PLIN1 protein are massively elevated, and completely replacing ADRP from the droplet surface. PLIN1 is the most abundant member of the PERILIPIN (PLIN) family, which all been characterized as lipid droplet associated proteins. PLIN1 is found predominantly surrounding the outer surface of a lipid droplet in adipocytes, It plays a dual role in adipocyte lipid mobilization as it acts as a barrier in basal lipolysis but also promotes stimulated lipolysis (Martinez-Botas, Anderson et al. 2000). Lipolysis is triggered by β-adrenergic signaling via protein kinase A (PKA)-mediated phosphorylation of PLIN1(Tansey, Huml et al. 2003). phosphorylated PLIN1 releases the ATGL activator CGI-58 and provides a docking site by which phosphorylated HSL gains access to substrates at the surface of LDs(Lass, Zimmermann et al. 2006). Thereby, PKA dependent phosphorylation sites on PLIN1is an essential step in β-adrenergic induced lipolysis (Figure 5).

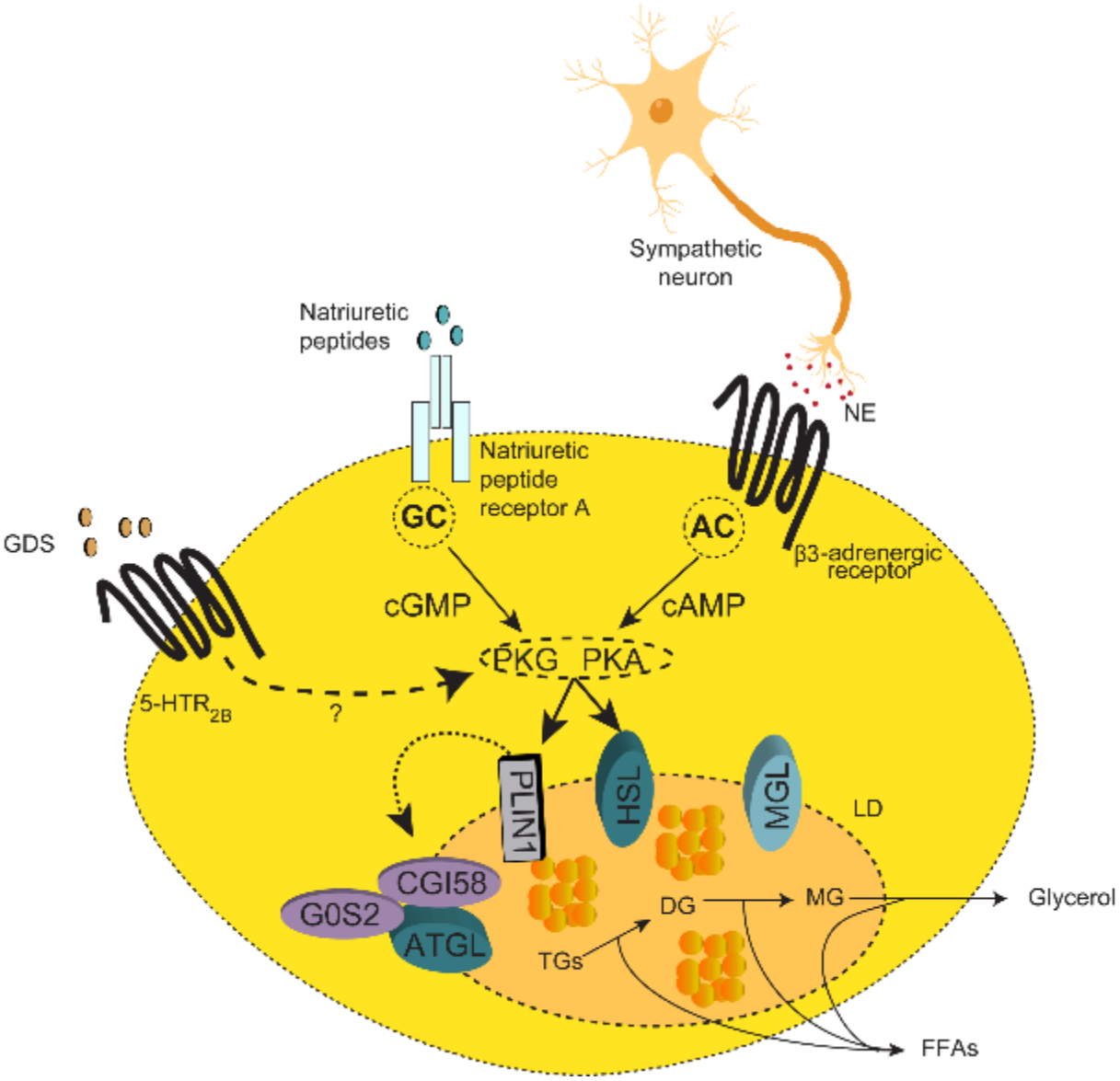

Figure 5. Overview of the lipolytic pathways in lipid droplets.

The lipolytic cascade is mainly activated through β-adrenergic signaling in a PKA-dependent manner. PKA phosphorylates HSL and PLIN-1 resulting in the recruitment of the lipolytic machinery (ATGL, and MGL) and thereby the sequential hydrolysis of TG into FA and glycerol. Similarly, natriuretic peptides activate lipolysis via PKG. Additionally, gut-derived serotonin (GDS) binds to 5-Hydroxytryptamine receptor 2B (5-HTR2B) to conduct its signaling cascade via PKG to promote lipolysis adapted and modified from (Arner and Langin 2014).

4.7 Insulin-mediated deactivation of lipolysis

Physiologically, there is no doubt that insulin is the most important hormonal inhibitor of lipolysis. As observed in the fed state, the rise of circulating insulin levels is enough to highly suppress adipocyte lipolysis. The mechanism by which insulin was shown to inhibits

lipolysis begins from the binding of insulin to its receptor on target cells. Insulin binding results in autophosphorylation and activation of the receptor which leads to the activation of PI-3 kinase which in turn lowers cyclic AMP concentrations, leading to a decrease in the activity of HSL (Figure 3) (Choi, Tucker et al. 2010). Furthermore, an increasing line of evidence suggesting an inhibitory role of insulin on the transcription of *Atgl*. A leading study showed that insulin-mediated activity of mTORC1 (also known as mammalian target of rapamycin complex 1) induces the expression of the transcription factor Early Growth Response 1 (Egr1), which in turn exerts a negative transcriptional effect upon its binging to the *Atgl* promoter (Chakrabarti, Kim et al. 2013). Similarly, insulin signaling was also shown to inhibit the nuclear translocation of the forkhead transcription factor O1 (FOXO1), thereby reducing the ability of FOXO1 to induce the transcription of *Atgl* upon its bind to *Atgl* promoter (Chakrabarti and Kandror 2009).

5 MAPK6

5.1 Mitogen-activated protein kinases

Mitogen-activated protein kinases (MAPKs) are a family of serine/threonine/tyrosine kinases are known to be committed to transducing environmental stimuli into the conduction of various cellular responses, including mitogenic factors, cellular stress, cytokines and cell adherence etc. (Cargnello and Roux 2011). External stimuli trigger multiple cellular responses by activating various signaling cascades that can coordinate the activation of defined intra-cellular programs. The cellular responses to these external physical and chemical stimuli are fundamental cellular processes such as cell growth, proliferation, differentiation, migration and apoptosis. MAPKs are among the most ancient signal transduction pathways and are widely used throughout evolution. Their expression was first characterized in an array of unicellular eukaryotes and been encountered in higher multicellular organisms form fungi, plants and animals. The importance of the MAPK signaling pathway lead to its extensive study until date. MAPK signaling consists of a relay of events mostly triggered by phosphorylation where a MAPK is activated by MAPK kinases (MAPKK), which in turn is activated by MAPK kinase kinases (MAPKKK).

These protein kinases at each level can be referred to by the generic names as MAPK, MAPKK (or MAP2K), and MAPKKK (or MAP3K). In humans, there are at least 11 members of the MAPK superfamily (Cargnello and Roux 2011) that are categorized into six groups based on their sequence homology. There are at least six different groups of MAPK that have been identified in humans cells: the extracellular signal-regulated protein kinases (ERK1, ERK2); c-Jun N-terminal kinases (JNK1, JNK2, JNK3) p38s (p38a, p38b, p38g, p38d); ERK5; ERK3s (ERK3, p97 MAPK, MAPK4); ERK7s (ERK7, ERK8). Each group of MAPK works through a separate signal transduction pathway in response to different external stimuli. MAPKs can be categorized into two subfamilies based on their structure, phospho-acceptor site and the activating signals: typical MAPKs and atypical MAPKs. Typical MAPK signaling is a three-tiered network consisting of protein kinases activated in response to various signals including growth factors. Their activation loop consists of a characteristic T-X-Y (Threonine-Any amino acid- Tyrosine) motif (New and Han 1998). These MAPKs are phosphorylated at both (T and Y) residues on the activation loop, hence are activated by dual-specificity protein kinases. Some of the conventional MAPKs are ERK1, ERK2, ERK5, JNK 1, JNK2, JNK3 and p38 MAPK. ERK1 and ERK2 are known to be activated by mitogens such as growth factor

signals, whereas p38 MAPKs and JNK are primarily activated by stress signals and proinflammatory cytokines. While the typical MPAK signaling pathways have been well-studied, activation signals and upstream regulators of atypical MAPKs are poorly understood. Atypical MAPKs have an activation loop where tyrosine in classical MAPKs is replaced with glycine or glutamic acid. ERK3, ERK4, ERK-7 belong to this category.

5.2 ERK3 regulation

ERK3 (Mapk6) was identified in the early 1990s by homology cloning using Erk1 derived probs. The ERK3 proteins share nearly 50% homology to ERK1/2 within their kinase domain but have distinct structural features that make them atypical compare to the other MAPKs. Moreover, ERK3 has a unique C-terminal extension that is absent in classical MAP kinases(Zhu, Zhao et al. 1994). Structurally, ERK3 is most closely related to the MAP kinase Erk4 (Mapk4). The two proteins share around 73% amino acid analogy in the kinase domain. They both possess a single phosho-acceptor site in the S-E-G (Ser-Glu-Gly) motif instead of the classical T-X-Y (Thr-X-Tyr) motif found in the typical MAPKs activation loop (Al-Mahdi 2015). Taken together, these similarities in structure and organization between ERK3 and ERK4 genes suggesting a burst of gene duplication arose from a common ancestor (Coulombe and Meloche 2007)(Figure 5). notably, ERK3 and ERK4 genes are the only MAP kinase genes whose expression is restricted to vertebrates, implying a role in more specialized vertebrate-specific physiological processes. The sequencing of the Erk3 gene revealed a coding sequence for 721 amino acids but shows a molecular mass of 100 kDa possibly due to posttranslational modifications. The physiological function of Erk3 remains to be elucidated. Developmental studies indicated the temporal increase of ERK3 expression during embryonic development, increasing at the time of early organogenesis, while gradually declining toward birth (Klinger, Turgeon et al. 2009). In adult animals, *Erk3* mRNA is found to be ubiquitously expressed in most tissues, with the highest levels found in the testis, central nervous system and skeletal muscle. In vitro studies have shown that Erk3 expression is upregulated during terminal differentiation of model cell lines into neurons or myotubes (Hoeflich, Eby et al. 2006, Klinger, Turgeon et al. 2009, Brand, Schumacher et al. 2012)on the protein level, ERK3 is highly unstable protein, with rapid turnover mediated by ubiquitination and proteasomal degradation (Coulombe, Rodier et al. 2004). These findings suggest a tight intracellular regulatory mechanism for always keeping a level of availability of ERK3 protein, which gets stabilized when its activity is needed. Indeed, studies had shown a time-dependent stabilization of ERK3 protein during in-vitro differentiation of PC12 and C2C12 cells into the neuronal and muscle lineage,

respectively(Coulombe, Rodier et al. 2003). Moreover, ERk3 protein was shown to shuttle around the cell between the nucleus, cytoplasm and the plasma membrane (Al-Mahdi, Babteen et al. 2015). ERK3 nuclear export is regulated by a CRM1 (chromosome region maintenance 1). Moreover, the same study showed that the nuclear export of ERK3 increases as cells progress through the S phase, while during the early phases of the subsequent cell cycle ERK3 localized back to the Golgi (Julien, Coulombe et al. 2003). Besides, another study reported that the proteolytic cleavage of ERK3 is required for its release from the Golgi, given that the nuclear form of the protein was carboxy-terminally truncated (Bind, Kleyner et al. 2004). This evidence supports the existence of a peculiar mechanism of ERK3 activation and suggests that ERK3 localization is strictly connected to its regulatory function of the cell cycle. So far, only limited number of studies had investigated the kinetic activity of Erk3. Importantly, Ek3 was identified as a for class I p21 activated kinases (Pak) that binds at Ser189, within the Erk3 activation loop, thereby regulating its subcellular (De La Mota-Peynado, Chernoff et al. 2011). Another substrate that has been described for ERK3 is MK5 also referred to as PRAK. ERK3 interaction motif termed" FRIEDE" is shown to be essential for binding to the C-terminal region of MK5. This FRIEDE motif is located within the L16 extension C-terminal to the common docking domain in ERK3 (Figure 6). Hence, MK5 presents a physiological substrate on ERK3, where its binding via this region of the induces a significant conformational alternation which promotes its activation (Åberg, Torgersen et al. 2009).

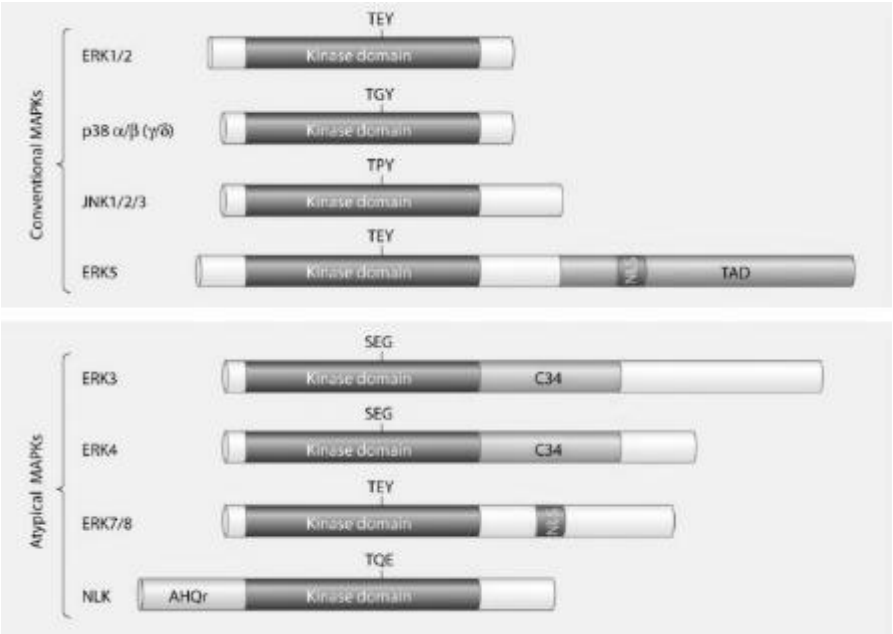

Figure 6. Structure of conventional and atypical MAP kinases.

Conventional MAP kinases possess a conserved Thr-X-Tyr motif in the activation loop of their kinase domain, whereas this motif is absent in atypical MAP kinases, apart from Erk7. All MAP kinases comprise the Ser/Thr kinase domain surrounded by N- and C-terminal regions of varying lengths. Additionally, other domains exist in some MAP kinases: a transactivation domain (TAD), a nuclear localization sequence (NLS), a conserved extended C-terminal region (C34) and an Ala-/His-/Glu- rich domain (AHQr) (Cargnello and Roux 2011).

5.3 Cofactor MK5

MK5, belong to a family that harbors 11 MAPK-activated protein kinases (MAPKAPK), which have been described in mammals. MK5 is a 54 kD Ser/Thr kinase, among all the other MAPKAPKs that are exclusively phosphorylated by conventional MAPKs, MK5 is the only MAPKAPK that is a substrate for both conventional and atypical MAPKs. The *Mk5* gene, in its sequence and even its protein folding, is conserved throughout the vertebrates while absent in invertebrates (Kostenko, Dumitriu et al. 2012). In mammalian cells, MK5 participates in several biological functions, it stimulates the transcriptional activity of p53 which involved in tumor suppression. MK5 was also shown to be involved in cellular proliferation and differentiation, anxiety-related behavior and the rearrangements of the F- actin cytoskeleton (Chen, Hitomi et al. 2000, Gerits, Van Belle et al. 2007, Sun, Yoshizuka et al. 2007, Kostenko, Johannessen et al. 2009). Moreover, it was shown that MK5 phosphorylates FOXO1 at serine 215, thereby placing a negative feedback for Ras proliferative signaling and promoting cellular senescence (Chen, Hitomi et al. 2000, Chow, Timblin et al. 2013). MK5 is ubiquitously expressed, with the highest expression observed in the brain, heart and platelets (Gerits, Shiryaev et al. 2009). A rising number of studies had defined the specific role of MK5 in the studied o Structurally, MK5 has both nuclear localization signal (NLS) and nuclear export signal (NES), thus allowing the protein to shuttle between the nucleus and the cytoplasm(Engel, Schultz et al. 1995, Zu, Ai et al. 1995). Unlike the other MAPKAPKs that have their NLS and NES are located on distinct C-terminal regions, in MK5, the two signals overlap giving it a unique characteristic for its binding with ERK3 and ERK4. MK5 also contains a p38MAPK docking motif, which overlaps with the NLS (Kostenko, Dumitriu et al. 2011). Furthermore, MK5 was shown to interact with ERK3, this interaction occurs in a defined motif termed" FRIEDE" which has been shown to be essential for binding to the C-terminal region of MK5 (Åberg, Torgersen et al. 2009).

5.4 Regulatory role of PKA

Protein kinase A (PKA) is a family of enzymes whose activity is dependent on cellular levels of cyclic AMP (cAMP). PKA is also known as cAMP-dependent protein kinase PKA which is found to be ubiquitously expressed in all mammalian cells. Due to this fact, a large number of studies aimed to investigate deeply its physiological and biochemical role, therefore making it is one of the best characterized members of the large protein kinase superfamily. PKA is a heterotetrameric enzyme comprising two regulatory and two catalytic subunits. The binding of cAMP to PKA regulatory subunits unleashes the active catalytic subunits thus allowing them to phosphorylate a number of protein substrates, both nuclear and cytosolic. A critical review in the PKA literature in the context of its role as a regulator of atypical MAPKs shows clear hints for the role of PKA in regulating the ERK3/MK5 pathway. On one hand, PKA phosphorylates UBE3A at T485 and inhibits its activity(Jason, Berrios et al. 2015). Ube3a also known as E6AP is an E3 ubiquitin ligase shown target ERK3 and its complex and direct them for proteasomal degradation(Coulombe, Rodier et al. 2004). On the other hand, β-adrenergic stimulation rapidly phosphorylates a ubiquitin-specific protease 20 (USP20) in a PKA dependent manner (Kommaddi, Jean-Charles et al. 2015). USP20 belongs to deubiquitinating enzymes (DUBs) family, USP20 upon its phosphorylations, deubiquitinates the ERK3 protein complex resulting in the stabilization of the kinase complex (Mathien, Déléris et al. 2017). Furthermore, upon its activation, PKA induces nucleocytoplasmic redistribution of MK5 at serine 115. In this regard, the overexpression of phosphor-deficient mutated of MK5 at S115A redistribute MK5 to the cytoplasm, while MK5 S115D overexpression leads to its nuclear distribution (Kostenko, Shiryaev et al. 2011).

6 AIMS OF THE STUDY

Energy metabolism is a field of biology that has received much attention in the few decades. The dramatic increase in the incidences of obesity and type 2 diabetes worldwide and the urgent need for new pharmacological therapies have greatly stimulated the research in this area. This present study aims to better understand the signaling cascades involved in the hormonal regulation of metabolism in the adipose tissue. We aim through our approach, using an unbiased screening method, to identify the kinases within the signaling cascades which are implicated in the response of adipocytes to lipolytic signals evoked by the major hormones such as catecholamines and gut-derived serotonin. After the unraveling of a novel kinase, that has a high impact in the regulation of lipolysis in the adipocytes, we aim through the use of multiple molecular biology techniques to get further insights and detail the molecular events promoting the activation of this kinase and the following signaling pathway evoked by its activity. Furthermore, we aim through the generation of a specific mouse model, bearing the deletion of this kinase specifically in the adipose tissue, to the study the physiological impact of our candidate kinase on the adipose tissue metabolic functions and its relevance on the whole-body energy hemostasis. The planed experiment on these mice will be performed in mice fed standard diet most importantly in mice in which an obese and diabetic phenotype would be induced by a high-fat diet feeding. Untimely, after a careful investigation of the possible beneficial impact of the inhibition our candidate signaling pathway on the metabolic fitness of obese mice, we aim to proceed with our investigative efforts to characterize the possible favorable impact caused by the administration of a pharmacological inhibitor, targeting our candidate signaling pathway, on the metabolic profile of obese mice.

Overall, the proposed experimental strategy will allow us to identify new components of signaling machinery regulating the metabolism of adipose tissue at basal and pathophysiological conditions. It will also allow us to get further insights into the complex network of signaling molecules promoting the development of metabolic disorders such as obesity. Ultimately, we aim to test the impact of a potential targeted drug to combat obesity and its associated metabolic diseases.

RESULTS

6.1 Screening for kinases regulating lipolysis in adipocytes.

6.1.1 Optimization and validation of transfection protocol

To identify novel protein kinases, that regulate lipolysis upon beta-adrenergic and/or serotonin stimulation (Figure 7 A), we developed an interfering RNA (siRNA)-based screen for silencing genes in 3T3-L1-derived adipocytes. The method used required several optimization steps as compared to previously published protocols to ensure a higher transfection efficiency (Echeverri and Perrimon 2006, Kilroy, Burk et al. 2009). Moreover, to guarantee specific deletion efficiency we utilized a combination of four specific targeting sequences (smart pools) of siRNAs per target. Our developed method lowers the off-target effect of a specific sequence since the optimized RNA concentration of transfection was calculated as a combination of pooled sequences. Differentiated cells were transfected at a state of full differentiation into adipocytes (corresponding to day 10 after initiation of differentiation). Since at this stage these cells are in their non-dividing stage and containing a high amount of lipids in droplets. Furthermore, we optimized our protocol to transfect these adipocytes in suspension to further increase the transfection efficacy, we configured the optimal ratio of siRNA and transfection reagent and we pre-coated plates with Matrigel to ensure adipocytes attachment to the surface (Figure 7 B).

Next, we verified the specificity and the efficiency of our transfection method using a siRNA-mediated silencing of *Atgl*, a key enzyme mediating lipolysis in adipocytes. Western blot analysis of transfected cells showed an efficient depletion of ATGL protein in differentiated 3t3l1 cells (Figure 7C). Moreover, taking into our advantage ATGL function as the major lipase regulating lipolysis, we next conducted a lipolysis assay on differentiated adipocytes transfected with either non-targeting control sequences or with siRNA against *Atgl* (siAtgl). Two days post-transfection, cells were serum-starved for 2 hours then stimulated as indicated below (Figure 7D, E). Interestingly, Cells stimulated with a combination of beta-adrenergic agonist; isoproterenol and agonist of the receptor of serotonin, Htr2b, (BW-723C86) showed the highest induction of lipolysis as shown by the release of FFA (Figure 7D,) and Glycerol (Figure 7E) into the media. As expected, in the cells depleted from *Atgl*, lipolysis induced by either Htr2b agonist, isoproterenol alone or both in combination, was completely abolished. These results further confirm the efficiency of the used transfection protocol and highlight that

the combination of both Htr2b agonist and beta-adrenergic agonists fully activates lipolysis in differentiated adipocytes.

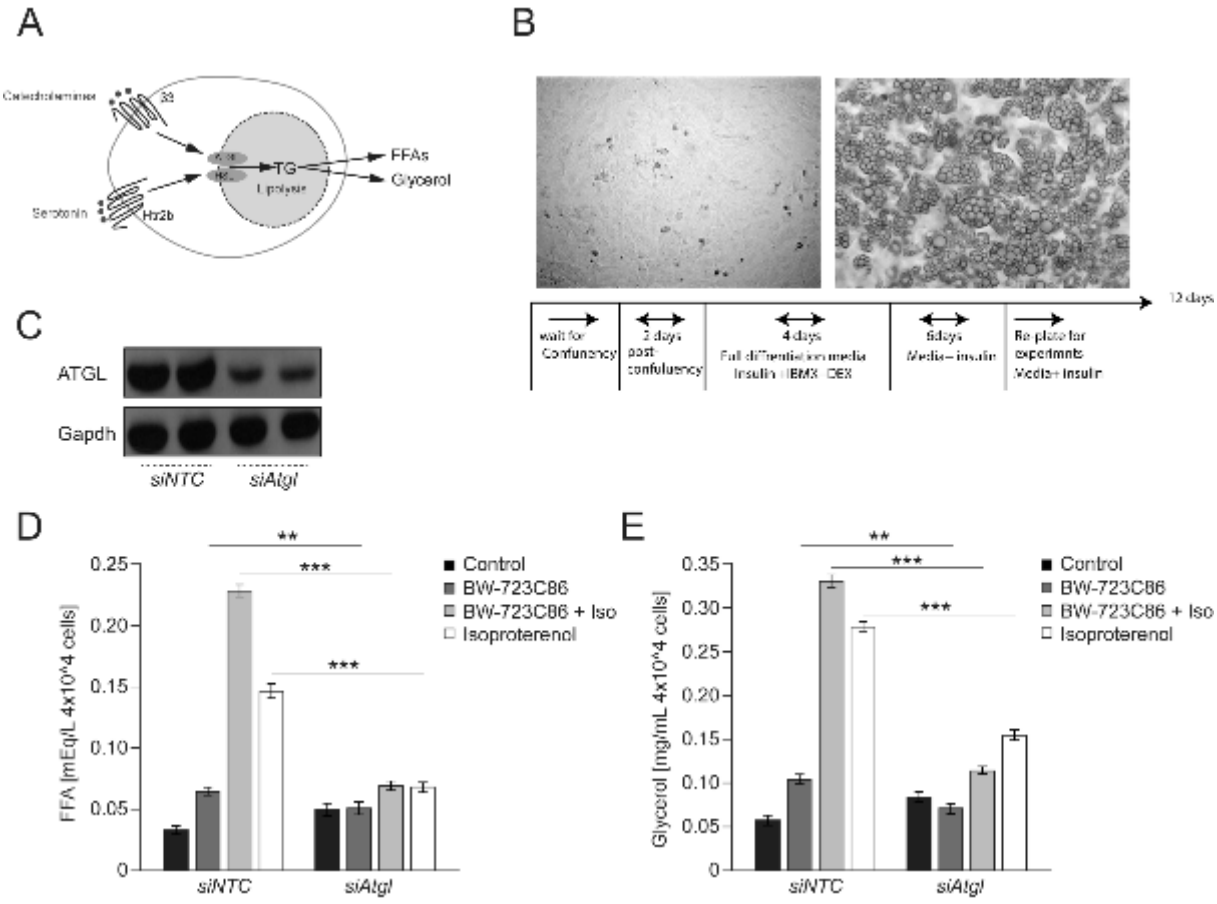

Figure 7. Study model for identification of novel kinases regulating lipolysis.

(A) Schematic representation of the study model. (B) Schematic representation of the differentiation protocol (lower panel) and a representative photo of the undifferentiated (upper-left panel) and differentiated into adipocytes (upper-right panel) 3T3L1 cells (C) Western blot (WB) analysis of *Atgl* and GAPDH abundance in extracts isolated from differentiated 3T3L1 cells transfected with siRNA against *Atgl.* Free fatty acids (FFAs) (D) and glycerol (d) output from 3T3L1 adipocytes transfected and stimulated as indicated. n=3 for each experiment, for graphs - data presented as average +/- SEM, ** P ≤0.01, *** P ≤0.001.

6.1.2 Screening revealed novel kinases regulating lipolysis

Our first aim was to achieve an unbiased identification of novel kinases regulating lipolysis, We designed a high throughput screening strategy to assess the impact of kinase-mediated signaling on the rate of lipolysis evoked by the combination of both β-adrenergic agonist, isoproterenol (Iso), and the HTR2B agonist, BW-723C86, in differentiated adipocyte-like cells 3T3L1 (Figure 8). During the primary screening, we utilized a randomly allocated kinase library of 715 predicted kinases in the mouse genome with the addition of both positive and negative

controls. FFA release was measured separately from all experimental conditions then each was normalized to the total DNA content present in the same experimental well. Fold change was then calculated from the average value compared to the respective control condition. Data collected from siRNA screens were further normalized relative to the normal standard distribution to define the Z-score (also called Z-value) for each point (Birmingham, Selfors et al. 2009). Then, hit-samples were ranked according to the Z-score which typically belongs to less than -2 or more than +2, then we applied P-value as additive criteria to select the hits. Results from the primary screening showed that silencing of 48 kinases resulted in decreased lipolysis (FFAs output), whereas depletion of 69 kinases enhanced it in 3T3L1-derived adipocytes. Finally, selected hits in the primary screen were further validated in a secondary screen using a different set of siRNA sequences in order to confirm the phenotype observed in the primary screen.

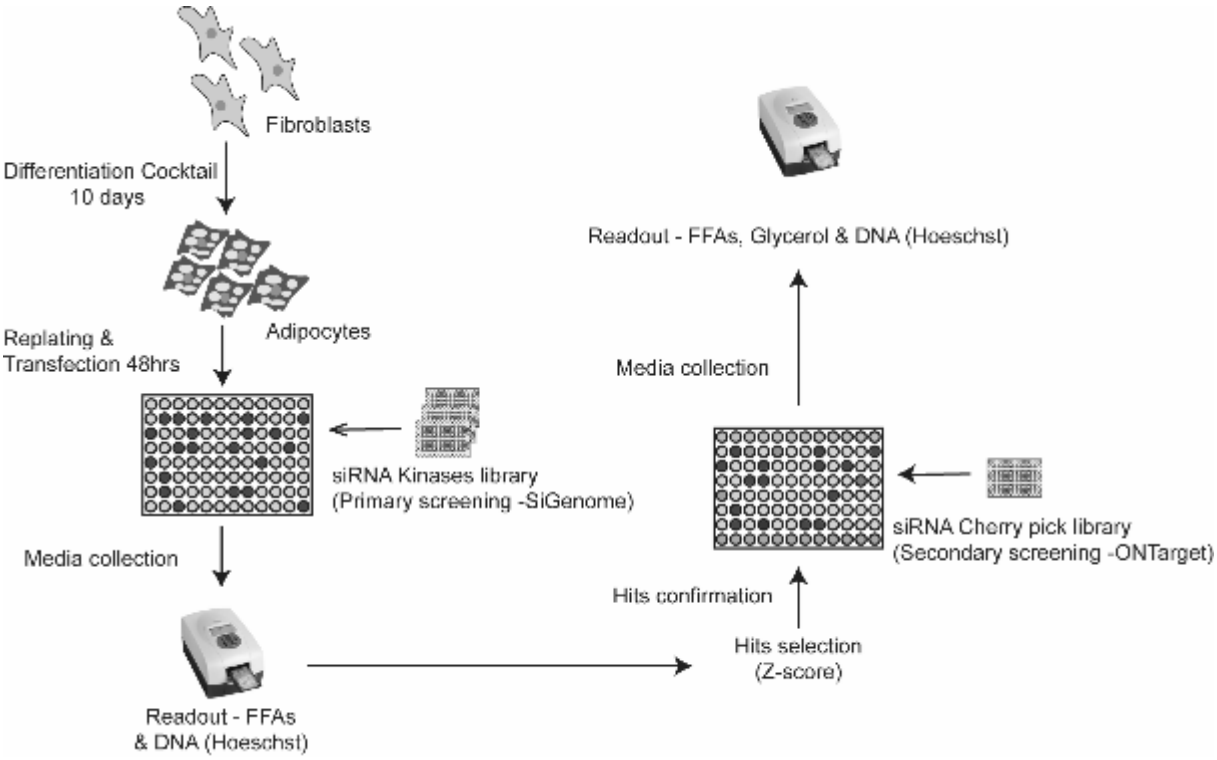

Figure 8. Design of the screen for kinases regulating lipolysis.

Schematic representation of the screening strategy.

6.1.3 Validation of ERK3, a central regulator of lipolysis

For a secondary screen, we have selected 72 of the most up and down-regulated hits. We have utilized pools of different siRNA sequences to confirm our date. In a secondary screen, we

confirmed that silencing of 28 kinases reduced glycerol and FFA release while silencing of 23 enhanced it (Fig. 3a and b). Of note, Prkar1a, Prkar2b, Ndrg1, Raf1, Lats2, Peg3, and Trib3, which appeared on our screen were previously implicated in the regulation of lipolysis and different aspects of adipocytes function (Curley, Pinnock et al. 2005, Qi, Heredia et al. 2006, Kalderon, Azazmeh et al. 2012, Wang, Tao et al. 2013, Cai, El-Merahbi et al. 2017, Torres-Quesada, Mayrhofer et al. 2017). These results further confirm the screening efficacy. Importantly, we were interested to follow up on the highest hit that our screening had revealed. The silencing of Extracellular regulated kinase 3 (ERK3) inhibited lipolysis to the largest extent in both screens (Figure 9 A, B).

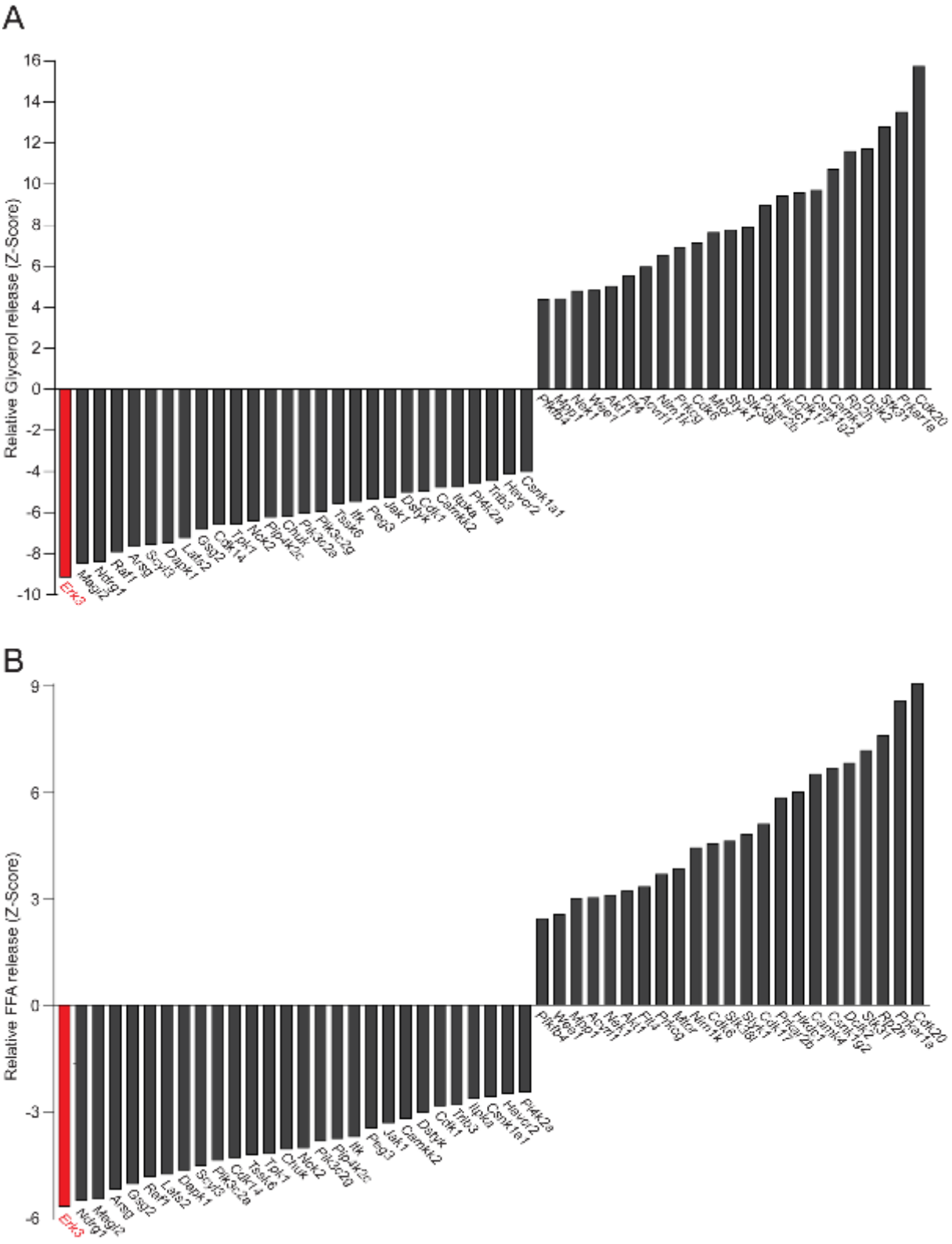

Figure 9. ERK3 is required for the induction of lipolysis.

(A) Relative rate of glycerol release (B) FFA release (Z-score), (n=4) from 3T3L1 cells transfected with indicated siRNA pools in response to the stimulation of Htr2b and beta-adrenergic agonists.

We were able to further validate these results by transfecting adipocytes in a larger setting. Indeed, siRNA sequences targeting *Erk3* were highly efficient in depleting *Erk3* in differentiated cells (Figure 10 A). Most importantly, however, the siRNA mediated depletion was highly specific, as the expression level of *Erk1* and *Erk2*, proteins sharing high homology with *Erk3*, was not altered (Figure 10 B). Consistently with our previous findings, the silencing of *Erk3* in adipocytes derived from 3T3L1 cells resulted in a strong inhibition of induced lipolysis evoked by β-adrenergic stimulation as well as by β- and HTR2B-agonists. These results were compared to a positive control from which differentiated cells were depleted from *Atgl* and exposed to the same stimulation. Of note, while induced lipolysis was largely attenuated, basal lipolysis seems to be unaffected (Figure 10 C, D). Moreover, aiming to avoid any false-positive results originated by an acquired mutation of a cell line. We harvested mesenchymal stem cells together with other adipocyte precursor cells found in the stromal vascular fraction (SVF) of subcutaneous white adipose tissue. After culturing these cells, we directed their differentiation toward an adipocyte like cells using the same differentiation protocol as mentioned above. After achieving the differentiation of these primary cells into mature adipocytes we transfected these cells following the same transfection protocol as performed in the 3T3L1 cell line. Interestingly, the silencing of *Erk3* in primary derived adipocytes resulted in a similar reduction of agonists-induced lipolysis as showed before in the cell line. FFA and Glycerol levels (Figure 10 E, F) were highly reduced upon stimulation when compared to cells transfected with a non-targeting siRNA.

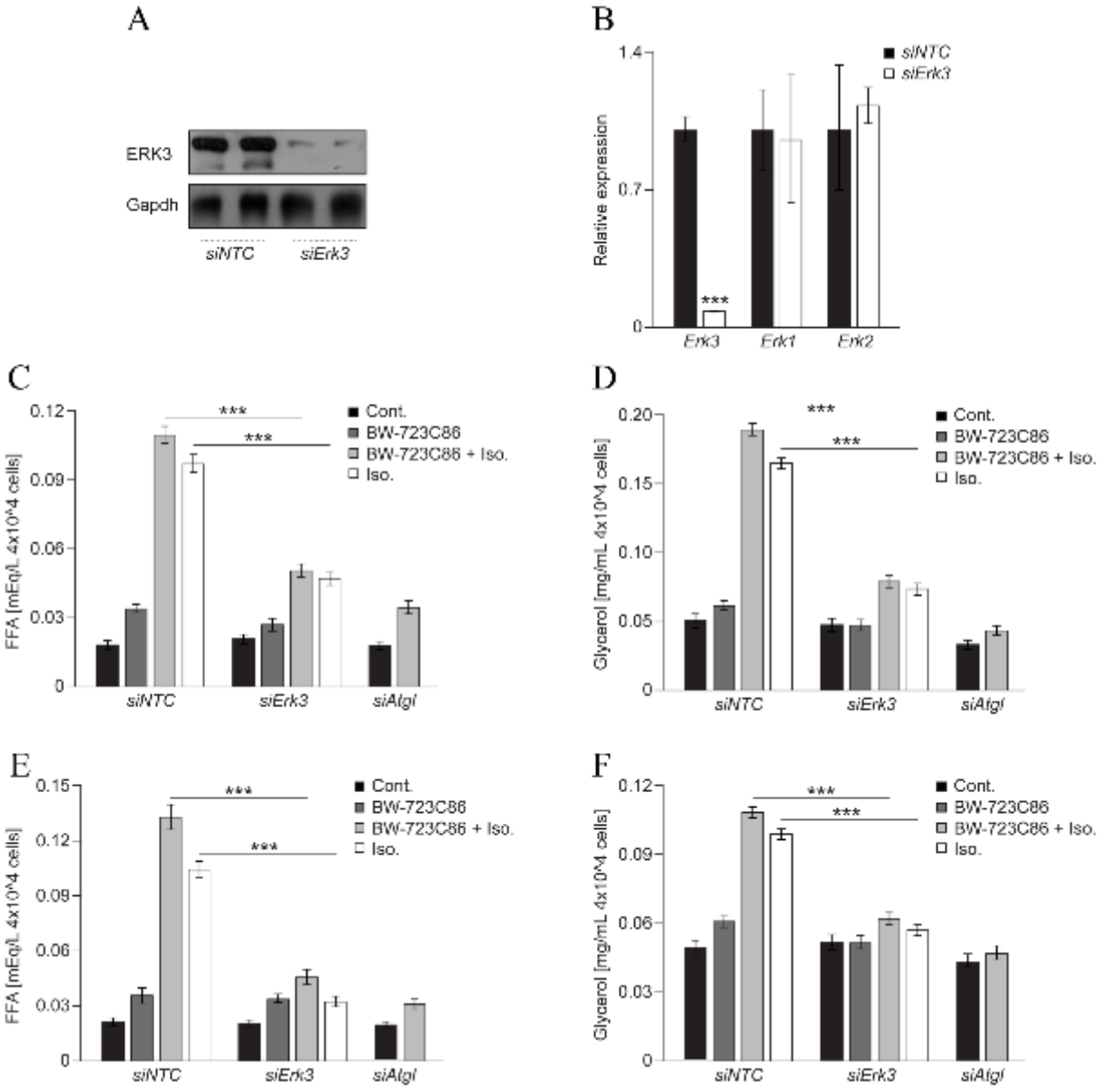

Figure 10. siErk3 selectively inhibits ERK3 in promoting lipolysis.

(A) WB for ERK3 on extracts from 3T3L1 adipocytes transfected with specific siRNAs (n=2). (B) Relative expression of indicated genes in adipocytes transfected with *Erk3*-specific or control NTC siRNA (n=3). (C) FFAs and (D) Glycerol output from 3T3L1 adipocytes transfected with specified siRNAs and stimulated as indicated (n=3). (E) FFA and (D) glycerol release from stromal-vascular cell (SVC)-derived adipocytes transfected with specific siRNAs and stimulated by the β-agonist Isoproterenol (Iso.) and/or the HTR2b agonist BW-723C86 as indicated (n=3). For graphs - data presented average +/- SEM, *** $P \leq 0.001$.

6.1.4 The prolonged deletion of *Erk3* reduced lipid accumulation in adipocytes.

To study the effect of prolonged deletion of Erk3 gene, throughout pre-adipocytes differentiation, on major adipocyte functions including TG accumulation and induced hydrolysis. We generated stable cell lines by plasmid-mediated overexpression of a transient

shRNA sequence targeting *Erk3* mRNAs. Western blot (Figure 11A) followed by QPCRs (Figure 11B) analysis showed an efficient shRNA mediated *Erk3* knockdown (sh*Erk3*) in generated 3t3 L1 cells. In line with our siRNA results, knockdown of *Erk3* attenuated induced lipolysis to a similar rate as observed before. These conclusions were drawn as a result of the analysis of FFA and Glycerol release to the media upon stimulation with beta-adrenergic agonists following the same experimental conditions as performed previously (Figure 11C, D).

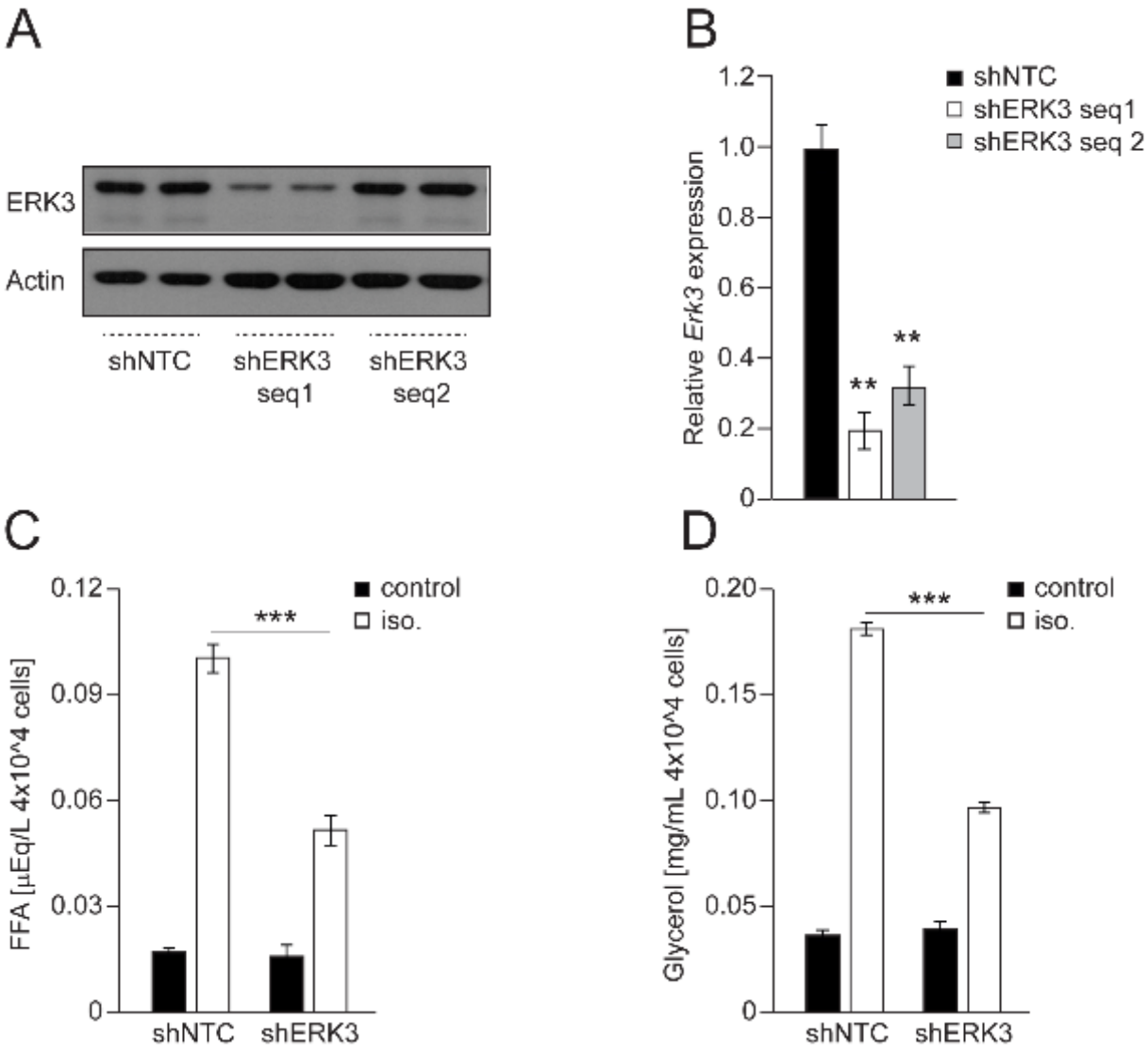

Figure 11. *ShErk3* blocks induced lipolysis.

(A, B) WB and relative expression analysis of ERK3 knockdown in 3T3L1 cells transfected with *Erk3* shRNA or non-targeting shRNA (n=2). (C) FFAs and (D) glycerol release from *shErk3* transfected 3T3L1 adipocytes and control cells (n=3). For graphs - data presented average +/- SEM, *** P ≤0.001.

Furthermore, using an AdipoRed assay in cells depleted of *Erk3*, we observed a significant decrease in the TG content, as reflected by a fluoresces staining of TGs, after 10 days of differentiation as compared to their corresponding control cells (shNTC) (Figure 12A). Moreover, Oil-Red-O staining also revealed less TG accumulation, as well as smaller lipid droplets within the cells (Figure 12 B). Taken together, results from both knockdown models, we could conclude that ERK3 protein plays an active role in adipocyte maturation and lipid accumulation. Most importantly, however, ERK3 is primarily responding to lipolytic stimuli in regulating the rate of lipolysis. Hence, further studies are mainly focusing on understating the detailed role of ERK3 in adipocytes.

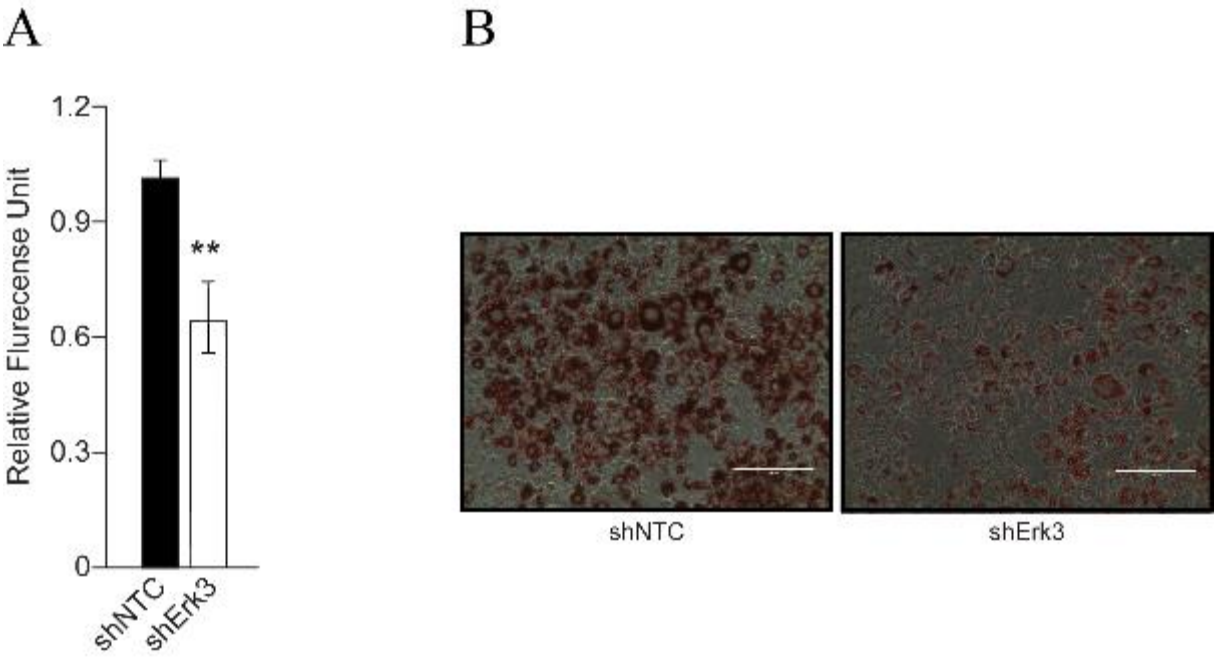

Figure 12. Long term depletion of Erk3 affected decrease TG deposition in adipocytes.

(A) Relative fluoresces of Adipored staining 3T3L1 cells transfected with *Erk3* shRNA or non-targeting shRNA. (B) light microscopy image of Oil-red-O stained 3T3L1 cells transfected with *Erk3* shRNA or non-targeting shRNA. For graphs - data presented average +/- SEM, ** P ≤0.01.

6.2 β-adrenergic activation of PKA leads to stabilization of ERK3

6.2.1 ERK3 is stabilized during adipocytes differentiation

Mitogen-activated protein (MAP) kinases are mainly stable enzymes that are regulated by phosphorylation and subcellular targeting. However previous reports showed that extracellular signal-regulated kinase 3 (ERK3), unlike other MAP kinases, ERK3 is an unstable protein that is constitutively subjected to rapid proteasome-mediated degradation in quiescent cells,

(Coulombe, Rodier et al. 2003, Coulombe, Rodier et al. 2004). The biological relevance for cells to promote the stability or the abundance of a certain protein is often reflected in its importance at a specific cellular state. Our results have shown that ERK3 proteins level are low in the undifferentiated 3t3l1 but upon differentiation towards adipocyte like cells, ERK3 protein levels highly increased over the course of time (Figure 13A). Interestingly the *Erk3* mRNA relative expression showed no significant change upon differentiation (Figure 13B). Indicating that cellular regulation of ERK3 in differentiating adipocytes occurs as a post-translational modification rather than a transcriptional control of its expression.

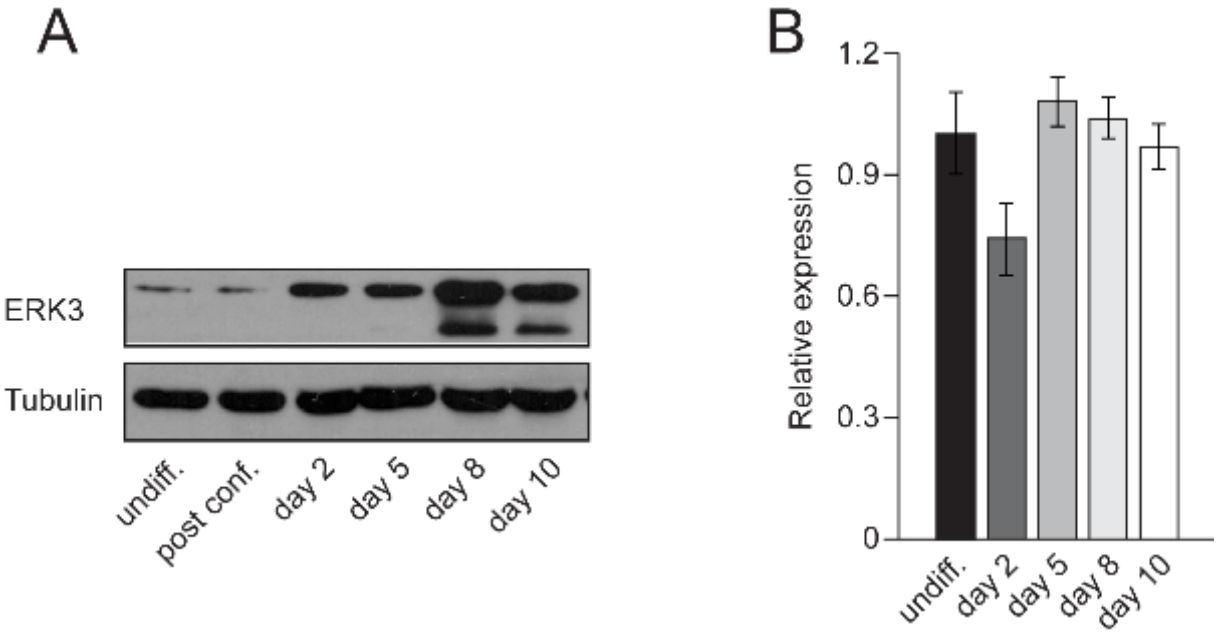

Figure 13. Post-transcriptional modification of ERK3 during adipocytes differentiation.

(A, B) WB and qPCR analysis of 3T3L1 cells during indicated time points. for graphs - data presented average +/- SEM.

6.2.2 Beta-adrenergic stimulation stabilizes ERK3.

Consistent with previous findings, we could confirm that the incubation of adipocytes with pharmacological proteasomal inhibitors, the peptide-aldehyde MG-132 or the *Streptomyces* metabolite lactacystin, lead to the stabilization of ERK3 protein in differentiated adipocytes (Figure 14A). Importantly, we found that the stimulation of adipocytes with β-adrenergic agonists (Iso) also lead to an increased ERK3 protein abundance (Figure 14A). The β-agonist and the proteasome inhibitor also stabilized the ectopically expressed Myc-

tagged ERK3 protein (Figure 14B). However, mRNA levels of *Erk3* were largely unaffected suggesting that the abundance of the protein is sole a post-translational modification (Figure 14C). Finally, blocking translation in adipocytes with cycloheximide resulted in a decreased abundance of ERK3 protein over time, which was highly rescued upon co-treatment with Iso (Figure 148D). This demonstrates that β-agonists stabilize ERK3 at the protein level, likely via inhibiting its proteasomal degradation.

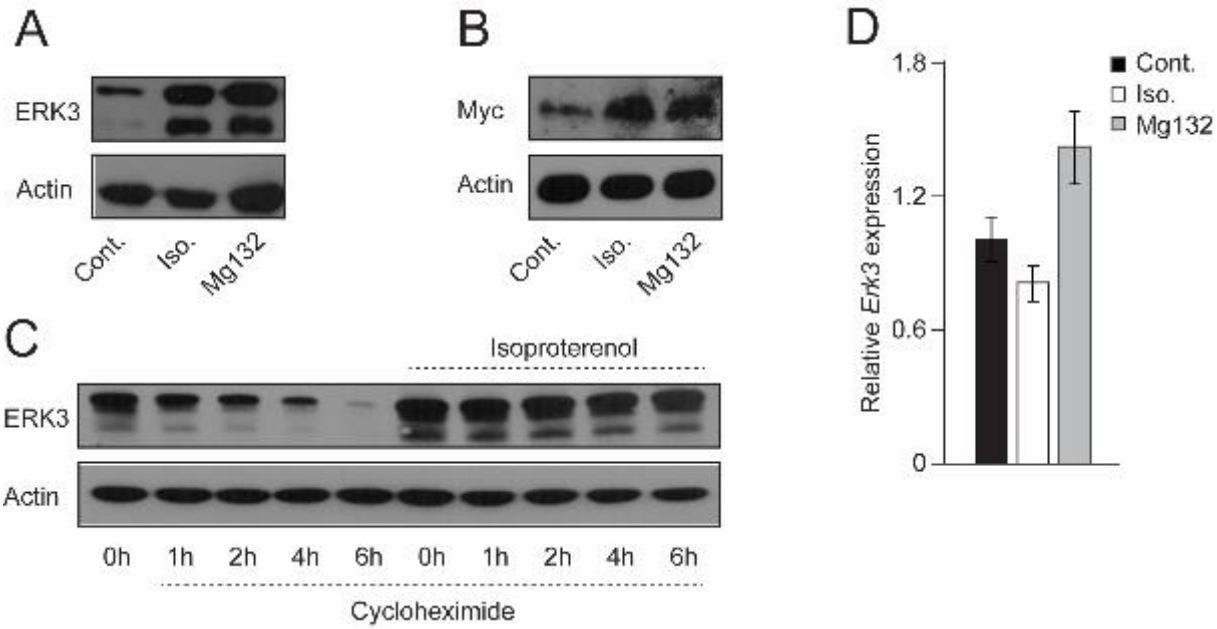

Figure 14. β-adrenergic signaling promotes ERK3 protein levels.

(A) WB for ERK3 on differentiated 3T3L1 cells stimulated as indicated (Iso. – Isoproterenol, proteasome inhibitor – Mg132). (B) WB analysis of indicated proteins on 3T3L1-derived adipocytes expressing Myc-tagged ERK3. (C) ERK3 levels over periods on 3T3L1 cells treated with cyclohexamide and stimulated as indicated. (D) Relative expression of *Erk3* in 3T3L1 cells stimulated as shown. n=3 for each experiment, for graphs - data presented average +/- SEM.

6.2.3 Elevation of cAMP levels promotes ERK3 stability independent of Beta-adrenergic receptor.

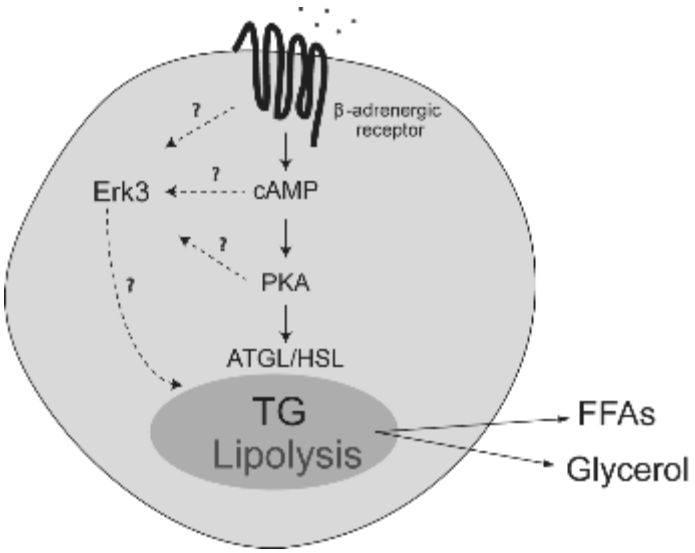

Figure 15. The experimental hypothesis of possible mechanisms of ERK3 action in adipocytes.

As it commonly that adrenaline released from the innervated neurons directly binds to its adrenergic receptor on the surface of adipocytes, triggering a series of events leading to the elevation of cAMP levels, which activates protein kinase A (PKA) and the later induces lipolysis (Arner and Langin 2014). Next, we aimed to identify the mechanism by which β-adrenergic agonists stimulate ERK3 levels and promote lipolysis in adipocytes. We postulated several hypotheses by which ERK3 could be intracellularly stimulated and how it could mediate its action in regulating lipolysis (Figure 15). To investigate if ERK3 stability is dependent on physical interaction with the adrenergic receptor, we used chemical elevators of cAMP as an approach to overpass the receptor and test this possibility. Interestingly, the elevation of cAMP levels (by forskolin or IBMX), independently of β-adrenergic receptors, was sufficient to stabilize ERK3 (Fig. 16A, B). Moreover, the stimulation of undifferentiated 3t3l1, cells that do not express yet any β-adrenergic receptors on their surface, with β-adrenergic agonists failed to induce the stability of ERK3 protein (Figure 16B). Additionally, stimulating HEK-293T cells, as another cell type that expresses β-adrenergic receptors, with β-adrenergic agonist or with IBMX lead to a profound stability of ERK3 protein (Figure 16C). Of note, treatment with proteasomal inhibitors was followed as a positive control that stabilizes ERK3 by blocking its proteasomal degradation. Therefore, here we showed that the binding of β-adrenergic agonists

on its receptor promotes the stability of by elevating intracellular cAMP levels independent of a physical interaction with the receptor.

Protein kinase A (PKA) belongs to a serine/threonine kinase family whose activity was reported to be dependent on cAMP binding to its regulatory subunits. Therefore, we were interested to investigate whether or not ERK3 is directly affected by cAMP or its stability is dependent on the activation of PKA. For this purpose, we used membrane-permeable PKA inhibitors, H89 or PKI 14-22, both of which have been shown to selectively inhibit PKA activity with high potency (Lochner and Moolman 2006). Pre-treatment with these inhibitors followed by co-stimulation with β-agonist inhibited the induced stabilization of ERK3 in adipocytes (Figure 16 D). Thus, we could conclude that β-adrenergic stimulation promotes PKA-dependent ERK3 stabilization.

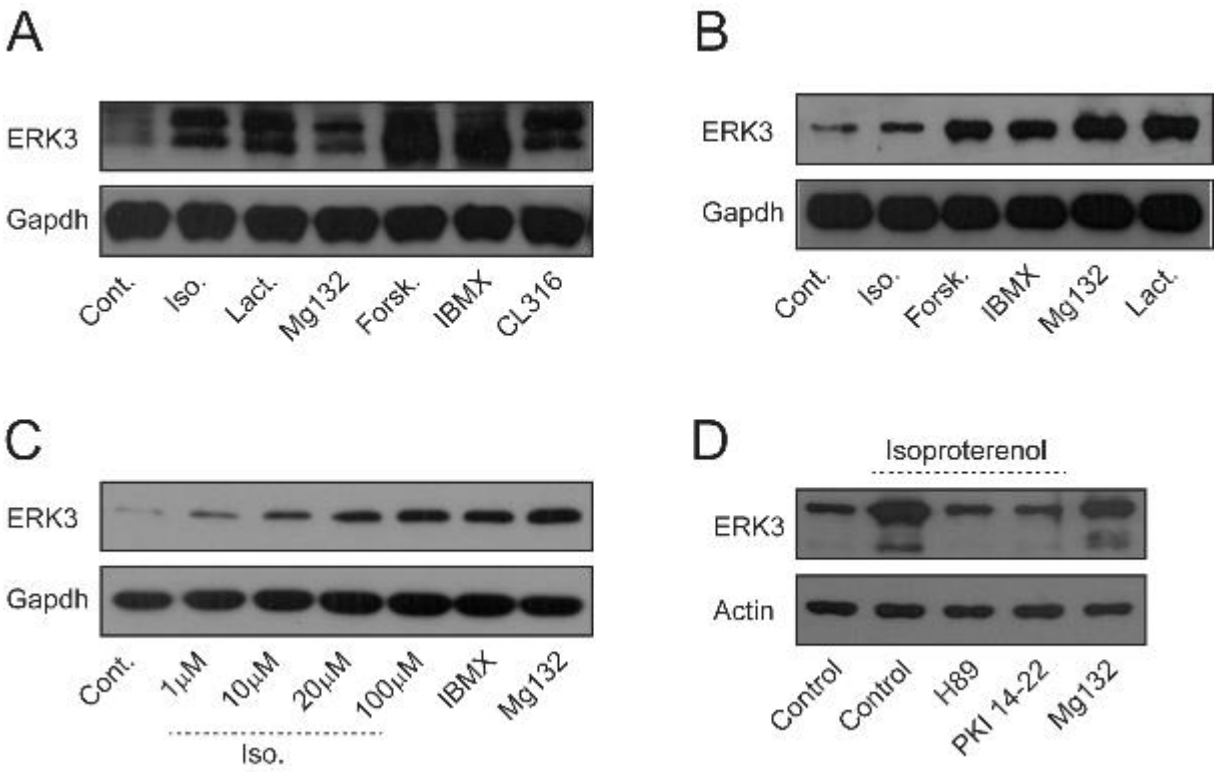

Figure 16. β-adrenergic signaling promotes ERK3 protein levels in a PKA dependent manner.

(A, D) WB for ERK3 on differentiated 3T3L1 cells, (B) undifferentiated 3t3L1 cells and (C) Hek 293T cells stimulated as indicated (Iso. – Isoproterenol, proteasome inhibitor – Mg132 and Lactacystin, cAMP elevators Forsk. – Forskolin and IBMX, PKA inhibitors – H89 and PKI 14-22). n=3 for each experiment.

6.3 PKA-mediated phosphorylation of MK5 promotes ERK3 stabilization and lipolysis

6.3.1 β-adrenergic stimulation promotes ERK3/MK5 stabilization in a PKA dependent manner.

It has been demonstrated before the interaction of PKA catalytic subunit with MK5 promotes the phosphorylation of MK5 at serine 115. Another paper indicated that this phosphorylation enables the translocation of MK5 from the nucleus to the cytoplasm (Gerits, Mikalsen et al. 2007, Kostenko, Shiryaev et al. 2011). On the other hand, a strong line of evidence indicated that the formation of a complex between ERK3 and MAP *kinase*-activated protein *kinase* 5 (MK5) renders both kinases from degradation and promotes the activation of MK5 (Schumacher, Laaß et al. 2004, Seternes, Mikalsen et al. 2004) while other research groups also indicated that the PKA activity renders the degradation of ERK3 and its associated complex, thereby promoting the complex stability (Jason, Berrios et al. 2015, Martínez-Noël, Luck et al. 2018). In light of these data, we hypothesized that following PKA activation in adipocytes, a translocation of MK5 to the cytoplasm could be inducing the formation of a complex with ERK3, this induces stability and promotes its biological functions. To verify this hypothesis, we started our molecular investigative approach by checking whether the stability of MK5 in adipocytes is affected by β-adrenergic stimulation. Indeed, our results indicate that the stability of Mk5 in differentiated adipocytes is highly induced upon β-adrenergic stimulation. Blocking protein synthesis in adipocytes using a pharmacological inhibitor, cycloheximide, decreased MK5 protein abundance over time. However, in adipocytes stimulated with β-adrenergic agonist for 2 hours prior to their treatment with cycloheximide, we observed a relevant delay in MK5 protein turnover (Figure 17). These results suggest a similar dependence on adrenergic stimulation for the stability of MK5 as previously observed in ERK3 protein.

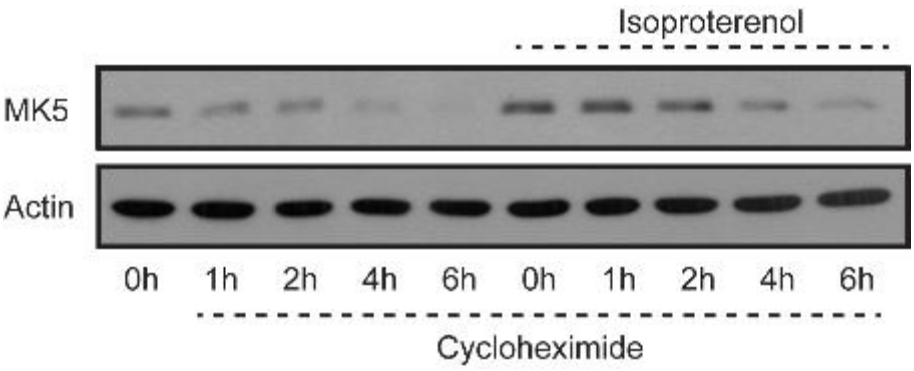

Figure 17. β-adrenergic stimulation promotes the stability of MK5.

WB analysis for MK5 on differentiated 3T3L1 cells stimulated as indicated (Cycloheximide, Isoproterenol).

Next, we tested whether our proposed regulatory mechanism truly applies to adipocytes. For this propose, we pretreated differentiated adipocytes with PKA pharmacological inhibitors (H89 and PKI 14-22) pre to their stimulation with β-agonist. In fact, pretreatment of cells with PKA inhibitors highly reduced MK5 stability in response to adrenergic stimulation in a similar manner to what we previously observed in ERK3 (Figure 18). To sum up, our results indicate that following β-adrenergic stimulation in adipocytes, PKA activity is crucial for the stability of both ERK3 and MK5 proteins.

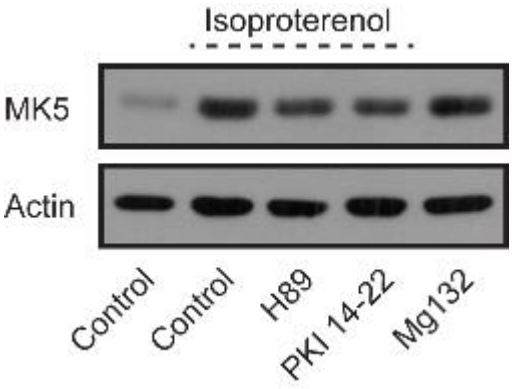

Figure 18. β-adrenergic stimulation promotes the stability of MK5 in a PKA dependent manner.

WB analysis for MK5 on differentiated 3T3L1 cells stimulated as indicated, n=3 (Isoproterenol, PKA inhibitors – H89 and PKI 14-22 and Mg132).

6.3.2 PKA activates MK5 translocation to the cytoplasm

As mentioned before, PKA-dependent phosphorylation of MK5 promotes its translocation from the nucleus to the cytoplasm (Kostenko, Shiryaev et al. 2011). This raises the possibility that, upon adipocyte stimulation, nuclear PKA-dependent phosphorylation of MK5 promotes its translocation, which might allow the cytoplasmic formation of a complex between MK5 and ERK3 as well as stabilization of both kinases. To prove this theory, we pretreated adipocytes with leptomycin B, a pharmacological compound that inhibits the interaction of exportin 1 with the Rev-type leucine-rich nuclear export signal (NES), thereby inhibiting MK5 among other proteins to be exported from the nucleus. Our results show that the stability of both MK5 and

ERK3 was highly reduced upon β-adrenergic stimulation when the cells were pre-treated with leptomycin B (figure 19A). These suggest that the regulation of this complex is happening in the cytoplasm. In order to provide further shreds of evidence in support of our theory, we applied a nuclear fractionation assay on differentiated adipocytes after their treatments with the indicated compounds (Figure 19B). Finally, we could confirm that the complex formation is occurring in the cytoplasm and in a PKA dependent manner.

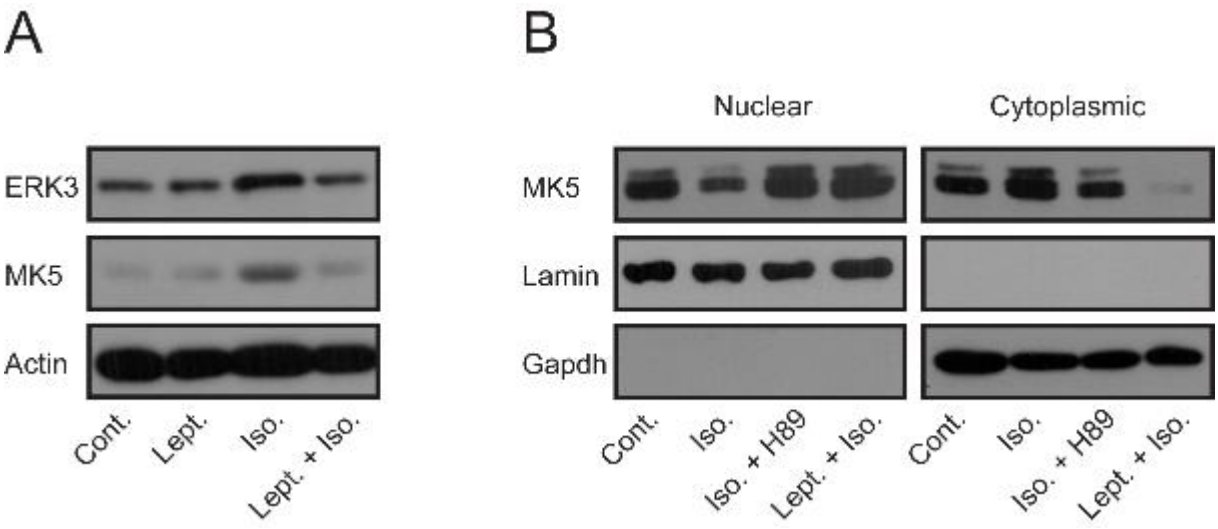

Figure 19. β-adrenergic stimulation promotes the nuclear export of MK5.

(A) WB analysis for MK5 on differentiated 3T3L1 cells stimulated as indicated. (B) MK5 levels in cytoplasmic and nuclear fractions of 3T3L1 cells treated as indicated. Lamin and Gadph are positive controls for the nuclear and cytoplasmic fractions, respectively (Iso – isoproterenol, Lept – Leptomycin B). n=3 of each experiment.

6.3.3 MK5 stability promotes lipolysis in differentiated adipocytes

Consequently, we hypothesized that a PKA/ERK3/MK5 signaling axis may regulate lipolysis induced by β-adrenergic stimulation. In support of this hypothesis, we further studied the molecular events evoked by β-adrenergic stimulation on MK5 stability. Interestingly, our primary screen revealed that the silencing of *Mk5* reduced the rate of lipolysis. We could reconfirm these results by repeating a siRNA-mediated depletion of *Mk5* in differentiated adipocytes. Indeed, the silencing of *Mk5* reduced β-adrenergic induced lipolysis as observed by analyzing FFA and Glycerol release to the media (Figure 20A, B). Notably, the silencing of *Mk5* resulted in a reduction level of lipolysis rate but not as robust as in comparison to the level previously observed upon ERK3 depletion. Importantly, the silencing of *Erk3* in adipocytes decreased the abundance of MK5 (Figure 20C). Similarly, the depletion of *Erk3* by siRNA did

not alter the expression level of *Mk5* as shown by the mRNA analysis of both genes (Figure 20D). Likewise, the silencing of *Mk5* resulted in a decreased abundance of ERK3 but did not affect its expression (Figure 20E, F). Also, stimulating 3t3l1 cells depleted from *Erk3* by a β-agonist did not alter the expression level of *Mk5* (Figure 20G). These results suggest that *Erk3* and *Mk5* transcriptional expression is independent of each other. However, our results indicate the stability of both proteins (MK5 and ERK3) are highly dependent on the abundance of the other.

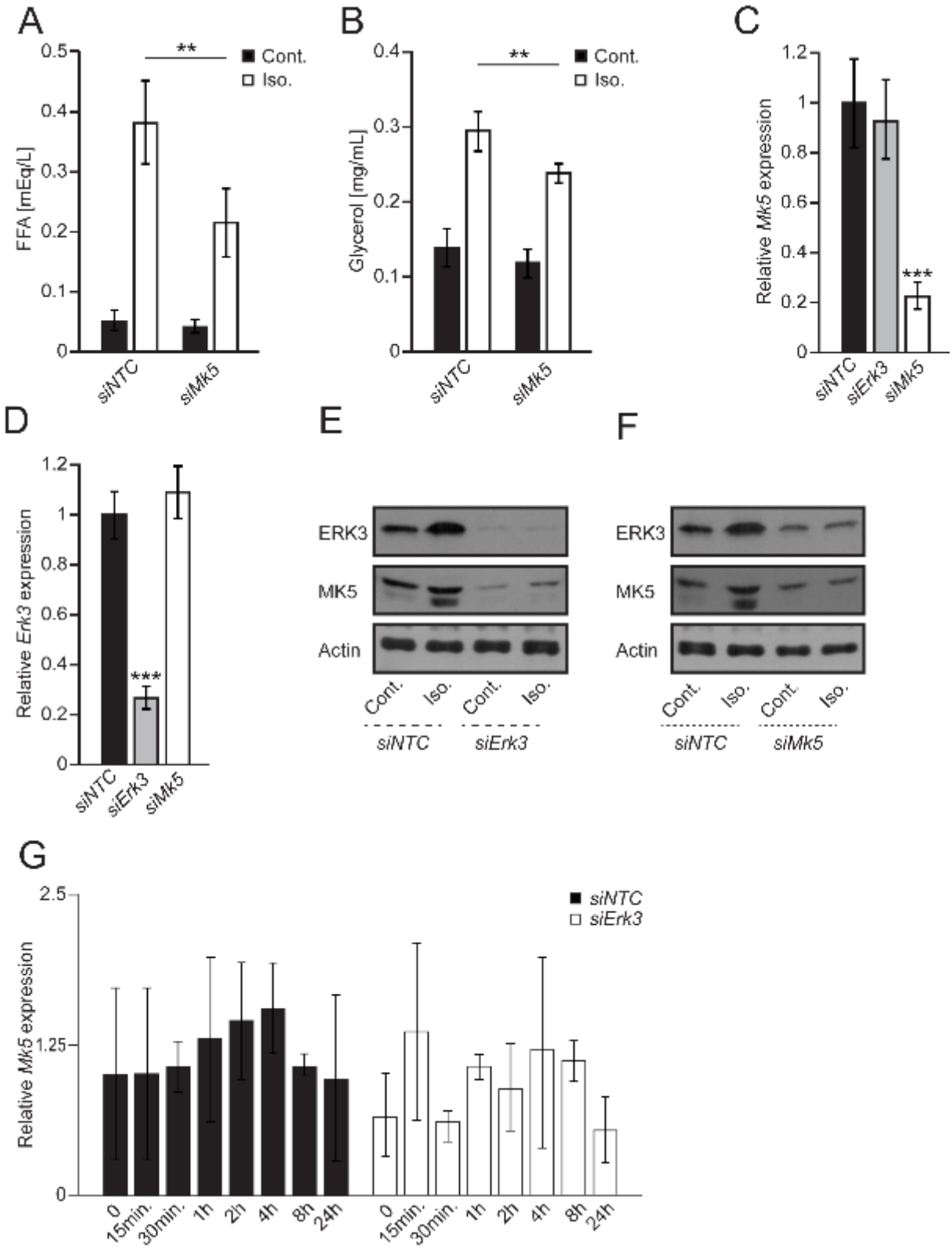

Figure 20. ERK3 stability is dependent on MK5 abundance.

(A, B) FFA and glycerol release in 3T3L1 cells transfected with either siMk5 or siNTC. (C, D) Relative expression of *Mk5* and ERK3 in 3T3L1 transfected with indicated siRNAs. (E, F) WB analysis of indicated proteins in 3T3L1 cells transfected with si*Mk5*, si*Erk3* or siNTC and

stimulated with either ISO of control media. (G) Relative expression of *Mk5* in 3T3L1 cells transfected with either siErk3 or siNtc, stimulated or control media, over the indicated time points. n=3 for each experiment. For graphs - data presented average +/- SEM, * P ≤0.05, ** P ≤0.01 and *** P ≤0.001.

6.3.4 MK5 phosphorylation at serine 115 promotes its function

Furthermore, independent studies on the molecular mechanism of MK5 performed in different cellular models had first demonstrated that following PKA activation, PKA catalytic subunit specifically translocates to the nuclease where it phosphorylates MK5 at serine 115(Kostenko, Shiryaev et al. 2011). Others showed that this specific phosphorylation of MK5 induces a conformational change in the folding of this protein allowing its translocation from the nucleus to the cytoplasmic, where it binds to ERK3 and activates the complex, independently of a physical interaction with PKA catalytic subunit (Perander, Keyse et al. 2016). To test this directly in adipocytes, we generated FLAG-tagged phospho-deficient and phospho-mimetic mutants of MK5 on serine 115 (MK5-S115A and MK5-S115E, respectively). Monitoring the cellular distribution of the exogenous MK5 upon overexpression of WT or indicated mutant forms. We observed that MK5-S115A localized primarily in the nucleus confirming that its phosphorylation is essential for its cytoplasmic translocation. Moreover, while MK5-WT was found in both compartments, MK5-S115E presented solely cytoplasmic localization (Figure 21A). Consistently, in the absence of β-agonist stimulation, overexpression of MK5-S115E mutation actively promoted the stability of ERK3 protein in differentiated adipocytes (Figure 18B). Importantly, β-adrenergic stimulation boosted the stability of ERK3 in MK5-WT overexpressing cells, to a higher extent than observed in the control cells (Figure 21B).

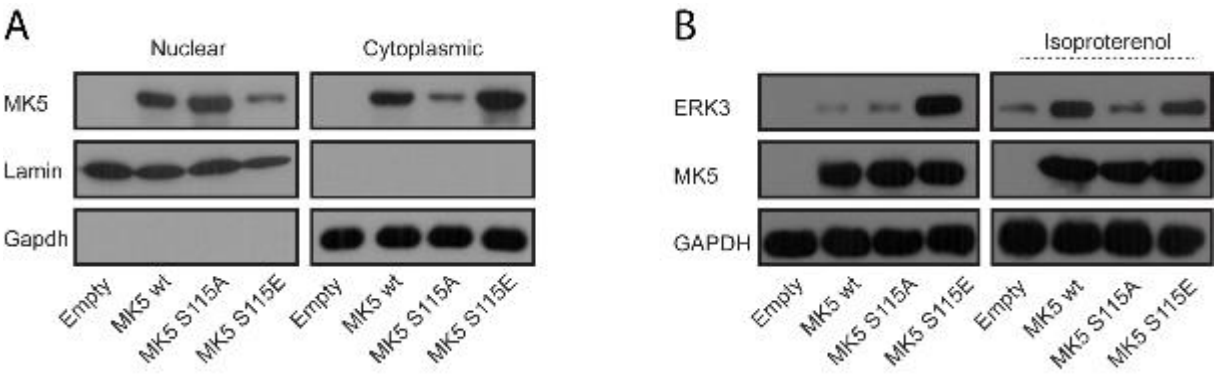

Figure 21. The phosphorylation of MK5 on S115 determines its cytoplasmic localization.

(A) The abundance of MK5 in the nucleus and cytoplasm of adipocytes expressing indicated MK5 mutants. Lamin and Gadph are positive controls for the nuclear and cytoplasmic fractions, respectively. (B) WB analysis of ERK3 and MK5 in adipocytes expressing indicated MK5 mutants. n=3 for each experiment.

On the other hand, the overexpression of MK5-S115E in differentiated adipocytes promoted a direct formation of a complex with the endogenous ERK3 as observed in our co-immune precipitation analysis. of note, since our assay was performed under basal conditions, without β-adrenergic stimulation, the binding of the WT-Mk5 to the endogenous ERK3 protein was very weak (Figure 22A). Importantly, MK5-WT protein abundance and its relative expression levels were not different from the overexpressed MK5 mutants (Figure 22A, B). Moreover, exogenous expression of MK5 or its mutants did not alter the endogenous mRNA expression level of *Erk3* (Figure 22C). Nevertheless, pharmacological inhibition of PKA activity successfully blocked β-adrenergic stimulation from promoting the interaction between MK5 and ERK3 proteins in adipocytes (Figure 22D). Finally, we performed further functional analysis on these differentiated adipocytes, bearing this overexpression of MK5 or its indicated mutants. Our results revealed a significant increase in basal lipolysis rate in MK5-S115E overexpressing adipocytes (Figure 22E). On the other hand, in adipocytes depleted from *Erk3*, MK5-S115E mutations could not trigger any increase in the basal lipolysis rate. Of note, β-agonist stimulation on these cells saturated the system and we could not observe a significant difference between the experimental conditions (Figure 22E). Taken together, these results directly reflect the dependence of PKA phosphorylation on MK5 serine 115, which is required to promote MK5 nuclear export and cytoplasmic complex formation with ERK. This further provides stability to the ERK3/MK5 complex and eventually triggers its activity in inducing lipolysis in adipocytes.

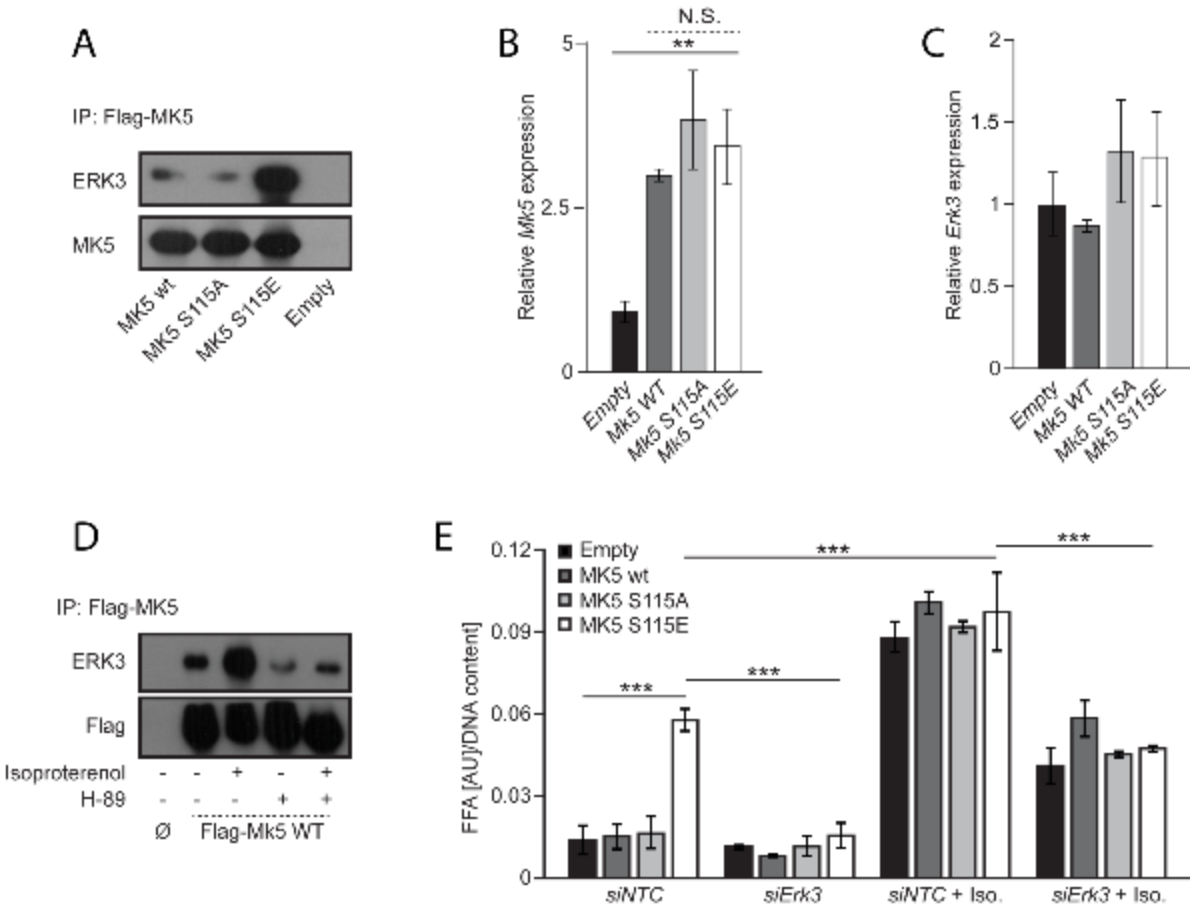

Figure 22. MK5 upon its phosphorylation enters a complex with ERK3.

(A) Immunoprecipitation (IP) using Flag antibody of indicated Flag-tagged mutants of MK5, (D) or Flag-tagged MK5 WT stimulated as indicated, followed by Western blot using specified antibodies against co-precipitated proteins. (B, C) Relative expression of *Mk5* and ERK3 in adipocytes overexpressing indicated Flag-tagged mutants of MK5. (E) FFA release in adipocytes overexpressing indicated Flag-tagged mutants of MK5 and stimulated with either isoproterenol or control media. n=3 for each experiment. For graphs - data presented average +/- SEM, * P ≤0.05, ** P ≤0.01 and *** P ≤0.001.

6.4 ERK3 knockdown affects adipocytes lipolytic machinery

6.4.1 High throughput RNA sequencing showed an altered adipose-related gene profile

We aimed next to identify genes and underlying pathways that could be altered in adipocytes upon the depletion of *Erk3*. For this purpose, we performed RNA sequencing analysis on the total RNA isolated from differentiated adipocytes depleted from *Erk3* by siRNA and compared to control cells transfected with a non-targeting sequence. Global transcriptomic analysis and further get set enrichment analysis revealed the down-regulation of major genes involved in lipolysis (Figure 23A, C) and lipogenesis (Figure 23B, D) pathways. Among those ATGL/pnpl2, Adcy10, HSL/Lipe, MGL and perilipin were highly down-regulated in adipocytes depleted

from *Erk3*. The downregulation of these genes provides a shred of strong evidence to support the reduction in the lipolysis rate shown above. On the other hand, since the alteration of genes involved in lipogenesis is often associated development of obesity and diabetes, we were also interested to investigate the impact of *Erk3* depletion in adipocytes on the expression of lipogenic genes. Indeed, our global transcriptomic assessment revealed a significant downregulation in major genes involved in the lipid biosynthesis pathways. Among these genes are key enzymes such as fatty acid synthase (FASN), long-chain-fatty-acid-CoA ligase 1 (Acsl1), phosphoenolpyruvate carboxykinase (Pck1), free fatty acid receptor-4 (FFAR4), Lipase H (LIPH) and several other mentioned our lipogenesis gene enrichment heat map (Figure 23B).

However further validation was required to confirm our findings.

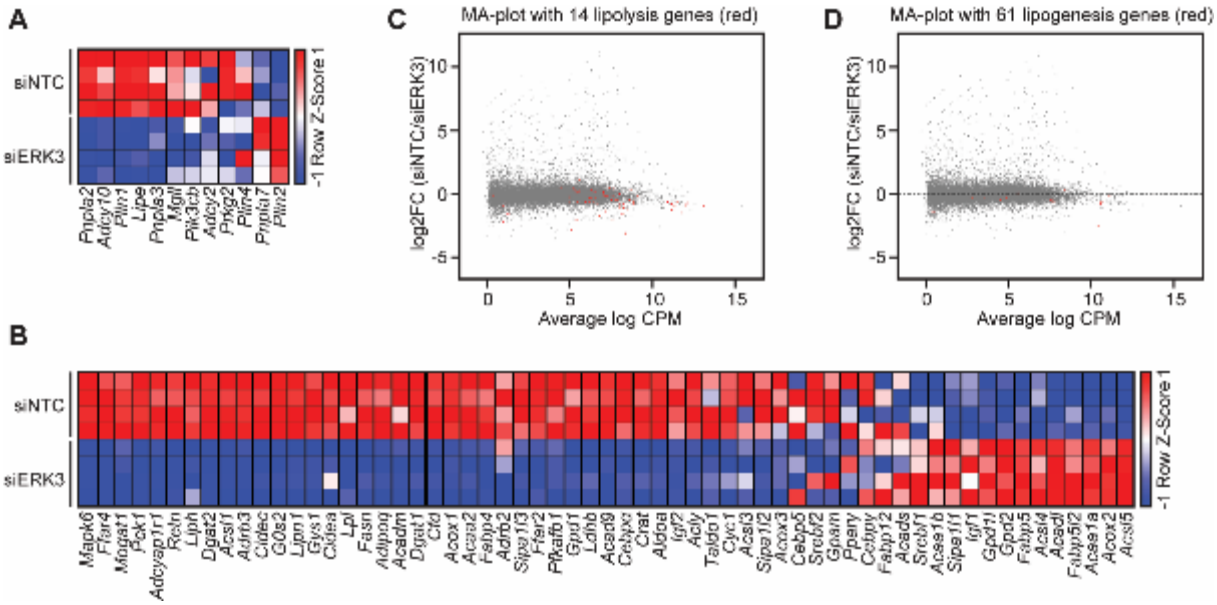

Figure 23. ERK3 depletion altered the expression profile of adipocytes.

(A, B) RNA-sequencing based heat map of the expression patterns of indicated genes. (C, D) MAplot showing RNA sequencing results. Differential expression and average abundance [indicated as log2 fold change (FC) and log countspermillion (CPM)] of all genes were calculated with EdgeR. Lipolysis and lipogenesis related genes are highlighted in red (n=4).

6.4.2 Validation of transcriptomic selected hits.

To verify the reliability of our sequencing data, we performed a qPCR analysis on total mRNA isolated from independent sets of differentiated adipocytes transfected with si*Erk3* or NTC. Consistently, QPCR confirmed reduced expression of the major lipolytic enzymes including

Atgl, in adipocytes depleted of *Erk3* (Figure 24A). Equally important, western blot analysis showed that the ATGL protein level was reduced in adipocytes depleted of *Erk3* (Figure 24B). Moreover, WB and QPCR analysis performed on 3T3L1 cells transfected with *Erk3* shRNA and control cells showed a reduction in transcription of *Atgl* which also was evident on the protein level respectively (Figure 24C, D). On the contrary, the expression of PPAR-gamma nor C/EBP-Alpha (key regulators of adipocytes differentiation) were not altered in both tested models. Hence, upon its stability, ERK3 is promoting the transcription of *Atgl* (Figure 24D, E, F).

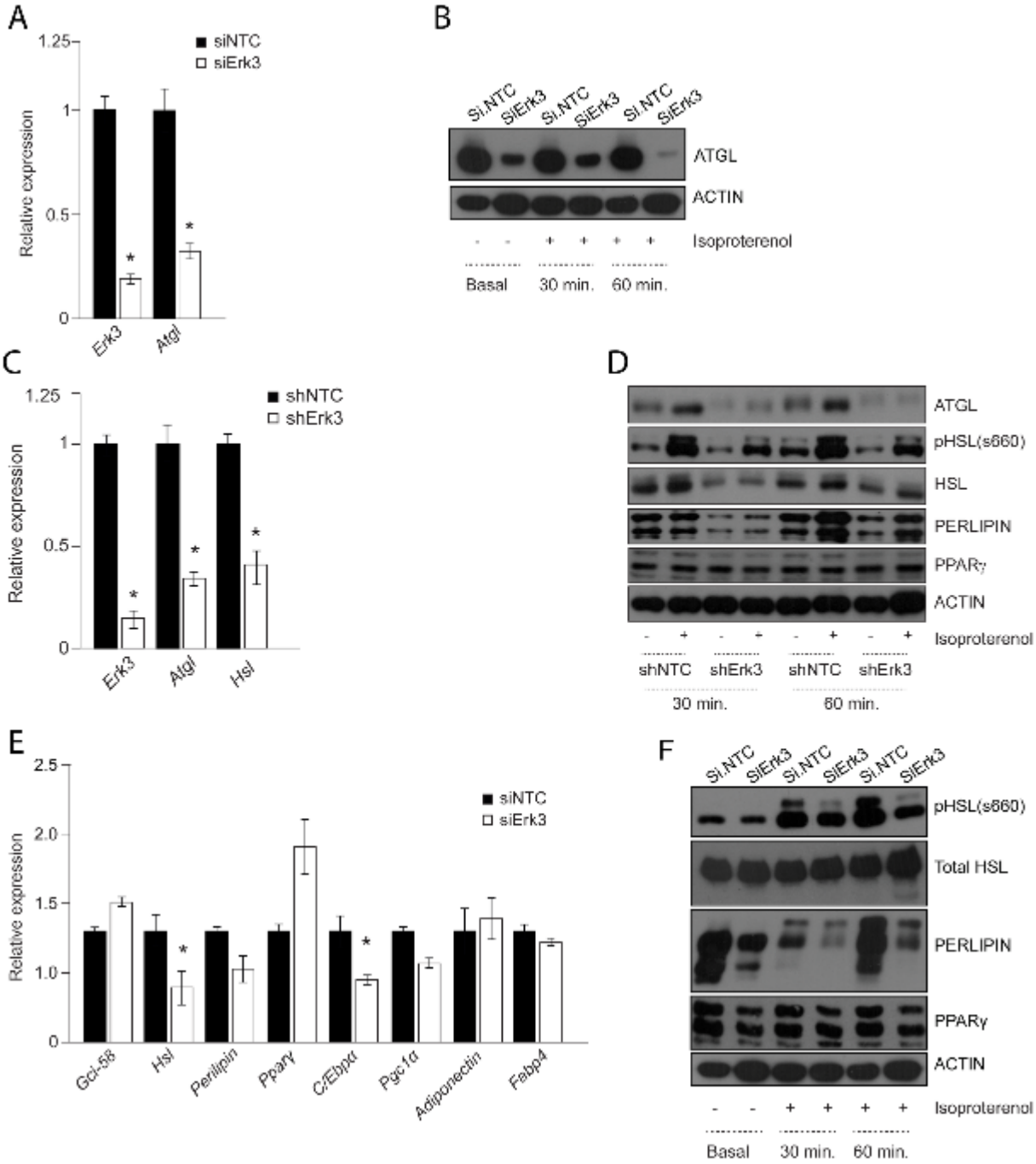

Figure 24. ***Erk3*** **depletion altered the expression of major genes involved in lipolysis**.

(A, E), (B, F) Relative expression and WB analysis respectively of indicated genes in 3T3L1 cells transfected with either si*Erk3* or siNTC. (C, D) Relative expression and WB analysis of indicated genes respectively in 3T3L1 cells stably expressing either sh*Erk3* or shNTC. n=3 for each experiment. For graphs - data presented average +/- SEM, ** P ≤0.01.

6.4.3 ATGL, a key regulator of triglyceride hydrolysis

Lipolysis mediated by β-adrenergic stimulation in adipocytes occurs by a complex proteome comprised of specific acyl-glycerol lipases and their regulators (Kraemer and Shen 2002). Importantly, ATGL is responsible for the bulk of triacylglycerol hydrolase activity in adipocytes. Therefore, we were interested to investigate whether the re-introduction of ATGL in adipocytes, depleted from *Erk3* (Figure 25A), is sufficient to restore the lipolytic rate. In fact, overexpression of ATGL in 3T3L1 cells depleted from *Erk3* restored the lipolysis rate induced by β-agonist to a similar level than observed in wild type cells (Figure 25B). Moreover, since transcriptional events occurring in adipocytes upon β-adrenergic stimulation, which is utilized by the EKR3 pathway, may require longer periods to be translated into biological effects. Therefore, we have assessed, through WBs and qPCRs, the detailed timing of β-adrenergic activation of ERK3. We could observe a rapid increase in ERK3 stability in adipocytes after stimulation by β-agonist then a peak in its abundance two hours later (Figure 25C). Interestingly, *Atgl* expression was substantially increased 30 minutes after stimulation in parallel with increasing ERK3 stability (Figure 25D). Respectively, the silencing of ERK3 ameliorated the expression and abundance of ATGL in adipocytes even after stimulation with β agonist. In parallel, the induction of lipolysis was rapid upon the β-agonist. The levels of FFAs and glycerol release to the media by the differentiated adipocytes kept on increasing at later time points in control cells but not in the ERK3-deficient adipocytes (Figure 25E). Therefore, a β-adrenergic-induced ERK3 pathway is required rather for sustaining lipolysis after the initial phase of the TG release. However, the molecular mechanism that underlies the regulatory effect of ERK3 on *Atgl* expression in adipocytes warrants further detailed exploration.

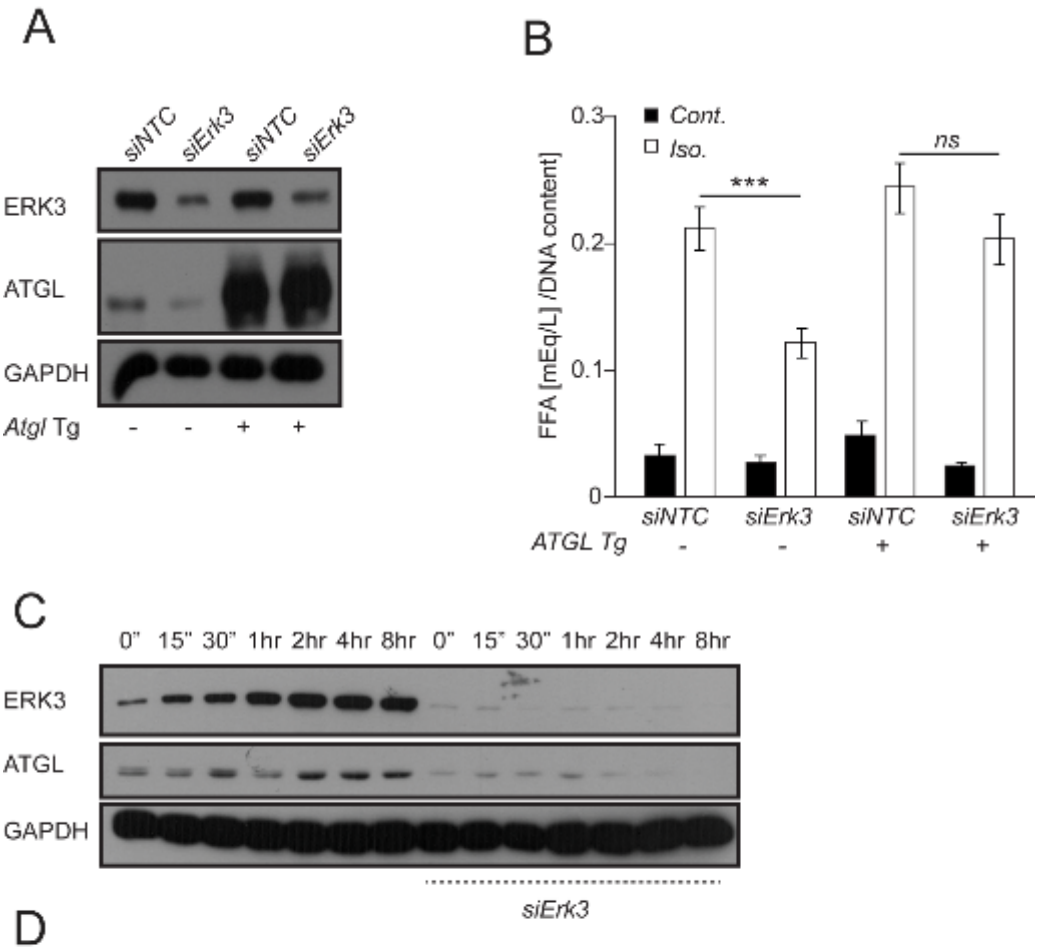
A
siNTC
siErk3
siNTC
siErk3
ERK3
ATGL
GAPDH
Atgl Tg
- - + +
B
Cont.
Iso.
FFA [mEq/L] /DNA content
0.3
0.2
0.1
0
***
ns
siNTC
siErk3
siNTC
siErk3
ATGL Tg
- - + +
C
0" 15" 30" 1hr 2hr 4hr 8hr 0" 15" 30" 1hr 2hr 4hr 8hr
ERK3
ATGL
GAPDH
siErk3
D
siNTC
siErk3
Relative Atgl expression
6
3
0
0 15min. 30min. 1h 2h 4h 8h 24h 0 15min. 30min. 1h 2h 4h 8h 24h
E
siNTC
siErk3
FFA [mEq/L]
0.6
0.4
0.2
0
basal 15" 30" 60" 2hr 4hr 8hr 24hr

Figure 25. ERK3 targets the transcription regulation of *Atgl*.

(A, B) WB on indicated proteins analysis of 3T3L1 cells stably overexpressing *Atgl*, transfected with either si*Erk3* or siNtc. (B) FFA release of 3T3L1 cells stably overexpressing *Atgl*, transfected with either si*Erk3* or siNtc, stimulated with isoproterenol or control media. (C) WB analysis of indicated proteins, (D) Relative expression of *Atgl*, (E) FFA release into the media in 3T3L1 cells transfected with either si*Erk3* or siNtc, stimulated or control media, over the indicated time points. n=3 for each experiment. For graphs - data presented average +/- SEM, * $P \leq 0.05$, ** $P \leq 0.01$ and *** $P \leq 0.001$.

6.4.4 ERK3/MK5 pathway promotes nuclear translocation of FOXO1 to drive *Atgl* expression

Combined with our previous observations that the abundance of ERK3 in positively regulating the transcription of Atgl (Figure 20A), together with the stated findings that β-adrenergic stimulation is inducing cytoplasmic stability of ERK3/MK5 Complex. We hypothesize the existence of an intermediate mediator regulating the transcription of *Atgl* in the nucleus. Forkhead box protein O family members are transcription factors that function broadly in regulating homeostasis, including insulin and glucose metabolism (Dong, Copps et al. 2008). Previous studies provided evidence that strongly supports the notion that MK5 phosphorylates FOXO1 at serine 215, which results in transcriptional activation of a select subset of FOXO1 target genes. On the other hand, a rising number of papers showing a direct link between FOXO1 activity and ATGL expression (Chakrabarti and Kandror 2009, Kress, Cannell et al. 2011, Chow, Timblin et al. 2013). In fact, we could show that the siRNA-mediated deletion of *Foxo1* reduced *Atgl* expression to a similar extent as observed in adipocytes depleted from *Erk3* or MK5 (Figure 26A). Taken, together with that, the depletion of *Foxo1* reduced Atgl expression; we next applied a lipolysis assay on adipocytes depleted from *Foxo1* by siRNA. In fact, lipolysis was highly reduced in *Foxo1* depleted cells when compared to siNTC transfected cells after their stimulation with isoproterenol (Figure 26B). To further assess, if ERK3/MK5 dependent expression of *Atgl* occurs through a FOXO1 dependent manner. We selectively depleted *Foxo1* in adipocytes expressing MK5-S115E, cells previously shown an active increase in the abundance and stability of ERK3/MK5 complex. In comparison with cells overexpressing MK5WT or an empty vector, we observed a significant increase in the transcriptional expression levels of *Atgl* at the basal conditions (Figure 26C). In parallel, stimulation with β-agonist resulted in the induction of *Atgl* expression in adipocytes, especially, which have overexpression of MK5-S115E mutant. Furthermore, the silencing of *Foxo1* highly ameliorated this induced expression of *Atgl* under all tested experimental conditions (Figure 26C).

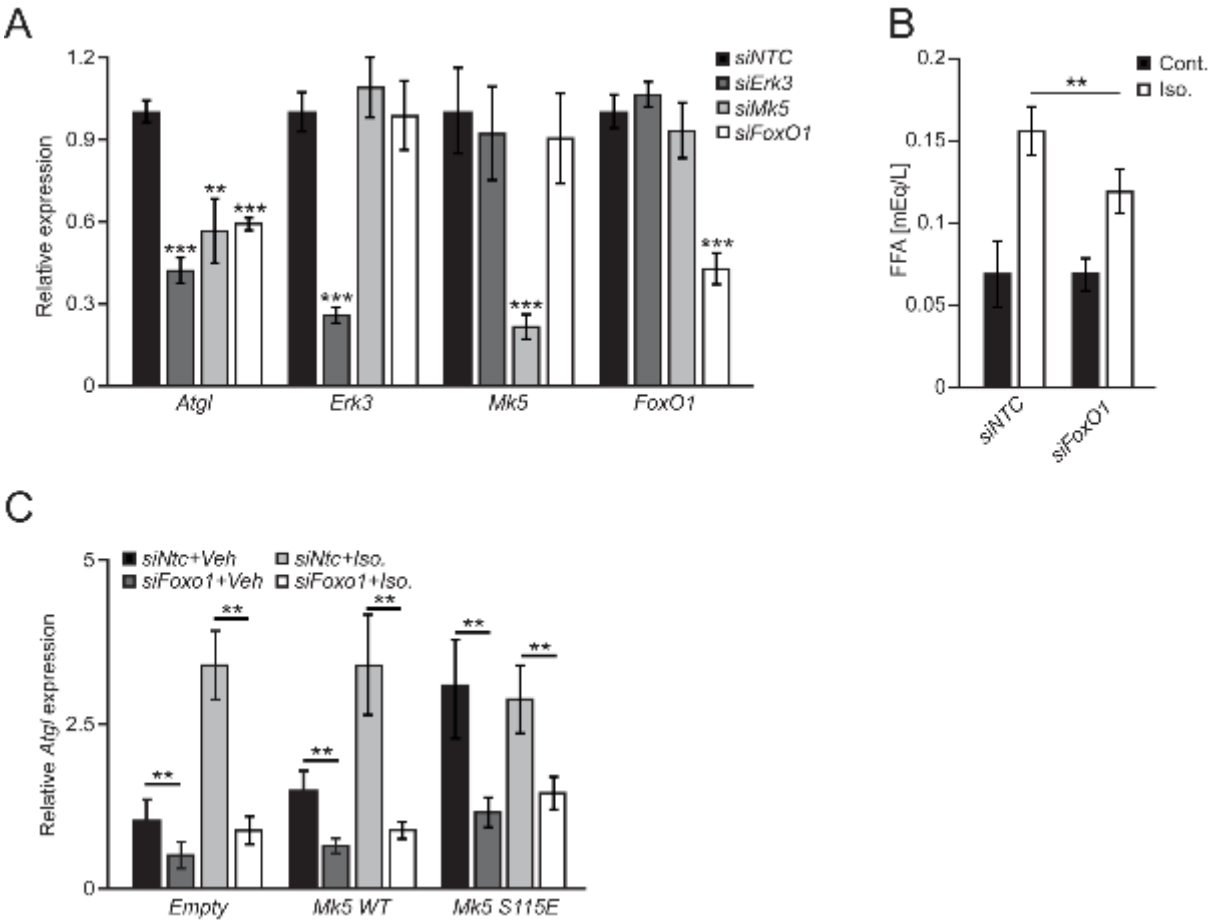

Figure 26. ERK3/MK5 promotes FOXO1-mediated transcription of *Atgl*.

(A) Relative expression of indicated genes in adipocytes overexpressing indicated Flag-tagged mutants of MK5 transfected with siRNA against *Erk3*, *Mk5*, *Foxo1* and NTC. (B) FFA release in adipocytes transfected with either *Foxo1* or NTC siRNAs and stimulated with isoproterenol or control media. (C) Relative expression of *Atgl* in adipocytes overexpressing the indicated Flag-tagged mutants of MK5 and transfected with siRNA against *Foxo1* or NTC then stimulated with isoproterenol or control media. n=3 for each experiment. For graphs - data presented average +/- SEM, * P ≤0.05, ** P ≤0.01 and *** P ≤0.001.

FOXO1 is a critical and direct regulator for *Atgl* expression. Although FOXO1 regulation has been widely studied in several cell types, pathways regulating FOXO1 in adipocytes have not been fully elucidated. For its activity as a transcription factor, FOXO1 has to translocate to the nucleus to mediate its action on target genes. Therefore, we applied confocal imaging to help us visualize FOXO1 nuclear/cytoplasmic trafficking upon β-adrenergic stimulation in adipocytes. Indeed, under basal conditions, FOXO1 was found wildly distributed throughout the cells. However, upon β-adrenergic stimulation, FOXO1 was mainly found residing in the nucleus (Figure 27A). Moreover, siRNA-mediated depletion of either *Erk3* or *Mk5* in

differentiated adipocytes majorly altered the cytoplasmic/nuclear trafficking of FOXO1 in response to β adrenergic stimulation. In fact, after a double-blinded observation on FOXO1 cellular localization in 200 cells per condition in 3 independent experiments (Figure 27B), we could conclude that in adipocytes depleted from *Erk3* or *Mk5*, β-adrenergic stimulation failed to induce nuclear translocation of FOXO1 proteins, as we mainly observed FOXO1 protein residing in the cytoplasm and was not responsive adrenergic signaling in *Erk3* or *Mk5* depleted conditions (Figure 27A, B).

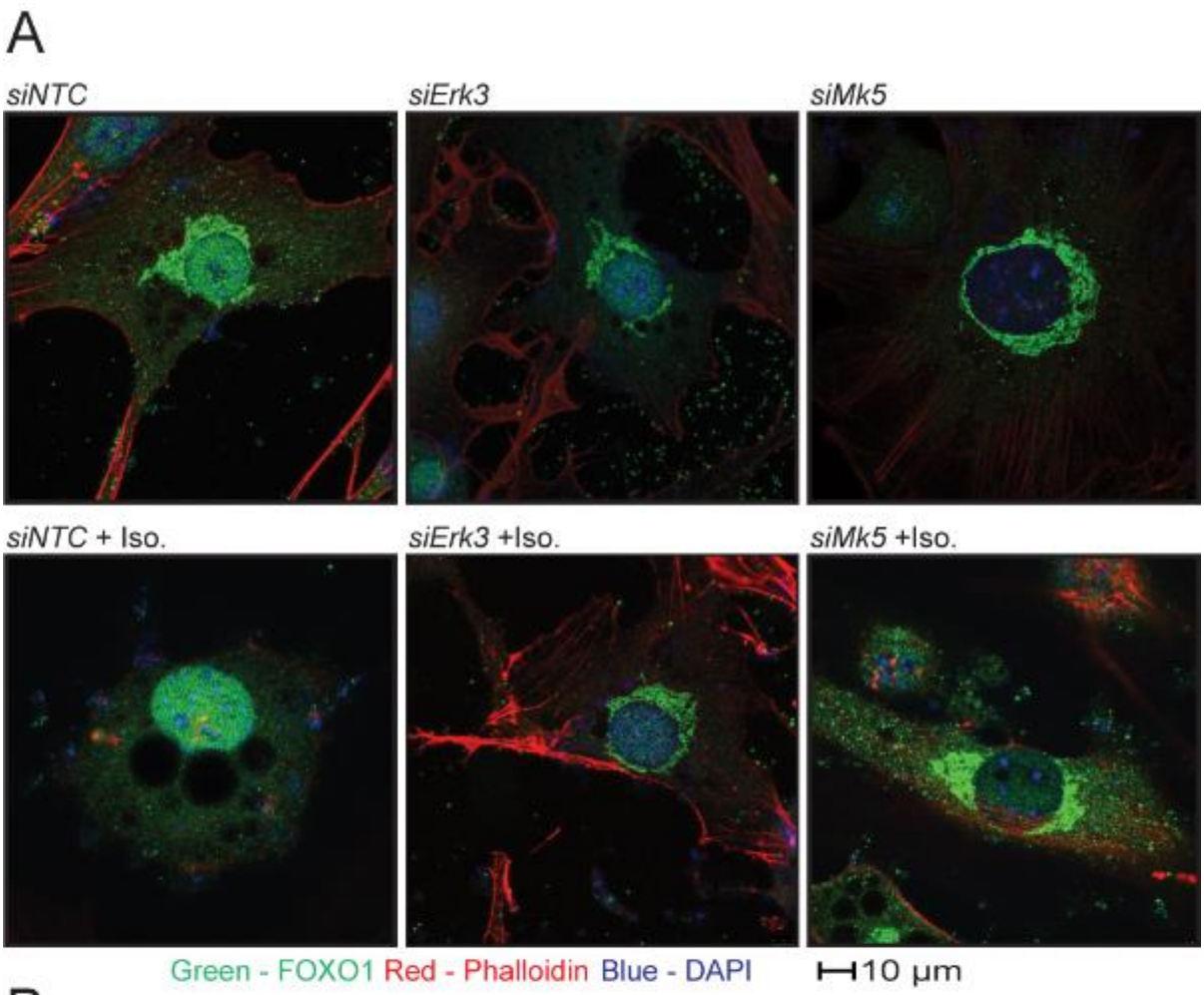

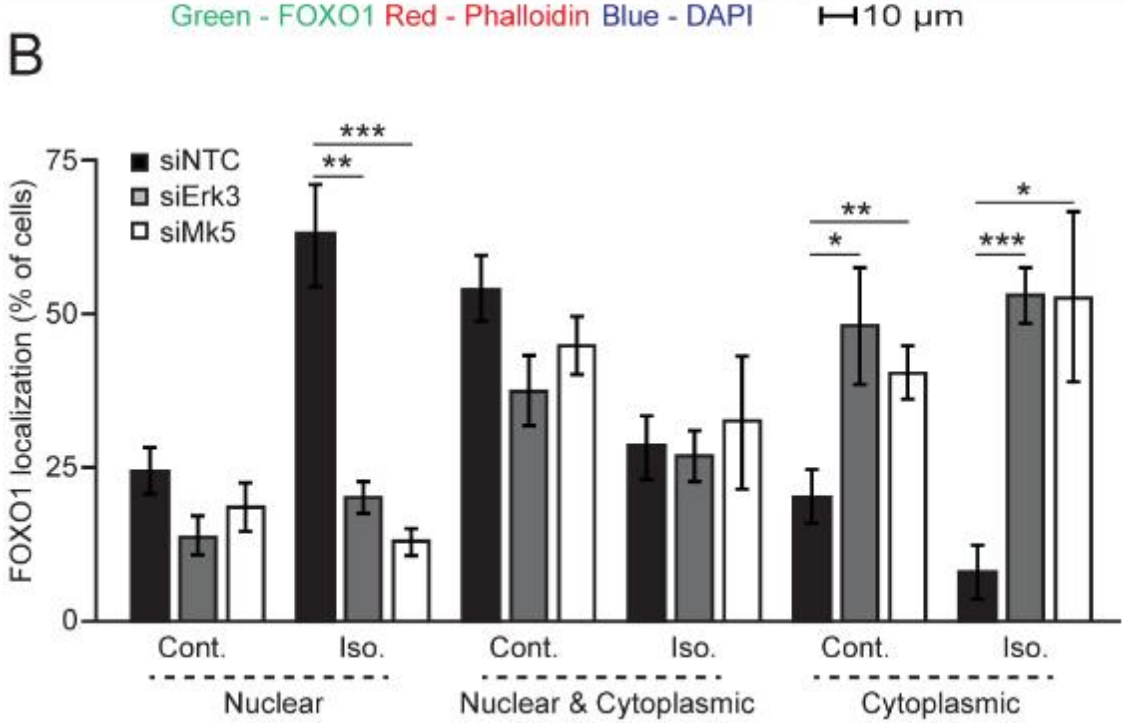

Figure 27. β-adrenergic mediated FOXO1 nuclear translocation in ERK3/MK5 depleted cells.

(A) Representative images of FOXO1 staining on 3T3L1 cells transfected with indicated siRNAs, stimulated as shown for 2h and the (B) corresponding quantifications of specific

localizations. N=3 to 4 for each experiment, for graphs - data presented average +/- SEM, * P≤0.05, ** P ≤0.01, *** P≤0.001.

Together with our findings, that the depletion of Ekr3 reduces *Atgl* expression and eventually leading to the decease of its protein levels. On the other hand, MK5 was shown to phosphorylate members of the FOXO family (including FOXO1) on serine 215, which later induces its translocation to the nucleus. We next were interested to further study Foxo1 mediated transcription of *Atgl*. For this purpose, we next applied a chromatin immune precipitation assay on differentiated adipocytes to fish out FOXO1 DNA-binding partners. Indeed, we found that FOXO1 directly binds to the *Atgl* promoter, which eventually promotes its transcription (Figure 28A). Knowing that MK5 phosphorylates members of the FOXO family on serine 215, which is conserved among all the FOXO members (including FOXO1) (Kress, Cannell et al. 2011, Chow, Timblin et al. 2013) We next generated phospho-deficient and phospho-mimetic mutants of FOXO1 (FOXO1 S215A and FOXO1 S215D, respectively). Next, we analyzed the basal localization of the exogenous HA- FOXO1 protein in adipocytes, or its mutants, following a nuclear fractionation assay. Using an HA-tag antibody, WB quantifications revealed that FOXO1 S215A is primarily localized in the cytoplasm while FOXO1 S215D mainly localized in the nucleus (Figure 28B). Therefore, we hypothesized that upon its phosphorylation by the ERK3/MK5 complex, FOXO1 was translocating to the nucleus to bind with the *Atgl* promoter. For this purpose, we performed a CHIP assay in ERK3-deficient adipocytes. Interestingly, we observed a reduced binding of FOXO1 to the *Atgl* promoter in 3T3L11-differentiated adipocytes depleted from *Erk3* compared to control cells (Figure 28C). Moreover, we could obtain similar results using primary differentiated adipocytes, isolated from either subcutaneous adipose tissue (Figure 28D) or from brown adipose tissue depot (Figure 28E), of $Erk3^{f/f}$ mice and compared to their littermates carrying the genetic deletion of *Erk3* specifically in adipocytes ($Erk3^{Adipo.\Delta/\Delta}$). Finally, we reconfirmed these findings by a so-called rescue experiment where we observed that the expression of the phospho-mimetic FOXO1 mutant (S215D), but not wild-type or phospho-deficient (S215A) FOXO1, promoted the binding of FOXO1 to the *Atgl* promoter in adipocytes depleted of *Erk3* (Figure 28F). Altogether, these data suggest that ERK3/MK5 drives lipolysis by phosphorylating FOXO1 at S215, thereby promoting its nuclear translocation and eventually the transcription of *Atgl*.

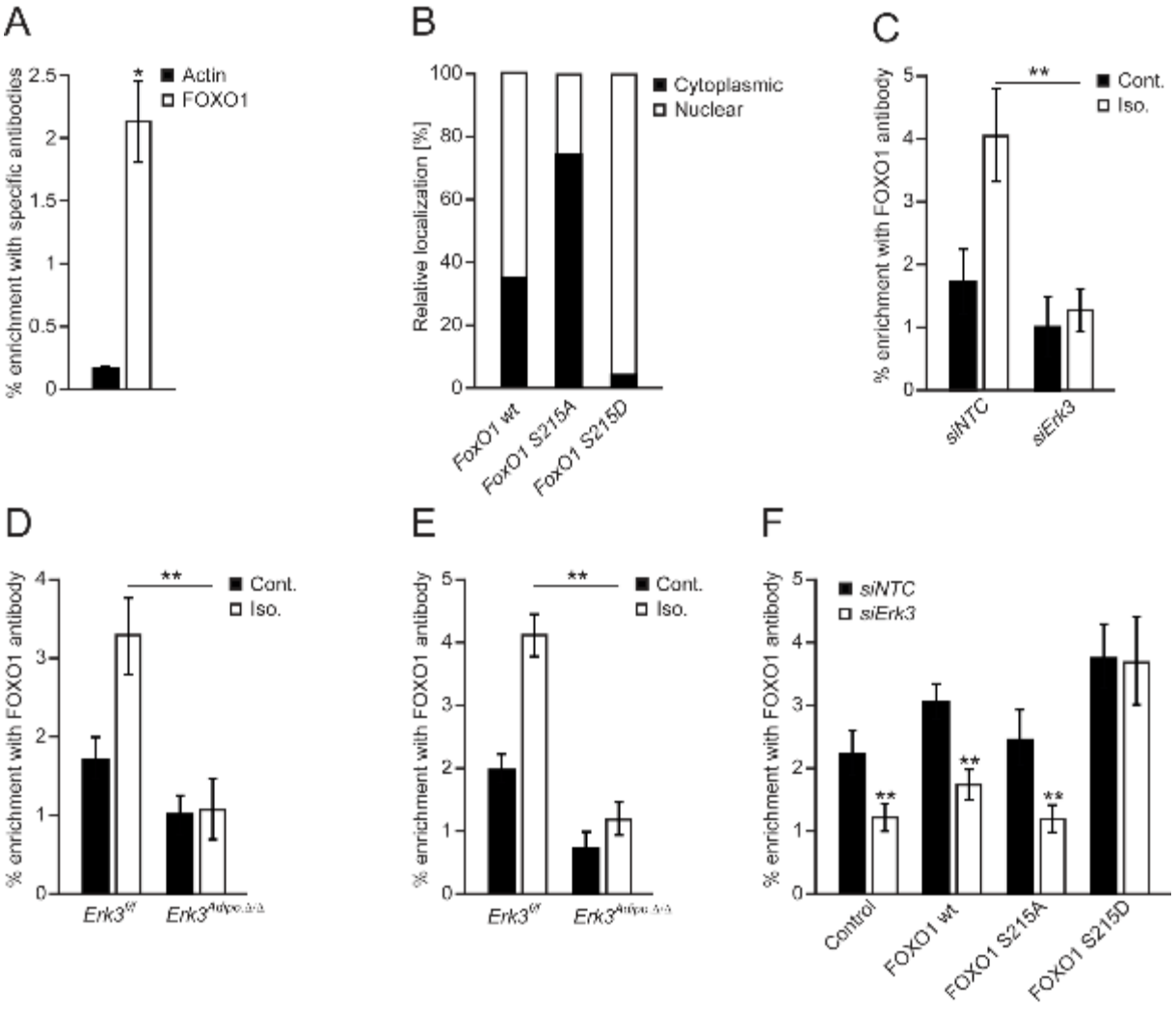

Figure 28. ERK3/MK5 promotes FOXO1-mediated transcription of *Atgl*.

(A) Chromatin immunoprecipitation of *Atgl* promoter using FOXO1 and actin antibody from 3T3L1. (B) Relative localization of indicated FOXO1 mutants in the cytoplasmic and nuclear fraction of the adipocytes. (C) Chromatin immunoprecipitation of *Atg*l promoter using FOXO1 antibody from 3T3L1 cells transfected with *Erk3* or NTC siRNA, (D) SVC-derived subcutaneous adipocytes and (E) SVC-derived brown adipocytes, stimulated for 2h as shown, or (F) overexpressing specific FOXO1 mutants.

6.5 ERK3 regulates β-adrenergic induced lipolysis in adipose tissue and adaptive thermogenesis

6.5.1 Murine adipose tissue requires ERK3 to perform lipolysis.

ERK3 is a constitutively active kinase (Coulombe, Rodier et al. 2003, Coulombe, Rodier et al. 2004) whose abundance is regulated during tissues and tumor development. Consistently, ERK3 was shown to be implicated in lung development and carcinogenesis (Klinger, Turgeon et al. 2009, Long, Foulds et al. 2012). However, its role in adipose tissue has been previously

poorly investigated. Under physiological conditions, the body primarily responds to food deprivation by the increase of the secretion of stress hormones (catecholamines), thereby initiating a lipolytic response in adipose tissue depots. Taken together with the induced stability of ERK3 upon β-adrenergic stimulation we were then interested to investigate the role of ERK3 *in vivo*. Consistently, we found that elevated levels of ERK3 protein in epi-gonadal white adipose tissue (EpiWAT) as well as in brown adipose tissue (BAT) of mice subjected to short-term fasting (Figure 29 A, B). On the other hand, pharmacological induction of β-adrenergic stimulation following an intraperitoneal injection of a specific β3 agonist (CL316,253) in mice, led to an increase of ERK3 protein levels in EpiWAT of CL injected mice, compared with mice injected with a vehicle (saline) (Figure 29C). These data suggest that ERK3 is highly involved in driving the lipolysis rate under physiological conditions.

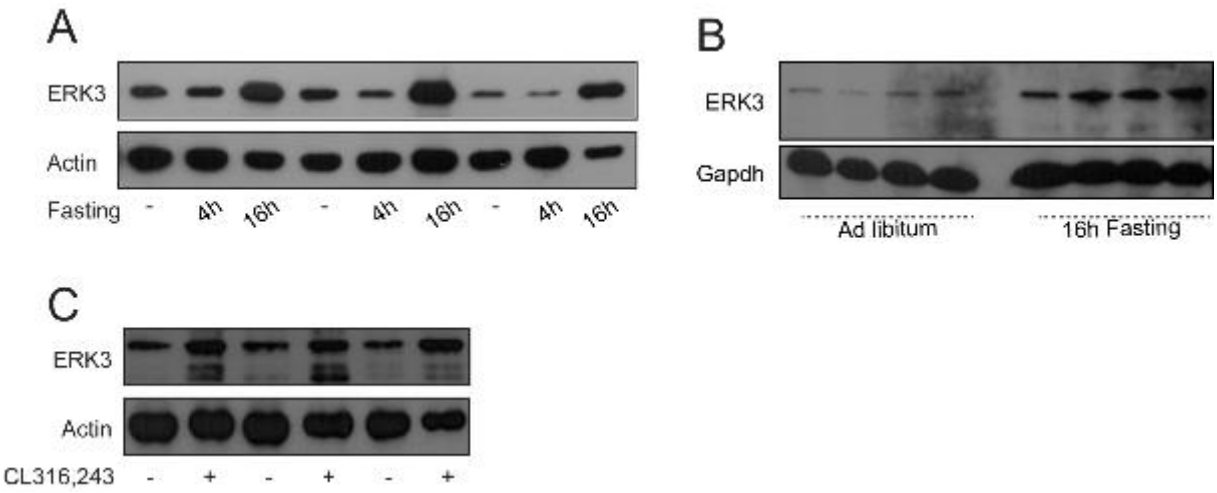

Figure 29. ERK3 regulation in mice adipose tissue.

(A) ERK3 protein levels in EpiWAT of mice fasted for indicated time points (n=3). (B) ERK3 protein levels in BAT of mice fasted for indicated time points (n=4) (C) ERK3 levels in mice injected with β-agonist CL316243 or vehicle control (n=3).

To obtain close mechanistic insights on ERK3 regulation in vivo especially in response to lipolysis stimuli in the adipose tissue we generated mice with conditional knockout of *Erk3*. At first, we crossed *Erk3* floxed mice (Figure 30A) with the adiponectin Cre mice line to generate mice deficient for *Erk3* specifically in adipocytes (explained in the methods section). First, we verified the deletion efficiency and specificity at the protein level. Our western blot analysis revealed the ubiquitous distribution of ERK3 protein in all tested organs while showing the highest abundance levels in the adipose tissue (Figure 24A). Importantly, adipose tissues

isolated from *Erk3*$^{Adipo.\Delta/\Delta}$ mice, carrying the genetic deletion of *Erk3* specifically in adipocytes, showed an efficient deletion of ERK3 protein in the adipose tissue (EpiWAT, SubWAT, and BAT) (Figure 30B).

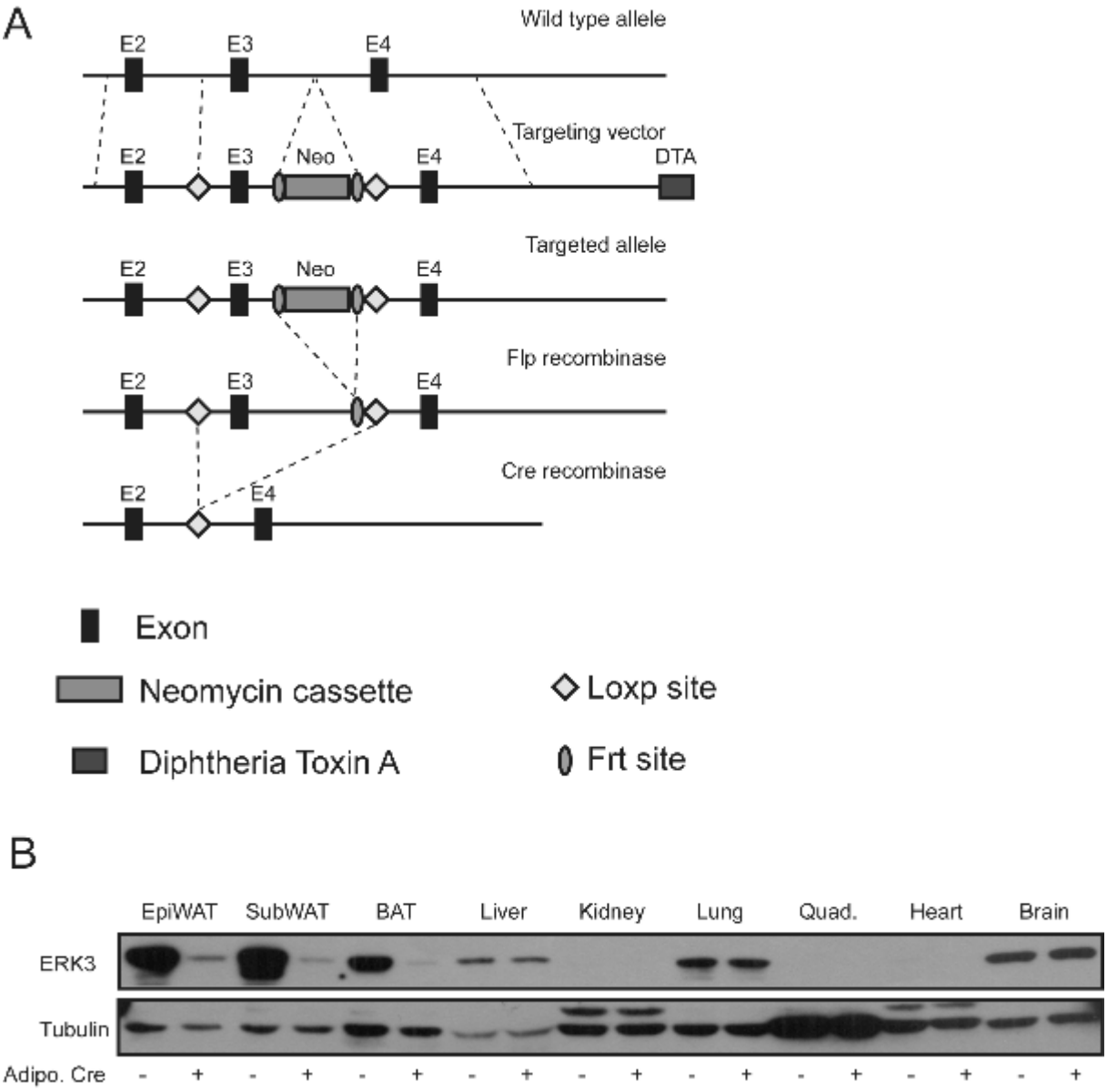

Figure 30. Generation of mice deficient for ERK3 specifically in adipocytes.

(A) Schematic representation of the targeting strategy for the generation of *Erk3*-deficient mice. (B) WB confirming specific deletion of *Erk3* in different adipose tissue depots of *Erk3*$^{Adipo.\Delta/\Delta}$ mice (n=3).

Consistently with our previous results obtained *in vitro*, FFAs and glycerol levels were highly attenuated in the blood of *Erk3*$^{Adipo.\Delta/\Delta}$ mice following β3-agonist stimulation as compared to

their control animals *Erk3*$^{f/f}$ (Figure 31 A, B). Thus, ERK3 is required for stimulation-induced lipolysis in adipocytes in animals.

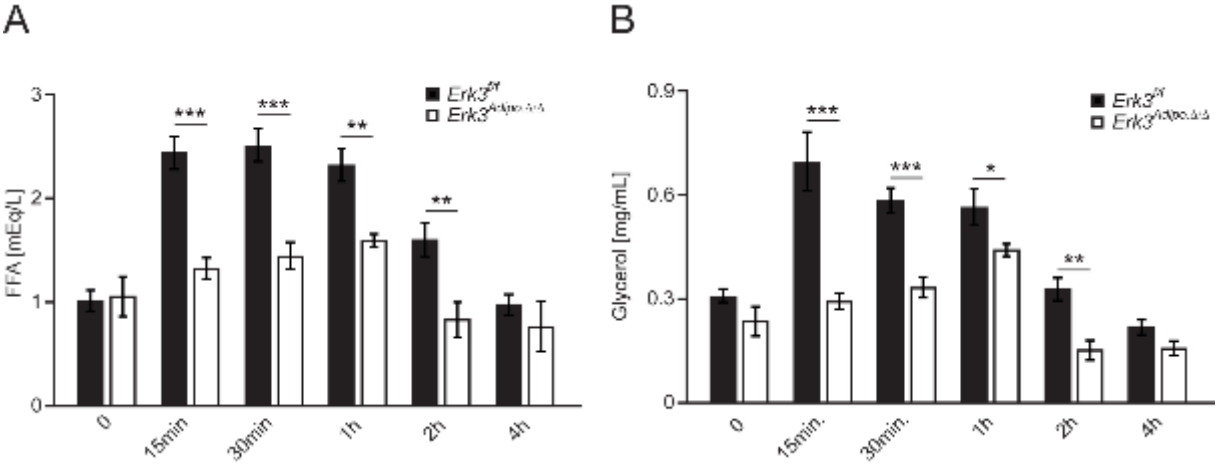

Figure 31. **ERK3 promotes lipolysis in-vivo**.

(A, B) FFAs and Glycerol release in circulation respectively after injection of β-agonist (CL316243) for indicated time in mice with adipocyte-specific deletion of *Erk3* (*Erk3*$^{Adipo.\Delta/\Delta}$) or control animals (*Erk3*$^{f/f}$) (n=6). Data presented as average +/- SEM, * P≤0.05 ** P≤0.01, *** P≤0.001.

Furthermore, based on our *in vitro* data, we investigated through mechanistic approaches, the classical lipolytic pathway that could be altered by the depletion of Ekr3 in adipocytes. The knockdown of *Erk3* in adipose tissue resulted in decreased *Atgl* transcription as well as the translated proteins level (Figure 32A, B). Moreover, the deletion of *Erk3* in adipose tissue also leads to a decrease in the abundance of MK5 protein (Figure 32C). Thus, ERK3 is required for lipolysis in adipocytes *in vitro* and *in vivo*.

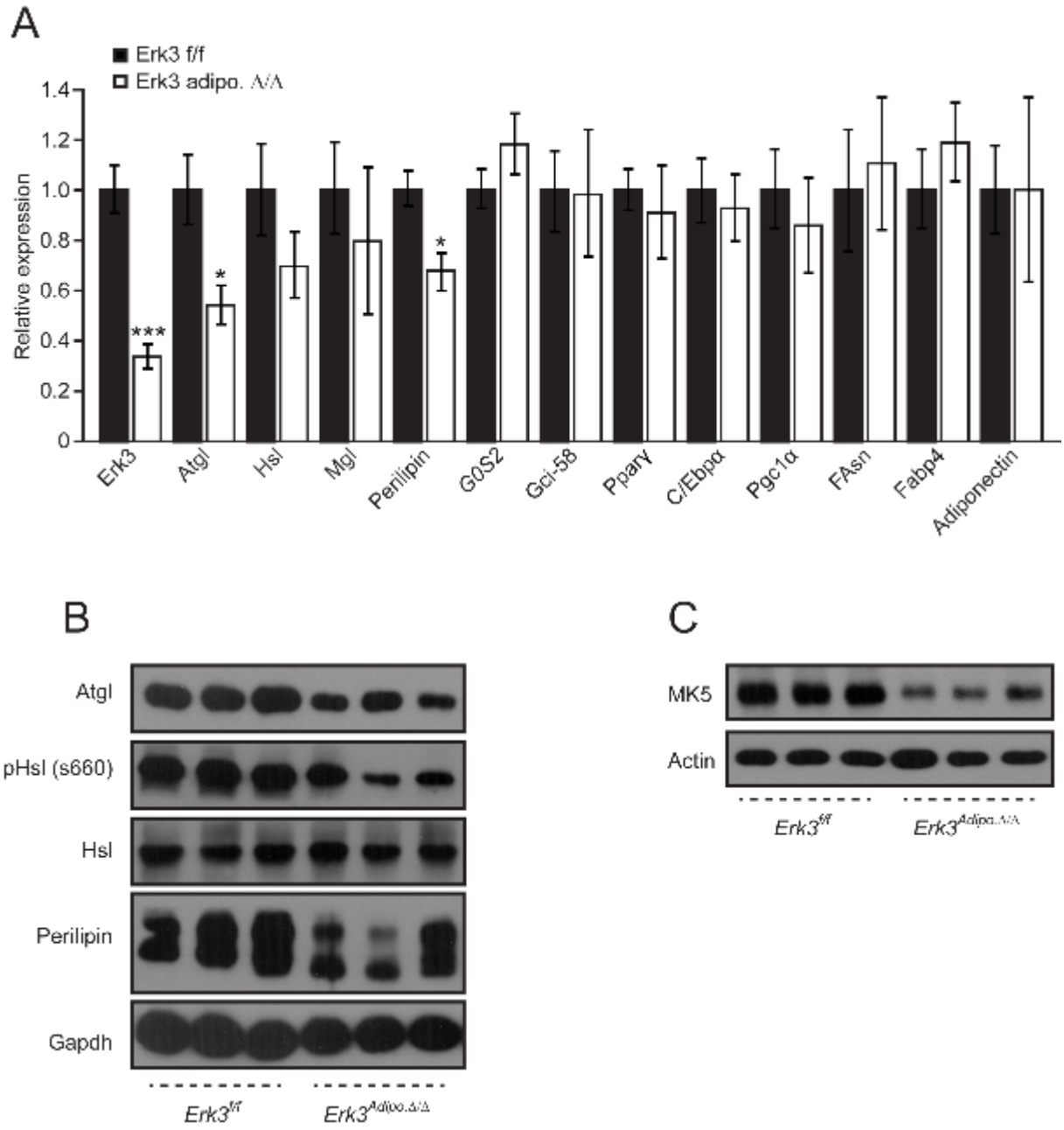

Figure 32. *Erk3* deletion in adipocytes alters the mice's major adipocyte functional genes.

(A) Relative expression of indicated genes in mice adipose tissue with adipocyte-specific deletion of *Erk3* (*Erk3*$^{\Delta adipo.\Delta/\Delta}$) or control animals (*Erk3*$^{f/f}$) (n=6). (B, C) WB analysis of indicated proteins in mice adipose tissue with adipocyte-specific deletion of *Erk3* (*Erk3*$^{\Delta adipo.\Delta/\Delta}$) or control animals (*Erk3*$^{f/f}$) (n=6). For graphs, data presented as average +/- SEM, * P≤0.05, *** P≤0.001.

6.5.2 Deletion of ERK3 protects against diet-induced obesity and enhanced metabolic fitness

Obesity contributes to numerous systemic diseases, reduces the quality of life, and shortens life expectancy (Kalyani, Corriere et al. 2014). Taking together our presented results linking ERK3 to the beta-adrenergic induced lipolysis trough MK5/ FOXO1/*Atgl*. Next, we decided to test the impact of ERK3 on the development of obesity and diabetes *in vivo*. The body weight development of indicated mice was monitored over a period of 14 weeks while fed Ad. libitum a normal chow diet (ND). *Erk3*$^{Adipo.\Delta/\Delta}$ mice presented similar body weight gain as their corresponding control animals (Figure 33).

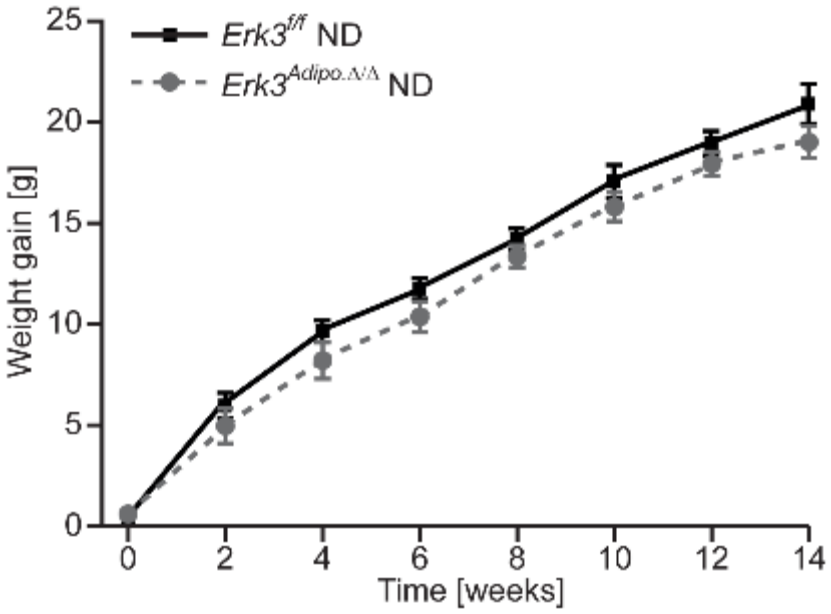

Figure 33. Deletion of *Erk3* in adipocytes effects on body weight gain in mice on ND.

Bodyweight evolution on *Erk3*$^{Adipo.\Delta/\Delta}$ and *Erk3*$^{f/f}$ mice fed a normal diet (ND) (n=8). Data presented as average +/- SEM.

Measurement of body mass composition is an important factor to consider in the fields of obesity and diabetes. Using nuclear magnetic resonance (NMR) technique, we were able to rapidly acquire distinct measurements of fat mass, lean mass, and fluids in a noninvasive method and without the use of anesthetics. Thus, after using NMR to examine *Erk3*$^{Adipo.\Delta/\Delta}$ mice as well as their controls; we did not notice any major difference between both genotypes regarding the total body fat and lean mass (Figure 34A, B). Additionally, there was also no major difference in the organ weight of major tested organs (Figure 34C).

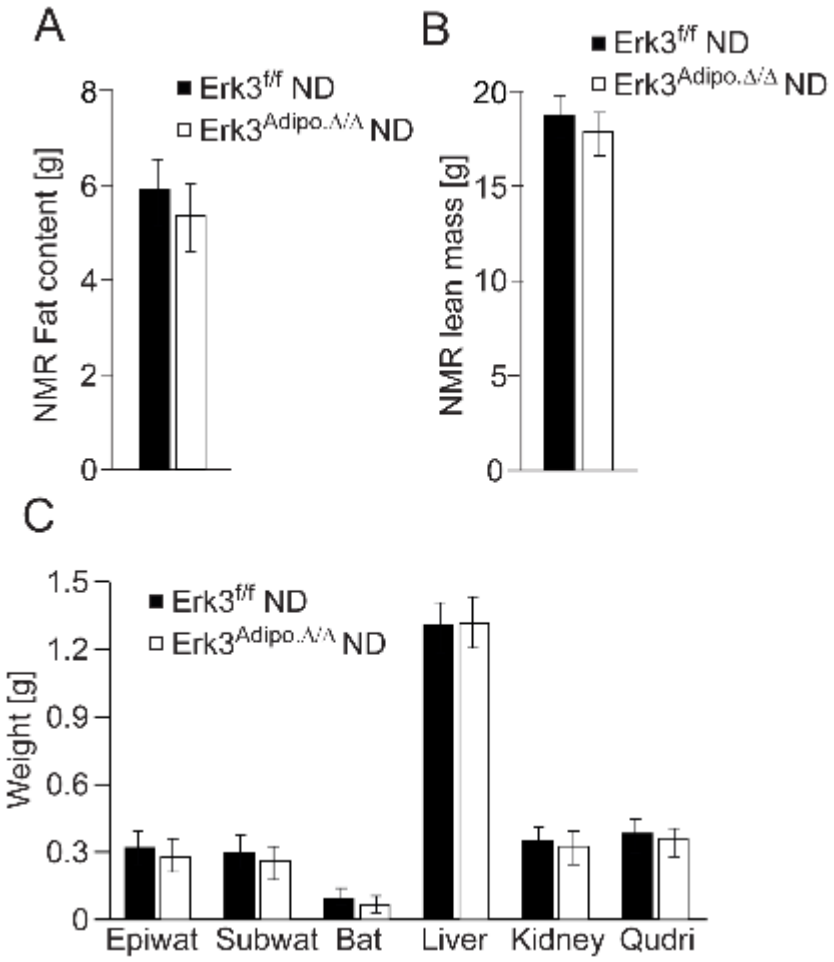

Figure 34. Effect of *Erk3* deletion in mice adipocytes on their body composition.

(A) NMR analysis of mice with *Erk3* deletion in mice adipocytes and their controls showing fat content, (B) lean mass, after 14 weeks of ND feeding. (C) organ weight of mice with *Erk3* deletion in mice adipocytes and their controls. N=8, data presented as average +/- SEM.

However, after applying the glucose tolerance test (GTT), we noticed a significant metabolic improvement in the fasting glucose level in $Erk3^{Adipo.\Delta/\Delta}$ mice compared to their respective controls $Erk3^{f/f}$ mice (Figure 25A). However, after administrating each mouse with a respective dose of glucose, we did not notice any change in the average glucose clearance ability from the circulation when values were normalized to the initial fasting glucose of each mouse (Figure 35B). The systematic response of peripheral organs to insulin stimulation was also assessed by an inulin tolerance test (ITT). Similarly, fasting glucose showed an improvement in $Erk3^{Adipo.\Delta/\Delta}$ mice, while the normalized insulin sensitivity was not altered between the genotypes. (Figure 35B). Hence, these data suggest a mild improvement in fasting glucose of $Erk3^{Adipo.\Delta/\Delta}$ mice, however, a metabolic challenge is needed to further access any effect of ERK3 on the general metabolic fitness.

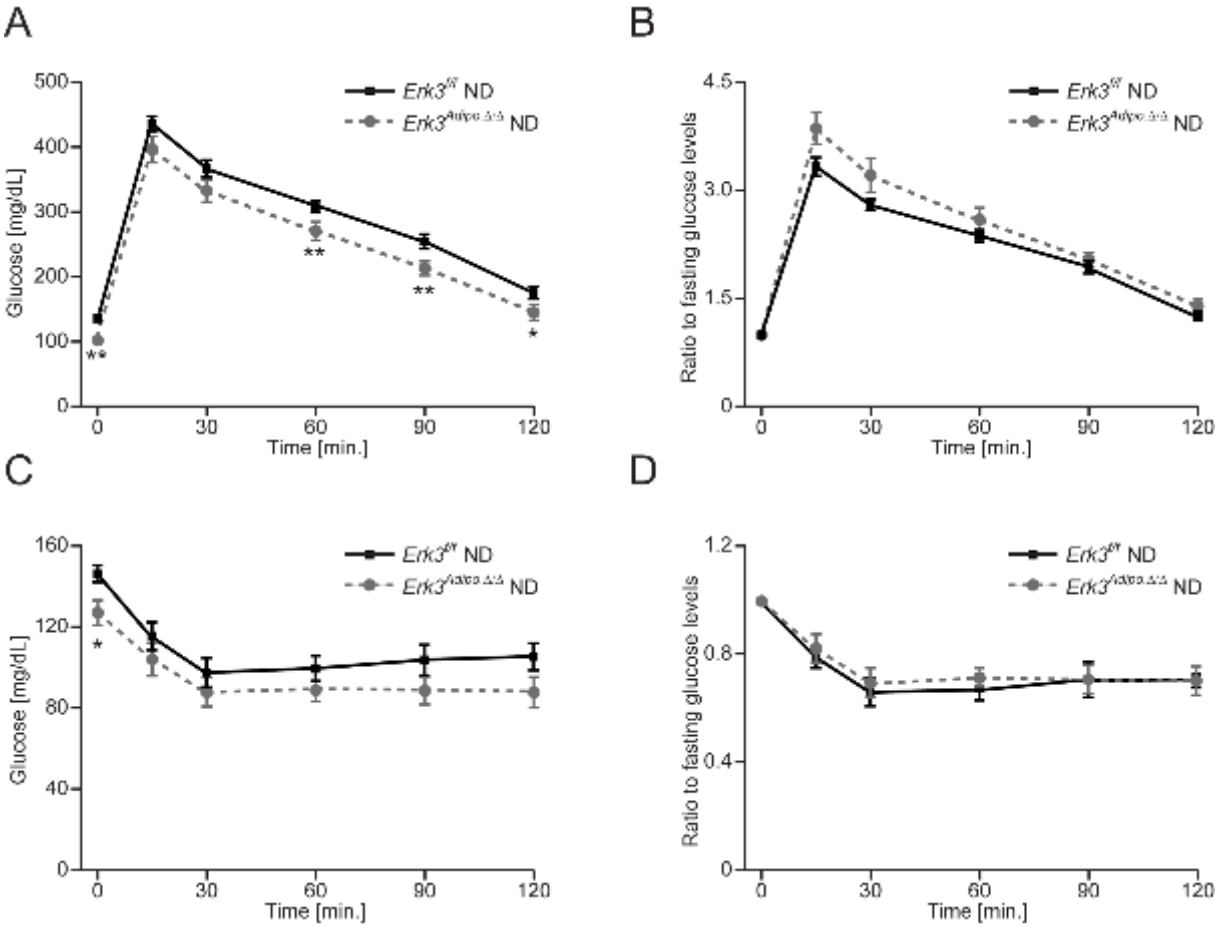

Figure 35. Glucose tolerance and insulin sensitivity in mice with *Erk3* deletion under ND.

(A, B) Glucose tolerance test and its respective normalization to fasting glucose, (C, D) insulin tolerance test and its respective normalization to fasting glucose, in on $Erk3^{Adipo.\Delta/\Delta}$ and $Erk3^{f/f}$ mice fed a normal diet. Data presented as average +/- SEM, * P≤0.05, ** P≤0.01.

To mimic the pathophysiological mechanisms and metabolic alterations associated with obesity in our mice models, we fed $Erk3^{Adipo.\Delta/\Delta}$ mice together with their control littermates $Erk3^{f/f}$ Ad.libitum with a High-fat diet, thereby providing the mice with 5.21 Kcal per gram or food. In fact, while monitoring the body weight gain over time, both genotypes scored a substantial increase in their body weight gain, indicating signs of obesity. However, $Erk3^{Adipo.\Delta/\Delta}$ mice have gained significantly less weight with respect to their control mice. Moreover, these data suggest that the depletion of *Erk3* specifically in adipocytes protected these mice from HFD induced obesity (Figure 36).

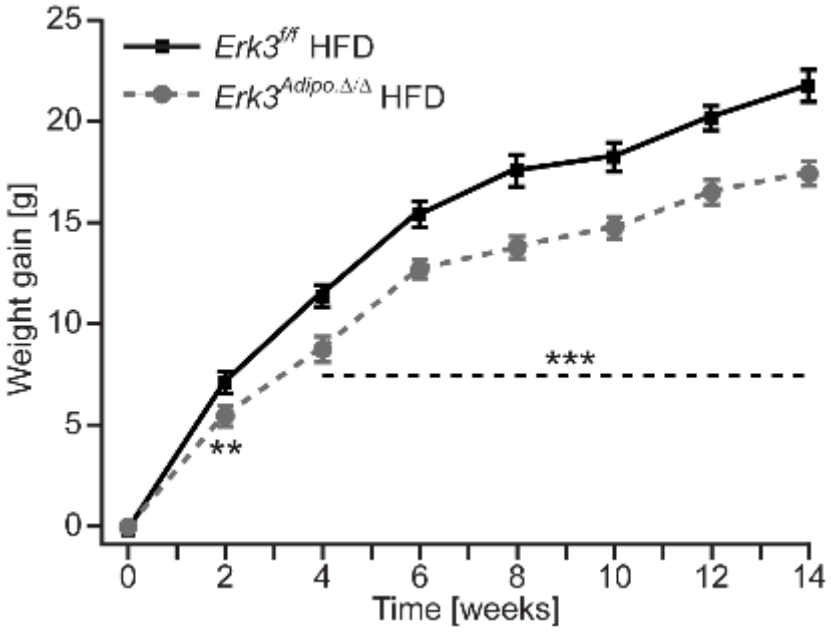

Figure 36. **Deletion of *Erk3* in adipocytes effects on body weight gain in mice on a high-fat diet.**

Bodyweight evolution on *Erk3*$^{Adipo.\Delta/\Delta}$ and *Erk3*$^{f/f}$ mice fed a high-fat diet (HFD) (n=11). Data presented as average +/- SEM, ** P≤0.01, *** P≤0.001.

Moreover, *Erk3*$^{Adipo.\Delta/\Delta}$ mice, under an HFD, showed an enhanced ability to efficiently clear injected glucose from their circulation after being challenged with a defined dose of glucose as compared to their respective controls (Figure 37A, B). This metabolic improvement was further defined in *Erk3*$^{Adipo.\Delta/\Delta}$ mice from their general fasting blood glucose levels (Figure 37C) and a clear trend of improvement in their sensitivity to insulin stimulation when challenged under the experimental conditions of an Insulin tolerance test. (Figure 37D).

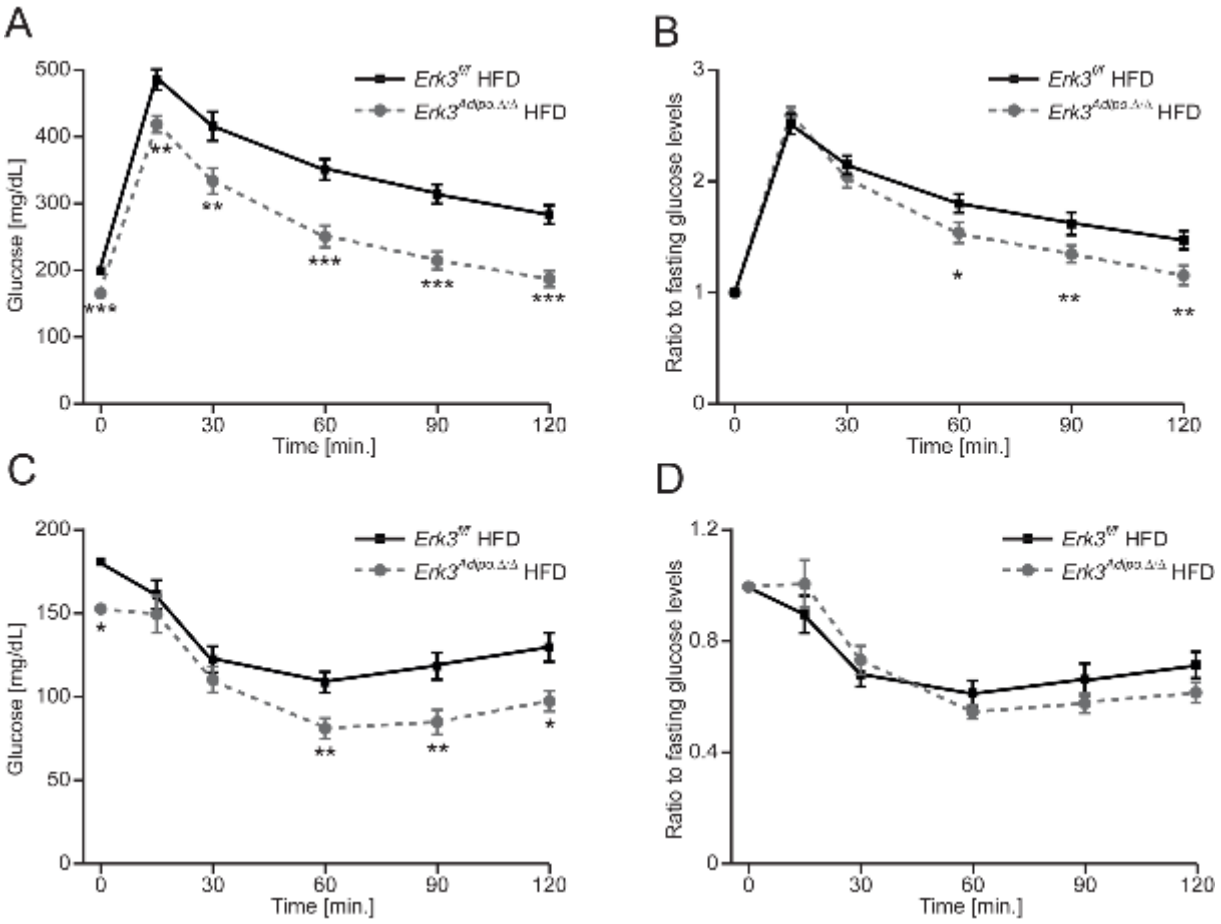

Figure 37. Glucose tolerance and insulin sensitivity in mice with *Erk3* deletion under a High-fat diet.

(A, B) Glucose tolerance test and its respective normalization to fasting glucose, (C, D) insulin tolerance test and its respective normalization to fasting glucose, in on $Erk3^{Adipo.\Delta/\Delta}$ and $Erk3^{f/f}$ mice fed a normal diet. Data presented as average +/- SEM, * P≤0.05, ** P≤0.01.

Furthermore, analysis of body composition using NMR detected reduced fat mass in $Erk3^{Adipo.\Delta/\Delta}$ under HFD feeding (Figure 38A, B). Detailed analysis of isolated organ weight revealed a smaller mass of major adipocytes depots (EpiWat, SubWat, and BAT) (Figure 38C).

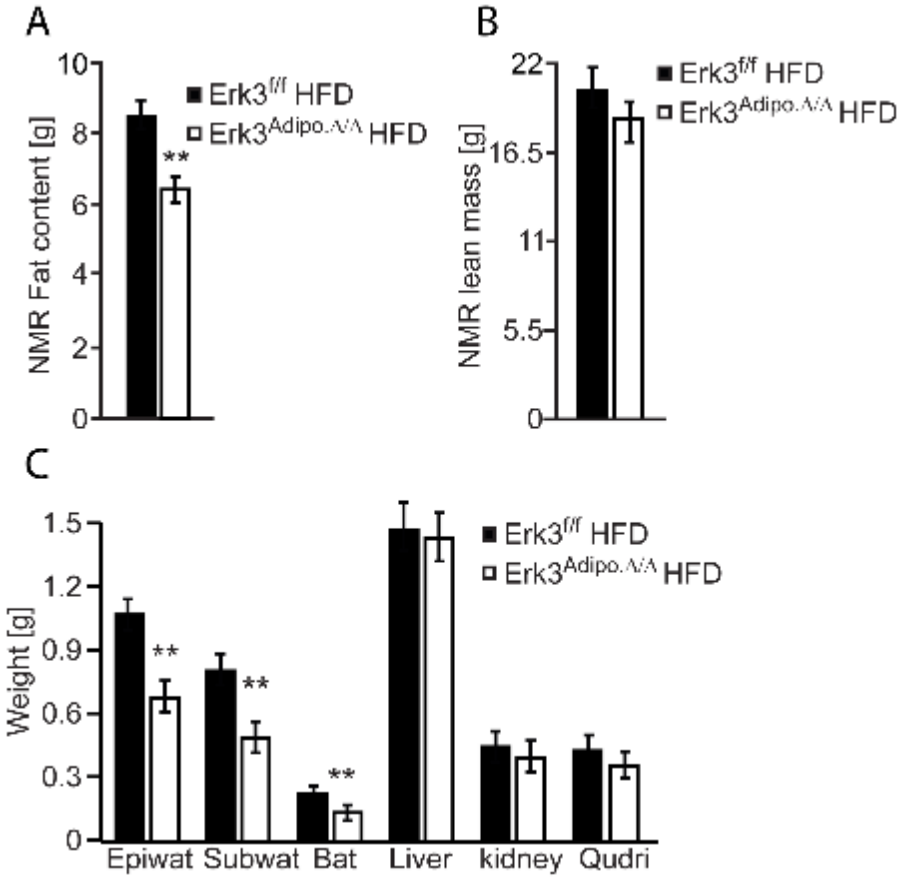

Figure 38. Effect of *Erk3* deletion in mice adipocytes on their body composition.

(A) NMR analysis of mice with *Erk3* deletion in mice adipocytes and their controls showing fat content, (B) lean mass, after 14 weeks of ND feeding. (C) organ weight of mice with *Erk3* deletion in mice adipocytes and their controls. N=11, data presented as average +/- SEM. * P≤0.05, ** P≤0.01.

Histological analysis of subcutaneous white adipose tissue revealed a large reduction in adipocytes size (Figure 39A), which was further quantified using a semi-automated imaging software (Figure 39B). Moreover, a careful observation also shed the light on the appearance of multilocular cells within subcutaneous adipose tissue (SubWAT) of *Erk3*$^{Adipo.\Delta/\Delta}$ (Figure 39A), suggesting a so-called "beige phenotype". Histological analysis of the brown adipose depots also showed a large tendency of less fat accumulation within the brown adipocytes (Figure 39C). These findings render us further attention and investigations in the metabolic phenotype of *Erk3*$^{Adipo.\Delta/\Delta}$ mice.

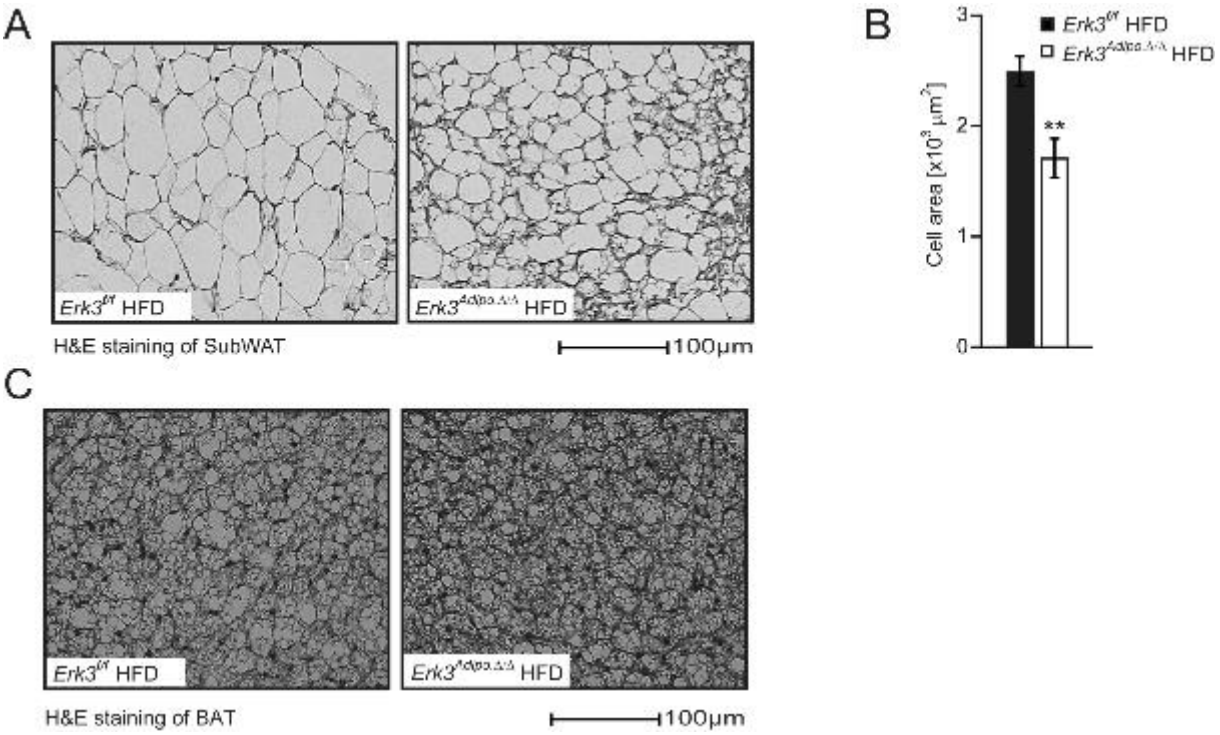

Figure 39. The deletion of *Erk3* decreases overall adipocyte size in mice fed HFD.

(A) Representative H&E staining of (A) SubWAT and (C) BAT, from *Erk3*$^{Adipo.\Delta/\Delta}$ and control mice, fed HFD. (B) Average adipocytes size was analyzed using the ImageJ software. Data are presented as mean ± SEM (n=8/genotype) ** P≤0.01.

Mechanistically, the lowered lipolysis in *Erk3*$^{Adipo.\Delta/\Delta}$ mice was caused by a reduced lipolytic activity because of impaired *Atgl* expression. A rising number of reports linked reducing ATGL action with the protection against obesity and diabetes by mechanisms that are not fully elucidated (Haemmerle, Lass et al. 2006, Arner and Langin 2014, Schreiber, Hofer et al. 2015). Moreover, FOXO1 promotes differentiation of adipocytes and suppresses the expression of uncoupling protein 1 (UCP1), which drives energy expenditure and therefore counteracts lipid accumulation (Nakae, Kitamura et al. 2003, Nakae, Cao et al. 2008, Nakae, Cao et al. 2012, Liu, Tao et al. 2016, Kita, Nakae et al. 2019, Peng, Xiao et al. 2019). Thus, inhibition of ERK3/MK5 signaling, which could be achieved by specific inhibitors, might represent an attractive strategy to ameliorate obesity. Driven by these conclusions, we were interested to investigate the impact of ERK3 in respect to its active metabolic role in the development of obesity. Therefore, we place mice in metabolic cages and monitored their vital signature over a period of time. Indeed, *Erk3*$^{Adipo.\Delta/\Delta}$ mice fed on a normal chow diet revealed a remarkably increased energy expenditure when compared to control animals (Figure 40A), while food intake and voluntary movements were unchanged (Figure 40B, C).

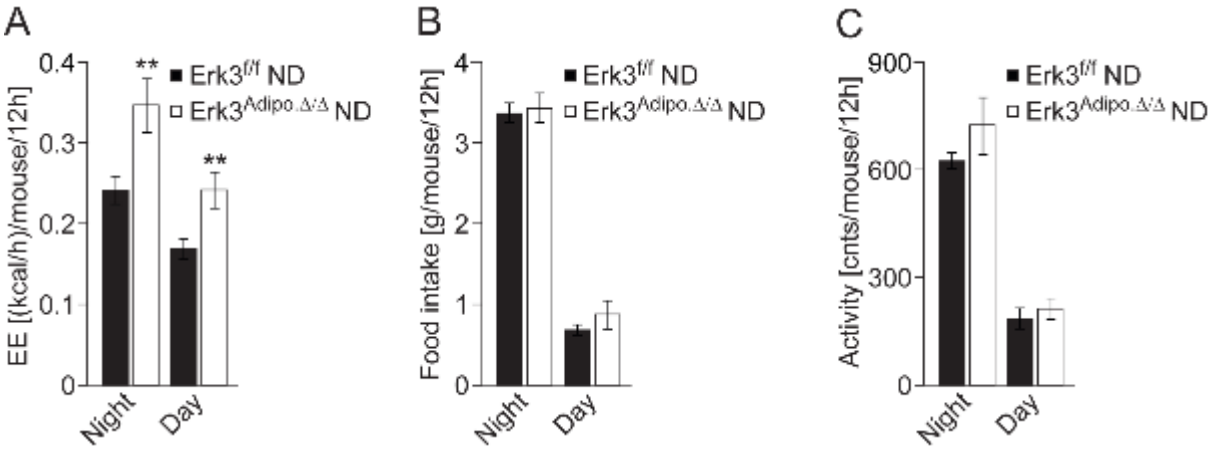

Figure 40. Enhanced energy expenditure in *Erk3*$^{Adipo.\Delta/\Delta}$ fed on ND.

(A) Energy expenditure, (B) food intake and (C) voluntary activity of *Erk3*$^{Adipo.\Delta/\Delta}$ *and Erk3*$^{f/f}$ mice fed on normal chow diet. (n=8). Data presented as average +/- SEM. ** P≤0.01.

These phenotypes prompted us further to analyze the effect of *Erk3* deletion in adipocytes on energy expenditure under a high-fat diet. Consistently with the previous findings, *Erk3* deletion in obese mice also resulted in higher energy expenditure (Figure 41A) without significantly affecting activity or food intake of these mice (Figure 41B, C).

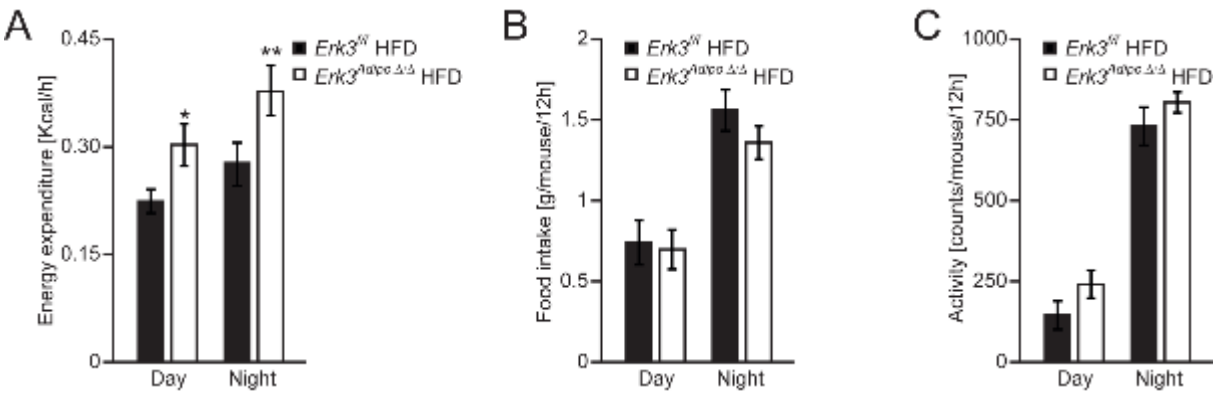

Figure 41. Enhanced energy expenditure in *Erk3*$^{Adipo.\Delta/\Delta}$ fed on an HFD.

(A) Energy expenditure, (B) food intake and (C) voluntary activity of *Erk3*$^{Adipo.\Delta/\Delta}$ *and Erk3*$^{f/f}$ mice fed on normal chow diet. (n=8). Data presented as average +/- SEM. * P≤0.05,** P≤0.01.

Elevated expression of UCP1 in different adipose tissue depots drives the energy dissipation of adipocytes which can increase the energy expenditure of the entire organism and prevent the development of obesity (Kajimura, Spiegelman et al. 2015). In the HFD-fed *Erk3*$^{Adipo.\Delta/\Delta}$ mice, we found increased expression of *Ucp1* and associated thermogenic genes in SubWAT (Figure

42A) and brown adipose tissue (Figure 42B). Consistently, UCP1 protein levels were elevated in SubWAT (Figure 42C).

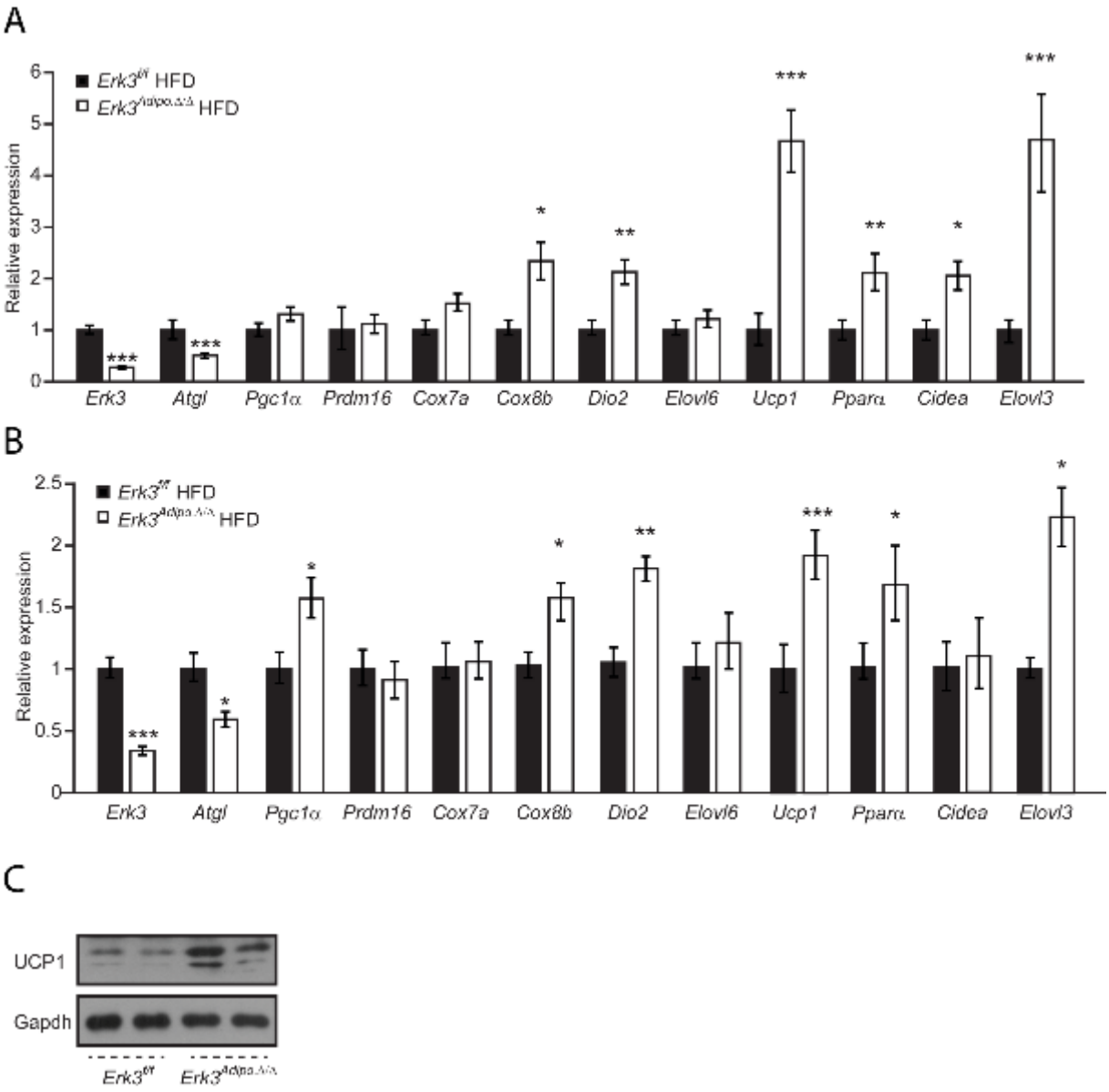

Figure 42. Thermogenic genes induced in *Erk3*$^{Adipo.\Delta/\Delta}$ mice adipose tissue fed on HFD.

(A) Relative expression of indicated thermogenic genes in SubWAT and (B) BAT of *Erk3*$^{Adipo.\Delta/\Delta}$ mice fed HFD. (C) WB analysis of UCP1 in SubWAT of *Erk3*$^{Adipo.\Delta/\Delta}$ mice fed HFD. n=6, for graphs data presented as average +/- SEM. * P≤0.05, P≤0.01, *** P≤0.001.

Moreover, silencing of *Mk5*, *Erk3* or *Foxo1* was sufficient to promote expression of *Ucp1* in 3T3L1-derived adipocytes (Figure 43A) suggesting that ERK3/MK5/FOXO1 axis exerts negative feedback on *Ucp1* expression and presumably energy dissipation by adipocytes. Indeed, isolated primary adipocytes from brown and SubWAT, differentiated and transfected

with the indicated siRNAs also showed the same elevation of *Ucp1* expression level as observed in the cell line (Figure 43B, C). Moreover, depletion of any of either *Erk3*, *Mk5* or *Foxo1* had also a high impact on the expression levels of key thermogenic genes in either primary isolated white adipocytes (Figure 43D) or in primary brown adipocytes (Figure 43E).

Next, we were interested in investigating the effect of *Erk3* deletion on the cellular metabolism of adipocytes. Therefore, we performed a seahorse experiment on primary isolated adipocytes from BAT. Our results indicate an increased oxygen consumption rate and decoupling activity in $Erk3^{Adipo.\Delta/\Delta}$ mice compared to adipocytes isolates from $Erk3^{f/f}$ BAT cells (Figure 37F, G). Thus, depletion of *Erk3* inhibits lipolysis by reducing FOXO1-mediated *Atgl* expression but at the same time promotes *Ucp1* expression and energy dissipation by brown as well as white adipose tissue thereby protecting against obesity and diabetes. Therefore, based on this hypothesis, we verified the binding of FOXO1 to the *Ucp1* promoter in our cellular models. Chip assay on primary isolated adipocytes form SubWat and BAT showed a high binding potential of FOXO1 to the *Ucp1* promoter. Importantly, this binding was significantly attenuated in adipocytes depleted from Erk3 (Figure 43H, I).

FOXO1-dependent suppression of *Ucp1* expression and energy expenditure appears to exert a dominant role over ATGL-dependent lipolysis. In parallel, it was previously shown that the ablation of *Ucp1* induces obesity and abolishes diet-induced thermogenesis, while this is released in mice living at thermoneutrality (Feldmann, Golozoubova et al. 2009). In light of these findings, we housed $Erk3^{Adipo.\Delta/\Delta}$ and $Erk3^{f/f}$ mice under thermal neutral temperate just after weaning and fed them with an HFD Ad. Libitum. Interestingly, even with HFD feeding, mice of both genotypes gained rapid but similar body weight. This indicates that the observed changes in body weight gain and energy dissipation can be abolished under thermo-neutral conditions (Figure 43J).

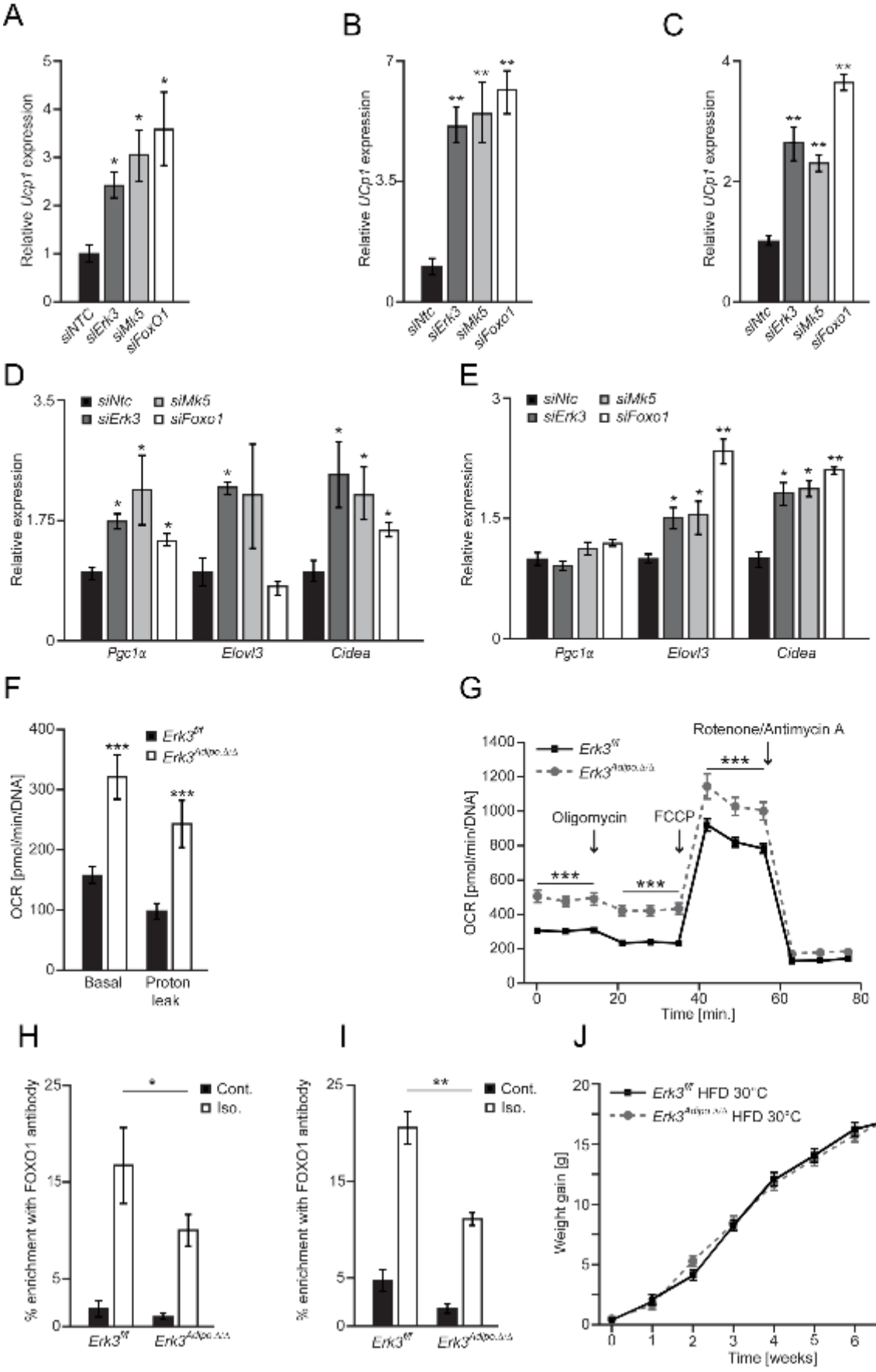
A
Relative Ucp1 expression
siNTC
siErk3
siMk5
siFoxO1
B
Relative UCp1 expression
siNtc
siErk3
siMk5
siFoxo1
C
Relative UCp1 expression
siNtc
siErk3
siMk5
siFoxo1
D
siNtc
siMk5
siErk3
siFoxo1
Relative expression
Pgc1α
Elovl3
Cidea
E
siNtc
siMk5
siErk3
siFoxo1
Relative expression
Pgc1α
Elovl3
Cidea
F
Erk3fl
Erk3Adipo.Δ/Δ
OCR [pmol/min/DNA]
Basal
Proton leak
G
Erk3fl
Erk3Adipo.Δ/Δ
Rotenone/Antimycin A
Oligomycin
FCCP
OCR [pmol/min/DNA]
Time [min.]
H
Cont.
Iso.
% enrichment with FOXO1 antibody
Erk3fl
Erk3Adipo.Δ/Δ
I
Cont.
Iso.
% enrichment with FOXO1 antibody
Erk3fl
Erk3Adipo.Δ/Δ
J
Erk3fl HFD 30°C
Erk3Adipo.Δ/Δ HFD 30°C
Weight gain [g]
Time [weeks]

Figure 43. ERK3/MK5/FOXO1 pathway in adipocytes suppresses energy dissipation and promotes obesity.

(A, B, C) Relative expression of *Ucp1* or indicated siRNAs in differentiated 3T3L1 cells, SubWAT and BAT primary derived adipocytes respectively (n=4). Relative expression of indicated genes in SVC-derived white (D) and brown (E) -derived adipocytes transfected with indicated siRNAs (n=4). (F) Oxygen consumption rate (OCR) in response to indicated substances as well as (C) OCR annotated to the indicated cellular processes in *Erk3*-deficient SVC differentiated into brown adipocytes. (H) Chromatin immunoprecipitation of *Ucp1* promoter using FOXO1 antibody from and SVC-derived brown adipocytes (I) and white adipocytes stimulated for 2h as shown (n=3). Bodyweight evolution of mice with indicated genotypes fed HFD and maintained at thermoneutral conditions n=7. Data presented as average +/- SEM, * P ≤0.05, ** P ≤0.01, *** P ≤0.001.

6.6 Induced inhibition of the ERK3/MK5 pathway improves metabolic fitness

6.6.1 Inactivation of ERK3 in obese mice prevents further body weight gain and improves insulin sensitivity.

Erk3$^{Adipo.\Delta/\Delta}$ mice provided us with the unique experimental model to test the physiological relevance of ERK3 protein in the protection from diet-induced obesity. However, the major limitation was that in this model, lies in the fact that ERK3 was always knocked out in adipocytes throughout the mouse development and growth. To circumvent this limitation; we then tested if the deletion of ERK3 in mice with established obesity can inhibit further body weight gain and improve glycemia. For this purpose, we have crossed *Erk3*$^{f/f}$ with a tamoxifen-inducible adiponectin promoter-driven CRE line (*Erk3*$^{Ind.Adipo.\Delta/\Delta}$) and induced deletion of ERK3 with tamoxifen administration after the development of obesity in mice. After induction of ERK3 deletion in *Erk3*$^{Ind.Adipo.\Delta/\Delta}$ mouse model, we first validated its specific deletion in adipocytes. As observed after western blot analysis, ERK3 been specifically deleted adipocytes while other organs were not affected (Figure 44).

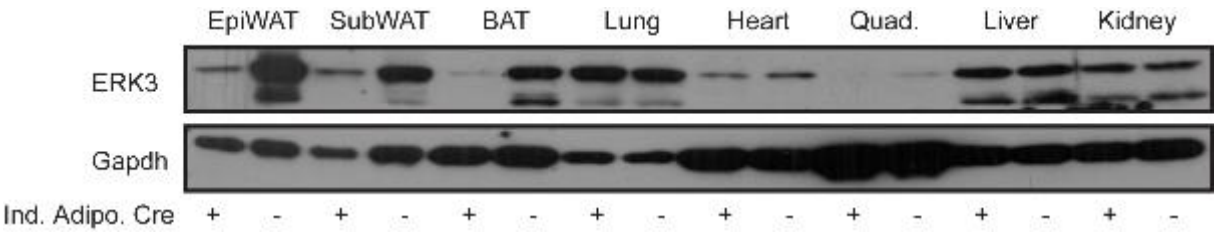

Figure 44. Deletion efficacy of ERK3 in an induced adiponectin-Cre mouse model.

WB analysis of ERK3 in indicated organs isolated from *Erk3*$^{Ind.Adipo.\Delta/\Delta}$ mice and their controls *Erk3*$^{f/f.}$, n=3.

Furthermore, while monitoring body weight development over a period of 9 weeks, mice of both genotypes gained weight equally. However, after the administration of the respective dose of tamoxifen equally to both genotypes, we observed a clear difference in the continuous weight gain development *Erk3*$^{Ind.Adipo.\Delta/\Delta}$ mice did not further gain weight like corresponding control animals (Figure 45).

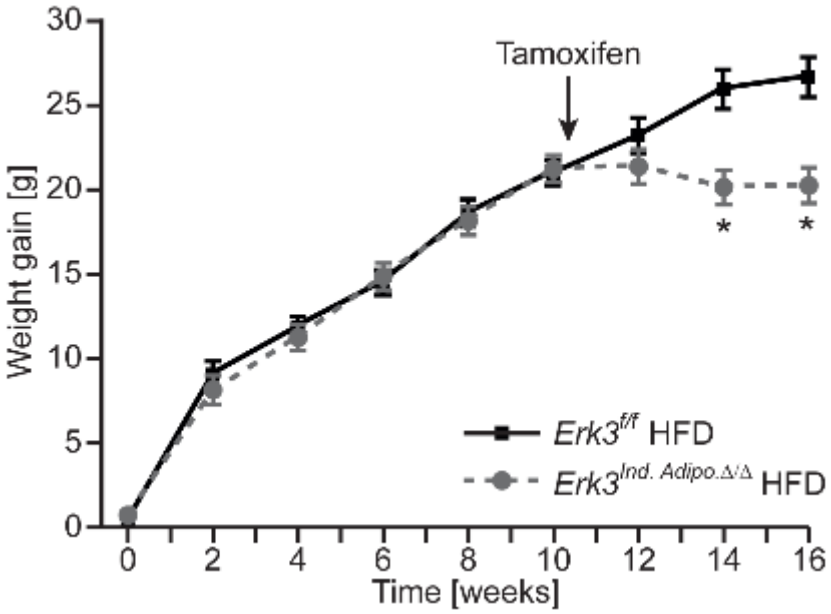

Figure 45. Induced deletion of Ek3 in obese mice improves their resistance to HFD.

Bodyweight evolution on *Erk3*$^{IndAdipo.\Delta/\Delta}$ and *Erk3*$^{f/f}$ mice fed a high-fat diet (HFD) (n=11). Data presented as average +/- SEM, *P≤0.05.

Consistently, adipose tissue of *Erk3*$^{Ind.Adipo.\Delta/\Delta}$ mice were smaller while the weight of other organs was not affected (Figure 46A). Furthermore, NMR monuments also showed a reduction in the total fat mass found in *Erk3*$^{Ind.Adipo.\Delta/\Delta}$ mice compared to their controls (Figure 46B).

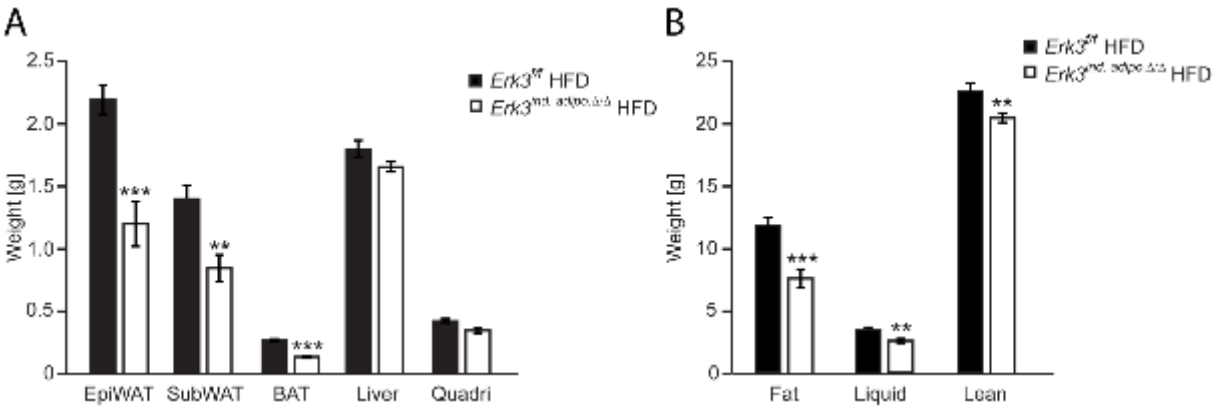

Figure 46. Effects of induced *Erk3* deletion in mice adipocytes on their body composition.

(A) Organ weight of mice with *Erk3* deletion in mice adipocytes and in control animals (B) NMR analysis of mice with induced *Erk3* deletion in mice adipocytes and control animals showing the fat content, lean mass, and body fluids after 16 weeks of HFD feeding. N=8, data presented as average +/- SEM. ** P≤0.01, ** P≤0.001.

We next aimed through histological analysis to compare adipocyte cell size and size distribution from the subcutaneous fat depot and to determine the association of the induced *Erk3* deletion with the observed metabolic profile of $Erk3^{Ind.Adipo.\Delta/\Delta}$ (Figure 47A). Our results indicate an alteration in the size distribution of adipocytes of $Erk3^{Ind.Adipo.\Delta/\Delta}$; we could observe a reduction in the average size of adipocytes (Figure 47B) but more specifically an increase in the fraction of small adipocytes (Figure 47C).

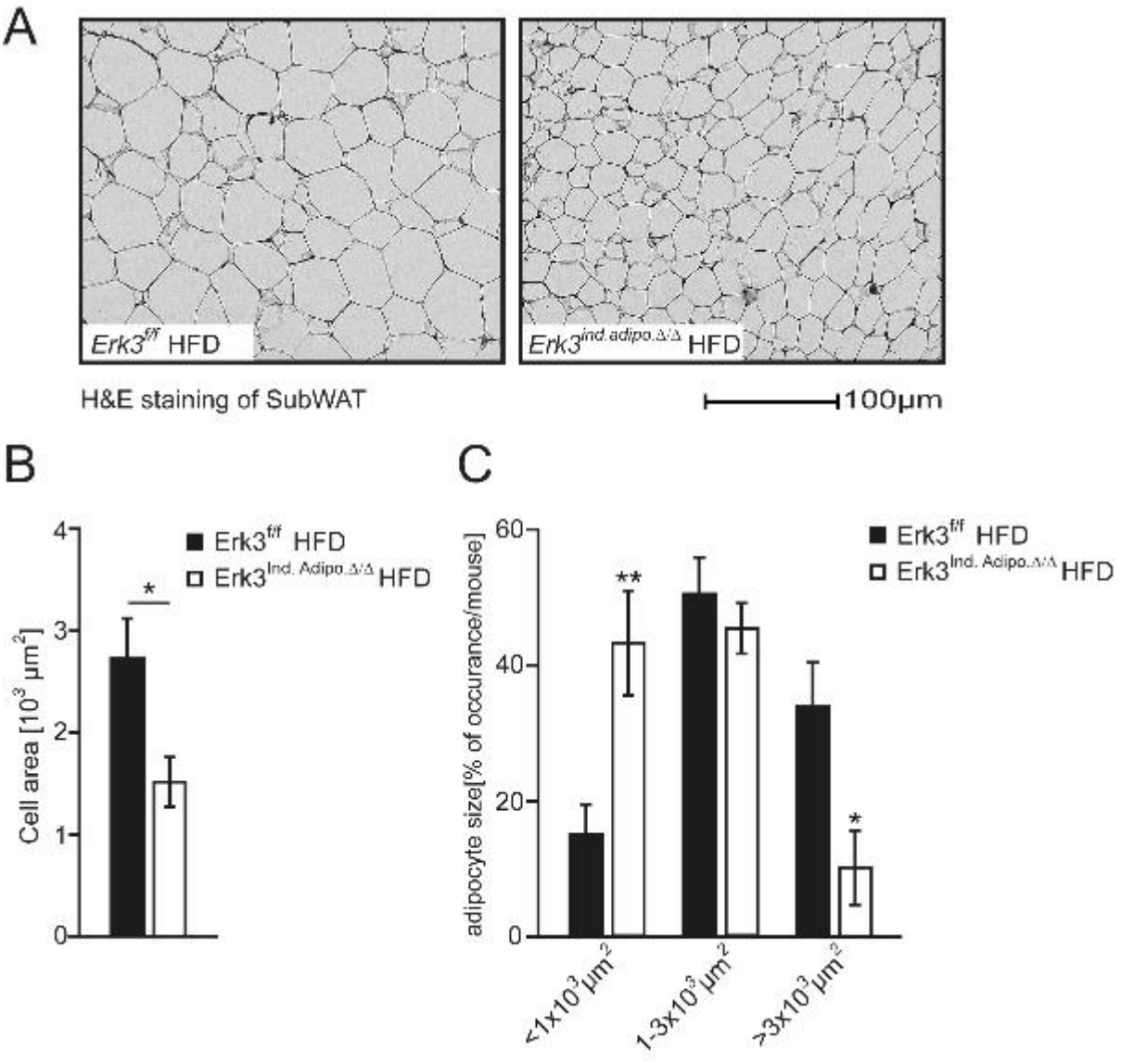

Figure 47. Induced Deletion of ERK3 **decreases overall adipocyte size in mice fed HFD.**

(A) Representative H&E staining of SubWAT and from *Erk3*$^{Ind.Adipo.\Delta/\Delta}$ and control mice fed HFD. (B) Average adipocytes size and (C) size distribution analyzed using the ImageJ software. Data are presented as mean ± SEM (n=8/genotype) ** P≤0.01.

Consistent with previous results, indirect calorimetry analysis also revealed that *Erk3*$^{Ind.Adipo.\Delta/\Delta}$ mice displayed elevated energy expenditure, but the induced deletion of ERK3 in adipocytes did not influence food intake and voluntary movements (Figure 48A-C).

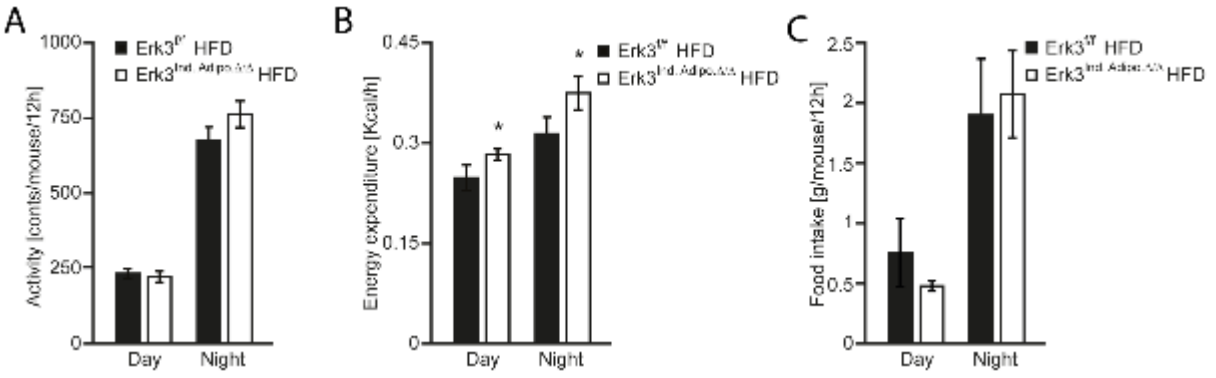

Figure 48. Enhanced energy expenditure in *Erk3*$^{Ind.Adipo.\Delta/\Delta}$ fed on HFD.

(A) Voluntary activity, (B) Energy expenditure and (C) food intake of *Erk3*$^{Ind.Adipo.\Delta/\Delta}$ and *Erk3*$^{f/f}$ mice fed on a high-fat diet. (n=8). Data presented as average +/- SEM. * P≤0.05.

Furthermore, we were interested to investigate whether induced deletion of ERK3 in obese mice could improve in in systemic regulation of glucose homeostasis. Thus, indicated mice were challenged with a glucose tolerance test, for which the fasted mice received a defined dose of glucose and the glucose levels were monitored at defined time points as performed in previous models. Remarkably, induced deletion of ERK3 in obese mice improved glucose tolerance as the glucose concentration in circulation was lowering in these mice at much faster rates than for control mice (Figure 49A). Moreover, we complemented our study with an ITT on the same mice. Importantly, we observed a significant improvement in insulin sensitivity in *Erk3*$^{Ind.Adipo.\Delta/\Delta}$ mice compared to control littermates (Figure 49B). As a response to the insulin challenge, the blood glucose concentrations of mice lacking *Erk3* in adipocytes dropped at much faster rates compared to controls littermates. Together these results indicate that the induction of *Erk3* deletion on obese mice adipocytes was sufficient for mice to increase their sensitivity to insulin and thus clearing glucose faster from circulation.

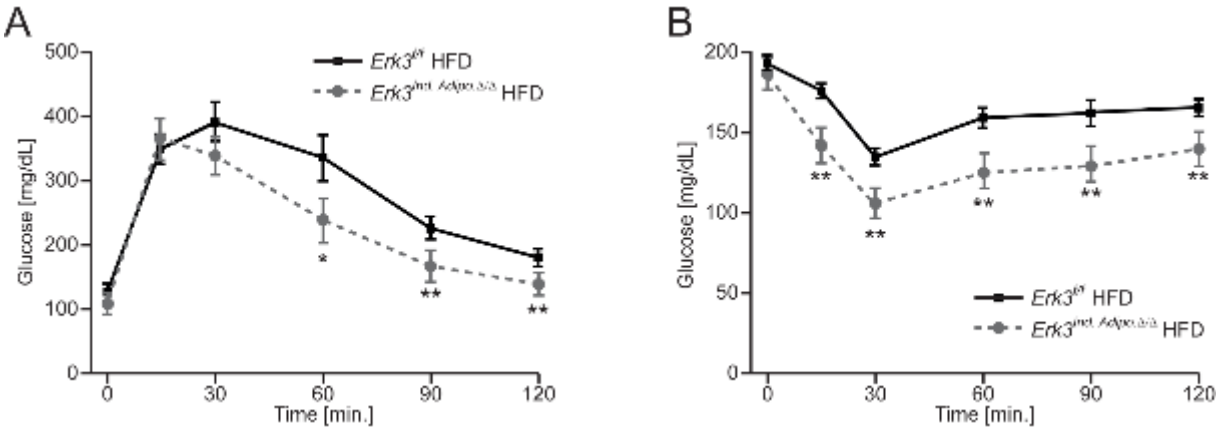

Figure 49. Glucose tolerance and insulin sensitivity in mice with induced *Erk3* deletion under a High-fat diet.

(A) Glucose tolerance and (B) insulin sensitivity of *Erk3*$^{Ind.Adipo.\Delta/\Delta}$ and *Erk3*$^{f/f}$ mice fed on a high-fat diet. (n=8). Data presented as average +/- SEM. * P≤0.05.

6.6.2 Pharmacological inhibition of MK5 improves metabolic fitness.

The genetic approaches used to study the molecular events that govern the development of metabolic syndrome, helped us widen our understanding of the complexity of the disease. As we noted, our transgenic mouse model had shown promising results in the general improvement of the organism's metabolic fitness when challenged with an obesogenic diet. Hence, our data also suggest that the reduction of lipolysis and induction of energy expenditure by the inhibition of ERK3/MK5 activity could be an attractive approach to combat obesity and associated diabetes.

Based on the presented data here, we proceeded with testing a pharmacological approach in inhibiting ERK3/MK5 using MK5 chemical inhibitor (MK5i) GLPG0259 in adult mice as an attempt to reduce induced- lipolysis in response to adrenergic stimulation and further study its metabolic impact on the whole body. This drug has been already approved for the phase II clinical trial for reducing inflammation caused by rheumatoid arthritis (Westhovens, De Keyser et al. 2013), Indeed, one-week of daily oral-administration of MK5i in mice significantly reduced *Atgl* expression level in subcutaneous adipose tissue depots as compared to control mice administered with vehicle only (Figure 50A). Functionally, the treatment of mice with GLPG0259 significantly reduced mice adipose tissue response to β-adrenergic stimulation as observed by the attenuated release of FFAs to the circulation following an intraperitoneal injection of β-adrenergic agonist (CL316243) (Figure 50B). Moreover, the treatment of adult mice with MK5i significantly reduced adipose tissue response to β-adrenergic stimulation as

observed by the attenuated release of FFAs to the circulation (Figure 50B). Furthermore, transcriptional profiling in both adipose tissue depots (SubWAT and BAT) showed a significant increase in major thermogenic genes including *Ucp1* (Figure 50C, D).

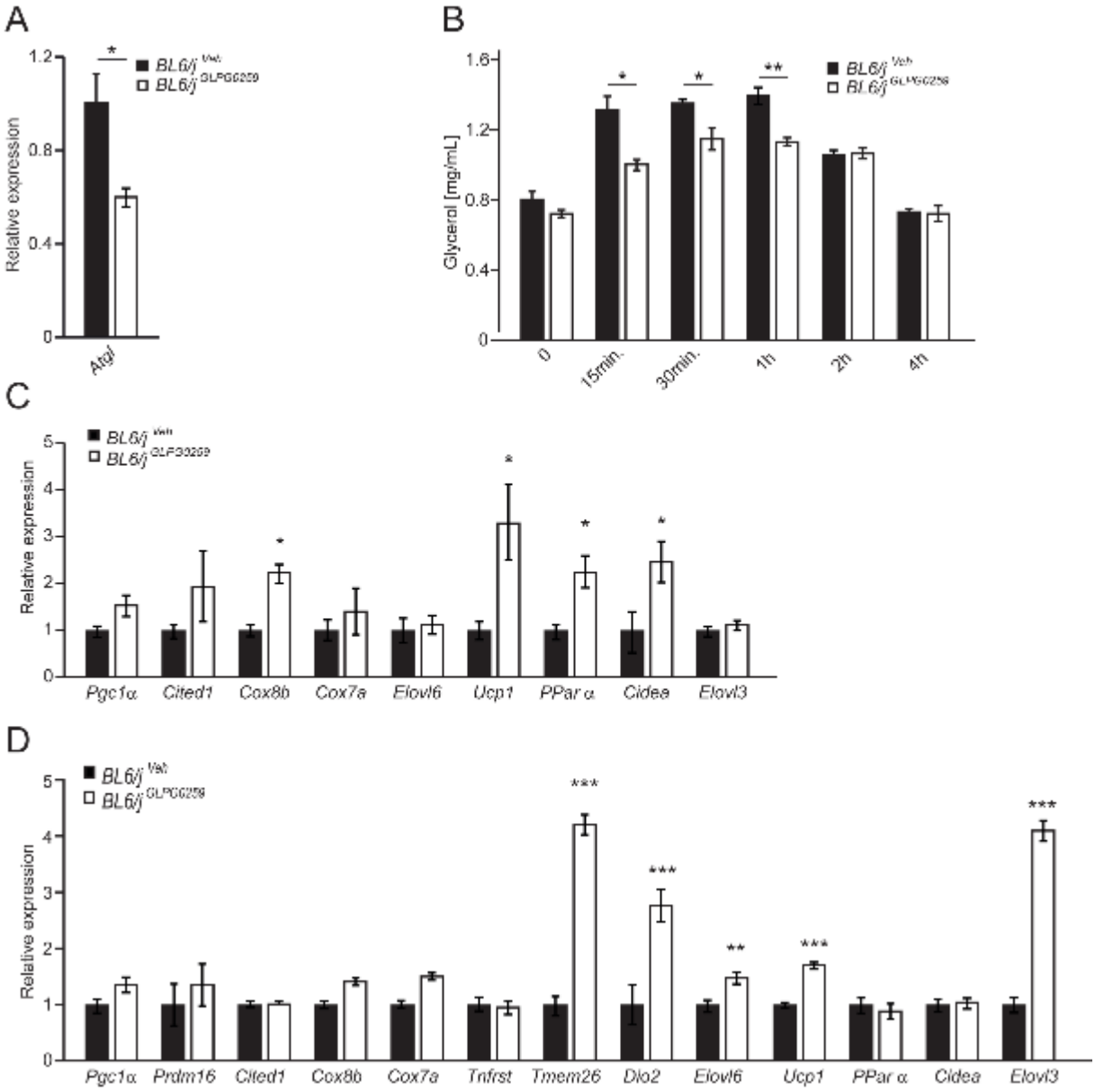

Figure 50. Pharmacological inhibition of MK5 in mice improved thermogenic activity.

(A) Relative expression of *Atgl* in SubWAT from GLPG0259 administered mice and their respective vehicle control mice (n=5). (B) Glycerol released in circulation after injection of β-agonist (CL316243) for indicated times in BL6/J mice that have been orally administered with GLPG0259 inhibitor (10mg/kg) or vehicle control for one consecutive week (n=5). (C, D) Relative expression of indicated genes in the SubWAT and BAT from GLPG0259 administered mice and their respective vehicle control mice (n=5). Data presented as average +/- SEM. * P≤0.05, ** P≤0.01, *** P≤0.01.

6.6.3 Oral treatment of MK5i improved metabolic fitness in obese mice on an HFD

Next, we were interested in further verifying the efficacy of our pharmacological MK5 inhibitor concerning its potential protective effect form diet-induced obesity and possible improvement of the body's metabolic fitness using our diet-induced-obesity mouse model. Therefore, to assess whether MK5i could have a potential protective effect from diet-induced obesity, we started administering mice with a daily oral dose (10 mg/kg) of the inhibitor 9 weeks after initiating the obesogenic diet. Interestingly, during the first 9 weeks, all mice gained similar weight. However, over the time span after inhibitor administration, treated mice gained significantly less body weight as compared to vehicle mice (Figure51).

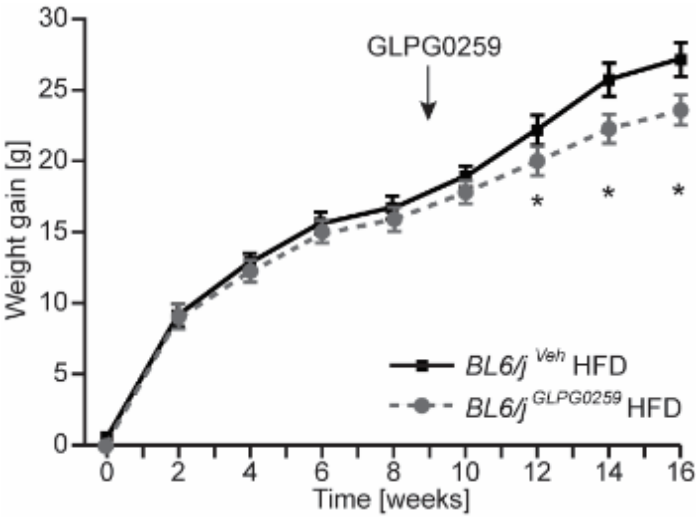

Figure 51. Oral treatment of MK5i reduced body weight gain in obese mice on an HFD.

Bodyweight evolution on BL6/j^{GLPG0259} and wild type BL6/j mice fed on an HFD (n=15). Data presented as average +/- SEM, * P≤0.05.

After a period of continues HFD feeding, the observed reduction in body weight in mice on MK5i was highly due to a decrease in mice adiposity as observed in our NMR analysis which revealed an average reduction of the Fat mass (Figure 52A), whereas lean mass had barely changed (Figure 52A). Furthermore, similar intermediation of these results could be drawn from the average organ weights, which revealed a significant reduction in the weight of EpiWAT, SubWAT and interscapular brown adipose tissue (BAT), while the weight of other tested organs showed no significant change between MK5i administrated animals compared with controls (Figure 51B).

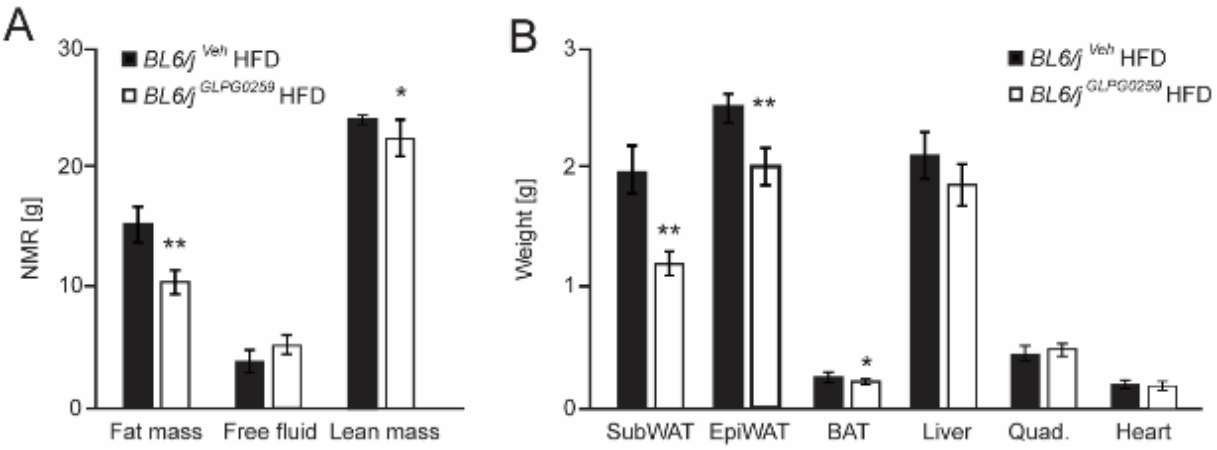

Figure 52. Effect of MK5i oral treatment on the body composition of obese mice.

(A) NMR analysis of on BL6/j^{GLPG0259} and wild type BL6/j mice fed on an HFD showing fat mass, free fluid, and lean mass. (B) Organ weight of indicated organs isolated from BL6/j^{GLPG0259} and wild type BL6/j mice. N= 15, Data presented as average +/- SEM, * P≤0.05, ** P≤0.001.

As serum lipolytic bi-products (FFA and Glycerol) levels are usually highlighted in their association with obesity-related insulin resistance, type 2 diabetes. Next, we tested the impact if MK5i administration on the levels of FFA and glycerol in circulation since they are especially linked to the severity of the metabolic syndrome. Interestingly our results presented a reduction in the circulating FFA and glycerol in their serum of MK5i-treated mice compared to control mice, while both fed HFD *Ad. Libitum* (Figure 53 A, B). Of note, moderate fasting (4 hrs.) displayed reduced levels of FFAs and glycerol in circulation compared to *Ad. Libitum* feeding in both MK5i mice and their control littermates (Figure 53 A, B). These data suggest that MK5i is beneficial for reducing the lipotoxicity associated with a high-fat diet consumption.

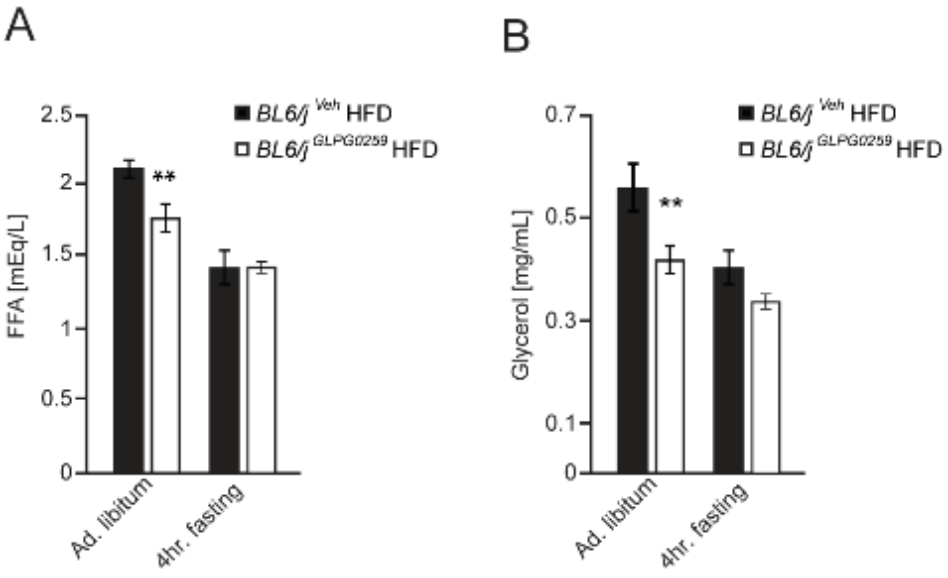

Figure 53. MK5i attenuates induced-lipolysis in-vivo.

(A, B) FFAs and Glycerol levels in the circulation in BL6/j^{GLPG0259} and wild type BL6/j mice fed on an HFD *Ad. Libitum* or fasted for 4 hours. Data presented as average +/- SEM, ** P≤0.001.

As insulin insensitivity presents the hallmark of T2D, we next examined whether MK5i could help in improving insulin sensitivity and glucose tolerance. Indeed, glucose tolerance (Figure 54A) and insulin tolerance tests (Figure 54B) showed an efficient and significant improvement in plasma glucose clearance, after insulin as well as after glucose injection, in HFD-fed MK5i-treated mice compared with their vehicle-treated littermates. Thus, these data indicate a positive effect of MK5i treatment in improving mice insulin sensitivity and glucose tolerance.

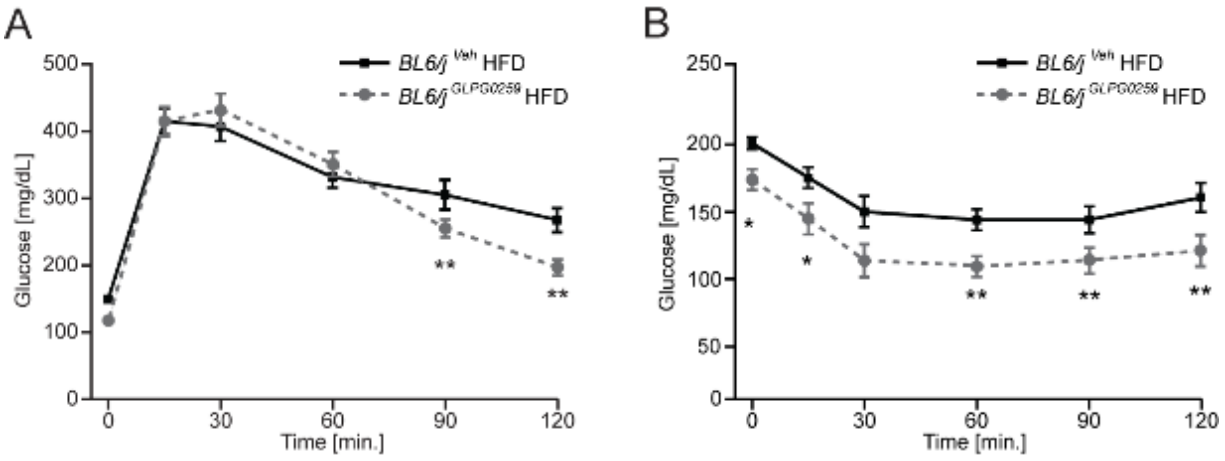

Figure 54. The effect of MK5i oral treatment improves glucose tolerance and insulin sensitivity in obese mice under an HFD.

(A, B) Glucose tolerance test (GTT) and insulin tolerance test (ITT) performed on BL6/j^{GLPG0259} and wild type BL6/j mice fed on an HFD. N=15, Data presented as average +/- SEM, * P≤0.05, ** P≤0.001.

Sympathetic activation of adipose tissue plays an essential role in maintaining energy balance by stimulating lipolysis and promoting energy expenditure (Betz and Enerbäck 2015). We thought to explore the possibility if MK5i may affect energy expenditure in our obese mouse model. Therefore, HFD-fed mice, treated with a continuous daily dose of MK5i, were separated in metabolic cages for indirect calorimetry measurements. Indeed, MK5i-treated mice presented an elevation in their energy expenditure profile as compared to control animals (Figure 55A), while voluntary activity (Figure 55B), food intake (Figure 55C) as well as respiratory exchange rate (Figure 55D) remained unchanged.

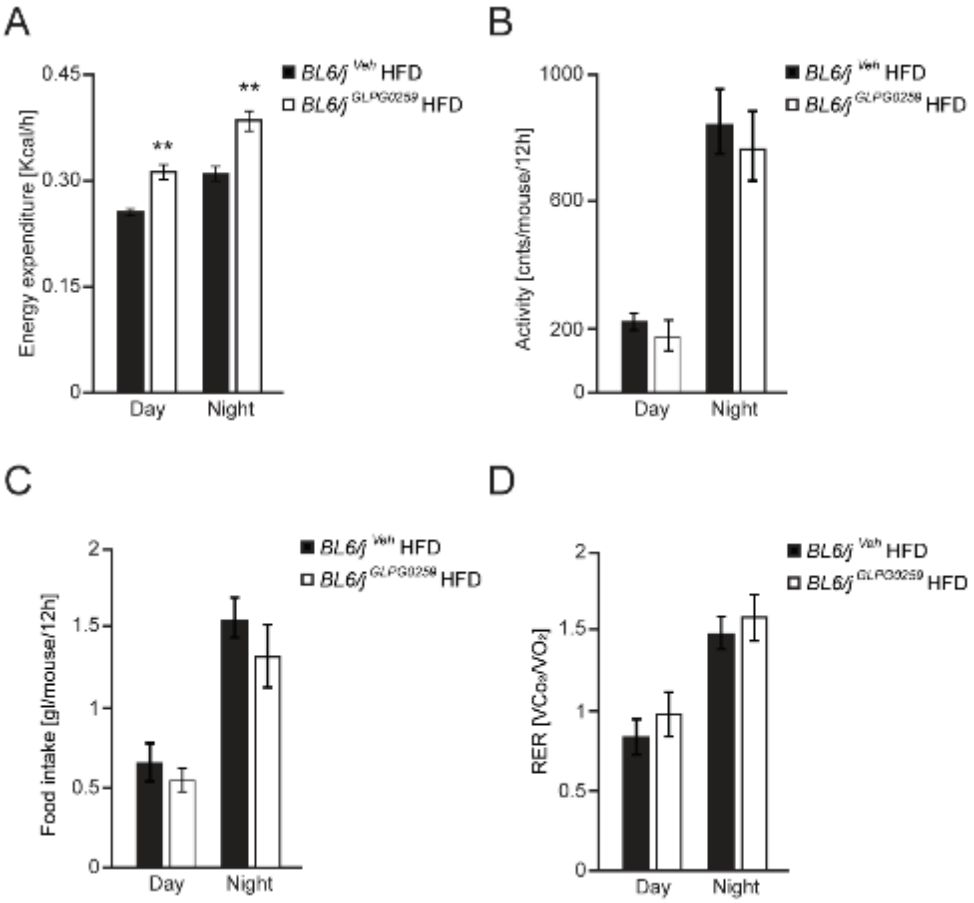

Figure 55. Enhanced energy expenditure in MK5i treated obese mice.

(A) Energy expenditure, (B) voluntary activity, (C) food intake and (D) respiratory exchange rate of BL6/j^{GLPG0259} and wild type BL6/j mice fed on an HFD. N=15, Data presented as average +/- SEM, ** P≤0.001.

7 DISCUSSION

7.1 Identification of kinases regulating lipolysis

The growing worldwide burden of obesity and its associated co-morbidities and pathologies had led to it being defined as a global pandemic (Blüher 2019). The identification of factors that modulate pathological consequences of obesity is a vital step towards the development of novel therapeutic approaches to the treatment of insulin resistance and other aspects of metabolic syndrome.

In this study (El-Merahbi, Viera et al. 2020) we sought to perform an siRNA-based screen to identify kinase that could be efficiently translated to future druggable kinases to target lipolysis hyperactivity in obesity and cancers. A similar approach was demonstrated by another research group, which performed a high-throughput, image-based screen to identify kinases involved in brown adipocyte development (Perdikari, Kulenkampff et al. 2017). Despite the difference in the research question, their screening method was based on lentiviral-mediated knockdown using a short hairpin RNA (shRNA) library. While lentiviral-mediated knockdown shares similar genetic specificity with siRNA based depletion, our experience, as well as other studies, showed a lower transfection efficiency and a longer recovery time needed for the adipocytes after their transfection compared to siRNA based transfection, all of which could possess a negative impact the interpretation of the screening results (Isidor, Winther et al. 2016). Therefore, we chose to proceed with a siRNA-based screen to identify kinase implicated in the regulation of lipolysis rate. Upon stimulation with the mixture of hormones (beta-adrenergic and serotonergic agonists) which normally evoke triglycerides degradation the released lipolytic bi products are collected for measurement using colorimetric assays. of note, to avoid the passive diffusion of FFA back to the stimulated adipocytes, we coupled the stimulation media with an FFA-free BSA, as a substrate shown to bind liberated lipids and not interfere with the colorimetric measurements (Alsabeeh, Chausse et al. 2018). Importantly, our primary screen with a library of siRNAs pools against 706 kinases, yielded a high number of kinases that showed a clear impact on regulating adipocytes' response to the combined hormonal stimulation. However, taking into consideration the appearance of possible false-positive results due to crossmatch of siRNA sequences or an unknown technical error made during the experimental procedure, we repeated the screen on a group of selected hits, using a different targeting pool of sequences for each selected kinase. Importantly, after considering appropriate bio-statistical recommendations for high-throughput screening (Birmingham, Selfors et al.

2009), we were able to validate in the performed secondary screen about 72 kinases, all which their depletion in differentiated adipocytes was co-regulating the lipolysis rate (Figure 9). Our findings that ERK3 is an essential kinase in regulating lipolysis does not discard the involvement of other important kinases in regulating lipolysis as also observed in our screening. In fact, we are currently investigating the role of Magi2 in lipolysis; we had previously reported the role of Ndrg1, the third hit in our kinase screen, as an important factor in promoting adipocyte differentiation and its lipolytic function by inducing Pparγ expression. There we demonstrated that the expression of *Atgl* and *Hsl*, which are defined targets of Pparγ (Karbowska and Kochan 2012), was reduced in the absence of Ndrg1 (Cai, El-Merahbi et al. 2017), thereby further validating the observed reduction of lipolysis rate upon adrenergic stimulation. Equally, the role played by Raf1 in lipolysis has been previously reported (Kalderon, Azazmeh et al. 2012). Raf1 is a member of the mitogen-activated protein kinase family, as noted Raf1 inhibition reduces isoproterenol-induced adenyl cyclase activity, thereby reducing lipolysis. Moreover, lats2 was to play a role in regulating PPARγ-induced adipocyte differentiation (An, Kang et al. 2013). Similarly, the role of *Peg3, Cdk1, camkk2 and Trib3* have been also documented in regulating lipolysis and other aspects of adipocytes function (Curley, Pinnock et al. 2005, Kurat, Wolinski et al. 2009, Lin, Ribar et al. 2011, Liu, Zhang et al. 2012). on the other hand, our screen revealed that silencing of two regulatory subunits of a multi-subunit complex of PKA (*Prkar1a* and *Prkar2b*, which inhibits PKA activation (Torres-Quesada, Mayrhofer et al. 2017)) enhances the lipolysis rate. Taken together, here we shed the light on the role of several kinases in the process of lipolysis. These data suggest that the regulation of lipolysis is a complex process that requires the involvement and activity of many of the key proteins that requires a lot attention and future investigating.

7.2 An overseen role of ERK3 in adipocyte biology

Importantly among the kinases hits, the silencing of ERK3 resulted in the most prominent suppression of lipolysis rate. The role of Ekr3 in adipocytes biology has been mentioned previously but left poorly characterized(Ross, Erickson et al. 2002). Here, we show that upon adipocytes differentiation, ERK3 protein levels are drastically increased, thus providing a shred of solid evidence for the importance of this protein for the function of adipocytes. Among the known factors not identified in the screen were the classical members of the MAPK family, this could be due to an overseen false-negative results that are between the common limitations when performing a high-throughput screening (Zhang, Ferrer et al. 2007). Importantly, extracellular-regulated kinase (ERK) 1/2 and c-Jun N-terminal kinase (JNK) 1/2/3 previously

reported to promote triglycerides degradation in adipocytes (Greenberg, Shen et al. 2001, Gehart, Kumpf et al. 2010, Hong, Song et al. 2018). The metabolic roles of ERK 1/2 in adipocyte proliferation, differentiation, and insulin action have been well studied (Taniguchi, Emanuelli et al. 2006). In the regard of lipolysis, Erk2 was shown to respond to stress stimuli, phosphorylating β3 adrenergic receptor on S247, which was claimed to be a critical regulatory step in enhanced adipocyte lipolysis upon stimulation(Hong, Song et al. 2018). Furthermore, possible crosstalk between the cAMP and classical ERK signaling pathways has been previously discussed in the literature. For example, the beta-adrenergic induced elevation of cAMP was shown to activate c-Raf (MAPKKK), a component of the classical MAPK pathway (Roskoski Jr 2012). After its activation, c-Raf phosphorylates MEK1/2 which in turn, phosphorylates and activates ERK1/2 to promote lipolysis (Ikoma-Seki, Nakamura et al. 2015). As an attempt to strengthen the link between ERK1/2 and lipolysis, a later study investigated the effect of general MEK inhibitors on (PD184352 and PD0325901) on induced lipolysis in 3T3-L1 adipocytes. Indeed, authors of this study (Ozaki, Awazu et al. 2016) showed that the treatment with MEK inhibitors ameliorated lipolysis in adipocytes, they overlooked the fact that treatment with MEK inhibitors that prevent ERK1/2 activation led to a large reduction in ERK3 protein levels (Hoeflich, Eby et al. 2006). Together, these findings provide an evidence point that ERK3 biological activity in adipocytes has been previously overseen and a detailed investigation of the mechanisms of ERK3 pathways in the context of adipocytes biological function is urgently needed.

Here in this study, we used various molecular techniques to detail the mechanistic pathway of ERK3 in adipocytes. Furthermore, we provided noteworthy physiological evidence on the biological role of ERK3 in adipose tissue in mice models.

7.3 A mechanistic overview of the post-translational regulation of ERK3 stability.

It is commonly known that the *Erk3* gene is ubiquitously expressed in different cell types while its activity is mainly regulated by its cellular availability or in other words its abundance (Cheng, Boulton et al. 1996). In cellular models, *Erk3* mRNA was shown to be continuously transcribed and its expression levels were independent of the cellular state. On the other hand, ERK3 protein was shown to be very unstable in highly proliferating cells and its stability increases with cellular differentiation that is coupled with cell cycle arrest (Coulombe, Rodier et al. 2003). A similar mechanistic regulation is shared with other cellular proteins, like hypoxia-inducible factor-1 (HIF-1) as an example. Likewise, HIF-1 RNA is actively been transcribed, translated and then rapidly degraded by the E3 ubiquitination system (Nakagawa, Kohara et al. 2016).

However, an external stimulus, as hypoxia is generally in the case of HIF-1 (Semenza 2014) or adrenergic stimulation as in the case of ERK3 in adipocytes, leads to the activation or inactivation of the cellular mechanisms leading to the inhibition of the degradation and the induced stability of these proteins. Another example of ERK3 stability was observed in immune cells, the study showed that after anti-CD3 stimulation in T cells, increased transcription of *Erk3* is accompanied by a massive accumulation of its protein in activated cells (Marquis, Boulet et al. 2014). ERK3 is shown to be constitutively phosphorylated in its activation loop and was found to remain active during their presence in its respective cellular state, independently from a known activator (Déléris, Rousseau et al. 2008). Moreover, same authors further demonstrated that ERK3 has a single Ser-Glu-Gly phospho-acceptor motif which gets phosphorylated downstream of class I p21 activated kinases (PAKs) in a RAC- or CDC42-dependent manner (Déléris, Trost et al. 2011) Here, we showed that upon beta-adrenergic stimulation, the elevation of intracellular cAMP leads to ERK3 protein stabilization in adipocytes (Figure 14). This suggests that unlike the classical Erk signaling, in adipocytes ERK3 responds to catecholamines signals mainly arriving from innervated neurons. As a result of the activation of the adrenergic receptor on adipocytes, an elevation cAMP, the secondary messenger, was sufficient to promote the stability of this protein in a PKA dependent manner. Furthermore, we strengthen our observations with additional investigations in the ERK3 pathway specifically in adipocytes as it has been studied before in this cell type. Furthermore, we showed that adrenergic stimulation promotes complex formation between ERK3 and MK5 which is a critical cofactor in prolonging its stability and abundance in adipocytes (Figure 14, 17). Importantly, using chemical inhibitors against PKA activity, we could confirm that the stability ERK3/MK5 complex occurs in a PKA-dependent manner (Figure 16, 18). Together with our functional observations, showing the importance of ERK3 in prompting lipolysis in adipocytes, these mechanistic insights in adipocytes provides an additional physiological relevance to the ERK3/MK5 interaction that has been previously characterized in different cell lines(Schumacher, Laaß et al. 2004, Seternes, Mikalsen et al. 2004, Kant, Schumacher et al. 2006). A previous study showed that pretreating adipose tissue explants with MEK inhibitor significantly reduced adrenergic-included lipolysis(Hong, Song et al. 2018). With the explained notion about the un-specificity of MEK inhibitor, our finding showing that genetic depletion of *Mk5* by siRNA leads to a reduction in lipolysis rate while a constitutive overexpression of a phospho-mimicking mutant form of MK5 S115E, a phosphosite important for its binding with ERK3, promoted the stability of ERK3 and induced lipolysis independent of adrenergic stimulation (Figure 21, 22). Moreover, consistent with our in vitro experiments, we could

observe significant stability of ERK3 protein in mice adipose upon fasting, as it is a physiological state of activation of adrenergic signaling (Figure 23). MK5 was shown to follow the same transcriptional profile as MK5 transcripts have been detected during embryogenesis and then remained ubiquitously expressed in human and murine cell types (Natale, Paliga et al. 2004, Ewen, Jackson et al. 2010). Ubiquitinated MK5 has been detected in rabbit reticulocyte lysate and mouse embryonic fibroblasts, suggesting proteasomal degradation of MK5 is a contentious event that starts to occur from the early development (Sahadevan and Allen 2017). Importantly, as observed in our study, as well as by others (Seternes, Mikalsen et al. 2004), the depletion of either ERK3 or MK5 would highly affect the stability and the abundance of the other protein. In fact, ERK3 and MK5 act synergically in studied cellular models (Schumacher, Laaß et al. 2004, Déléris, Trost et al. 2011) as well in our study here. Consistently between tested models, upon activation of PKA, MK5 cytoplasmic translocation occurs leading to a complex formation with ERK3. Moreover, we had further elucidated the active role of the ERK3/MK5 complex in promoting the phosphorylation at serine 256, eventually promoting a nuclear translocation of the forkhead transcription factor 1 (FOXO1) which ultimately induce the transcription of Atgl (Figure 26).

FOXO1 is a major transcription factor that was shown to regulate many important metabolic pathways in the liver, fat tissue, and hypothalamus(Nakae, Cao et al. 2008, Henriques, Machado et al. 2019). In the liver, FOXO1 binds and promotes transcription of glucose 6-phosphatase and phosphoenolpyruvate carboxykinase, which are key enzymes stimulating gluconeogenesis and glycogenolysis (Matsumoto, Pocai et al. 2007, Wu, Pan et al. 2018). Insulin stimulation promotes the binding of FOXO1 to the ApoC3 promoter and enhances its transcription leading to elevation of plasma triglyceride levels (Altomonte, Cong et al. 2004).
In adipose tissue, FOXO1 has several transcriptional targets. it has been shown that FOXO1 binds to the promoter sites of peroxisome proliferator-activated receptor-gamma (PPARγ) DNA and represses its transcription thereby suppressing adipogenesis (Nakae, Kitamura et al. 2003). Interestingly, it has been demonstrated that insulin stimulation leads to the degradation of FOXO1 protein (Matsuzaki, Daitoku et al. 2003). Increasing evidence, including in this study, points out the role of adrenergic-PKA activity in the stability and activity of FOXO1. Several reports showed that FOXO1 suppresses the expression of genes regulating energy dissipation, including *Ucp1*, in white and brown adipocytes (Nakae, Cao et al. 2008, Nakae, Cao et al. 2012, Liu, Tao et al. 2016, Kita, Nakae et al. 2019, Peng, Xiao et al. 2019). However, a recent study indicated that in brown adipose tissue of mice fed ND, FOXO1 does not affect *Ucp1* and *in*

vitro under specific culture conditions deletion of FOXO1 might even decrease *Ucp1* expression in brown adipocytes (Jung, Hung et al. 2019). These results came opposing with a previous study showing an increased binging of the FOXO1 transcription factor to *Pgc1* a and *Ucp1* promoters in brown adipose tissue in response to forskolin stimulation, an intracellular cAMP chemical elevator (Ortega-Molina, Efeyan et al. 2012). Additionally, another group had studied the binging of FOXO1 to the *Atgl* prompter in white adipose tissue observed a reduced binding of FOXO1 in response to insulin stimulation. Taken together, our study provides additional evidence suggesting that adrenergic signaling counteracts insulin stimulation regarding FOXO1 binding to *Atgl* as well and *Ucp1* promoters (Figure 27,28).

7.4 Counteracting the metabolic syndrome by inhibiting lipolysis and inducing energy expenditure

During the past decades, intensive research focus in the metabolic field was put on different strategies to control energy balance in order to help overcome the manifestation of metabolic diseases. Given the biological function exerted by the ERK3/MK5/FOXO1 pathway on adipose, in the regulation of adipocytes lipolysis and effecting its thermogenesis, it was critical to explore physiological aspect by which this pathway could affect the organism's adipose tissue function and the whole-body hemostasis. Therefore, we generated a mouse model deficient for *Erk3* specifically in adipocytes under a constant or an inducible adiponectin promoter. Consistently with our *in-vitro* studies, the deletion of *Erk3* specifically in adipocytes resulted in markedly reduced levels of lipolytic products in the circulation of mice injected with the β3-receptor agonist (CL316243) (Figure 31). In this regard, several studies found that the attenuation of lipolysis rate by inhibiting lipolytic enzymes (ATGL and HSL) results not only in better insulin sensitivity, but also ameliorates diet-induced obesity (Zimmermann, Strauss et al. 2004, Kienesberger, Lee et al. 2009, Schweiger, Romauch et al. 2017, De Koster, Nelli et al. 2018). Deletion of *Atgl* in the whole body or all the depots of adipose tissue results in decreased energy dissipation in mice upon cold exposure especially during the time of food deprivation (Ahmadian, Abbott et al. 2011, Schreiber, Diwoky et al. 2017). However, in mice deficient for *Atgl* in the whole body (except for the cardiac muscle) and mice treated with Atglistatin, which were fed HFD and maintained at room temperature, energy expenditure was not decreased (Schreiber, Hofer et al. 2015, Schweiger, Romauch et al. 2017). Moreover, mice treated with Atglistatin display higher UCP1 levels in adipose tissue (Schweiger, Romauch et al. 2017). Similarly, the deletion of CGI-58 in brown adipose tissue, which partially blocks lipolysis, does not block energy dissipation by adipocytes in mice fed ad libitum (Shin, Ma et al. 2017, Shin,

Shi et al. 2018). likewise, the deletion of *Foxo1*, the upstream transcription factor that promotes *Atgl* expression, showed to have a similar metabolic phenotype in obese mice models as what is described by *Atgl* inhibition. In fact, a mouse genetic model of *Foxo1* haploinsufficiency reported its protective effect against high-fat diet-induced insulin resistance with enhanced peroxisome Pparγ activation in adipose tissue (Kim, Li et al. 2009). Moreover, treatment with AS1842856, a selective FOXO1 pharmacological inhibitor, showed to suppress adipogenesis (or adipocyte hyperplasia) but also Fine-tuned mice metabolism by an increase in their energy expenditure and provided a protective effect from diet-induced obesity(Zou, Liu et al. 2014, Cheng 2015, Pandey, Kumar et al. 2016). Moreover, a study identified fat mass and obesity-associated gene (FTO), as a direct substrate for *Foxo1* mRNA. Using FTO pharmacological inhibitor the authors could also replicate FOXO1 inhibition metabolic phenotype (Peng, Xiao et al. 2019). However, caution should be carried out when using antagonists to silence FOXO1 in a chronic and systemic way as FOXO1 plays pleiotropic roles in different tissues (Cheng and White 2011). Considering the presented limitation of these previous studies, we anticipate from genetically knocking down *Erk3* in adipocytes, that it will inhibit ERK3/MK5 complex from phosphorylating FOXO1 specifically at Ser256 while rendering FOXO1 protein intact. In fact, we observed a protective role of ERK3 deletion specifically in adipocytes on the development of diet-induced obesity (Figure 27, 28). Interestingly, mice depleted form *Erk3* in adipocytes, placed on an HFD showed promising signs of enhanced metabolic fitness as displayed by improved insulin sensitivity, glucose tolerance and increased energy expenditure (Figure 36-38). Moreover, histological analysis revealed a reduced adipocytes' size and the emergence of multilocular adipocytes (beige adipocytes) within the subcutaneous fat mass (Figure 39) which is associated by transcriptional upregulation in thermogenic markers in SubWAT and BAT. Hence, our data suggest that the reduction of lipolysis and induction of energy expenditure by the inhibition of ERK3/MK5/FOXO1 activity could be an attractive approach to combat obesity and associated diabetes.

7.5 Pharmacological approaches in the treatment of obesity and associated metabolic diseases.

Currently, there are five approved drugs or combinations that are present on the market for the treatment of obesity: orlistat, lorcaserin, liraglutide, phentermine/topiramate, and bupropion/naltrexone. These medications have demonstrated efficacy to achieve clinically

important weight losses and improve cardiometabolic risk markers, with a reasonable risk-benefit balance.

Orlistat is a tetrahydrolipstatin with potent and selective lipase inhibitory activity that decreases fat absorption by reducing triglyceride hydrolysis(Heck, Yanovski et al. 2000). However, despite an observed beneficial effect in weight loss, most patients reported a side effect related to fat malabsorption and related gastrointestinal tract syndromes (Song, Ruan et al. 2018). Lorcaserin is a benzazepine derivative and a selective serotonin type 2C receptor (5-HT2C) agonist that reduces food intake by reducing apatite. However, It was removed from the market in the United States in 2020 due to its increased risk of cancer (Voelker 2020). Another line of drugs that are used to reduce apatite and elevate energy expenditure lies in the combination of phentermine, an atypical amphetamine analog, with topiramate, an anti-epileptic drug, or with bupropion, an anti-depressant drug which stimulates the neuronal release of αmelanocyte-stimulating hormones. These drugs showed its effectiveness in a wide range of case studies, however, it is associated with common side effects including, vomiting, dizziness, confusion, trouble concentrating and in some cases problems with speech or memory(Pappa, Filippatos et al. 2018, Hsia, Gosselin et al. 2020, Singh and Singh 2020).

The role of glucagon-like peptide-1 (GLP-1) in the pathophysiology of obesity has long been studied before the development of the drug liraglutide, as a GLP-1 receptor agonist. The binding of liraglutide to its receptor improves pancreatic beta-cell function and insulin sensitivity in diabetic and obese patients(Holst 2007, Marso, Daniels et al. 2016). While a licensed low dose of this drug, with acceptable nausea as a side effect, was shown its effectivity in only 15-30% of administered patients (Mohanty 2017), a higher dose is proven to be glycemically more effective but consistently associated with unacceptable tolerability (Barrington, Chien et al. 2011, Nauck, Petrie et al. 2016).

Considering the limitations of the presented pharmacological drugs concerning their side effects but most importantly to their effectiveness on a larger population of obese and diabetic patients. We find it is yet urgent for new drug development to tangle the rising number of obese and diabetic patients worldwide. Here, we shed light on our innovative approach with the administration of MK5 inhibitor (MK5i) GLPG0259 in adult mice as an attempt to reduce induced- lipolysis in response to adrenergic stimulation. This drug has been already approved for the phase II clinical trial for reducing inflammation caused by rheumatoid arthritis and shows very mild side effects (Westhovens, De Keyser et al. 2013), Indeed, already after one-week of daily oral-administration of MK5i in mice, we observed a significant reduction in *Atgl*

expression level while an elevation in several thermogenic genes in both subcutaneous adipose tissue depots as compared to control mice administered with vehicle only (Figure 50). Functionally, treatment of adult obese mice with MK5i, fine-tuned their metabolic fitness. This mainly observed by obese mice being protected from further weight gain while it did not influence mice apatite as do difference was observed in their food intake (Figure 51, 54). Furthermore, a metabolic switch toward a browning phenotype in adipose tissue allowed obese mice to dissipate a had higher energy expenditure as heat, while it did not alter their voluntary activity normal behavior (Figure 54). Together with a lower level of circulating FFAs (Figure 52), treatment of MK5i leads for a metabolic improvement in obese mice to become more insulin sensitive and glucose tolerant (Figure 53), while no signs of illness were observed throughout the time frame of drug administration. Given that the pharmacokinetic and the safety of this chemical compound had been previously addressed before proceeding to the performed clinical trials (Namour, Vanhoutte et al. 2012), we find it essential to proceed further in our future investigation in studying the detailed mechanistic pathway of this drug and later to assess its potential beneficial metabolic effect on humans.

For this purpose, we aim our future experiments to investigate the potential impact of MK5i on adipocytes lipogeneses through functional assays and transcriptional profiling of lipogenic genes as well as functional analysis of adipocytes lipid accumulation in vitro. To achieve this aim we will image and quantify the possible effect of MK5i on the accumulation of TGs throughout the time course of adipocytes differentiation using Adipored and Oil-red-O (specific intracellular TG red stains). Moreover, while glucose is the main substrate for *de novo* lipogenesis, we will be measuring the potential effect of MK5i on the incorporation of stable isotope-labeled glucose D-[3-3H], during adipocytes differentiation as well as in response to insulin stimulation.

Next, we aim to better understand the mechanisms by which MK5 inhibitor elevates energy expenditure. As we previously noted that BAT presents a major organ in responding to adrenergic signaling and dissipating energy as heat. Our data here indicates that obese mice administered MK5i present an elevated energy expenditure. However, since the administered drug is acting systemically, it is still not clear if brown or beige adipocytes are responsible for this molecular elevation in energy expenditure. To address this question, we aim to apply several *in-vitro* functional assays on primarily isolated pre-adipocytes that their differentiation was directed towards brown/beige adipocytes lineage in combination or absence of MK5i treatment. Using this cellular platform, we will be able to apply fluorescent labeling techniques, to image mitochondrial fission and fusion in our adipocyte's models in response to MK5i

treatment. Of note, it has been previously reported by our group (Löffler, Mayer et al. 2018) and others, that studying the mitochondrial dynamics together with the measurement of oxygen consumption rate using a seahorse analyzer, could provide an important shred of evidence to explain the observed elevated cellular energy expenditure in obese MK5i treated mice.

Finally, additional histological characterization of metabolic organs in mice fed an HFD in the presence and absence of an MK5 inhibitor would beneficial to help further elucidate the response of each organ to the MK5i drug administration as well to spot any pathological reactions as a side effect associated by its prolonged administration. In this regard, we aim to check the possible emergence of multi-locular beige adipocytes in the subcutaneous adipose tissue depot which is shown be a beneficial effect in obese patients contributing in the of their elevation in energy expenditure by actively dissipating more energy as heat (Beiroa, Imbernon et al. 2014, Claussnitzer, Dankel et al. 2015).

8 CLOSING REMARKS

In a translational point of view, a novel treatment that might be an effective tool against obesity must have a well-characterized mechanism of action, a favorable risk-benefit balance with unimportant side effects and be both easy to deliver and affordable (Hainer and Aldhoon-Hainerová 2014, Jackson, Breen et al. 2015). Previously, we demonstrated that β-adrenergic stimulation stabilizes ERK3 leading to the formation of a complex with the co-factor MK5 thereby driving lipolysis. Importantly, we provided evidence that targeted deletion of ERK3 in mouse adipocytes inhibits lipolysis, but elevates energy dissipation, promoting lean phenotype and ameliorating diabetes. Based on our results, pharmacological targeting of the ERK3/MK5 pathway might be a valid strategy to treat obesity and associated diabetes. Taken together, we identified a signaling axis that can link and fine-tune the transcriptional response leading to lipolysis and energy dissipation in adipocytes (Figure 56). We speculate that inhibition of ERK3/MK5 signaling, which was achieved by a specific MK5 inhibitor, might represent an attractive strategy for a future translational approach. We also proposed additional follow-up experiments that would provide an essential shred of evidence to strengthen our understanding of the mechanistic pathway of MK5i. Finally, and after performing all the necessary missing experiments, we would be more confident to proceed forward with researching our pharmacotherapeutic drug in clinical trials, ultimately aiming to ameliorate the advert impact of obesity and diabetes in diseased patients.

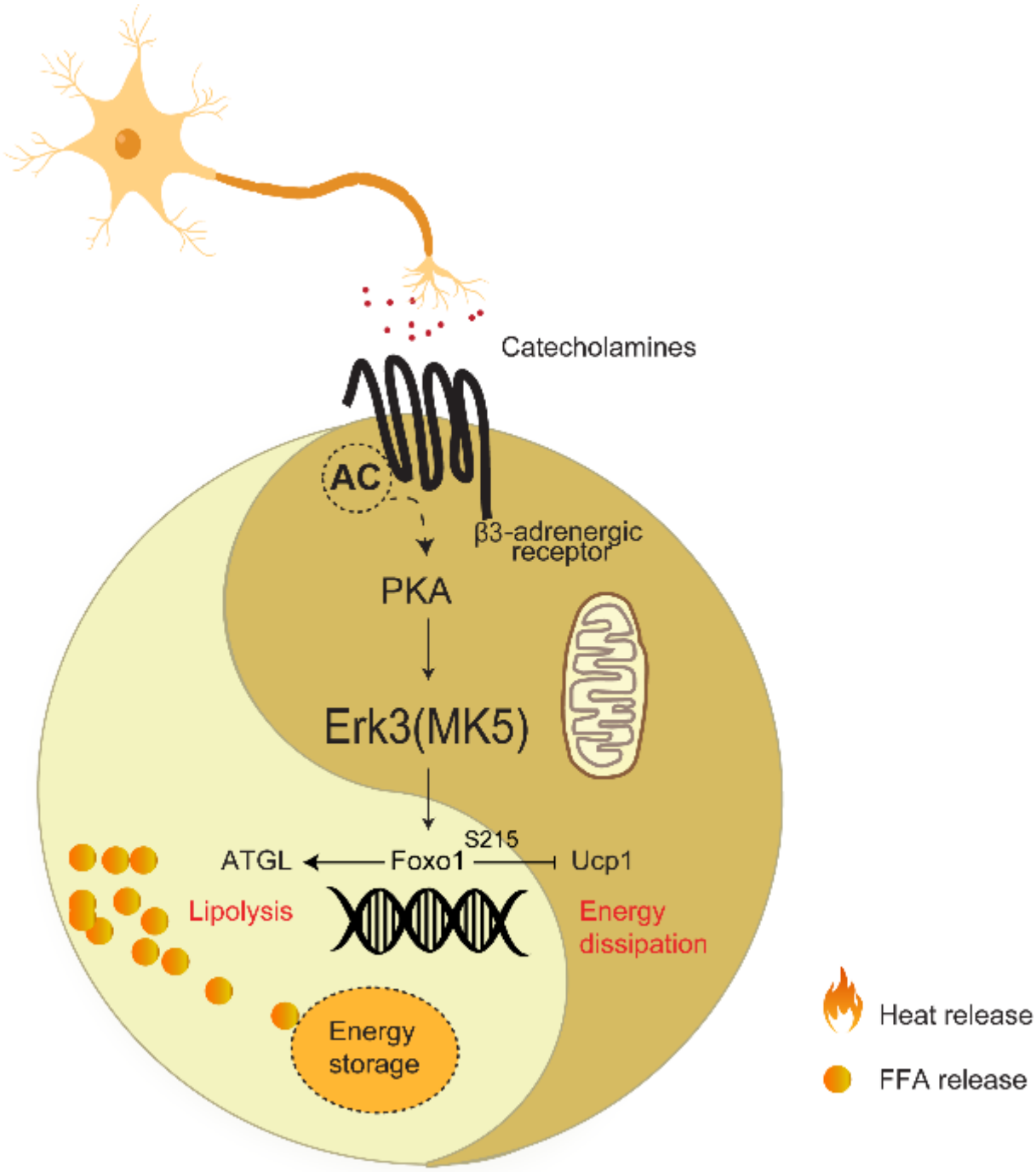

Figure 56. Graphical conclusion.

9 MATERIALS

9.1 Chemicals and reagents

Table 1: List of chemicals and reagents used in this thesis.

1,4-Dithiothreitol (DTT)	Sigma-Aldrich	#10197777001
12-molybdophosphoric acid	Alfa Aesar	#56166
2'-deoxynucleoside 5'-triphosphate (dNTP) mix (2 mM each):	Thermo Fisher Scientific	#R0242
Acetic acid	Roth	#3738.1
Acrylamide	AppliChem	#A4989
Adenosine monophosphate (AMP)	Sigma-Aldrich	#A1752
AdipoRed dye	Lonza	#PT-7009
Agar	Sigma-Aldrich	#A1296
Agarose	Roth	#2267.4
Albumin fraction V	Roth	#8076.2
Ammonium bicarbonate (NH_4HCO_3)	Sigma-Aldrich	#09830
Ammonium chloride (NH_4Cl)	Sigma-Aldrich	#A9434
Ammonium peroxidisulphate (APS)	Roth	#9592.2
Ampicillin	Sigma-Aldrich	#A0166
Antimycin A	Sigma-Aldrich	#A8674
Bovine serum albumin (BSA)	Sigma-Aldrich	#A7030
Bromophenol blue	Roth	#A512.1
Calcium chloride ($CaCl_2$)	Merck	#8222622500
Carbonyl cyanide-4-(trifluoromethoxy) phenylhydrazone (FCCP)	Roth	#CN93.1
Collagenase D	Roche	#359009
Chloroform ($CHCl_3$)	Roth	#1479.3
Crystal violet	Sigma-Aldrich	#B0770
DNA loading dye solution, 6x	Sigma-Aldrich	#33120-M
DharmaFECT duo	Thermo Fisher Scientific	#T-2010-03

Distilled water (UltraPure)	Thermo Fisher Scientific	#10977-035
Dry milk, fat-free	Roth	#T145.4
Enhanced chemiluminescence (ECL) substrate	Thermo Fisher Scientific	#14155048
Eosin G solution	Bio-Rad	#170-5061
Ethanol; absolute	Roth	#3139.2
Ethanol; denatured	Roth	#5054.1
Ethyl acetate	Roth	#K928.3
Ethylenediaminetetraacetic acid (EDTA)	Sigma-Aldrich	#34858
Formalin	Roth	#8040.1
Formic acid	Sigma-Aldrich	#HT501128
Formic acid (98-100%) for LC/MS	Sigma-Aldrich	#106526
Free fatty acid (FFA) standard	Sigma-Aldrich	#5.33002
Free Glycerol Reagent	Sigma-Aldrich	#F6428
GeneRuler 1 kbp DNA ladder	Wako Diagnostics	#276-76491
GeneRuler 100 bp DNA ladder	Thermo Fisher Scientific	#SM0311
Glucose	Thermo Fisher Scientific	#SM0241
Glycerol	Roth	#X997.2
Glycerol standard	Roth	#3783.1
Glycine	Roth	#3790.3
Goat serum	Sigma-Aldrich	#G8790
Hoechst 33342 dye	Sigma-Aldrich	#34859-M
Hydrochloric acid (HCl)	Thermo Fisher Scientific	#62249
Hydrogen peroxide (H_2O_2)	Sigma Aldrich	#30721
Hydrophobic pen; Roti®-Liquid barrier marker	Sigma-Aldrich	#31642
Isopropanol	Sigma-Aldrich	#I6125
Magnesium chloride ($MgCl_2$)	Sigma-Aldrich	#62840
Magnesium sulfate ($MgSO_4$)	Roth	#KK36.1

Mayer's hematoxylin solution	Sigma-Aldrich	#M2643
Methanol (MeOH)	Sigma-Aldrich	#MHS16
Methanol (MeOH)	Sigma-Aldrich	#34860
Midori green advance DNA stain	Roth	#4627.3
Mounting medium; Roti®-Mount	Nippon Genetics	#MG04
Myc tagged magnetic beads	Thermo Fisher Scientific	#88803
Nonidet P-40 (NP-40)	Sigma-Aldrich	#N5252
NuPAGE® *lithium dodecyl sulfate* (LDS) sample buffer	Sigma-Aldrich	#74385
NuPAGE® Novex® 4-12% Bis-Tris gels	Thermo Fisher Scientific	#NP0007
NuPAGE™ MOPS SDS running buffer (20X)	Thermo Fisher Scientific	#NP0321PK2
Oil Red O	Sigma-Aldrich	#O0625
Oligomycin	Sigma-Aldrich	#O1008
PageRuler® prestained protein ladder	Calbiochem	#495455
Paraformaldehyde (PFA)	Thermo Fisher Scientific	#26619
Phosphate-buffered saline (PBS)	GE Healthcare	#17-0456-01
Pierce™ IP Lysis Buffer	Sigma-Aldrich	#P7943
Pierce™ Protein A/G Magnetic Beads	Thermo Fisher Scientific	#87787
PowerUp™ SYBR™ green master mix	Promega	#V5280
ProLong Gold Antifade Mountant with *4',6-diamidino-2-phenylindole* (DAPI) mounting reagent	Thermo Fisher Scientific	#A25742
Protease and phosphatase inhibitor (PPI) cocktail (100x)	Thermo Fisher Scientific	#P36931
QIAzol lysis reagent	Thermo Fisher Scientific	#78442
Quick Start™ Bradford 1x dye reagent	Qiagen	#79306

Sodium chloride (NaCl)	Thermo Fisher Scientific	#LC6060
Sodium dodecyl sulfate (SDS) pellets	Roth	#3957.1
Sodium hydroxide (NaOH)	Roth	#CN30.2
Sulfuric acid (H_2SO_4)	Roth	#P031.1
Tetramethylethylenediamine (TEMED)	Sigma-Aldrich	#30743-M
TRIS base	Sigma-Aldrich	#T7140
Triton X-100	Roth	#AE15.4
Tween 20	Roth	#8952.2
Tyloxapol (Triton WR1339)	Roth	#9127.1
UltraPure™ distilled water (Dnase/Rnase Free)	Sigma-Aldrich	#T0307
Urea	Thermo Fisher Scientific	#10977-035
Xylazine	Sigma-Aldrich	#U0631
Xylol	cp-pharma	Xylavet
Yeast extract	Roth	#9713.3
β-mercaptoethanol	Sigma-Aldrich	#70990
Matrigel	Corning	Cat#: 354230 I7378
Indomethacin	Sigma-Aldrich	Cat#:
3-Isobutyl-1-methylxanthine	Sigma-Aldrich	Cat#: I5879
Dexamethasone	Sigma-Aldrich	Cat#: D4902
Insulin solution human	Sigma-Aldrich	Cat#: I9278
3,3′,5-Triiodo-L-thyronine sodium salt (T3)	Sigma-Aldrich	Cat#: T6397
Isoproterenol hydrochloride	Sigma-Aldrich	Cat#: 1351005
MG-132	Tocris biotech	Cat#: 1748
Forskolin	Sigma-Aldrich	Cat#: F6886
CL 316243 disodium salt	Tocris biotech	Cat#: 1499
lactacystin	Sigma-Aldrich	Cat#: L6785
Cyclohexamide	Sigma-Aldrich	Cat#: C1988
leptomycin B	Tocris biotech	Cat#: 1987
H-89 dihydrochloride hydrate	Sigma-Aldrich	Cat**#:** B1427

PKI 14-22 amide, myristoylated	Tocris biotech	Cat#: 2546
BW 723C86 hydrochloride	Tocris biotech	Cat#: 1059
Fatty acid-free BSA	Sigma-Aldrich	Cat**#:** A7030
Oligomycin	Calbiochem	Cat#: 95455
Carbonyl cyanide 4-(trifluoromethoxy)phenylhydrazone (FCCP)	Sigma-Aldrich	Cat#: C2920
Rotenone	Sigma-Aldrich	Cat#: R8875
Antimycin A	Sigma-Aldrich	Cat#: A8674
Hoechst 33342 Solution	Thermo Scientific	Cat#: 62249
poly-L-lysine	Sigma-Aldrich	Cat#: P2636
Phalloidin–Atto 647N	Sigma-Aldrich	Cat#: 65906
GLPG0259	Medkoo	Cat#: 15986
Tamoxifen	Sigma-Aldrich	Cat#: T5648

Table 2. Buffers and solutions

All buffers and solutions were prepared in distilled, deionized water (ddH_2O) obtained from a MilliQ Water Purification System unless stated otherwise. pH was adjusted with HCl or NaOH, respectively.

Blocking buffer (WB) *TRIS buffered saline with tween* (TBST) 5% BSA or fat-free dry milk	50x Tris-acetate-EDTA (TAE) 2 mM TRIS 5.7% Acetic acid 10% EDTA (0.5 M stock)
Blocking buffer (IF) PBS 0.5% BSA 10% Normal goat serum	1x TAE 2% 50x TAE
Crystal violet staining solution 2% Crystal violet (90%) 20% Ethanol	10x Running/Transfer buffer 250 mM TRIS 1.92 M Glycine
Fixation solution 4% PFA (in PBS)	1x Running buffer 10% 10x Running buffer

	0.5% SDS (20% stock)
<u>5x Laemmli buffer (SDS-PAGE)</u> 300 mM TRIS, pH 6.8 (2 M stock) 10% SDS 50% Glycerol 25% β-mercaptoethanol spatual tip Bromophenol blue	<u>1x Transfer buffer</u> 10% 10x Transfer buffer 20% Methanol
<u>Lysis buffer (WB)</u> 20 mM TRIS, pH 7.5 (1 M stock) 150 mM NaCl (5 M stock) 20 mM β-glycerophosphate 5 mM $MgCl_2$ 5% Glycerol 0.2% NP-40 0.2% Triton X-100 1x PPI (added before usage)	<u>Lysis buffer (DNA Extraction)</u> 100 mM TRIS, pH 8.5 (1 mM stock) 5 mM EDTA (0.5 M stock) 200 mM NaCl (5 M stock) 0.2% SDS (20% stock) → 0.1 mg/mL Proteinase K was added freshly before usage
<u>10x Tris-buffered saline (TBS), pH 7.6</u> 0.2 M TRIS 1.4 M NaCl	<u>10% separating gel (WB – 20 mL)</u> 9.8 mL ddH_2O 5 mL TRIS, pH 8.6 (1.5 mM stock) 5 mL Acrylamide (40% stock) 100 µL SDS (20% stock) 200 µL APS (10% stock) 20 µL TEMED
<u>1x TBS</u> 10% 10x TBS <u>1x TBST</u> 10% 10x TBS 0.1% Tween 20	<u>4% stacking gel (WB – 10 mL)</u> 8.2 mL ddH_2O 620 µL TRIS, pH 8.6 (1.5 mM stock) 946 µL Acrylamide (40% stock) 50 µL SDS (20% stock) 100 µL APS (10% stock) 10 µL TEMED
<u>LB Medium, pH 7.0</u>	<u>Mamalian Cells Freezing-Medium</u>

Trypton/Pepton aus Casein 10 g/L Yeast extract 5 g/L NaCl 171 mM	DMEM 50% FBS 40% DMSO 10%
<u>LB Plates</u> LB medium Agar 15 g/L	

Table 3: List of kits used in this thesis.

Commercial kit	**Manufacturer**	**Identifier**
BCA Protein Assay Kit	Thermo Fisher Scientific	#23227
CHIP KIT	Abcam	Cat#: Ab500
First Strand cDNA Synthesis Kit	Thermo Fisher Scientific	#K1612
NEFA Kit: NEFA-HR(2) R1 Set; NEFA-HR(2) R2 Set	Wako	#434-91795; #436-91995
NucleoBond® Xtra Midi	Macherey-Nagel	#740410.50
NucleoSpin® Gel and PCR Clean-up	Macherey-Nagel	#740609.250
NucleoSpin® Plasmid	Macherey-Nagel	#740588.250
Nuclear fraction NE-PER™ Nuclear and Cytoplasmic Extraction	Thermo Fisher Scientific	# 78833
Q5 site-directed mutagenesis kit	NEB	Cat#: E0552S
RNeasy Plus Universal Tissue Mini Kit	Qiagen	#73404
Seahorse XF Cell Mito Stress Test	Agilent Technologies	#103015-100
Serum TG Kit, Free Glycerol Reagent	Sigma-Aldrich	#F6428
Serum TG Kit, Triglyceride Reagent	Sigma-Aldrich	#T2449
Taq DNA Polymerase	Thermo Fisher Scientific	#EP0282

9.2 Oligonucleotides

Table 4: List of RT-qPCR primers used in this thesis.

Gene Name	**Forward (5'-3')**	**Reverse (5'-3')**
Erk1	TCCGCCATGAGAATGTTATAGGC	GGTGGTGTTGATAAGCAGATTGG

Erk2	TCAGATGAATTTTCGTTGGCAGA	GAGCACTTGGGTTACTCCACG
Erk3	CACATGAACTTGAACAGATGCA G	CAGTGCTTCTCGGCTGATCC
Mk5	CCT CAT TTC TAG CTT TTG GAC GA	CTG GGA GCC GGA ATT AGT GG
FoxO1	CCC AGG CCG GAG TTT AAC C	GTT GCT CAT AAA GTC GGT GCT
Atgl	CAACGCCACTCACATCTACGG	GGACACCTCAATAATGTTGGCA C
Prdm16	ACGGACAGGGCTTCTCCTAC	ATGGTGGTATCGAGGGTGGAA
Pgc-1α	AGC GCC GTG TGA TTT ACG TT	CCG CAG ATT TAC GGT GCA TT
Pparγ	GGAAGACCACTCGCATTCCTT	GTAATCAGCAACCATTGGGTCA
Ppar α	AACATCGAGTGTCGAATATGTGG	CCGAATAGTTCGCCGAAAGAA
Ucp1	AGG CTT CCA GTA CCA TTA GGT	CTG AGT GAG GCA AAG CTG ATT T
Rpl13a	CCC TCC ACC CTA TGA CAA GA	GCC CCA GGT AAG CAA ACT T
Fabp4	TTCGATGAAATCACC	GGTCGACTTTCCATC
G0S2	TAGTGAAGCTATACGTTCTGGGC	GTCTCAACTAGGCCGAGCA
perlipin	GGG ACC TGT GAG TGC TTC C	GTA TTG AAG AGC CGG GAT CTT TT
C/Ebp alfa	AAACAACGCAACGTGGAGA	GCGGTCATTGTCACTGGTC
Hsl	TTCTCCAAAGCACCTAGCCAA	TGTGGAAAACTAAGGGCTTGTT G
Adiponecti n	TGTTCCTCTTAATCCTGCCCA	CCAACCTGCACAAGTTCCCTT
Dio2	TGT CTG GAA CAG CTT CCT CC	CCA TCA GCG GTC TTC TCC G
Cedia	TGACATTCATGGGATTGCAGAC	GGCCAGTTGTGATGACTAAGAC
Cox7a	AGG ACG CAA AAT GAG GGC	TCT TGT GGG GGA AGG AGG
Cox8b	TGTGGGGATCTCAGCCATAGT	AGTGGGCTAAGACCCATCCTG
Tmem26	ACC CTG TCA TCC CAC AGA G	TGT TTG GTG GAG TCC TAA GGT C

Elovl3	TTC TCA CGC GGG TTA AAA ATG G	GAG CAA CAG ATA GAC GAC CAC
Elovl6	CCCGAACTAGGTGACACGAT	CCAGCGACCATGTCTTTGTA
Cited 1	AAC CTT GGA GTG AAG GAT CGC	GTA GGA GAG CCT ATT GGA GAT GT
Tnfrst9	CGT GCA GAA CTC CTG TGA TAA C	GTC CAC CTA TGC TGG AGA AGG

Table 5: List of siRNAs and DNA oligos used in this thesis.

siRNA	**Manufacturer**	**Identifier**
SMARTpool: siGENOME Human MAPK6 siRNA	GE Dharmacon	Cat.#:M-003594-02-0005
SMARTpool: siGENOME Mouse Mapkapk5 siRNA	GE Dharmacon	Cat.#:M-040095-01-0005
SMARTpool: siGENOME Mouse Foxo1 siRNA	GE Dharmacon	Cat.#:M-041127-00-0005
SMARTpool: siGENOME Mouse Pnpla2 siRNA	GE Dharmacon	Cat.#:M-040220-01-0005
SMARTpool: siGENOME Mouse Mapk6 siRNA	GE Dharmacon	Cat.#:M-040133-01-0005
SMARTpool: siGENOME Non-Targeting Pool	GE Dharmacon	Pool # 2

Unmodified DNA Oligos

Foxo1 S215D	GTC CCT TCA CGA CAA GTT TAT TCG AG	AGA TTG TGG CGA ATT GAA TTC
FOXO1 S215A	GTC CCT TCA CGC CAA GTT TA T TCG AG	AGA TTG TGG CGA ATT GAA TTC

MK5 S115A	TCA CAG AAT CGC CCA GCA CCG G	AAT AGC TCT CCC CCT TCC
MK5 S115E	TCA CAG AAT CGC CCA GCA CCG G	TCA CAG AAT CGA GCA GCA CCG GCA C
ShErk3	5'tgctgttgacagtgagcgaacacctgtaactaca aaacaatagtgaagccacagatgtattgttttgtagtt acaggtgtgtgcctactgcctcgga 3'	

9.3 Plasmids

Table 6: List of vectors, plasmids and constructs used in this thesis.

Plasmids	Manufacturer	Identifier
Plasmid: pGipz ShErk3	Addgene (modified)	Plasmin Map 1
Plasmid: cmycER3	This paper	Plasmid MAP 2
Plasmid: HA- FOXO1	Vector Builder	Plasmid MAP 3
Plasmid: 3xFLAG-MK5	Vector Builder	Plasmid MAP 4
Plasmid: pBABE vector	Addgene	RRID:Addgene_1764
Plasmid: psPAX	Addgene	RRID:Addgene_12260
Plasmid: pMD2.G	Addgene	RRID:Addgene_12259

9.4 Antibodies

9.4.1 Primary antibodies

Table 7: List of primary antibodies used in this thesis (for WB, IHC, IF and IP).

Antibody	Clone	Manufacturer	Reference no.
Rabbit anti-ERK3 clone	EP1720Y	Abcam	Cat# ab53277, RRID:AB_2140288

Rabbit anti-MAPKAPK-5 clone	D70A10	Cell Signaling Technology	Cat#: 7419 Cat# 7419, RRID:AB_10891810
Rabbit anti-FOXO1 clone	C29H4	Cell Signaling Technology	Cat# 2880, RRID:AB_2106495
Rabbit anti-ATGL		Cell Signaling Technology	Cat# 2138, RRID:AB_2167955
Rabbit anti-GAPDH		Sigma-Aldrich	Cat#: G9545
Rabbit anti-HSL		Cell Signaling Technology	Cat#: 4107
Rabbit anti-Phospho HSL Ser606		Cell Signaling Technology	Cat#: 4126
Rabbit anti-PPAR clone	C26H12	Cell Signaling Technology	Cat#: 2435
Rabbit anti-UCP1 clone	D9D6X	Cell Signaling Technology	Cat#: #14670
Rabbit anti-β3 Tubulin clone	D71G9	Cell Signaling Technology	Cat#: 5568
Myc-Tag	9B11	Cell Signaling	2276
α-Tubulin		Cell Signaling	2144
β-Actin		Sigma	A5441
Lamin B1 antibody	B10	Santa cruz	Cat:# SC-374015

9.4.2 Secondary antibodies

Table 8: List of secondary antibodies used in this thesis (for WB and IF).

Antibody	Manufacturer	Reference no.
Donkey anti-Rabbit IgG Alexa Fluor 488	Thermo Fisher Scientific	#A21206
Goat anti-Mouse IgG Alexa Fluor 488	Thermo Fisher Scientific	#A11001
Goat anti-Mouse IgG Alexa Fluor 594	Thermo Fisher Scientific	#A11005

Goat Anti-Mouse IgG Atto 647N	Sigma-Aldrich	#50185
Goat anti-Rabbit IgG Alexa Fluor 594	Thermo Fisher Scientific	#A11012
Goat anti-Rabbit IgG-HRP	GE Healthcare	#RPN4301
Sheep anti-Mouse IgG-HRP	GE Healthcare	#RPN4201

9.5 Enzymes

Table 9: List of enzymes used in this thesis.

Enzymes	Manufacturer	Identifier
EcoRI	NEB	#R0101
Proteinase K	Thermo Fisher Scientific	#EO0491
SalI	NEB	#R0138
T4 DNA ligase (5 U/µl)	Thermo Fisher Scientific	#EL0014
XhoI	NEB	#R0146

9.6 Cell culture reagents and media

Table 10: List of cell culture reagents and media used in this thesis.

Cell culture reagents and media	Manufacturer	Identifier
Dimethyl sulfoxide (DMSO)	Sigma-Aldrich	#D8418
DMEM-F12 Ham(4.5 g/L D-glucose)	Thermo Fisher Scientific	#11765054
DMEM (4.5 g/L D-glucose, 1 mM sodium pyruvate, 4.0 mM glutamine)	Thermo Fisher Scientific	#31966-021
DMEM (-glucose, -glutamine, -phenol red)	Thermo Fisher Scientific	#A1443001
Dulbecco's modified eagle media (DMEM) (1 g/L D-glucose) w/o amino acids	US Biological (Biomol)	#D9800-13.10

Dulbecco's phosphate-buffered saline (DPBS)	Thermo Fisher Scientific	#14190-094
Fetal bovine serum (FBS)	Thermo Fisher Scientific	#10270-106
GlutaMAX (100x)	Thermo Fisher Scientific	#35050-061
Nonessential amino acids (NEAA) (100x)	Thermo Fisher Scientific	#11140-050
OptiMEM	Thermo Fisher Scientific	#31985-047
Penicillin/Streptomycin (P/S) (10000 U/mL/10000 μg/mL)	Thermo Fisher Scientific	#15140-122
Sodium pyruvate (SP) (100 mM)	Thermo Fisher Scientific	#11360-039
Trypan blue stain	Thermo Fisher Scientific	#15250-061
Trypsin (0.05%)-EDTA	Thermo Fisher Scientific	#25300-054

9.7 Cell lines

Table 11. List of cell lines used in this thesis.

Human embryonic kidney (HEK) 293T cells were a generous gift from Prof. Dr. Eilers.

Platinum-E	Cell bio labs	Cat#: RV-101 RRID:CVCL_B488
HEK293T cells	ATCC	Cat# CRL-3216, RRID:CVCL_0063

3T3-L1	ATCC	Cat# CL-173, RRID:CVCL_0123
T37i	Provided by Marc Lombès	(Zennaro, Le Menuet et al. 1998)
One Shot™ TOP10 Chemically Competent *E. coli*	Thermo Fisher Scientific	#C404003

9.8 Mice and diets

Table 12: List of mouse strains used in this thesis.

Mouse line	Manufacturer	Identifier
Mouse: *Erk3 floxed* mice ($Erk3^{fl/fl}$)	Biocytogen	N/A
Mouse: B6;FVB-Tg(Adipoq-cre)1Evdr/J	The Jackson Laboratory	IMSR Cat# JAX:010803, RRID:IMSR_JAX:010803
Mouse: C57BL/6-Tg(Adipoq-cre/ERT2)1Soff/J	The Jackson Laboratory	IMSR Cat# JAX:025124, RRID:IMSR_JAX:025124
Mouse: C57BL/6J	The Jackson Laboratory	IMSR Cat# JAX:000664, RRID:IMSR_JAX:000664

Table 13: List of research diets used in this thesis.

Experimental diets	Manufacturer	Identifier
High-fat diet (HFD) with 58 kcal% fat w/sucrose	ResearchDiets	#D12331i
Normal diet (ND)	sniff Spezialdiäten	#V1125-3

9.9 Softwares

Table 14: List of software programs used in this thesis.

Software and algorithms	Manufacturer	Identifier
GPS Explorer	Applied Biosystems	Version 3.5
Illustrator CS6	Adobe	N/A
Image QuantTL	GE Healthcare	
ImageJ	NIH	https://imagej.nih.gov/ij/
LAS X	Leica	
A plasmid Editor - ApE	omicX	
MaxQuant		Version 1.6.2.2
QIAgility	Qiagen	Version 4.13.5
QuantStudio™ Design & Analysis Software	Thermo Fischer Scientific	
Trace finder software	Thermo Fischer Scientific	
Endnote		Version X9

10 METHODS

10.1 Pre-adipocyte culture and differentiation

3T3-L1 pre-adipocytes, Platinum-E and HEK293T cells were cultured and maintained in Dulbecco's modified eagle's medium (DMEM), 10% fetal bovine serum (FBS), 1% non-essential amino acids (NEAA) and 40µg/mL gentamycin. Stromal vascular cells (SVCs) were isolated from subcutaneous white adipose tissue (sWAT) or brown adipose tissue (BAT) of 5-9 weeks old mice as previously described in (Cai, El-Merahbi et al. 2017). Concisely, mice subcutaneous white adipose tissue (SubWAT) and brown adipose tissue (BAT) were sliced and digested in PBS containing 1mg/mL collagenase D, 5mM CaCl2 and 1% BSA for 40 minutes at 37 C. Adipose tissue are then passed through a 40µm mesh, washed in PBS by centrifugation and plated on Matrigel-coated plates in DMEM/F-12 containing 10% FBS 1% NEAA and 40µg/mL gentamycin. Two days post-confluence, preadipocytes differentiation was induced by 0.2 µM Indomethacin, 0.5 mM IBMX, 1 µM dexamethasone and 1.5 µg/mL insulin for the first 48 hours. Afterward, cells were maintained in complete medium with 1.5 µg/mL insulin for up to six additional days. In preadipocytes derived from BAT, additionally, T3 (2 nM) was added to the medium throughout differentiation. 3T3-L1 cells were differentiated into adipocytes according to the standard procedure demonstrated in figure1. Before treatment, differentiated adipocytes were washed twice with Phenol-Free DMEM then serum-starved for 2 hours in phenol red-free DMEM supplemented with 2% BSA. Afterwards and as indicated in experiments, treatments are added in following concentrations: Isoproterenol (1,10 µM), Mg-132 (10 µM), Forskolin (20uM), and IBMX(0.5mM), CL316,243 (10uM), lactacystin (Sigma) (20 µM), Cycloheximide (100ug/ml), H89 (20uM), PKI14-22 (20uM), leptomycin B1 (50nM), BW-723C86 (10uM).

10.2 Transient transfection with siRNA

Mature adipocytes, differentiated form 3t3-L1 or SVFs, were transfected with siRNA always-in suspension as follows: Mature adipocytes cultured on cell+ plates (Sarstedt) were detached with Accutase solution (Sigma) for 10min, spun down (5min, 300g) and counted. Indicated siRNAs smart pools and Dharmafect-Duo transfection reagent (Dharmacon) were diluted in Opti-MEM I Reduced Serum Medium separately before being mixed by pipetting. The siRNA-Duofect mix was

left to incubate for 30min at room temperature. Meanwhile, counted cells were then re-suspended in the culture medium, containing insulin, and added on top of the pre-incubated siRNA-Duofect mix. Finally, the mixture was added to Matrigel-coated culture plates or 96-well Seahorse plates. The final concentrations of Duofect, siRNA and cell number were adjusted per surface area in a ratio of 2.1 ul/cm^2 duofect, 1.25nM/cm^2 siRNA and $16.4x10^4$/cm^2 cells respectively. The cells were utilized for experiments 48hrs after transfection. All siRNA sequences were purchased as smart pools from Dharmacon.

10.3 Generation of stable cell lines

The Dharmacon GIPZ Lentiviral shRNA system was used to induce long-term gene silencing of *Erk3* gene, shRNA *Erk3* oligo was synthesized by following sequence below and cloned into a pGIPZ shRNA mir (a generous gift from Eilers lab, Biocenter, Würzburg) as followed below. between XhoI and EcoRI cloning sites.The pBABE- Puro Retroviral Vector system was used to overexpress ERK3 protein. Concisely, Myc tagged *Erk3* coding sequence was cloned from the human cDNA vector and inserted between EcoR1 and Sal1 in the pBABE vector. HA-Foxo1 and 3xFLAG-Mk5 overexpressing vectors were synthesized by Vectorbuilder by the insertion of their respective coding sequences in PLV-Puro lentivirus plasmid (plasmid map 3, 4). For HA-foxo1 s215A, D as well for 3xFLAG-MK5 S115A, E the following primers (Oligo primer list) were used to generate a point mutation on indicated sites using Q5 site-directed mutagenesis kit (NEB) following the manufacture recommendations. Lentiviral particles were packaged in HEK293T cells with psPAX (Adgene) and pMD2.G (Adgene) together with the targeted sequence or the scrambled control. Retroviral particles were produced using PlatinumE cells. Viral particles are collected and filtered by 40um filter papers then transduced in 3T3L1 cells. Cells were spinfected with viral supernatant with the addition of 4ug/ml polybrene (Sigma) then selected by Puromycin (5µg/mL, Thermo Fischer Scientific) for an additional 72 hours.

10.4 Molecular cloning

Cloning of the pGipz-shErk3 and the pBabe Puro-C-MYC-Erk3 plasmids were performed according to standard techniques. Briefly, The empty plasmid backbone was double-digested with high fidelity enzymes EcoRI and XhoI (as for pGIPZ shRNA mir) and EcoRI and SalI (pBabe Puro), respectively, in NEB CutSmart buffer for 1 h at 37°C followed by thermal inactivation for

10 min at 70°C. Subsequently, the DNA insert was amplified with the insertion of the respective sticky ends, digested as mentioned before. Both insert and its vector backbone was then separated on a 1% agarose gel at 90 V for 30 min. The specific bands were cut out and DNA was purified with a kit according to the manufacturer's instructions (NucleoSpin Gel and PCR Clean-up, Macherey-Nagel). Afterward, ligations with several different insert/backbone rations were performed with T4 ligase for 1.5 h at RT. The complete fusion was further verified by plasmids sequencing as a service provided from Eurofins Genomics

10.5 Transformation

One-Shot TOP10 chemically competent *E. coli* bacteria were used for transformation. Briefly, the ligated vector was added to the competent cells right after the thawing of the cells on ice. The mixture was then incubated on ice for 30 min before a heat shock at 42°C in a water bath for 30 *seconds* (s). Thereafter, 250 µL SOC-medium was added to the bacteria and incubated for 1 h at 37°C with continuous shaking at 250 rpm. The transformation mixture was plated on antibiotic-containing agar plates and incubated at 37°C overnight. Positive clones were picked and further cultured in LB-medium for Mini preps

10.6 Plasmid purification (Mini and Midi prep)

picked clones were cultured in LB-medium supplemented with respective antibiotics at 37°C and 225 rpm overnight. Part of the culture was used for plasmid purification using the mini prep kit (NucleoSpin Plasmid, Macherey-Nagel) according to the manufacturer's guidelines. Briefly, the Bactria were pelleted by centrifugation then resuspended using buffer A1. Cells are then lysed by adding A2 buffer for 5 min followed by neutralizing of the mixture by adding of buffer A3, and the lysate was clarified from precipitated proteins by centrifugation for 10 min at 11000 rpm. The clear supernatant was loaded onto the column and washed with buffer AW and buffer A4 (1 min, 11000 rpm, respectively). Finally, the plasmid was eluted with buffer AE (1 min, 11000 rpm). Sequencing confirmed successfully cloned plasmids (Eurofins). Positive mini cultures were used to inoculate 200 mL LB-medium for overnight culture. Plasmid purification of midi cultures was performed according to the manufacturer's protocol (NucleoBond Midi, Macherey-Nagel).

10.7 Generation of Viral particles

Lentiviral particles were packaged in HEK293T cells with psPAX (Addgene) and pMD2.G (Addgene) together with the targeted sequence or the scrambled control. Concisely, the respective packaging cells were cultured on a poly-L Lysine pre-coated plates. For plating, $1x10^6$ cells 6cm plate were seeded one day before the transfection (cells were 70-80% confluent at transfection). Transfection of the cells was carried out by using the Darmafect Duo transfection reagent according to the manufacturer's instructions. In brief, Lentiviral particles were packaged in HEK293T cells with targeted or scrambled control pGIPZ shRNA mir, psPAX and pMD2.G in a ratio of 10µg pgipz: 10µg psPAX: 4µg pMD2.G. Retroviral particles were produced using PlatinumE cells using 20 µg of the pBABe plasmid only. Afterward, 20 µL of the transfection reagent was mixed with 230 µL OptiMEM followed by the addition of an equal volume of plasmids in OptiMEM. The plasmid/transfection reagent mixture was incubated for 30 min at RT before adding it dropwise to the wells containing cells in an antibiotic-free growth medium. After overnight incubation, the transfection medium was replaced by a standard growth medium containing 1% P/S. 48 h and 72 hrs post-transfection, viral particles in the supernatant were collected and filtered then used for spinfection of 3T3l1 in combination with polybrene.

10.8 Lipolysis Assay

Determination of free glycerol and Free Fatty acids was performed as described before (Löffler, Mayer et al. 2018). In brief, adipocytes were washed twice with Phenol-Free DMEM then serum-starved for 2 hours in phenol red-free DMEM supplemented with 2% Fatty acid-free BSA, afterward stimulated with 1µM isoproterenol (Sigma) for 2 hours. The conditioned medium was then collected and analyzed. FFAs in the medium were measured using NEFA-reagents (Wako) and glycerol was quantified by free glycerol reagent (Sigma) according to the manufacturers' instructions. Values were normalized to the cell's total DNA content by Hoechst 33342 staining.

10.9 Lipogenesis assay

De novo lipogenesis assay was performed as described in (ALEX paper). Briefly, Indicated cells were incubated in lipogenic medium (DMEM w 25 mM glucose, 0.2 % FFA-free BSA and 4 µCi/mL 3H-acetate (Perkin Elmer)) at basal or insulin (100 nM) stimulated conditions for 6 hours.

After the extraction of total intracellular lipids, the amount of tritium incorporated into the newly formed lipids were measured in a lipid scintillation counter. Data were then normalized by the cells' total protein content (Bradford, Bio-Rad).

For Oil Red O staining, cultured cells were fixed with 4% PFA for 10 min at room temperature. Fixed cells are washed twice with ddH2O the 60% isopropanol for 5 min each then left o air dry. Afterward, cells' lipids content are stained with 0.375% Oil Red O solution (3:2 isopropanol:ddH2O, v/v) for 10min. Finally, excess oil red o was washed away by ddH2O (4 washes) then cells were ready for imaging under a light microscope.

10.10 Oxygen consumption

Mitochondrial respiration of brown adipocytes derived from the stromal-vascular fraction was determined by measuring the oxygen consumption rate (OCR) using the Seahorse XF Cell Mito Stress Test (103015-100; Agilent Technologies) in a Seahorse XFe96 Analyzer according to the manufacturer's protocol. Briefly, cells were incubated for 1 h with 180 µl Seahorse assay medium containing 1 mM sodium pyruvate, 2 mM glutamine, and 5 mM glucose. Subsequently, the cells were stimulated with 2 µM of oligomycin, 1 µM FCCP, and 0.75 µM rotenone/antimycin A. Cells are then fixed and the total DNA content was assessed by crystal violet staining. Absorbance was read at 595 in a Spark 10M microplate reader (Tecan) and the measurements were used to normalize the seahorse values.

10.11 Generation of mouse models

All experiments with mouse models were approved by the local institutional animal care (Regierung von Unterfranken, Germany) and conducted according to the guidelines and state regulations. Experiments were performed under animal protocol number AK 55.2-2531.01-124/13. Mice were maintained in a specific-pathogen-free facility with a 12-h light-dark cycle and given ad libitum access to water and standard chow diet (sniff Spezialdiäten) which was exchanged under indicated experimental conditions to High-fat diet (HFD) (ResearchDiets, D12331). All mice were closely monitored by the authors, facility technicians and by an independent veterinary scientist responsible for animal welfare.

Erk3 floxed mice (*Erk3*$^{fl/fl}$) were genetically engineered on the C57BL/6 background by Biocytogen Inc. Briefly, the targeting vector containing part of the *Erk3* gene was constructed as

demonstrated in Figure 30. Briefly, the selection neomycin (Neo) containing cassette flanked by two FLP sites was inserted between Exon (E) 3 and 4 together with the LoxP site. The second LoxP site was inserted between E2 and E3. At the 3'-end of the construct negative selection cassette containing diphtheria toxin was inserted. The resulting construct was linearized and electroporated into the BL6-derived ES-cells. Upon selection of positive clones and expansion of ES-cells in which homologs recombination took place, the ES cells were injected into the blastocyst and implanted into a pseudo-pregnant female. The resulting chimeric mice were crossed with the FLPe knock-in mice to remove the Neo cassette. The resulting *Erk3* flox mice ($Erk3^{f/f}$) were utilized for the generation of targeted deletion in tissues. For targeted deletion of *Erk3* in adipocytes, $Erk3^{f/f}$ mice were cross-bred with adiponectin promoter-driven Cre mice (adiponectin-Cre) (JAX stock 010803). As for the inducible model, $Erk3^{f/f}$ mice were cross-bred with adiponectin promoter-driven Cre-ERT2 mice (JAX stock 025124) 100 mg/kg tamoxifen was then administered orally when indicated in experiments above for five consecutive days to initiate deletion *Erk3*.

10.12 Animal Experiments

For induction of lipolysis, we injected mice deficient for *Erk3* in adipocytes ($Erk3^{Adipo.\Delta/\Delta}$) and corresponding control $Erk3^{f/f}$ animals with β-adrenergic agonist CL316,243 (CL) (Tocris Bioscience) intraperitoneally (i.p.) at a concentration of 2 mg/kg in 0.9% NaCl. Blood was sampled from the tail vein for metabolic studies as indicated on the corresponding figures.

The body weight gain of mice was monitored every other week. Body composition, including fat mass, lean mass and free fluids content, was analyzed by Nuclear Magnetic Resonance (NMR) using a Bruker's minispec LF50 body composition analyzer according to the manufacturer's instructions (Bruker Optik, Ettlingen, Germany) Indirect calorimetry measurements were done at the end using the Phenomaster system (TSE) as described before in (Viera, El-Merahbi et al. 2016). Briefly, mice were housed individually with ad libidum access to indicated food and water. After a 48-hour acclimation period, parameters were sampled for 72 hours in the fed stage. Locomotor activity was determined by consecutive photobeam breaks occurring in adjacent beams. All measurements were obtained every 10 min during a full light/dark cycle.

For blood glucose tolerance tests, mice fasted overnight, and glucose (2 g/kg) was administered intraperitoneal. For insulin sensitivity tests, mice were fasted for 4 hours before receiving an

intraperitoneal injection of 0.5 U/kg human insulin (Sigma). A blood drop was collected from the tail tip directly onto the test strip for the blood glucose measurement (Accu-Chek, Roche). Glucose concentrations were sampled in both conditions before and at 15, 30, 60, 90 and 120 min after injection.

10.13 Mouse genotyping

10.13.1DNA extraction from mouse tissue

After each mouse was clipped for numbering the clipped ear tissue was lysed in 500 µL DNA lysis buffer containing 0.1 mg/mL proteinase-K. Samples were placed in the thermomixer for overnight digestion with continuous shaking at 900 rpm at 55°C. Afterward, 100 µL of 5 M NaCl was added, samples were vortexed then centrifuged at 13000 rpm for 10 min at 4°C. Subsequently, the aqueous phase containing the nucleic acids (~500 µL) was isolated a new tube. DNA was precipitated with the addition of 500 µL of isopropanol followed by 30 min incubation at -20°C for 30 min to facilitate the process. after centrifugation at 13000 rpm for 10 min at 4°C, the supernatant was discarded and the precipitated nucleic acid pellet was washed with 1 mL of 70% ethanol and centrifuged again at 13000 rpm for 10 min at 4°C. DNA pellet was air-dried then solubilized in ddH2O. Genotyping of the mice was performed by a polymerase chain reaction (PCR) using specific primers.

10.13.2PCR for mouse genotyping

Table 15: PCR master mix applied for genotyping performed in this thesis.

Mix	1x
10x Thermo buffer - MgCl	2,4µl
MgCl	1,92µl
primer Frwd (10µM)	1,2µl
primer Rev (10µM)	1,2µl
dNTPs (2 mM stock)	0,96 µl
Taq polymerase (5 U/µL	0,2µl
H2O	14,12 µl

DNA	2 µl

Table 16. A chain reaction followed in genotyping for FLOX or Ert-Cre.

Step	Temperature	Time	Cycles
1	94°C	2 min	1x
2	94°C	20 sec	10x 0,5 °C decrease per cycle
3	65°C	15 sec	
4	68°C	10 sec	
5	94°C	15 sec	28 x
6	60°C	15 sec	
7	72°C	10 sec	
8	72 °C	2 min	1x
9	10 °C	hold	-

Table 17. A chain reaction followed in genotyping for Adipo-cre

Step	Temperature	Time	Cycles
1	95°C	3 min	1x
2	95°C	30 sec	28 x
3	54.2°C	1 min	
4	72°C	1 min	
5	72 °C	5 min	1x
6	4 °C	hold	∞

Table 18. Primers followed in genotyping protocols.

Genotyping Primers	Forward	Reverse
Adiponectin Cre	GGA TGT GCC ATG TGA GTC TG	ACG GAC AGA AGC ATT TTC CA
Adipoq-CreERT2	GAG TCT GCC TTT CCC ATG AC	ATC ACG TCC TCC ATC ATC C
LC-062-loxP	GTG GAT CCA CAC TCC TGT CTT AAG TC	GAA ACA CAG GCT CCA TGA ATC CAG

10.13.3Agarose gel electrophoresis

After amplification, PCR products were mixed with DNA loading dye and then separated on a 2% agarose gel. Briefly, the gel was made by adding 6 g of agarose to 300 mL 1x *TRIS-acetate-EDTA* (TAE) buffer and dissolved by heating it in the microwave followed by the addition of DNA stain (Midori Green Advance). The PCR products were then diluted in an appropriate amount of 6x loading dye and loaded together with the 100 bp DNA ladder onto the gel that was covered in 1x TAE. Separation of the samples and ladder was achieved at 120 V for 1 h followed by visualization using an *ultraviolet* (UV) device.

10.14 Histological analysis and cell size analysis

10.14.1Histological analyses

Tissues were isolated from mice, were washed with PBS then fixed in 4% paraformaldehyde. One day later, tissues were washed with 70% EtOH then placed in cassettes which allows its dehydration in an automated tissue processor. Tissues are then embedded in paraffin, cut in 5-µm sections and put on glass slides according to standard procedures.

10.14.2Hematoxylin and eosin staining

Hematoxylin and eosin (H&E) staining was performed according to standard laboratory procedures. In brief, dehydrated sections were deparaffinized in xylol (2x 10 min) and then proceeded with rehydration protocol in an alcohol gradient (100%, 100%, 95%, 90%, 80%, 70%, and 50%, 5 min each), followed by 5 min in ddH2O. Subsequently, the sections were stained with hematoxylin for 10 min, rinsed in tap water for 10 min, and put in ddH2O for an additional 5 min. Eosin counterstaining was performed for 2 min. Sections were dehydrated in an alcohol gradient (50%, 70%, 80%, 90%, 96%, 100%, and 100%, 2 min each) followed by xylol (2x 10 min). Finally, the sections were mounted in a xylene-based mounting medium (RotiMount. Digital images were captured using a Leica light microscope at 20X magnification. Measurement of adipocytes size and distribution was performed in a blinded fashion. Approximately 400 adipocytes per sample were measured using ImageJ software with the additional Adiposoft plugin.

10.14.3 Immunofluorescence microscopy

Immunofluorescent stainings were performed according to standard lab procedures. Indicated cells were seeded onto poly-L-lysine–treated glass coverslips in 12-well culture dishes and treated accordingly. Cells were washed in PBS before fixation with 4% paraformaldehyde for 10 min at room temperature. Cells were permeabilized with 0.5% Triton X-100 in PBS for 15 min at room temperature. To reduce nonspecific background noise, cell were blocked with PBS 5% (v/v) normal goat serum, 0.1% (v/v) Triton X-100, 0.05% (v/v) Tween 20. Primary antibody incubation was done for 16 hours in a humidified chamber at 4°C. After thorough washes, cells were incubated with Alexa Fluor 488 secondary antibody and Phalloidin–Atto 647N (Sigma) for 1 hour in the dark. Cells were then washed before being mounted onto glass slides using ProLong Gold mounting reagent (Life Technologies), which contained the nuclear stain 4′,6-diamidino-2-phenylindole (DAPI). Slides were visualized using Leica TCS SP8 confocal microscope.

10.15 Western blotting and immunoprecipitation of total and Subcellular fractionations

Total proteins were extracted from cells and tissues by a standard RIPA buffer supplemented with protease and phosphatase inhibitor (PPI) cocktail. Tissue pieces were homogenized with a homogenizing pestle, and cells were scraped from cell culture plates and forced through a 26 G

syringe needle for homogenization. Next, cell fragments were pelleted by centrifugation (13000 rpm, 10 min at 4°C) and the supernatant (protein lysate) was transferred to a new tube. Subcellular fractionations were performed using the NE-PER kit (Thermo-Scientific) according to the manufacturer's instructions. For immunoprecipitation (IP), indicated cells were lysed by Pierce IP Lysis buffer (Thermo-Scientific) and then IP using Flag-tag magnetic beads (M8823, Millipore) according to manufacturer's instructions. The lysis and wash buffers were all supplemented with protease and phosphatase inhibitors mix (Thermo-Scientific). Protein concentration was quantified using a BCA kit. Reduced protein extracts were mixed with appropriate loading dye, heated at 95 for 5 min then separated on 10% SDS-PAGE gels by electrophoresis and transferred PVDF membranes (Millipore) with wet transfer cells. Membranes were blocked in 5% (w/v) skim milk in TBS-T before overnight probing with indicated primary antibodies at 4 C, followed by TBST washes and incubation with corresponding secondary antibody. The signals were detected on Autoradiography Film with enhanced chemiluminescence solution (Biorad).

10.16 Real-time PCR analysis

Total RNA was extracted from tissue or cells using QIAzol Lysis Reagent according to the manufacturer's protocol. In brief, cells were scraped with 1 mL QIAzol Lysis Reagent and tissues were homogenized in the same amount of QIAzol Lysis Reagent using a benchtop homogenizer and incubated for 5 min at RT. Next, 0.2 mL of chloroform was added and incubated for 2-3 min at RT followed by phase separation (12000g, 15 min, 4°C). The aqueous phase was transferred to a new tube, mixed with 0.5 mL isopropanol, and incubated for 10 min at RT. After centrifugation (12000g, 15 min, 4°C), the supernatant was aspirated, and the pellet was washed in 1 mL 75% Ethanol. Following centrifugation (7500g, 5 min, 4°C), the supernatant was removed, and the pellet was air-dried for 10 min. An appropriate amount of RNase-free water was added and the RNA concentration and quality were assessed using a NanoDrop spectral photometer. For complementary DNA (cDNA) synthesis, First Strand cDNA Synthesis Kit was used according to the manufacturer's instructions. The master mix was heated up to 65°C in a thermal cycler for 5 min and cooled on ice afterward. Next, 9 µL of master mix 2 was added, incubated for 5 min at 25°C, and followed by 60 min at 37°C in a thermal cycler. Finally, the reaction was terminated with a heating step for 5 min at 70°C.

cDNA of cells was diluted 1:5 and from tissues 1:10 – 1:15 in RNase-free water. RT-qPCR was performed using PowerUp SYBR Green Master Mix as described below. The RT-qPCR samples and master mix were pipetted by a QIAgility and analyzed on a QuantStudio 5 Real-Time PCR System.

RT-qPCR mix:

2 µL	cDNA (diluted)
5 µL	PowerUp SYBR Green Master Mix
0.4 µL	forward primer (1:10 in H2O, stock: 1 µg/mL)
0.4 µL	reverse primer (1:10 in H2O, stock: 1 µg/mL)
2.2 µL	RNase-free water

The relative expression from the mRNAs of indicated genes was calculated using the comparative DDCT method normalized to the reference gene Rpl13a. The mouse primer sequences (sense and antisense) are listed in Table 4.

10.17 RNA sequencing

RNA-Sequencing was performed as described previously (Löffler, Mayer et al. 2018). Briefly, mRNA was isolated using the NEBNext® Poly(A) mRNA Magnetic Isolation Module (NEB) and library preparation was performed with the NEBNext® Ultra™ RNA Library Prep Kit for Illumina following the instruction manual. Libraries were size-selected using Agencourt AMPure XP beads (Beckman Coulter) followed by amplification with 12 PCR cycles. Library quantification and size determination were performed with the Experion Automated Electrophoresis System (Bio-Rad). The libraries were sequenced with an Illumina Genome Analyzer IIx or an Illumina NextSeq 500. The RNA-sequencing raw- and processed datasets, as well as information on data processing, can be found at accession number: GSE 142424.

10.18 Chromatin immunoprecipitation (Chip) assay

ChIP studies were carried out using the ChIP kit (Abcam) according to the manufacturer's instructions. Briefly, after crosslinking, nuclei extracted from indicated 3T3-L1 mature adipocytes were lysed and sonicated for 15 (on/off) cycles of 15 sec each. FOXO1 proteins were then immunoprecipitated from precleared lysates using the chip-grade FOXO1 antibody (Abcam) or

Actin antibody as a negative control. Protein-DNA complexes were eluted and treated with proteinase-K. Purified DNA was analyzed by quantitative PCR using SYBR green reaction with the following primers: 5′-AGGTTTCTAGTTTAGGATTGAAG-3′ and 5′-ACCTGAGCAGTAGTTATATACAT-3′ (–1041 to –1158 nt of the Atgl promoter) as described in Chakrabarti and Kandror (2009a) and the Ucp1 promoter primers (5′-CTGTTGTTGCTGCTGCTGTT-3′ and 5′-GGAAGCTGCAAGACCTATGG-3′) as described in (Ortega-Molina, Efeyan et al. 2012). The percentage of enrichment was calculated based on percent input DNA after adjusting for total input DNA: 100 × 2(adjusted input Ct − IP Ct).

10.19 Statistical analysis

The results are presented as mean values ± standard error of the mean (SEM). Significances were assessed by using a two-tailed Student's t-test for independent groups, or by using one-way or two-way analysis of variance (ANOVA), followed by a post hoc Tukey's test for multiple comparisons. P values of 0.05 or lower were considered as statistically significant (*p<0.05, **p<0.01, and ***p<0.001).

10.20 Plasmid maps

10.21 pGipz-Sherk3

NAME OF PLASMID: **pGIPZ ERK 3 seq 3** 11822 bp
CREATED BY: Rabih El Merahbi, 28.07.2015
VECTOR: pGIPZ NTC (Lentiviral shRNAmir - Thermo Scientific), 11688 bp
SELECTION MARKER: Amp, Puro

10.21.1shErk3 inserted sequence

TGCTGTTGACAGTGAGCGACAGAGTGTCAAACATGCTCTATAGTGAAGCCACAGAT
GTATAGAGCATGTTTGACACTCTGGTGCCTACTGCCTCGGAA

10.22 pBABE puro Erk3-Myc

pBABE puro Erk3-Myc, 7356 bp
CREATED BY: Rabih El Merahbi, 12.11.2015

VECTOR: pBABE-Puro (Cell Biolabs, RTV-001-PURO), 5169 bp

5’ cloning site: EcoRI (not destroyed)

3’ cloning site: SalI (not destroyed)

INSERT: Erk3-Myc (pEX-K4 Erk3-Myc, synthesized by Eurofins), 2199 bp (Insert)

5’ cloning site: EcoRI

3’ cloning site: SalI

SELECTION MARKER: Amp

MAP:

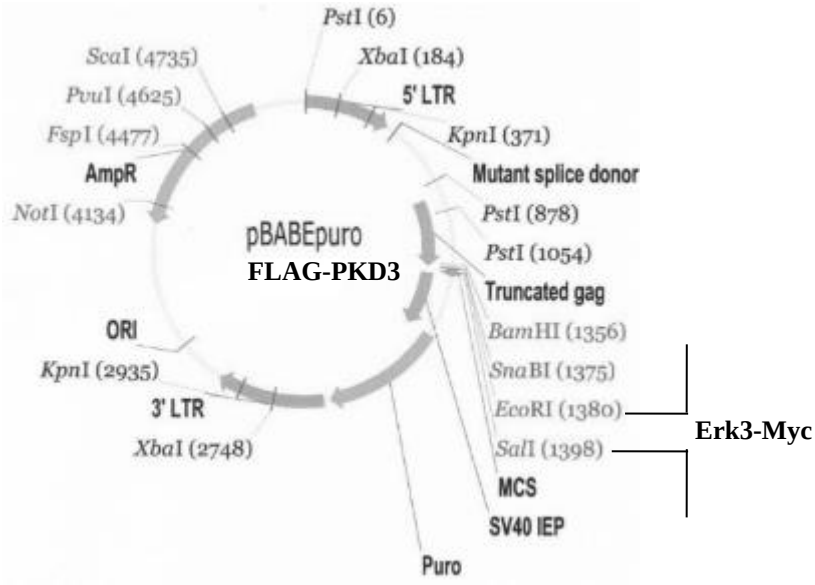

10.22.1 pBABE puro Erk3-Myc inserted sequence

atggcagagaaatttgaaagtctcatgaacattcatggttttgatctgggttctaggtatatggacttaaaaccattgggttgtggaggcaatgg
cttggtttttctgctgtagacaatgactgtgacaaaagagtagccatcaagaaaattgtccttactgatccccagagtgtcaaacatgctctac
gtgaaatcaaaattattagaagacttgaccatgataacattgtgaaagtgtttgagattcttggtcccagtggaagccaattaacagacgatgtg
ggctctcttacggaactgaacagtgtttacattgttcaggagtacatggagacagacttggctaatgtgctggagcagggccctttactggaa
gagcatgccaggcttttcatgtatcagctgctacgggggctcaagtatattcactctgcaaatgtactgcacagagatctcaaaccagctaatc
ttttcattaatacggaagacttggtgctgaagataggtgactttggtcttgcacggatcatggatcctcattattcccataagggtcatctttctga
aggattggttactaaatggtacagatctccacgtcttttactttctcctaataattatactaaagccattgacatgtgggctgcaggctgcatctttg
ctgaaatgctgactggtaaaaccctttttgcaggtgcacatgaacttgaacagatgcagctgattttagaatctattcctgttgtacatgaggaa
gatcgtcaggagcttctcagcgtaattccagtttacattagaaatgacatgactgagccacacaaacctttaactcagctgcttccaggaatta
gtcgagaagcactggatttcctggaacaaattttgacatttagccccatggatcggttaacagcagaagaagcactctcccatccttacatga

gcatatattcttttccaatggatgagccaatttcaagccatccttttcatattgaagatgaagttgatgatattttgcttatggatgaaactcacagtc
acatttataactgggaaaggtatcatgattgtcagttttcagagcatgattggcctgtacataacaactttgatattgatgaagttcagcttgatcc
aagagctctgtccgatgtcactgatgaagaagaagtacaagttgatccccgaaaatatttggatggagatcgggaaaagtatctggaggatc
ctgcttttgataccaattactctactgagccttgttggcaatactcagatcatcatgaaaacaaatattgtgatctggagtgtagccatacttgtaa
ctacaaaacgaggtcatcatcatatttagataacttagtttggagagagagtgaagttaaccattactatgaacccaagcttattatagatctttcc
aattggaaagaacaaagcaaagaaaaatctgataagaaaggcaaatcaaaatgtgaaaggaatggattggttaaagcccagatagcgcta
gaggaagcatcacagcaactggctggaaaagaaagggaaaagaatcagggatttgattttgattcctttattgcaggaactattcagcttagtt
cccagcatgagcctactgatgttgttgataaattaaatgacttgaatagctcagtgtcccaactagaattgaaaagtttgatatcaaagtcagtaa
gccaagaaaaacaggaaaaaggaatggcaaatctggctcaattagaagccttgtaccagtcttcttgggacagccagtttgtgagtggtgg
ggaggactgtttttttcataaatcagttttgtgaggtaaggaaggatgaacaagttgagaaggaaaacacttacactagttacttggacaagttct
ttagcaggaaagaagatactgaaatgctagaaactgagccagtagaggatgggaagcttggggagagaggacatgaggaaggatttctg
aacaacagtggggagttcctctttaacaagcagctcgagtccataggcatcccacagtttcacagtccagttgggtcaccacttaagtcaata
caggccacattaacaccttctgctatgaaatcttcccctcaaattcctcatcaaacatacagcagcattctgaaacatctgaactaaGAACA
AAAACTCATCTCAGAAGAGGATCTGTAA

10.23 HA-Foxo1

pLV[Exp]-Puro-CMV>HA/mFoxo1[NM_019739.3] , 9894 bp
CREATED BY: Vector builder, VB181004-1020nwp
SELECTION MARKER: Puromycin
Antibiotic Resistance: Ampicillin
MAP:

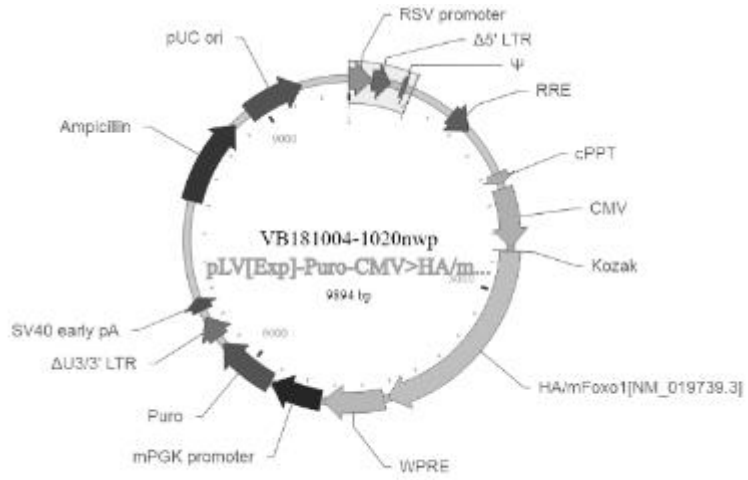

10.24 3xFLAG MK5

Plasmid name: pLV[Exp]-Puro-CMV>3xFLAG/mMapkapk5[NM_010765.2]

CREATED BY: Vector builder: VB181112-1103sva

SELECTION MARKER: Puromycin

Antibiotic Resistance: Ampicillin

MAP:

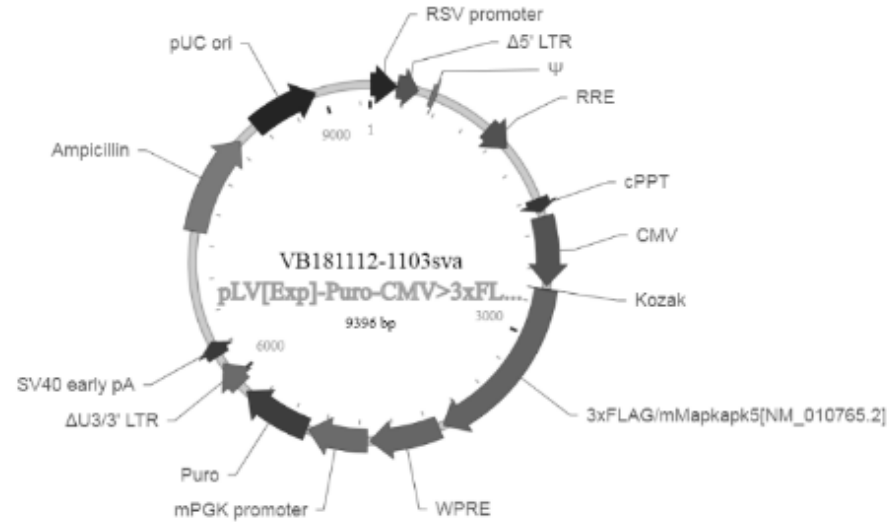

11 REFERENCES

Åberg, E., K. M. Torgersen, B. Johansen, S. M. Keyse, M. Perander and O.-M. Seternes (2009). "Docking of PRAK/MK5 to the atypical MAPKs ERK3 and ERK4 defines a novel MAPK interaction motif." Journal of Biological Chemistry **284**(29): 19392-19401.

Ahmadian, M., M. J. Abbott, T. Tang, C. S. Hudak, Y. Kim, M. Bruss, M. K. Hellerstein, H.-Y. Lee, V. T. Samuel and G. I. Shulman (2011). "Desnutrin/ATGL is regulated by AMPK and is required for a brown adipose phenotype." Cell metabolism **13**(6): 739-748.

Al-Mahdi, R. (2015). "Identification of novel roles and new modes of regulation for the atypical MAP kinases ERK3 and ERK4."

Al-Mahdi, R., N. Babteen, K. Thillai, M. Holt, B. Johansen, H. L. Wetting, O.-M. Seternes and C. M. Wells (2015). "A novel role for atypical MAPK kinase ERK3 in regulating breast cancer cell morphology and migration." Cell adhesion & migration **9**(6): 483-494.

Alsabeeh, N., B. Chausse, P. A. Kakimoto, A. J. Kowaltowski and O. Shirihai (2018). "Cell culture models of fatty acid overload: problems and solutions." Biochimica et Biophysica Acta (BBA)-Molecular and Cell Biology of Lipids **1863**(2): 143-151.

Altomonte, J., L. Cong, S. Harbaran, A. Richter, J. Xu, M. Meseck and H. H. Dong (2004). "Foxo1 mediates insulin action on apoC-III and triglyceride metabolism." The Journal of clinical investigation **114**(10): 1493-1503.

An, Y., Q. Kang, Y. Zhao, X. Hu and N. Li (2013). "Lats2 modulates adipocyte proliferation and differentiation via hippo signaling." PloS one **8**(8).

Anthonsen, M. W., L. Rönnstrand, C. Wernstedt, E. Degerman and C. Holm (1998). "Identification of novel phosphorylation sites in hormone-sensitive lipase that are phosphorylated in response to isoproterenol and govern activation properties in vitro." Journal of Biological Chemistry **273**(1): 215-221.

Antonopoulos, A. S., M. Margaritis, S. Verheule, A. Recalde, F. Sanna, L. Herdman, C. Psarros, H. Nasrallah, P. Coutinho and I. Akoumianakis (2016). "Mutual regulation of epicardial adipose tissue and myocardial redox state by PPAR-γ/adiponectin signalling." Circulation research **118**(5): 842-855.

Arner, P., S. Bernard, M. Salehpour, G. Possnert, J. Liebl, P. Steier, B. A. Buchholz, M. Eriksson, E. Arner and H. Hauner (2011). "Dynamics of human adipose lipid turnover in health and metabolic disease." Nature **478**(7367): 110-113.

Arner, P. and D. Langin (2014). "Lipolysis in lipid turnover, cancer cachexia, and obesity-induced insulin resistance." Trends Endocrinol Metab **25**(5): 255-262.

Arner, P. and D. Langin (2014). "Lipolysis in lipid turnover, cancer cachexia, and obesity-induced insulin resistance." Trends in Endocrinology & Metabolism **25**(5): 255-262.

Barbatelli, G., I. Murano, L. Madsen, Q. Hao, M. Jimenez, K. Kristiansen, J. Giacobino, R. De Matteis and S. Cinti (2010). "The emergence of cold-induced brown adipocytes in mouse white fat depots is determined predominantly by white to brown adipocyte transdifferentiation." American Journal of Physiology-Endocrinology and Metabolism **298**(6): E1244-E1253.

Barrington, P., J. Chien, H. Showalter, K. Schneck, S. Cui, F. Tibaldi, B. Ellis and T. Hardy (2011). "A 5‐week study of the pharmacokinetics and pharmacodynamics of LY2189265,

a novel, long‐acting glucagon‐like peptide‐1 analogue, in patients with type 2 diabetes." Diabetes, Obesity and Metabolism **13**(5): 426-433.
Bartz, R., J. K. Zehmer, M. Zhu, Y. Chen, G. Serrero, Y. Zhao and P. Liu (2007). "Dynamic activity of lipid droplets: protein phosphorylation and GTP-mediated protein translocation." Journal of proteome research **6**(8): 3256-3265.
Beiroa, D., M. Imbernon, R. Gallego, A. Senra, D. Herranz, F. Villarroya, M. Serrano, J. Fernø, J. Salvador and J. Escalada (2014). "GLP-1 agonism stimulates brown adipose tissue thermogenesis and browning through hypothalamic AMPK." Diabetes **63**(10): 3346-3358.
Bernard, C. (1856). Mémoire sur le pancréas: et sur le role du suc pancréatique dans les phénomènes digestits, particulièrement dans la digestion des matières grasses neulces, IB Baillière.
Betz, M. J. and S. Enerbäck (2015). "Human brown adipose tissue: what we have learned so far." Diabetes **64**(7): 2352-2360.
Betz, M. J. and S. Enerbäck (2018). "Targeting thermogenesis in brown fat and muscle to treat obesity and metabolic disease." Nature Reviews Endocrinology **14**(2): 77.
Bind, E., Y. Kleyner, D. Skowronska-Krawczyk, E. Bien, B. D. Dynlacht and I. Sánchez (2004). "A novel mechanism for mitogen-activated protein kinase localization." Molecular biology of the cell **15**(10): 4457-4466.
Birmingham, A., L. M. Selfors, T. Forster, D. Wrobel, C. J. Kennedy, E. Shanks, J. Santoyo-Lopez, D. J. Dunican, A. Long and D. Kelleher (2009). "Statistical methods for analysis of high-throughput RNA interference screens." Nature methods **6**(8): 569-575.
Birmingham, A., L. M. Selfors, T. Forster, D. Wrobel, C. J. Kennedy, E. Shanks, J. Santoyo-Lopez, D. J. Dunican, A. Long and D. J. N. m. Kelleher (2009). "Statistical methods for analysis of high-throughput RNA interference screens." **6**(8): 569-575.
Blüher, M. (2019). "Obesity: global epidemiology and pathogenesis." Nature Reviews Endocrinology **15**(5): 288.
Bouchard, C. (1991). "Current understanding of the etiology of obesity: genetic and nongenetic factors." The American journal of clinical nutrition **53**(6): 1561S-1565S.
Bowers, R. R., W. T. Festuccia, C. K. Song, H. Shi, R. H. Migliorini and T. J. Bartness (2004). "Sympathetic innervation of white adipose tissue and its regulation of fat cell number." American Journal of Physiology-Regulatory, Integrative and Comparative Physiology **286**(6): R1167-R1175.
Brand, F., S. Schumacher, S. Kant, M. B. Menon, R. Simon, B. Turgeon, S. Britsch, S. Meloche, M. Gaestel and A. Kotlyarov (2012). "The ERK3 (MAPK6)-MAPKAP kinase 5 signalling complex regulates septin function and dendrite morphology." Molecular and Cellular Biology: MCB. 06633-06611.
Bryant, N. J., R. Govers and D. E. James (2002). "Regulated transport of the glucose transporter GLUT4." Nature reviews Molecular cell biology **3**(4): 267-277.
Cai, K., R. El-Merahbi, M. Loeffler, A. E. Mayer and G. Sumara (2017). "Ndrg1 promotes adipocyte differentiation and sustains their function." Scientific reports **7**(1): 7191.
Cai, K., R. El-Merahbi, M. Loeffler, A. E. Mayer and G. Sumara (2017). "Ndrg1 promotes adipocyte differentiation and sustains their function." Scientific reports **7**(1): 1-9.
Cai, K., R. El-Merahbi, M. Loeffler, A. E. Mayer and G. Sumara (2017). "Ndrg1 promotes adipocyte differentiation and sustains their function." Sci Rep **7**(1): 7191.

Cannon, B. and J. Nedergaard (2004). "Brown adipose tissue: function and physiological significance." Physiological reviews **84**(1): 277-359.
Cao, J., J.-L. Li, D. Li, J. F. Tobin and R. E. Gimeno (2006). "Molecular identification of microsomal acyl-CoA: glycerol-3-phosphate acyltransferase, a key enzyme in de novo triacylglycerol synthesis." Proceedings of the National Academy of Sciences **103**(52): 19695-19700.
Cao, Y. (2013). "Angiogenesis and vascular functions in modulation of obesity, adipose metabolism, and insulin sensitivity." Cell metabolism **18**(4): 478-489.
Cargnello, M. and P. P. Roux (2011). "Activation and function of the MAPKs and their substrates, the MAPK-activated protein kinases." Microbiol. Mol. Biol. Rev. **75**(1): 50-83.
Cargnello, M. and P. P. J. M. M. B. R. Roux (2011). "Activation and function of the MAPKs and their substrates, the MAPK-activated protein kinases." **75**(1): 50-83.
Carlson, M. G., W. L. Snead and P. J. Campbell (1994). "Fuel and energy metabolism in fasting humans." The American journal of clinical nutrition **60**(1): 29-36.
Chakrabarti, P. and K. V. Kandror (2009). "FoxO1 controls insulin-dependent adipose triglyceride lipase (ATGL) expression and lipolysis in adipocytes." Journal of biological chemistry **284**(20): 13296-13300.
Chakrabarti, P. and K. V. Kandror (2009). "FoxO1 controls insulin-dependent adipose triglyceride lipase (ATGL) expression and lipolysis in adipocytes." J Biol Chem **284**(20): 13296-13300.
Chakrabarti, P., J. Y. Kim, M. Singh, Y.-K. Shin, J. Kim, J. Kumbrink, Y. Wu, M.-J. Lee, K. H. Kirsch and S. K. Fried (2013). "Insulin inhibits lipolysis in adipocytes via the evolutionarily conserved mTORC1-Egr1-ATGL-mediated pathway." Molecular and cellular biology **33**(18): 3659-3666.
Chen, G., M. Hitomi, J. Han and D. W. Stacey (2000). "The p38 pathway provides negative feedback for Ras proliferative signaling." Journal of Biological Chemistry **275**(50): 38973-38980.
Cheng, M., T. G. Boulton and M. H. Cobb (1996). "ERK3 is a constitutively nuclear protein kinase." Journal of Biological Chemistry **271**(15): 8951-8958.
Cheng, Z. (2015). "FoxO1: mute for a tuned metabolism?" Trends in Endocrinology & Metabolism **26**(8): 402-403.
Cheng, Z. and M. F. White (2011). "Targeting Forkhead box O1 from the concept to metabolic diseases: lessons from mouse models." Antioxidants & redox signaling **14**(4): 649-661.
Choe, S. S., J. Y. Huh, I. J. Hwang, J. I. Kim and J. B. Kim (2016). "Adipose tissue remodeling: its role in energy metabolism and metabolic disorders." Frontiers in endocrinology **7**: 30.
Choi, S. M., D. F. Tucker, D. N. Gross, R. M. Easton, L. M. DiPilato, A. S. Dean, B. R. Monks and M. J. Birnbaum (2010). "Insulin regulates adipocyte lipolysis via an Akt-independent signaling pathway." Molecular and cellular biology **30**(21): 5009-5020.
Chooi, Y. C., C. Ding and F. Magkos (2019). "The epidemiology of obesity." Metabolism **92**: 6-10.
Chouchani, E. T. and S. Kajimura (2019). "Metabolic adaptation and maladaptation in adipose tissue." Nature metabolism **1**(2): 189-200.
Chouchani, E. T. and S. J. N. m. Kajimura (2019). "Metabolic adaptation and maladaptation in adipose tissue." **1**(2): 189-200.

Chow, K. T., G. A. Timblin, S. M. McWhirter and M. S. Schlissel (2013). "MK5 activates Rag transcription via Foxo1 in developing B cells." Journal of Experimental Medicine **210**(8): 1621-1634.
Cinti, S. (2012). "The adipose organ at a glance." Disease models & mechanisms **5**(5): 588-594.
Cinti, S., G. Mitchell, G. Barbatelli, I. Murano, E. Ceresi, E. Faloia, S. Wang, M. Fortier, A. S. Greenberg and M. S. Obin (2005). "Adipocyte death defines macrophage localization and function in adipose tissue of obese mice and humans." Journal of lipid research **46**(11): 2347-2355.
Claussnitzer, M., S. N. Dankel, K.-H. Kim, G. Quon, W. Meuleman, C. Haugen, V. Glunk, I. S. Sousa, J. L. Beaudry and V. Puviindran (2015). "FTO obesity variant circuitry and adipocyte browning in humans." New England Journal of Medicine **373**(10): 895-907.
Coulombe, P. and S. Meloche (2007). "Atypical mitogen-activated protein kinases: structure, regulation and functions." Biochimica et Biophysica Acta (BBA)-Molecular Cell Research **1773**(8): 1376-1387.
Coulombe, P., G. Rodier, E. Bonneil, P. Thibault and S. Meloche (2004). "N-Terminal ubiquitination of extracellular signal-regulated kinase 3 and p21 directs their degradation by the proteasome." Molecular and cellular biology **24**(14): 6140-6150.
Coulombe, P., G. Rodier, S. Pelletier, J. Pellerin and S. Meloche (2003). "Rapid turnover of extracellular signal-regulated kinase 3 by the ubiquitin-proteasome pathway defines a novel paradigm of mitogen-activated protein kinase regulation during cellular differentiation." Mol Cell Biol **23**(13): 4542-4558.
Coulombe, P., G. Rodier, S. Pelletier, J. Pellerin and S. Meloche (2003). "Rapid turnover of extracellular signal-regulated kinase 3 by the ubiquitin-proteasome pathway defines a novel paradigm of mitogen-activated protein kinase regulation during cellular differentiation." Molecular and cellular biology **23**(13): 4542-4558.
Cousin, B., S. Cinti, M. Morroni, S. Raimbault, D. Ricquier, L. Penicaud and L. Casteilla (1992). "Occurrence of brown adipocytes in rat white adipose tissue: molecular and morphological characterization." Journal of cell science **103**(4): 931-942.
Cross, D. A., P. W. Watt, M. Shaw, J. Van Der Kaay, C. P. Downes, J. C. Holder and P. Cohen (1997). "Insulin activates protein kinase B, inhibits glycogen synthase kinase ‐ 3 and activates glycogen synthase by rapamycin ‐ insensitive pathways in skeletal muscle and adipose tissue." FEBS letters **406**(1-2): 211-215.
Cryer, A. (1981). "Tissue lipoprotein lipase activity and its action in lipoprotein metabolism." International Journal of Biochemistry **13**(5): 525-541.
Cunningham, S. A., M. R. Kramer and K. V. Narayan (2014). "Incidence of childhood obesity in the United States." New England Journal of Medicine **370**(5): 403-411.
Curley, J., S. Pinnock, S. Dickson, R. Thresher, N. Miyoshi, M. Surani and E. Keverne (2005). "Increased body fat in mice with a targeted mutation of the paternally expressed imprinted gene Peg3." The FASEB Journal **19**(10): 1302-1304.
Dalgaard, L. T. and O. J. D. Pedersen (2001). "Uncoupling proteins: functional characteristics and role in the pathogenesis of obesity and Type II diabetes." **44**(8): 946-965.
de Kloet, A. D. and J. P. Herman (2018). "Fat-brain connections: Adipocyte glucocorticoid control of stress and metabolism." Frontiers in neuroendocrinology **48**: 50-57.

De Koster, J., R. K. Nelli, C. Strieder-Barboza, J. de Souza, A. L. Lock and G. A. Contreras (2018). "The contribution of hormone sensitive lipase to adipose tissue lipolysis and its regulation by insulin in periparturient dairy cows." Scientific reports **8**(1): 1-11.
De La Mota-Peynado, A., J. Chernoff and A. Beeser (2011). "Identification of the atypical MAPK Erk3 as a novel substrate for p21-activated kinase (Pak) activity." Journal of Biological Chemistry **286**(15): 13603-13611.
de Meis, L., A. P. Arruda, R. M. da Costa and M. Benchimol (2006). "Identification of a Ca2+-ATPase in brown adipose tissue mitochondria regulation of thermogenesis by Atp and Ca2+." Journal of Biological Chemistry **281**(24): 16384-16390.
De Onis, M., M. Blössner and E. Borghi (2010). "Global prevalence and trends of overweight and obesity among preschool children." The American journal of clinical nutrition **92**(5): 1257-1264.
Déléris, P., J. Rousseau, P. Coulombe, G. Rodier, P. L. Tanguay and S. Meloche (2008). "Activation loop phosphorylation of the atypical MAP kinases ERK3 and ERK4 is required for binding, activation and cytoplasmic relocalization of MK5." Journal of cellular physiology **217**(3): 778-788.
Déléris, P., M. Trost, I. Topisirovic, P.-L. Tanguay, K. L. Borden, P. Thibault and S. Meloche (2011). "Activation loop phosphorylation of ERK3/ERK4 by group I p21-activated kinases (PAKs) defines a novel PAK-ERK3/4-MAPK-activated protein kinase 5 signaling pathway." Journal of Biological Chemistry **286**(8): 6470-6478.
Dong, X. C., K. D. Copps, S. Guo, Y. Li, R. Kollipara, R. A. DePinho and M. F. J. C. m. White (2008). "Inactivation of hepatic Foxo1 by insulin signaling is required for adaptive nutrient homeostasis and endocrine growth regulation." **8**(1): 65-76.
Eaton, S. B., M. J. Konner and L. Cordain (2009). Diet-dependent acid load, Paleolithic nutrition, and evolutionary health promotion, Oxford University Press.
Echeverri, C. J. and N. Perrimon (2006). "High-throughput RNAi screening in cultured cells: a user's guide." Nature Reviews Genetics **7**(5): 373-384.
Eissing, L., T. Scherer, K. Tödter, U. Knippschild, J. W. Greve, W. A. Buurman, H. O. Pinnschmidt, S. S. Rensen, A. M. Wolf and A. Bartelt (2013). "De novo lipogenesis in human fat and liver is linked to ChREBP-β and metabolic health." Nature communications **4**(1): 1-11.
El-Merahbi, R., J. T. Viera, A. L. Valdes, K. Kolczynska, S. Reuter, M. C. Löffler, M. Erk, C. P. Ade, T. Karwen and A. E. Mayer (2020). "The adrenergic-induced ERK3 pathway drives lipolysis and suppresses energy dissipation." Genes & Development.
Engel, K., H. Schultz, F. Martin, A. Kotlyarov, K. Plath, M. Hahn, U. Heinemann and M. Gaestel (1995). "Constitutive activation of mitogen-activated protein kinase-activated protein kinase 2 by mutation of phosphorylation sites and an A-helix motif." Journal of Biological Chemistry **270**(45): 27213-27221.
Ewen, K., A. Jackson, D. Wilhelm and P. Koopman (2010). "A male-specific role for p38 mitogen-activated protein kinase in germ cell sex differentiation in mice." Biology of reproduction **83**(6): 1005-1014.
Feldmann, H. M., V. Golozoubova, B. Cannon and J. J. C. m. Nedergaard (2009). "UCP1 ablation induces obesity and abolishes diet-induced thermogenesis in mice exempt from thermal stress by living at thermoneutrality." **9**(2): 203-209.
Ferrannini, E. and M. Stern (1995). "14 Primary Insulin Resistance: A Risk Syndrome." Diabetes: clinical science in practice: 200.

Ferre, P. and F. Foufelle (2007). "SREBP-1c transcription factor and lipid homeostasis: clinical perspective." Hormone Research in Paediatrics **68**(2): 72-82.
Fredrikson, G., P. Strålfors, N. O. Nilsson and P. Belfrage (1981). "Hormone-sensitive lipase of rat adipose tissue. Purification and some properties." Journal of Biological Chemistry **256**(12): 6311-6320.
Frontini, A., A. Vitali, J. Perugini, I. Murano, C. Romiti, D. Ricquier, M. Guerrieri and S. Cinti (2013). "White-to-brown transdifferentiation of omental adipocytes in patients affected by pheochromocytoma." Biochimica et Biophysica Acta (BBA)-Molecular and Cell Biology of Lipids **1831**(5): 950-959.
Garvey, W. T., L. Maianu, J. A. Hancock, A. M. Golichowski and A. Baron (1992). "Gene expression of GLUT4 in skeletal muscle from insulin-resistant patients with obesity, IGT, GDM, and NIDDM." Diabetes **41**(4): 465-475.
Gehart, H., S. Kumpf, A. Ittner and R. Ricci (2010). "MAPK signalling in cellular metabolism: stress or wellness?" EMBO Rep **11**(11): 834-840.
Gerits, N., T. Mikalsen, S. Kostenko, A. Shiryaev, M. Johannessen and U. Moens (2007). "Modulation of F-actin rearrangement by the cyclic AMP/cAMP-dependent protein kinase (PKA) pathway is mediated by MAPK-activated protein kinase 5 and requires PKA-induced nuclear export of MK5." Journal of Biological Chemistry **282**(51): 37232-37243.
Gerits, N., A. Shiryaev, S. Kostenko, H. Klenow, O. Shiryaeva, M. Johannessen and U. Moens (2009). "The transcriptional regulation and cell-specific expression of the MAPK-activated protein kinase MK5." Cellular & molecular biology letters **14**(4): 548.
Gerits, N., W. Van Belle and U. Moens (2007). "Transgenic mice expressing constitutive active MAPKAPK5 display gender-dependent differences in exploration and activity." Behavioral and Brain Functions **3**(1): 58.
Gibney, E. and C. Nolan (2010). "Epigenetics and gene expression." Heredity **105**(1): 4-13.
Giralt, M. and F. J. E. Villarroya (2013). "White, brown, beige/brite: different adipose cells for different functions?" **154**(9): 2992-3000.
Goldberg, I. J., R. H. Eckel and N. A. Abumrad (2009). "Regulation of fatty acid uptake into tissues: lipoprotein lipase-and CD36-mediated pathways." Journal of lipid research **50**(Supplement): S86-S90.
Greenberg, A. S., W.-J. Shen, K. Muliro, S. Patel, S. C. Souza, R. A. Roth and F. B. Kraemer (2001). "Stimulation of lipolysis and hormone-sensitive lipase via the extracellular signal-regulated kinase pathway." Journal of Biological Chemistry **276**(48): 45456-45461.
Guilherme, A., J. V. Virbasius, V. Puri and M. P. Czech (2008). "Adipocyte dysfunctions linking obesity to insulin resistance and type 2 diabetes." Nature reviews Molecular cell biology **9**(5): 367-377.
Hadi, M., C. C. Chen, M. Whatley, K. Pacak and J. A. Carrasquillo (2007). "Brown fat imaging with 18F-6-fluorodopamine PET/CT, 18F-FDG PET/CT, and 123I-MIBG SPECT: a study of patients being evaluated for pheochromocytoma." Journal of Nuclear Medicine **48**(7): 1077-1083.
Haemmerle, G., A. Lass, R. Zimmermann, G. Gorkiewicz, C. Meyer, J. Rozman, G. Heldmaier, R. Maier, C. Theussl, S. Eder, D. Kratky, E. F. Wagner, M. Klingenspor, G. Hoefler and R. Zechner (2006). "Defective lipolysis and altered energy metabolism in mice lacking adipose triglyceride lipase." Science **312**(5774): 734-737.

Hainer, V. and I. Aldhoon-Hainerová (2014). "Tolerability and safety of the new anti-obesity medications." Drug safety **37**(9): 693-702.
Halfon, N., K. Larson and W. Slusser (2013). "Associations between obesity and comorbid mental health, developmental, and physical health conditions in a nationally representative sample of US children aged 10 to 17." Academic pediatrics **13**(1): 6-13.
Heck, A. M., J. A. Yanovski and K. A. Calis (2000). "Orlistat, a new lipase inhibitor for the management of obesity." Pharmacotherapy: The Journal of Human Pharmacology and Drug Therapy **20**(3): 270-279.
Henriques, V., S. Machado, W. Link and B. I. Ferreira (2019). Monitoring the Transcriptional Activity of FOXO Transcription Factors by Analyzing their Target Genes. FOXO Transcription Factors, Springer**:** 103-113.
Himms-Hagen, J., A. Melnyk, M. Zingaretti, E. Ceresi, G. Barbatelli and S. Cinti (2000). "Multilocular fat cells in WAT of CL-316243-treated rats derive directly from white adipocytes." American Journal of Physiology-Cell Physiology **279**(3): C670-C681.
Hoeflich, K. P., M. T. Eby, W. F. Forrest, D. C. Gray, J. Y. Tien, H. M. Stern, L. J. Murray, D. P. Davis, Z. Modrusan and S. Seshagiri (2006). "Regulation of ERK3/MAPK6 expression by BRAF." International journal of oncology **29**(4): 839-849.
Holm, C. (2003). Molecular mechanisms regulating hormone-sensitive lipase and lipolysis, Portland Press Ltd.
Holm, C., T. Østerlund, H. Laurell and J. A. Contreras (2000). "Molecular mechanisms regulating hormone-sensitive lipase and lipolysis." Annual review of nutrition **20**(1): 365-393.
Holst, J. J. (2007). "The physiology of glucagon-like peptide 1." Physiological reviews **87**(4): 1409-1439.
Hondares, E., M. Rosell, J. Diaz-Delfin, Y. Olmos, M. Monsalve, R. Iglesias, F. Villarroya and M. J. J. o. B. C. Giralt (2011). "PPARα induces PGC-1α gene expression and contributes to the thermogenic activation of brown fat; involvement of PRDM16." jbc. M111. 252775.
Hong, S., W. Song, P.-J. H. Zushin, B. Liu, M. P. Jedrychowski, A. I. Mina, Z. Deng, D. Cabarkapa, J. A. Hall and C. J. Palmer (2018). "Phosphorylation of Beta-3 adrenergic receptor at serine 247 by ERK MAP kinase drives lipolysis in obese adipocytes." Molecular metabolism **12**: 25-38.
Horowitz, J. and R. Plant (1978). "Controlled cellular energy conversion in brown adipose tissue thermogenesis." American Journal of Physiology-Regulatory, Integrative and Comparative Physiology **235**(3): R121-R129.
Houten, S. M. and R. J. Wanders (2010). "A general introduction to the biochemistry of mitochondrial fatty acid β-oxidation." Journal of inherited metabolic disease **33**(5): 469-477.
Hsia, D. S., N. H. Gosselin, J. Williams, N. Farhat, J. Marier, W. Shih, C. Peterson and R. Siegel (2020). "A randomized, double‐blind, placebo‐controlled, pharmacokinetic and pharmacodynamic study of a fixed‐dose combination of phentermine/topiramate in adolescents with obesity." Diabetes, Obesity and Metabolism **22**(4): 480-491.
Hücking, K., M. Hamilton-Wessler, M. Ellmerer and R. N. Bergman (2003). "Burst-like control of lipolysis by the sympathetic nervous system in vivo." The Journal of clinical investigation **111**(2): 257-264.

Ikoma-Seki, K., K. Nakamura, S. Morishita, T. Ono, K. Sugiyama, H. Nishino, H. Hirano and M. Murakoshi (2015). "Role of LRP1 and ERK and cAMP signaling pathways in lactoferrin-induced lipolysis in mature rat adipocytes." PloS one **10**(10).
Isidor, M. S., S. Winther, A. L. Basse, M. C. H. Petersen, B. Cannon, J. Nedergaard and J. B. Hansen (2016). "An siRNA-based method for efficient silencing of gene expression in mature brown adipocytes." Adipocyte **5**(2): 175-185.
Jackson, V. M., D. M. Breen, J.-P. Fortin, A. Liou, J. B. Kuzmiski, A. K. Loomis, M.-L. Rives, B. Shah and P. A. Carpino (2015). "Latest approaches for the treatment of obesity." Expert opinion on drug discovery **10**(8): 825-839.
Jason, J. Y., J. Berrios, J. M. Newbern, W. D. Snider, B. D. Philpot, K. M. Hahn and M. J. Zylka (2015). "An autism-linked mutation disables phosphorylation control of UBE3A." Cell **162**(4): 795-807.
Julien, C., P. Coulombe and S. Meloche (2003). "Nuclear export of ERK3 by a CRM1-dependent mechanism regulates its inhibitory action on cell cycle progression." Journal of Biological Chemistry **278**(43): 42615-42624.
Jung, S. M., C.-M. Hung, S. R. Hildebrand, J. Sanchez-Gurmaches, B. Martinez-Pastor, J. M. Gengatharan, M. Wallace, D. Mukhopadhyay, C. M. Calejman and A. K. Luciano (2019). "Non-canonical mTORC2 Signaling Regulates Brown Adipocyte Lipid Catabolism through SIRT6-FoxO1." Molecular cell **75**(4): 807-822. e808.
Kahn, S. E., R. L. Hull and K. M. Utzschneider (2006). "Mechanisms linking obesity to insulin resistance and type 2 diabetes." Nature **444**(7121): 840-846.
Kajimura, S., B. M. Spiegelman and P. Seale (2015). "Brown and beige fat: physiological roles beyond heat generation." Cell metabolism **22**(4): 546-559.
Kalderon, B., N. Azazmeh, N. Azulay, N. Vissler, M. Valitsky and J. Bar-Tana (2012). "Suppression of adipose lipolysis by long-chain fatty acid analogs." Journal of lipid research **53**(5): 868-878.
Kalyani, R. R., M. Corriere and L. Ferrucci (2014). "Age-related and disease-related muscle loss: the effect of diabetes, obesity, and other diseases." The lancet Diabetes & endocrinology **2**(10): 819-829.
Kant, S., S. Schumacher, M. K. Singh, A. Kispert, A. Kotlyarov and M. Gaestel (2006). "Characterization of the atypical MAPK ERK4 and its activation of the MAPK-activated protein kinase MK5." Journal of Biological Chemistry **281**(46): 35511-35519.
Karbowska, J. and Z. Kochan (2012). "Fat-reducing effects of dehydroepiandrosterone involve upregulation of ATGL and HSL expression, and stimulation of lipolysis in adipose tissue." Steroids **77**(13): 1359-1365.
Kaufman, J., J. L. Montalvo-Ortiz, H. Holbrook, K. O'loughlin, C. Orr, C. Kearney, B.-Z. Yang, T. Wang, H. Zhao and R. Althoff (2018). "Adverse childhood experiences, epigenetic measures, and obesity in youth." The Journal of pediatrics **202**: 150-156. e153.
Khandekar, M. J., P. Cohen and B. M. Spiegelman (2011). "Molecular mechanisms of cancer development in obesity." Nature Reviews Cancer **11**(12): 886-895.
Kienesberger, P. C., D. Lee, T. Pulinilkunnil, D. S. Brenner, L. Cai, C. Magnes, H. C. Koefeler, I. E. Streith, G. N. Rechberger and G. Haemmerle (2009). "Adipose triglyceride lipase deficiency causes tissue-specific changes in insulin signaling." Journal of Biological Chemistry **284**(44): 30218-30229.
Kilroy, G., D. H. Burk and Z. E. Floyd (2009). "High efficiency lipid-based siRNA transfection of adipocytes in suspension." PloS one **4**(9).

Kim, J. J., P. Li, J. Huntley, J. P. Chang, K. C. Arden and J. M. Olefsky (2009). "FoxO1 haploinsufficiency protects against high-fat diet–induced insulin resistance with enhanced peroxisome proliferator–activated receptor γ activation in adipose tissue." Diabetes **58**(6): 1275-1282.
Kita, M., J. Nakae, Y. Kawano, H. Asahara, H. Takemori, H. Okado and H. Itoh (2019). "Zfp238 Regulates the Thermogenic Program in Cooperation with Foxo1." iScience **12**: 87-101.
Klinger, S., B. Turgeon, K. Lévesque, G. A. Wood, K. M. Aagaard-Tillery and S. Meloche (2009). "Loss of Erk3 function in mice leads to intrauterine growth restriction, pulmonary immaturity, and neonatal lethality." Proceedings of the National Academy of Sciences **106**(39): 16710-16715.
Kommaddi, R. P., P.-Y. Jean-Charles and S. K. Shenoy (2015). "Phosphorylation of the deubiquitinase USP20 by protein kinase A regulates post-endocytic trafficking of β2 adrenergic receptors to autophagosomes during physiological stress." Journal of Biological Chemistry **290**(14): 8888-8903.
Kooijman, S., J. K. van den Heuvel and P. C. Rensen (2015). "Neuronal control of brown fat activity." Trends in Endocrinology & Metabolism **26**(11): 657-668.
Kostenko, S., G. Dumitriu, K. J. Lægreid and U. Moens (2011). "Physiological roles of mitogen-activated-protein-kinase-activated p38-regulated/activated protein kinase." World journal of biological chemistry **2**(5): 73.
Kostenko, S., G. Dumitriu and U. Moens (2012). "Tumour promoting and suppressing roles of the atypical MAP kinase signalling pathway ERK3/4-MK5." Journal of molecular signaling **7**(1): 9.
Kostenko, S., M. Johannessen and U. Moens (2009). "PKA-induced F-actin rearrangement requires phosphorylation of Hsp27 by the MAPKAP kinase MK5." Cellular signalling **21**(5): 712-718.
Kostenko, S., A. Shiryaev, N. Gerits, G. Dumitriu, H. Klenow, M. Johannessen and U. Moens (2011). "Serine residue 115 of MAPK-activated protein kinase MK5 is crucial for its PKA-regulated nuclear export and biological function." Cellular and molecular life sciences **68**(5): 847-862.
Kostenko, S., A. Shiryaev, N. Gerits, G. Dumitriu, H. Klenow, M. Johannessen, U. J. C. Moens and m. l. sciences (2011). "Serine residue 115 of MAPK-activated protein kinase MK5 is crucial for its PKA-regulated nuclear export and biological function." **68**(5): 847-862.
Kraemer, F. B. and W.-J. Shen (2002). "Hormone-sensitive lipase control of intracellular tri-(di-) acylglycerol and cholesteryl ester hydrolysis." Journal of lipid research **43**(10): 1585-1594.
Kress, T. R., I. G. Cannell, A. B. Brenkman, B. Samans, M. Gaestel, P. Roepman, B. M. Burgering, M. Bushell, A. Rosenwald and M. Eilers (2011). "The MK5/PRAK kinase and Myc form a negative feedback loop that is disrupted during colorectal tumorigenesis." Molecular cell **41**(4): 445-457.
Kudo, N., A. J. Barr, R. L. Barr, S. Desai and G. D. Lopaschuk (1995). "High rates of fatty acid oxidation during reperfusion of ischemic hearts are associated with a decrease in malonyl-CoA levels due to an increase in 5′ -AMP-activated protein kinase inhibition of acetyl-CoA carboxylase." Journal of Biological Chemistry **270**(29): 17513-17520.

Kurat, C. F., H. Wolinski, J. Petschnigg, S. Kaluarachchi, B. Andrews, K. Natter and S. D. Kohlwein (2009). "Cdk1/Cdc28-dependent activation of the major triacylglycerol lipase Tgl4 in yeast links lipolysis to cell-cycle progression." Molecular cell **33**(1): 53-63.
Lafontan, M. and M. Berlan (1993). "Fat cell adrenergic receptors and the control of white and brown fat cell function." Journal of lipid research **34**(7): 1057-1091.
Lafontan, M. and D. Langin (2009). "Lipolysis and lipid mobilization in human adipose tissue." Progress in lipid research **48**(5): 275-297.
Lass, A., R. Zimmermann, G. Haemmerle, M. Riederer, G. Schoiswohl, M. Schweiger, P. Kienesberger, J. G. Strauss, G. Gorkiewicz and R. Zechner (2006). "Adipose triglyceride lipase-mediated lipolysis of cellular fat stores is activated by CGI-58 and defective in Chanarin-Dorfman Syndrome." Cell metabolism **3**(5): 309-319.
Lee, C., W. Li, R. Nishimura, M. Zhou, A. Batzer, M. Myers, M. White, J. Schlessinger and E. Skolnik (1993). "Nck associates with the SH2 domain-docking protein IRS-1 in insulin-stimulated cells." Proceedings of the National Academy of Sciences **90**(24): 11713-11717.
Lee, M.-J., Y. Wu and S. K. Fried (2010). "Adipose tissue remodeling in pathophysiology of obesity." Current opinion in clinical nutrition and metabolic care **13**(4): 371.
Lee, Y.-H., S.-N. Kim, H.-J. Kwon and J. G. Granneman (2017). "Metabolic heterogeneity of activated beige/brite adipocytes in inguinal adipose tissue." Scientific reports **7**: 39794.
Lee, Y.-H., A. P. Petkova, E. P. Mottillo and J. G. Granneman (2012). "In vivo identification of bipotential adipocyte progenitors recruited by β3-adrenoceptor activation and high-fat feeding." Cell metabolism **15**(4): 480-491.
Lin, F., T. J. Ribar and A. R. Means (2011). "The Ca2+/calmodulin-dependent protein kinase kinase, CaMKK2, inhibits preadipocyte differentiation." Endocrinology **152**(10): 3668-3679.
Listenberger, L. L., A. G. Ostermeyer-Fay, E. B. Goldberg, W. J. Brown and D. A. Brown (2007). "Adipocyte differentiation-related protein reduces the lipid droplet association of adipose triglyceride lipase and slows triacylglycerol turnover." Journal of lipid research **48**(12): 2751-2761.
Liu, J., W. Zhang, G. C. Chuang, H. S. Hill, L. Tian, Y. Fu, D. R. Moellering and W. T. Garvey (2012). "Role of TRIB3 in regulation of insulin sensitivity and nutrient metabolism during short-term fasting and nutrient excess." American Journal of Physiology-Endocrinology and Metabolism **303**(7): E908-E916.
Liu, L., Z. Tao, L. D. Zheng, J. P. Brooke, C. M. Smith, D. Liu, Y. C. Long and Z. Cheng (2016). "FoxO1 interacts with transcription factor EB and differentially regulates mitochondrial uncoupling proteins via autophagy in adipocytes." Cell death discovery **2**: 16066.
Lochner, A. and J. Moolman (2006). "The many faces of H89: a review." Cardiovascular drug reviews **24**(3 – 4): 261-274.
Löffler, M. C., A. E. Mayer, J. T. Viera, A. L. Valdes, R. El ‐ Merahbi, C. P. Ade, T. Karwen, W. Schmitz, A. Slotta and M. Erk (2018). "Protein kinase D1 deletion in adipocytes enhances energy dissipation and protects against adiposity." The EMBO journal **37**(22): e99182.
Löffler, M. C., A. E. Mayer, J. T. Viera, A. L. Valdes, R. El ‐ Merahbi, C. P. Ade, T. Karwen, W. Schmitz, A. Slotta and M. J. T. E. j. Erk (2018). "Protein kinase D1 deletion in adipocytes enhances energy dissipation and protects against adiposity." **37**(22).

Long, W., C. E. Foulds, J. Qin, J. Liu, C. Ding, D. M. Lonard, L. M. Solis, I. I. Wistuba, S. Y. Tsai and M.-J. Tsai (2012). "ERK3 signals through SRC-3 coactivator to promote human lung cancer cell invasion." The Journal of clinical investigation **122**(5): 1869-1880.
MacLean, P. S., J. A. Higgins, M. R. Jackman, G. C. Johnson, B. K. Fleming-Elder, H. R. Wyatt, E. L. Melanson and J. O. Hill (2006). "Peripheral metabolic responses to prolonged weight reduction that promote rapid, efficient regain in obesity-prone rats." American Journal of Physiology-Regulatory, Integrative and Comparative Physiology **290**(6): R1577-R1588.
Mancuso, P. (2016). "The role of adipokines in chronic inflammation." ImmunoTargets and therapy **5**: 47.
Marquis, M., S. Boulet, S. Mathien, J. Rousseau, P. Thebault, J.-F. Daudelin, J. Rooney, B. Turgeon, C. Beauchamp and S. Meloche (2014). "The non-classical MAP kinase ERK3 controls T cell activation." PloS one **9**(1).
Marso, S. P., G. H. Daniels, K. Brown-Frandsen, P. Kristensen, J. F. Mann, M. A. Nauck, S. E. Nissen, S. Pocock, N. R. Poulter and L. S. Ravn (2016). "Liraglutide and cardiovascular outcomes in type 2 diabetes." New England Journal of Medicine **375**(4): 311-322.
Marti, A., M. Moreno-Aliaga, J. Hebebrand and J. Martinez (2004). "Genes, lifestyles and obesity." International Journal of Obesity **28**(3): S29-S36.
Martinez-Botas, J., J. B. Anderson, D. Tessier, A. Lapillonne, B. H.-J. Chang, M. J. Quast, D. Gorenstein, K.-H. Chen and L. Chan (2000). "Absence of perilipin results in leanness and reverses obesity in Lepr db/db mice." Nature genetics **26**(4): 474-479.
Martínez-Noël, G., K. Luck, S. Kühnle, A. Desbuleux, P. Szajner, J. T. Galligan, D. Rodriguez, L. Zheng, K. Boyland and F. Leclere (2018). "Network analysis of UBE3A/E6AP-associated proteins provides connections to several distinct cellular processes." Journal of molecular biology **430**(7): 1024-1050.
Mathien, S., P. Déléris, M. Soulez, L. Voisin and S. Meloche (2017). "Deubiquitinating enzyme USP20 regulates extracellular signal-regulated kinase 3 stability and biological activity." Molecular and cellular biology **37**(9): e00432-00416.
Matsumoto, M., A. Pocai, L. Rossetti, R. A. DePinho and D. Accili (2007). "Impaired regulation of hepatic glucose production in mice lacking the forkhead transcription factor Foxo1 in liver." Cell metabolism **6**(3): 208-216.
Matsuzaki, H., H. Daitoku, M. Hatta, K. Tanaka and A. Fukamizu (2003). "Insulin-induced phosphorylation of FKHR (Foxo1) targets to proteasomal degradation." Proceedings of the National Academy of Sciences **100**(20): 11285-11290.
McGarry, J. and D. Foster (1980). "Regulation of hepatic fatty acid oxidation and ketone body production." Annual review of biochemistry **49**(1): 395-420.
McMorrow, A. M., R. M. Connaughton, F. E. Lithander and H. M. Roche (2015). "Adipose tissue dysregulation and metabolic consequences in childhood and adolescent obesity: potential impact of dietary fat quality." Proceedings of the Nutrition Society **74**(1): 67-82.
Menendez, J. A. and R. Lupu (2007). "Fatty acid synthase and the lipogenic phenotype in cancer pathogenesis." Nature Reviews Cancer **7**(10): 763-777.
Mohanty, B. (2017). "Lower Cardiovascular Risk with Diabetic Drugs: A Paradigm Shift from Glucocentricity to Cardio Protectiveness." Diabetes Case Rep **2**(123): 2.

Murano, I., G. Barbatelli, A. Giordano and S. Cinti (2009). "Noradrenergic parenchymal nerve fiber branching after cold acclimatisation correlates with brown adipocyte density in mouse adipose organ." Journal of anatomy **214**(1): 171-178.
Murphy, S., S. Martin and R. G. Parton (2009). "Lipid droplet-organelle interactions; sharing the fats." Biochimica et Biophysica Acta (BBA)-Molecular and Cell Biology of Lipids **1791**(6): 441-447.
Nakae, J., Y. Cao, F. Hakuno, H. Takemori, Y. Kawano, R. Sekioka, T. Abe, H. Kiyonari, T. Tanaka and J. Sakai (2012). "Novel repressor regulates insulin sensitivity through interaction with Foxo1." The EMBO journal **31**(10): 2275-2295.
Nakae, J., Y. Cao, M. Oki, Y. Orba, H. Sawa, H. Kiyonari, K. Iskandar, K. Suga, M. Lombes and Y. Hayashi (2008). "Forkhead transcription factor FoxO1 in adipose tissue regulates energy storage and expenditure." Diabetes **57**(3): 563-576.
Nakae, J., T. Kitamura, Y. Kitamura, W. H. Biggs III, K. C. Arden and D. Accili (2003). "The forkhead transcription factor Foxo1 regulates adipocyte differentiation." Developmental cell **4**(1): 119-129.
Nakagawa, K., T. Kohara, Y. Uehata, Y. Miyakawa, M. Sato-Ueshima, N. Okubo, M. Asaka, H. Takeda and M. Kobayashi (2016). "PIAS3 enhances the transcriptional activity of HIF-1α by increasing its protein stability." Biochemical and biophysical research communications **469**(3): 470-476.
Nakamura, K. and S. F. Morrison (2008). "A thermosensory pathway that controls body temperature." Nature neuroscience **11**(1): 62-71.
Namour, F., F. P. Vanhoutte, J. Beetens, S. Blockhuys, M. De Weer and P. Wigerinck (2012). "Pharmacokinetics, safety, and tolerability of GLPG0259, a mitogen-activated protein kinase-activated protein kinase 5 (MAPKAPK5) inhibitor, given as single and multiple doses to healthy male subjects." Drugs in R&D **12**(3): 141-163.
Natale, D. R., A. J. Paliga, F. Beier, S. D'souza and A. J. Watson (2004). "p38 MAPK signaling during murine preimplantation development." Developmental biology **268**(1): 76-88.
Nauck, M. A., J. R. Petrie, G. Sesti, E. Mannucci, J.-P. Courrèges, M. L. Lindegaard, C. B. Jensen and S. L. Atkin (2016). "A phase 2, randomized, dose-finding study of the novel once-weekly human GLP-1 analog, semaglutide, compared with placebo and open-label liraglutide in patients with type 2 diabetes." Diabetes care **39**(2): 231-241.
New, L. and J. J. T. i. c. m. Han (1998). "The p38 MAP kinase pathway and its biological function." **8**(5): 220-228.
Okemah, J., J. Peng and M. Quinones (2018). "Addressing clinical inertia in type 2 diabetes mellitus: a review." Advances in therapy **35**(11): 1735-1745.
Organization, W. H. (2002). The world health report 2002: reducing risks, promoting healthy life, World Health Organization.
Ortega-Molina, A., A. Efeyan, E. Lopez-Guadamillas, M. Muñoz-Martin, G. Gómez-López, M. Cañamero, F. Mulero, J. Pastor, S. Martinez and E. Romanos (2012). "Pten positively regulates brown adipose function, energy expenditure, and longevity." Cell metabolism **15**(3): 382-394.
Ouzzahra, Y., G. Havenith and B. Redortier (2012). "Regional distribution of thermal sensitivity to cold at rest and during mild exercise in males." Journal of Thermal Biology **37**(7): 517-523.

Ozaki, K.-i., M. Awazu, M. Tamiya, Y. Iwasaki, A. Harada, S. Kugisaki, S. Tanimura and M. Kohno (2016). "Targeting the ERK signaling pathway as a potential treatment for insulin resistance and type 2 diabetes." American journal of physiology-endocrinology and metabolism **310**(8): E643-E651.
Pandey, A., G. S. Kumar, A. Kadakol, V. Malek and A. Bhanudas Gaikwad (2016). "FoxO1 inhibitors: the future medicine for metabolic disorders?" Current diabetes reviews **12**(3): 223-230.
Pappa, E., T. D. Filippatos and M. S. Elisaf (2018). "Naltrexone ER/Bupropion ER for the treatment of obesity." Hellenic Journal of Atherosclerosis **7**(4).
Park, H., V. K. Kaushik, S. Constant, M. Prentki, E. Przybytkowski, N. B. Ruderman and A. K. Saha (2002). "Coordinate regulation of malonyl-CoA decarboxylase, sn-glycerol-3-phosphate acyltransferase, and acetyl-CoA carboxylase by AMP-activated protein kinase in rat tissues in response to exercise." Journal of Biological Chemistry **277**(36): 32571-32577.
Paulo, E., D. Wu, Y. Wang, Y. Zhang, Y. Wu, D. L. Swaney, M. Soucheray, D. Jimenez-Morales, A. Chawla and N. J. Krogan (2018). "Sympathetic inputs regulate adaptive thermogenesis in brown adipose tissue through cAMP-Salt inducible kinase axis." Scientific reports **8**(1): 1-14.
Peng, S., W. Xiao, D. Ju, B. Sun, N. Hou, Q. Liu, Y. Wang, H. Zhao, C. Gao and S. Zhang (2019). "Identification of entacapone as a chemical inhibitor of FTO mediating metabolic regulation through FOXO1." Science translational medicine **11**(488): eaau7116.
Perander, M., S. M. Keyse and O.-M. Seternes (2016). "New insights into the activation, interaction partners and possible functions of MK5/PRAK." cell **12**: 13.
Perdikari, A., E. Kulenkampff, C. Rudigier, H. Neubauer, G. Luippold, N. Redemann and C. Wolfrum (2017). "A high-throughput, image-based screen to identify kinases involved in brown adipocyte development." Sci. Signal. **10**(466): eaaf5357.
Petrovic, N., T. B. Walden, I. G. Shabalina, J. A. Timmons, B. Cannon and J. Nedergaard (2010). "Chronic peroxisome proliferator-activated receptor γ (PPARγ) activation of epididymally derived white adipocyte cultures reveals a population of thermogenically competent, UCP1-containing adipocytes molecularly distinct from classic brown adipocytes." Journal of Biological Chemistry **285**(10): 7153-7164.
Popkin, B. M., L. S. Adair and S. W. Ng (2012). "Global nutrition transition and the pandemic of obesity in developing countries." Nutrition reviews **70**(1): 3-21.
Prentki, M., E. Joly, W. El-Assaad and R. Roduit (2002). "Malonyl-CoA signaling, lipid partitioning, and glucolipotoxicity: role in β-cell adaptation and failure in the etiology of diabetes." Diabetes **51**(suppl 3): S405-S413.
Qi, L., J. E. Heredia, J. Y. Altarejos, R. Screaton, N. Goebel, S. Niessen, I. X. MacLeod, C. W. Liew, R. N. Kulkarni and J. Bain (2006). "TRB3 links the E3 ubiquitin ligase COP1 to lipid metabolism." science **312**(5781): 1763-1766.
Robbins, D. C., E. Danforth Jr, E. S. Horton, R. L. Burse, R. F. Goldman and E. A. Sims (1979). "The effect of diet on thermogenesis in acquired lipodystrophy." Metabolism **28**(9): 908-916.
Robbins, D. C., E. S. Horton, O. Tulp and E. A. Sims (1982). "Familial partial lipodystrophy: complications of obesity in the non-obese?" Metabolism **31**(5): 445-452.
Robidoux, J., T. L. Martin and S. Collins (2004). "β-adrenergic receptors and regulation of energy expenditure: a family affair." Annu. Rev. Pharmacol. Toxicol. **44**: 297-323.

Rosen, E. D. and B. M. Spiegelman (2014). "What we talk about when we talk about fat." Cell **156**(1-2): 20-44.
Rosenwald, M., A. Perdikari, T. Rülicke and C. Wolfrum (2013). "Bi-directional interconversion of brite and white adipocytes." Nature cell biology **15**(6): 659-667.
Roskoski Jr, R. (2012). "ERK1/2 MAP kinases: structure, function, and regulation." Pharmacological research **66**(2): 105-143.
Ross, S. E., R. L. Erickson, I. Gerin, P. M. DeRose, L. Bajnok, K. A. Longo, D. E. Misek, R. Kuick, S. M. Hanash and K. B. Atkins (2002). "Microarray analyses during adipogenesis: understanding the effects of Wnt signaling on adipogenesis and the roles of liver X receptor α in adipocyte metabolism." Molecular and cellular biology **22**(16): 5989-5999.
Sahadevan, P. and B. G. Allen (2017). "MK5: A novel regulator of cardiac fibroblast function?" IUBMB life **69**(10): 785-794.
Sahu-Osen, A., G. Montero-Moran, M. Schittmayer, K. Fritz, A. Dinh, Y.-F. Chang, D. McMahon, A. Boeszoermenyi, I. Cornaciu and D. Russell (2015). "CGI-58/ABHD5 is phosphorylated on Ser239 by protein kinase A: control of subcellular localization." Journal of lipid research **56**(1): 109-121.
Schreiber, R., C. Diwoky, G. Schoiswohl, U. Feiler, N. Wongsiriroj, M. Abdellatif, D. Kolb, J. Hoeks, E. E. Kershaw and S. Sedej (2017). "Cold-induced thermogenesis depends on ATGL-mediated lipolysis in cardiac muscle, but not brown adipose tissue." Cell metabolism **26**(5): 753-763. e757.
Schreiber, R., P. Hofer, U. Taschler, P. J. Voshol, G. N. Rechberger, P. Kotzbeck, D. Jaeger, K. Preiss-Landl, C. C. Lord, J. M. Brown, G. Haemmerle, R. Zimmermann, A. Vidal-Puig and R. Zechner (2015). "Hypophagia and metabolic adaptations in mice with defective ATGL-mediated lipolysis cause resistance to HFD-induced obesity." Proc Natl Acad Sci U S A **112**(45): 13850-13855.
Schumacher, S., K. Laaß, S. Kant, Y. Shi, A. Visel, A. D. Gruber, A. Kotlyarov and M. Gaestel (2004). "Scaffolding by ERK3 regulates MK5 in development." The EMBO journal **23**(24): 4770-4779.
Schweiger, M., M. Paar, C. Eder, J. Brandis, E. Moser, G. Gorkiewicz, S. Grond, F. P. Radner, I. Cerk and I. Cornaciu (2012). "G0/G1 switch gene-2 regulates human adipocyte lipolysis by affecting activity and localization of adipose triglyceride lipase." Journal of lipid research **53**(11): 2307-2317.
Schweiger, M., M. Romauch, R. Schreiber, G. F. Grabner, S. Hütter, P. Kotzbeck, P. Benedikt, T. O. Eichmann, S. Yamada and O. Knittelfelder (2017). "Pharmacological inhibition of adipose triglyceride lipase corrects high-fat diet-induced insulin resistance and hepatosteatosis in mice." Nature communications **8**(1): 1-15.
Schweiger, M., M. Romauch, R. Schreiber, G. F. Grabner, S. Hutter, P. Kotzbeck, P. Benedikt, T. O. Eichmann, S. Yamada, O. Knittelfelder, C. Diwoky, C. Doler, N. Mayer, W. De Cecco, R. Breinbauer, R. Zimmermann and R. Zechner (2017). "Pharmacological inhibition of adipose triglyceride lipase corrects high-fat diet-induced insulin resistance and hepatosteatosis in mice." Nat Commun **8**: 14859.
Schweiger, M., R. Schreiber, G. Haemmerle, A. Lass, C. Fledelius, P. Jacobsen, H. Tornqvist, R. Zechner and R. Zimmermann (2006). "Adipose triglyceride lipase and hormone-sensitive lipase are the major enzymes in adipose tissue triacylglycerol catabolism." Journal of Biological Chemistry **281**(52): 40236-40241.

Seale, P., S. Kajimura, W. Yang, S. Chin, L. M. Rohas, M. Uldry, G. Tavernier, D. Langin and B. M. J. C. m. Spiegelman (2007). "Transcriptional control of brown fat determination by PRDM16." **6**(1): 38-54.
Semenza, G. L. (2014). "Oxygen sensing, hypoxia-inducible factors, and disease pathophysiology." Annual Review of Pathology: Mechanisms of Disease **9**: 47-71.
Seternes, O. M., T. Mikalsen, B. Johansen, E. Michaelsen, C. G. Armstrong, N. A. Morrice, B. Turgeon, S. Meloche, U. Moens and S. M. Keyse (2004). "Activation of MK5/PRAK by the atypical MAP kinase ERK3 defines a novel signal transduction pathway." The EMBO journal **23**(24): 4780-4791.
Shin, H., Y. Ma, T. Chanturiya, Q. Cao, Y. Wang, A. K. Kadegowda, R. Jackson, D. Rumore, B. Xue and H. Shi (2017). "Lipolysis in brown adipocytes is not essential for cold-induced thermogenesis in mice." Cell metabolism **26**(5): 764-777. e765.
Shin, H., H. Shi, B. Xue and L. Yu (2018). "What activates thermogenesis when lipid droplet lipolysis is absent in brown adipocytes?" Adipocyte **7**(2): 143-147.
Sidossis, L. and S. Kajimura (2015). "Brown and beige fat in humans: thermogenic adipocytes that control energy and glucose homeostasis." The Journal of clinical investigation **125**(2): 478-486.
Singh, A. K. and R. Singh (2020). "Pharmacotherapy in obesity: a systematic review and meta-analysis of randomized controlled trials of anti-obesity drugs." Expert review of clinical pharmacology **13**(1): 53-64.
Song, B. and D. M. Thomas (2007). "Dynamics of starvation in humans." Journal of mathematical biology **54**(1): 27-43.
Song, J., X. Ruan, M. Gu, L. Wang, H. Wang and A. O. Mueck (2018). "Effect of orlistat or metformin in overweight and obese polycystic ovary syndrome patients with insulin resistance." Gynecological Endocrinology **34**(5): 413-417.
Song, Z., A. M. Xiaoli and F. Yang (2018). "Regulation and metabolic significance of de novo lipogenesis in adipose tissues." Nutrients **10**(10): 1383.
Stanley, S., S. Pinto, J. Segal, C. A. Pérez, A. Viale, J. DeFalco, X. Cai, L. K. Heisler and J. M. Friedman (2010). "Identification of neuronal subpopulations that project from hypothalamus to both liver and adipose tissue polysynaptically." Proceedings of the National Academy of Sciences **107**(15): 7024-7029.
Stefan, N. and H.-U. Häring (2013). "Circulating fetuin-A and free fatty acids interact to predict insulin resistance in humans." Nature medicine **19**(4): 394.
Strålfors, P. and P. Belfrage (1983). "Phosphorylation of hormone-sensitive lipase by cyclic AMP-dependent protein kinase." Journal of Biological chemistry **258**(24): 15146-15152.
Sun, K., J. Tordjman, K. Clément and P. E. Scherer (2013). "Fibrosis and adipose tissue dysfunction." Cell metabolism **18**(4): 470-477.
Sun, P., N. Yoshizuka, L. New, B. A. Moser, Y. Li, R. Liao, C. Xie, J. Chen, Q. Deng and M. Yamout (2007). "PRAK is essential for ras-induced senescence and tumor suppression." Cell **128**(2): 295-308.
Tabarés Seisdedos, R. (2017). "Health effects of overweight and obesity in 195 countries over 25 years." New England Journal of Medicine, 2017, vol. 377, num. 1, p. 13-27.
Taniguchi, C. M., B. Emanuelli and C. R. Kahn (2006). "Critical nodes in signalling pathways: insights into insulin action." Nature reviews Molecular cell biology **7**(2): 85-96.

Tansey, J. T., A. M. Huml, R. Vogt, K. E. Davis, J. M. Jones, K. A. Fraser, D. L. Brasaemle, A. R. Kimmel and C. Londos (2003). "Functional studies on native and mutated forms of perilipins a role in protein kinase A-mediated lipolysis of triacylglycerols in Chinese hamster ovary cells." Journal of Biological Chemistry **278**(10): 8401-8406.
Taskén, K. and E. M. Aandahl (2004). "Localized effects of cAMP mediated by distinct routes of protein kinase A." Physiological reviews **84**(1): 137-167.
Torres-Quesada, O., J. E. Mayrhofer and E. Stefan (2017). "The many faces of compartmentalized PKA signalosomes." Cellular signalling **37**: 1-11.
van der Lans, A. A., J. Hoeks, B. Brans, G. H. Vijgen, M. G. Visser, M. J. Vosselman, J. Hansen, J. A. Jörgensen, J. Wu and F. M. Mottaghy (2013). "Cold acclimation recruits human brown fat and increases nonshivering thermogenesis." The Journal of clinical investigation **123**(8): 3395-3403.
Van Gaal, L. F., I. L. Mertens and E. Christophe (2006). "Mechanisms linking obesity with cardiovascular disease." Nature **444**(7121): 875-880.
van Loon, L. J., R. Koopman, J. H. Stegen, A. J. Wagenmakers, H. A. Keizer and W. H. Saris (2003). "Intramyocellular lipids form an important substrate source during moderate intensity exercise in endurance‐trained males in a fasted state." The Journal of physiology **553**(2): 611-625.
Viera, J. T., R. El-Merahbi, B. Nieswandt, D. Stegner and G. Sumara (2016). "Phospholipases D1 and D2 suppress appetite and protect against overweight." PloS one **11**(6): e0157607.
Voelker, R. (2020). "FDA Assesses Potential Cancer Risk Associated With Weight Loss Drug." Jama **323**(7): 600-600.
Wallace, D. C., W. Fan and V. Procaccio (2010). "Mitochondrial energetics and therapeutics." Annual Review of Pathology: Mechanisms of Disease **5**: 297-348.
Wang, Q. A., C. Tao, R. K. Gupta and P. E. Scherer (2013). "Tracking adipogenesis during white adipose tissue development, expansion and regeneration." Nature medicine **19**(10): 1338.
Wearing, S. C., E. M. Hennig, N. M. Byrne, J. R. Steele and A. P. Hills (2006). "Musculoskeletal disorders associated with obesity: a biomechanical perspective." Obesity reviews **7**(3): 239-250.
Westhovens, R., F. De Keyser, D. Rekalov, E. L. Nasonov, J. Beetens, A. Van der Aa, P. Wigerinck, F. Namour, F. Vanhoutte and P. Durez (2013). "Oral administration of GLPG0259, an inhibitor of MAPKAPK5, a new target for the treatment of rheumatoid arthritis: a phase II, randomised, double-blind, placebo-controlled, multicentre trial." Annals of the rheumatic diseases **72**(5): 741-744.
White, M. F. (2002). "IRS proteins and the common path to diabetes." American Journal of Physiology-Endocrinology And Metabolism **283**(3): E413-E422.
Wu, J., P. Boström, L. M. Sparks, L. Ye, J. H. Choi, A.-H. Giang, M. Khandekar, K. A. Virtanen, P. Nuutila and G. Schaart (2012). "Beige adipocytes are a distinct type of thermogenic fat cell in mouse and human." Cell **150**(2): 366-376.
Wu, Y., Q. Pan, H. Yan, K. Zhang, X. Guo, Z. Xu, W. Yang, Y. Qi, C. A. Guo and C. Hornsby (2018). "Novel mechanism of Foxo1 phosphorylation in glucagon signaling in control of glucose homeostasis." Diabetes **67**(11): 2167-2182.

Zechner, R., P. C. Kienesberger, G. Haemmerle, R. Zimmermann and A. Lass (2009). "Adipose triglyceride lipase and the lipolytic catabolism of cellular fat stores." Journal of lipid research **50**(1): 3-21.
Zennaro, M.-C., D. Le Menuet, S. Viengchareun, F. Walker, D. Ricquier and M. Lombès (1998). "Hibernoma development in transgenic mice identifies brown adipose tissue as a novel target of aldosterone action." The Journal of clinical investigation **101**(6): 1254-1260.
Zhang, X. D., M. Ferrer, A. S. Espeseth, S. D. Marine, E. M. Stec, M. A. Crackower, D. J. Holder, J. F. Heyse and B. Strulovici (2007). "The use of strictly standardized mean difference for hit selection in primary RNA interference high-throughput screening experiments." Journal of biomolecular screening **12**(4): 497-509.
Zhu, A. X., Y. Zhao, D. E. Moller and J. S. Flier (1994). "Cloning and characterization of p97MAPK, a novel human homolog of rat ERK-3." Molecular and cellular biology **14**(12): 8202-8211.
Zhu, X., Q. He and Z. Lin (2003). "Effects of catecholamines on human preadipocyte proliferation and differentiation." Zhonghua zheng xing wai ke za zhi= Zhonghua zhengxing waike zazhi= Chinese journal of plastic surgery **19**(4): 282-284.
Zimmermann, R., J. G. Strauss, G. Haemmerle, G. Schoiswohl, R. Birner-Gruenberger, M. Riederer, A. Lass, G. Neuberger, F. Eisenhaber and A. Hermetter (2004). "Fat mobilization in adipose tissue is promoted by adipose triglyceride lipase." Science **306**(5700): 1383-1386.
Zou, P., L. Liu, L. Zheng, L. Liu, R. E. Stoneman, A. Cho, A. Emery, E. R. Gilbert and Z. Cheng (2014). "Targeting FoxO1 with AS1842856 suppresses adipogenesis." Cell Cycle **13**(23): 3759-3767.
Zu, Y.-L., Y. Ai and C.-K. Huang (1995). "Characterization of an autoinhibitory domain in human mitogen-activated protein kinase-activated protein kinase 2." Journal of Biological Chemistry **270**(1): 202-206.
Zucoloto, F. S. (2011). "Evolution of the human feeding behavior." Psychology & Neuroscience **4**(1): 131-141.

12 ANNEX

12.1 List of abbreviations

18F-FDG	Fluorodeoxyglucose
5-HTR2B	5-Hydroxytryptamine Receptor 2b
ABHD5	A/B Hydrolase Domain-Containing Protein-5
AC	Adenylyl Cyclase
ACC1	Acetyl-Coa Carboxylases 1
ACSL1	Long-Chain-Fatty-Acid-Coa Ligase 1
ADCY10	Adenylate Cyclase 10
ADRP	Adipocyte Differentiation-Related Protein
AHQR	Ala-/His-/Glu- Rich Domain
AMP	Adenosine Monophosphate
APOC3	Apolipoprotein C3
AT	Adipose Tissue
ATGL	Adipose Triglyceride Lipase
ATP	Adenosine Triphosphate
BAT	Brown Adipose Tissue
BMI	Body Mass Index
BrdU	Bromodeoxyuridine / 5-Bromo-2'-Deoxyuridine
BSA	Bovine Serum Albumin
C/EBP	CCAAT-Enhancer-Binding Proteins (Or C/Ebps
C34	cluster of diffrentiation 34
CAMKK2	Calcium/Calmodulin Dependent Protein Kinase Kinase 2
CAMP	S Cyclic Amp
CD36	cluster of diffrentiation 36
CD42	Glycoprotein Ib
CGI-58	Comparative Gene Identification 58
CHIP	Chromatin Immunoprecipitation
CHREBP	Carbohydrate Response Element-Binding Protein
CPM	Countspermillion
CPT1	Carnitine Palmitoyltransferase 1
CRM1	Chromosome Region Maintenance 1
DAPI	Prolong Gold Antifade Mountant with 4’,6-Diamidino-2-Phenylindole
DMEM	Dulbecco's Modified Eagle Media
DMSO	Dimethyl Sulfoxide
DNL	De Novo Lipogenesis
DNTP	2'-Deoxynucleoside 5'-Triphosphate

DPBS	Dulbecco's Phosphate-Buffered Saline
DTT	1,4-Dithiothreitol
ECL	Enhanced Chemiluminescence
EDTA	Ethylenediaminetetraacetic Acid
EGR1	Early Growth Response 1
EPIWAT	Epi-Gonadal White Adipose Tissue
ERK1, ERK2	Extracellular Signal-Regulated Protein Kinases 1,2
FADH	Flavin Adenine Dinucleotide
FASN	Fatty Acid Synthase
FATP1	Fatty Acid Transport Protein-1
FBS	Foetal Bovine Serum
FCCP	Carbonyl Cyanide-4-(Trifluoromethoxy) Phenylhydrazone
FFA	Free Fatty Acids
FFAR4	Free Fatty Acid Receptor-4
FOXO1	Forkhead Transcription Factor O1
G0S2	The G0/G1 Switch Gene 2
GDS	Gut-Derived Serotonin
GLP-1	Glucagon-Like Peptide-1
GLUT4	Glucose Transporter-4
GLYCEROL-3P	Glycerol-3 Phosphate
GPCRS	G-Protein Coupled Receptors
GTT	Glucose Tolerance Test
HFD	High-Fat Diet
HIF-1	Hypoxia-Inducible Factor-1
HSL	Hormone-Sensitive Lipase
HTR2B	5-Hydroxytryptamine Receptor 2b
IBMX	3-Isobutyl-1-Methylxanthine
IP	Immunoprecipitation
IRS	Insulin Receptor Substrate
ISO	Isoproterenol
ITT	Inulin Tolerance Test
JNK1, JNK2, JNK3	C-Jun N-Terminal Kinases
LATS2	Large Tumor Suppressor Kinase 2
LD	Lipid Droplets
LDS	Lithium Dodecyl Sulfate
LEP	Leptomycin B
LIPH	Lipase H
MAPK	Mitogen-Activated Protein Kinases
MAPKKK	Mapk Kinase Kinases
MGL	And Monoglyceride Lipase
MK5	Map Kinase-Activated Protein Kinase 5

MK5i	Mk5 Chemical Inhibitor
MTORC1	Mammalian Target Of Rapamycin Complex 1
NADH	Nicotinamide Adenine Dinucleotide
ND	Normal Diet
NDRG1	N-Myc Downstream Regulated 1
NE	Norepinephrine
NEAA	Nonessential Amino Acids
NEFA	Non-Esterified Fatty Acids
NES	Nuclear Export Signal
NLS	Nuclear Localization Sequence
NMR	Nuclear Magnetic Resonance
NP-40	Nonidet P-40
OCR	Oxygen Consumption Rate
P/S	Penicillin/Streptomycin
PAK	Class I P21 Activated Kinases
PBS	Phosphate-Buffered Saline
PCK1	Phosphoenolpyruvate Carboxykinase
PCR	Polymerase Chain Reaction
PEG3	Paternally Expressed 3
PET	Positron Emission Tomography
PFA	Paraformaldehyde
PGC-1	Peroxisome Proliferator-Activated Receptor Gamma Coactivator 1-Alpha
PI3K	Phosphatidylinositol 3-Kinase
PKA	Protein Kinase A
PLIN1	Perilipin 1 Gene
PNPLA2	Patatin Like Phospholipase Domain Containing 2
POA	Preoptic Area
PPARΓ	Peroxisome Proliferator-Activated Receptor-Gamma
PPI	Protease and Phosphatase Inhibitor
PRAK	P38-Regulated/Activated Protein Kinase
PRKAR1A	Protein Kinase Camp-Dependent Type Ii Regulatory Subunit Alpha
PRKAR2B	Protein Kinase Camp-Dependent Type Ii Regulatory Subunit Beta
PRMD16	Pr Domain Containing 16
RT-qPCR	Quantitative Reverse Transcription Pcr
SDS	Sodium Dodecyl Sulfate
SDS-PAGE	Sodium Dodecyl Sulphate-Polyacrylamide Gel Electrophoresis
S-E-G	(Ser-Glu-Gly) Motif
ShNTC	Shrna-Non-Targeting Control
shRNA	Short Hairpin RNA
SIRNA	Small Interfering Rna

SP	Sodium Pyruvate
SREBP1	Sterol Regulatory Element-Binding Protein 1
SVF	Stromal Vascular Fraction
T2D	Type 2 Diabetes Mellitus
TAD	Transactivation Domain
TAE	Tris-Acetate-Edta
TBST	Tris Buffered Saline with Tween
TEMED	Tetramethylethylenediamine
TG	Triglycerides
TNFA	Tumor Necrosis Factor A
TRIB3	Tribbles Homolog 3
T-X-Y	(Threonine-Any Amino Acid- Tyrosine) Motif
UBE3A	Ubiquitin-Protein Ligase E3a
UCP1	Uncoupling Protein 1
USP20	Ubiquitin-Specific Protease 20
VLDL	Very-Low-Density Lipoproteins
WAT	White Adipose Tissue
WB	Western Blot
WHO	World Health Organization
B-AR	B-Adrenergic Receptors

12.2 List of figures

12.3 List of Tables.

12.4 Publications

12.4.1 Original articles

El-Merahbi R*, Trujillo Viera J, Loza Valdes A, Kolczynska K, Reuter S, Löffler MC, Erk M, Ade CP, Karwen T, Mayer AE, Eilers M and Sumara G. Adrenergic-induced ERK3 pathway drives lipolysis and suppresses energy dissipation. Genes and Development, 2020.

Mayer, AE., Löffler, MC., Schmitz, W., Erk, M., **El-Merahbi R**., Zhang, T., Braun, U., Heikenwalder M., Leitges, M., Schulze, A., Sumara, G. Hepatic Protein Kinase D3 provides the

negative feedback on cholesterol and TG synthesis by suppressing insulin signaling. Science Signaling 12.593 (2019): eaav9150.

Löffler, MC., Mayer, AE., Trujillo Viera, J., Loza Valdes, A., **El-Merahbi R**., Ade, CP.,Karwen, T., Schmitz, W., Slotta, A., Erk, M., Janaki-Raman, S., Matesanz, N., Torres, JL., Marcos, M., Sabio, G., Eilers, M., Schulze, A., Sumara, G. Protein kinase D1 deletion in adipocytes enhances energy dissipation and protects against adiposity. EMBO J. 2018 Nov 15; 37(22).

Cai, K., **El-Merahbi R.,** Loeffler M., Mayer, AE., Sumara, G. NDRG1 promotes adipocyte differentiation and sustains their function. Sci Rep. 2017; 7: 7191

Trujillo Viera J, **El-Merahbi R***, Nieswandt B, Stegner D, Sumara G. Phospholipases D1 and D2 suppresses appetite and protect against overweight. PloS one. 2016;11(6).

Mouhieddine TH, Nokkari A, Itani MM, Chamaa F, Bahmad H, Monzer A, **El-Merahbi R,** Daoud G, Eid A, Kobeissy FH, Abou-Kheir W. Metformin and ara-a effectively suppress brain cancer by targeting cancer stem/progenitor cells. Frontiers in neuroscience. 2015 Nov 23;9:442.

Abou-Kheir W, Eid A**, El-Merahbi R**, Assaf R, Daoud G. A unique expression of keratin 14 in a subset of trophoblast cells. PloS one. 2015;10(10).

El-Merahbi R*, Liu YN, Eid A, Daoud G, Hosry L, Monzer A, Mouhieddine TH, Hamade A, Najjar F, Abou-Kheir W. Berberis libanotica Ehrenb extract shows anti-neoplastic effects on prostate cancer stem/progenitor cells. PLoS One. 2014;9(11).

12.4.2 Reviews

El-Merahbi R., Löffler M., Mayer, A., Sumara, G. The roles of peripheral serotonin in metabolic homeostasis. FEBS letters. 2015; 589, 1728-1734

13 ACKNOWLEDGMENTS

This Ph.D. has been for me a complex journey in the world of academic science. As frustrating and exhausting some days could be, it was overall a very rewarding experience, that shaped my personal and professional development. I wish to thank all the people whose assistance was a milestone in the completion of my Ph.D.

I wish to express my deepest gratitude to my scientific advisor Dr. Grzegorz Sumara for giving me excellent projects and for supervising me through my Ph.D.. Thank you for providing me with a solid infrastructure and the remarkable opportunities that helped me shape my scientific career. I deeply appreciate your careful revision of all my work and many thanks for your patience, support, and guidance that proved to be monumental towards the success of my Ph.D.

I would like to pay my special regards to the rest of my thesis committee: Prof. Antje Gola, and Prof. Christian Wolfrum for their collaborative support to my work and their insightful comments and constructional critics which incented me to widen my research from various perspectives. I truly appreciate your personal support and great advice.

I am very thankful for Prof. Dr. Manfred Gessler who agreed to be the chairperson during my thesis defense.

I wish to show my gratitude to our collaborators, Prof. Martin Eilers and Dr. Carsten Ade, for lending us their expertise and provided us with reagents and especially for performing the RNA sequencing experiments.

I gratefully acknowledge the funding sources that made my Ph.D. work possible. I was funded by The Deutsche Forschungsgemeinschaft (DFG), and the European Research Council.

My Ph.D. work was done in Rudolf-Virchow-Zentrum, I am very thankful for the fruitful retreats, seminars and social events. Thanks to groups Wehman and Heinze who gave me access to their microscope facilities, A special thanks for Ahmad-Gholamreza Fazeli, who took care of me when

I first started. Thank you for being a good friend and for your scientific support and guidance throughout the years.

I am so honored to be a member of the Graduate School of Life Sciences at the University of Würzburg. I am very grateful for the excellent platform that GSLS provides to the doctoral candidates, including all the interesting workshops, organized lecture seminars and symposiums. All which helped me build up my personal and intrapersonal skills.

I will forever be thankful to my mentor Dr. Wassim Abu Kheir who provided me with the opportunity to join his marvelous team at AUBMC as a Master student. Wassim has been a great source of inspiration for me; his passion, enthusiasm and love for science are contagious. I am very grateful for his continuous personal support even after leaving his lab and I am very proud of his friendship above all.

A huge thanks for all the present and formal members of AG Sumara: Mona, Alex, Jonathan, Angel, Till, Manu, Saskia, Vanessa, Karina, Kasia and all others with whom I shared amazing trips, fruitful discussions on various topics and also excellent collaborative work on separate projects. I am very honored by all my students whom I had the chance to supervise during my Ph.D. Especially I am very proud of my talented student Saskia Router and particularly thankful for her outstanding help in this project.

Special thanks to Jonathan to whom I consider my wingman! Thank you for the great time on the personal and professional level. In the middle of my Ph.D., an Angel from Mexico joined the team during the time of my frustration peak. Angel, the talented scientist, with his amazing personality lifted the spirits of our team and with his extra chili attitude. I will never forget our trip to Palma together with Till and Jonathan which marked a great friendship that I hope to cherish through life.

I would like to thank my academic friends in Wurzburg and in Lebanon, having said that it was hard for non-academics to understand our crazy lifestyle. To all with whom I spent an amazing time at parties, BBQs, trips or some casual drinks. You all filled my time with Joy and made this Ph.D. a wonderful experience that I will never forget.

Among the academics comes my favourite scientist who quickly became my partner in life. Hana Ghanawi, I wouldn't thank you here for all your love and care nor it's the place here to thank you for all the amazing moments that we shared in trips and everyday life or even for always being there for me and understanding all the crazy working times, but here I would like to thank you for correcting my Thesis and all the constructive critics that you gave on my research as well as on my professional career.

Last but not the least, I would like to thank my family: my dad, my mom, my brother and two sisters for their constant support and believing in me. We grew up in Lebanon in difficult and challenging times. I am very grateful for my parents for all their extra-ordinary support throughout my life. It was only because of your continuous encouragement and guidance that I was able to overpass my difficult times and look forward to a brighter future. You believed in me in times it was unrealistic for anyone else to see what you saw in me.

To my Father Bassam who taught me how to handle the challenging life,

To my Mother Yassmin who taught me how to love myself and others,

I dedicate this Thesis to you…

13.1 Affidavit

I hereby declare that my thesis entitled, "**Adrenergic-induced ERK3 pathway drives lipolysis and suppresses energy dissipation**" is the result of my own work. I did not receive any help or support from commercial consultants. All sources and/or materials applied are listed and specified in the thesis.

Furthermore, I confirm that this thesis has not yet been submitted as part of another examination process neither in identical nor in a similar form.

Würzburg, MAY 2020 _____

Rabih El Merahbi

13.2 Eidesstattliche Erklärung

Hiermit erkläre ich an Eides statt, die Dissertation „**Der adrenerge induzierte ERK3-Signalweg verstärkt Lipolyse und unterdrückt Energiedissipation**" eigenständig, d.h. insbesondere selbstständig und ohne Hilfe eines kommerziellen Promotionsberaters, angefertigt und keine anderen als die von mir angegebenen Quellen und Hilfsmittel verwendet zu haben.

Ich erkläre außerdem, dass die Dissertation weder in gleicher noch in ähnlicher Form bereits in einem anderen Prüfungsverfahren vorgelegen hat.

Würzburg, April 2020 _____

Rabih El Merahbi